UNIVERSITY OF SOUTHAMPTON

FACULTY OF ENGINEERING, SCIENCE & MATHEMATICS

School of Chemistry

An exploration of supramolecular tape-like assemblies formed by pyridine dicarboxylates

by

Jonathan Edward Cheesewright

Supervisor: Dr. M. C. Grossel
Advisor: Dr. R. C. Brown

Thesis for the degree of Doctor of Philosophy

September 2009

UNIVERSITY OF SOUTHAMPTON

ABSTRACT

FACULTY OF ENGINEERING, SCIENCE & MATHEMATICS
SCHOOL OF CHEMISTRY

Doctor of Philosophy

AN EXPLORATION OF SUPRAMOLECULAR TAPE-LIKE ASSEMBLIES FORMED BY PYRIDINE DICARBOXYLATES

By Jonathan Edward Cheesewright

This investigation builds on a previous survey of the solid-state behaviour of pyridinedicarboxylate diesters, an overview of which is presented in Chapter 1. These compounds have been shown to form tape-like assemblies, mediated by a novel triple hydrogen bond motif.

Chapter 2 examines the behaviour of a small subset of these compounds in solution, some of which appear to form tape-like aggregates, as studied by ^{1}H NMR spectroscopy. Variable temperature Raman spectroscopy has been used to observe the disruption of the crystal architecture as the sample is heated past its melting point, and the increased strength of the tapes formed by the 2,6-diesters compared to those of the 3,5-analogues has been quantitatively demonstrated by DSC.

The results of X-ray diffraction studies on the single crystals of a number of diesters formed with naphthalene and anthracene side-arms are described in Chapter 3. This series of compounds has allowed the effect of changing both the length of the alkyl linker and its position of attachment to the polyaromatic to be considered.

The solid-state behaviour of a number of chlorinated and methylated diesters are compared in Chapter 4. Chapter 5 examines the crystal architecture of a number of asymmetrical monoesters and the behaviour of these systems is compared to that of the analogous diesters.

Chapter 6 details the progress made towards the use of the 2,6-pyridinedicarboxylate synthon in the synthesis of functional materials. The solid-state behaviour of a number of other pyridine derivatives prepared during the course of the present study is described in Chapter 7.

Contents

Declaration of authorship

I, Jonathan Edward Cheesewright, declare that the thesis entitled "*An exploration of supramolecular tape-like assemblies formed by pyridine dicarboxylates*" and the work presented in the thesis are both my own, and have been generated by me as the result of my own original research. I confirm that:

- this work was done wholly or mainly while in candidature for a research degree at this University;
- where any part of this thesis has previously been submitted for a degree or any other qualification at this University or any other institution, this has been clearly stated;
- where I have consulted the published work of others, this is always clearly attributed;
- where I have quoted from the work of others, the source is always given. With the exception of such quotations, this thesis is entirely my own work;
- I have acknowledged all main sources of help;
- where the thesis is based on work done by myself jointly with others, I have made clear exactly what was done by others and what I have contributed myself;
- none of this work has been published before submission.

Signed: J E Cheesewright

Date: 29th September 2009

Acknowledgements

There are a number of people without whom this thesis would never have been started, let alone completed and hopefully I have remembered to acknowledge and thank them all. (If not I'm very sorry!)

Firstly, my thanks are due to "the Boss," Martin, who not only offered me the chance to do a PhD but has provided me with a number of interesting, rewarding and memorable experiences throughout my time in Southampton.

My thanks also go to members of the Grossel group past and present (Polski, James, Michael, Dan, Alex, Georgina, the Andrews, Alan, Richard, Francesco and Alain) who have smiled and nodded as I've outlined another idea for how we could "improve" the lab - the value of your patience and camaraderie over the last four years is immeasurable. Equally patient have been the project students and interns that have worked with me (Richard, Scott, William, Chris and Rick) and I'm still not entirely sure who learnt more from whom!

Within the Chemistry Department there a number of people who have helped with my various questions and sometimes unusual requests; Neil Wells and Joan Street in NMR, John Langley and Julie Herniman in mass spec' and Sally, Nanou, Bevy in the admin offices are but a few. I am indebted to Mark Light, Pete Horton and Simon Coles for their patience with all my X-ray and DSC related questions, to Andrea Russell and the members of her research group, particularly Jon Speed, for their assistance with all things Raman, and to my advisor, Richard Brown. Finally thanks are due to the glassblowers who's names I can never seem to learn but who's skill has been of great value on numerous occasions, and to Karl, Graham and Tony in stores for their continued patience and (almost) limitless good humour!

As part of my project I was fortunate enough to experience the world of academia across the Channel and Professor Batail and his research group, especially Dr. Abdelkrim El-Ghayoury, are to be thanked for giving me such a warm welcome and tolerating my complete lack of useable French!

Away from the bench a number of people have provided me with all manner of distractions from the serious business of chemistry. The members of SUHC, StageSoc and ShowStoppers have given me many good memories and a plethora of photos to go with them. The leaders and young people of the 25th Southampton Sea Scout Group have played a large part in my last couple of years in Southampton and will be greatly missed. My housemates from the last four years (Alan, Andrew and Louise and Sarah & Andy M) have been exceptionally tolerant of my numerous comings and goings, particularly so of the late-night clattering and large piles of laundry that seem to follow a weekend away.

There are also a number of people who I am especially proud to be able to call friends and who have always been on hand when things haven't worked out quite as well as I'd hoped. So to Tim, Bourbon, Neil, Andrew and Lauren - thank you!

Last but by no means least, my parents have been a source of immense support and encouragement, to say nothing of providing an endless supply of tea and cake to help me keep typing. This thesis is dedicated to them.

Abbreviations

The following abbreviations have been used in the text.

Ar	Aromatic
Bn	Benzyl
Bpt	Boiling point
CIF	Crystallographic Information File
CSD	Cambridge Structure Database
DCC	1,3-Dicyclohexylcarbodiimide
DCM	Dichloromethane
DMAP	4-Dimethylamino pyridine
DMF	Dimethylformamide
DMSO	Dimethyl sulfoxide
DSC	Differential scanning calorimetry
EDT-TTF	4,5-Ethylenedithio-tetrathiafulvalene
EPSRC	Engineering and Physical Sciences Research Council
EtOAc	Ethyl acetate
ES-	Negative electrospray
ES+	Positive electrospray
Et	Ethyl
FTIR	Fourier transform infrared
Fw	Formula weight
HRMS	High resolution mass spectrum
IR	Infrared
LDA	Lithium diisopropylamide
Me	Methyl
MeCN	Acetonitrile
Mpt	Melting point
MS	Mass spectrum
NCS	National Crystallography Service
NMR	Nuclear magnetic resonance
Ph	Phenyl

Py	Pyridyl
rt	Room temperature
TGA	Thermal Gravimetric Analysis
THF	Tetrahydrofuran
TLC	Thin layer chromatography
TMS	Tetramethylsilane
TTF	Tetrathiafulvalene

1- Introduction

1.1 - Supramolecular chemistry and crystal engineering

The concepts of supramolecular chemistry are important in a whole spectrum of different fields since they deal with the non-covalent interactions between molecules. Consequently supramolecular chemistry is important in areas ranging from the understanding of biological systems and the design of new drugs, to the synthesis of new materials using molecular templates and the design and manufacture of functional systems such as molecular machines and devices.

The roots of the discipline can be traced back to the work of Lehn[1] and Pederson.[2] Pederson's crown ethers were the first neutral, synthetic molecules capable of binding alkali metal cations and the classic demonstration of using a crown ether, such as dicyclohexano-18-crown-6 (**1**), to drive the solvation of potassium permanganate in an aprotic solvent is still shown to undergraduates today (Figure 1).

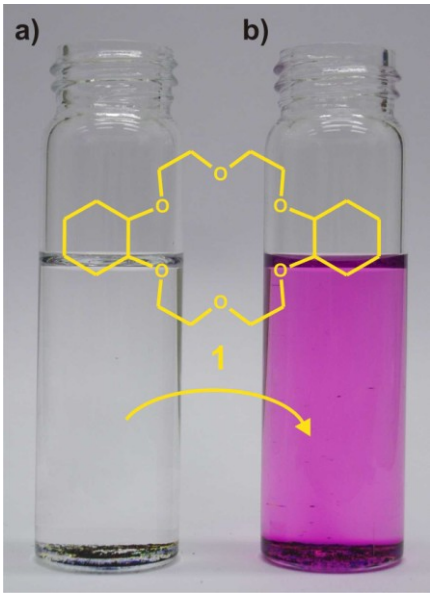

*Figure 1: (a) $KMnO_4$ is insoluble in toluene; (b) addition of **1** draws the permanganate anion into solution by forming a soluble complex with the potassium cation.*

More recently, supramolecular chemists have examined how molecules can be assembled to replicate the behaviour of mechanical or electronic components. Stoddart[3] has described the use of a catenane as two- or three-state switch and De Silva[4] has examined how small molecules can act as logic gates. For example, the fluorescence of compound **2** is dependent on the binding of three different cations (a sodium ion at site *a*, a proton at site *b* and a zinc ion at site *c*); whilst the binding of one or two ions produces a small increase in fluorescence, a major change is only observed if all three ions bind together.

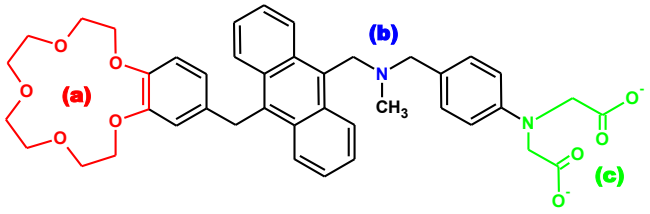

2[4]

Lee *et al.*[5] have described the behaviour of supramolecular "springs" formed from complexes of silver ions with pyridine ligands. Studies of aqueous solutions of the resulting coordination polymers showed that they form helical assemblies, the pitch of which can be altered by heating or cooling.

Not all supramolecular systems have a macroscopic analogue; Bonifazi *et al.*[6] have exploited intermolecular interactions between small molecules to produce nanoparticles. Varying the stoichiometric ratios of the components allows the size and volume distribution of these systems to be tuned. Others have used supramolecular assemblies as a means to a synthetic end. MacGillivray,[7] for example, has used small molecules as supramolecular templates to control the photocyclisation of olefins. Further examples of the role of supramolecular assemblies in photochemistry will be highlighted later in this chapter.

Supramolecular templates have also been used in the preparation of nano-structured semiconductors; Nandhakumar *et al.*[8] have exploited the ordered arrays formed by the self-assembly of liquid crystals, using them as templates for the preparation of nano-structured, thin films of lead telluride.

Supramolecular assembly is also fundamental to our understanding of biochemistry. From the pairing of bases in a DNA double helix, to the folding of proteins and the action of enzymes, the principles of supramolecular chemistry are essential to life. As Branco and Schneider note in their recent review[9] the principles of supramolecular chemistry are becoming increasingly important in the design of new drug delivery systems, to say nothing of the process of designing drugs themselves.

At the core of supramolecular chemistry is an understanding of how and why molecules interact with each other: the concept of molecular recognition. For two molecules to associate with each other and form interactions they must have functional groups that are complimentary to each other, both in terms of their chemistry (the simplest example being the interaction between a positive and a negative charge), and in terms of their geometry (the functional groups must be able to align themselves in space to allow a favourable interaction to occur).

In 1894 Fischer[10] used the mechanical example of a lock and key to explain how enzymes were able to recognise sugar molecules for metabolism. This simple analogy is now routinely used to illustrate how molecular selectivity can be achieved by combining several chemically complimentary interactions in a specific configuration. A different molecule may have the same combination of functional groups but if they are not arranged in the correct configuration, recognition will not take place.

A schematic illustration of this is presented in Figure 2; the host lock contains four sites of interaction, two positive and two negative. Consequently any potential guest key must contain the complimentary charges (i.e. two negative and two positive). Both of the guest keys (A and B) fulfil this

criterion, but only in key A are these charged sites arranged in a geometrically complimentary configuration to that of the lock. Consequently guest A is able to bind to the host (the key can open the lock) whilst guest B is repelled.

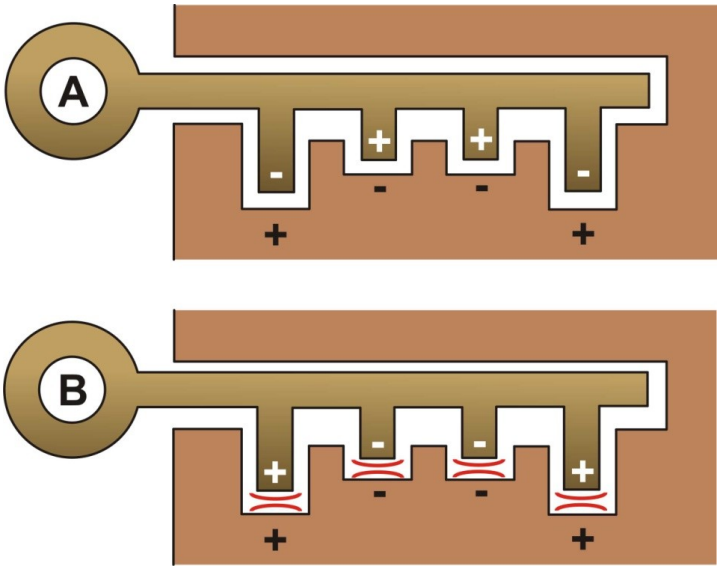

Figure 2: Schematic illustration of the concepts of molecular recognition based around Fischer's lock and key model.[10]

Dunitz[11] has observed that a crystal is a perfect example of a supermolecule. In a crystal, self-recognition by an individual molecule (or recognition between groups of molecules in the case of multi-component "co-crystals") can lead to macroscopic assemblies that are easily visible to the naked eye, but in which the smallest repeating unit is measured in Ångströms - some 6-7 orders of magnitude smaller.

Crystal engineering is a branch of supramolecular chemistry and its origins can be traced back to work by Schmidt[12] on the development of organic solid-state photochemistry.[13, 14] Supramolecular chemists working in the field of crystal engineering are interested in understanding how intermolecular interactions influence the behaviour of molecules in the crystalline solid-state. This knowledge can be used to design molecules that will form crystals with specific properties or that have the ability to perform specific functions (for example systems which have non-linear optical properties or that can act as superconductors).[13, 15, 16] Desiraju[14] elegantly summarised this objective

when he commented that *"crystal engineering is the rational design of functional molecular solids."*

In his recent review on the subject, Desiraju[14] states that within crystal engineering there are three distinct processes: the study of intermolecular interactions; the study of the effect of these interactions on crystal packing with the aim of defining a "design strategy;" and the study of how variations in packing can be used to fine-tune the properties of the crystal.

As has already been mentioned, the first of these stages is relevant not just to crystal engineering but to the entirety of supramolecular chemistry and, as Stoddart *et al.*[17] write, *"the design of a set of matching molecules that will self-assemble efficiently and selectively to form ordered supramolecular arrays in the solution and solid-states requires a precise understanding of all the non-covalent bonding forces that can exist between the components of a particular supramolecular array."* Stoddart[18] provides an elegant demonstration of this in the "one-pot" synthesis of molecular Borromean rings. In this example, supramolecular interactions between a metal centre, a bipyridyl unit and 2,6-diformylpyridine are exploited to direct the self-assembly of 18 individual components to form three interlinked rings (Figure 3).

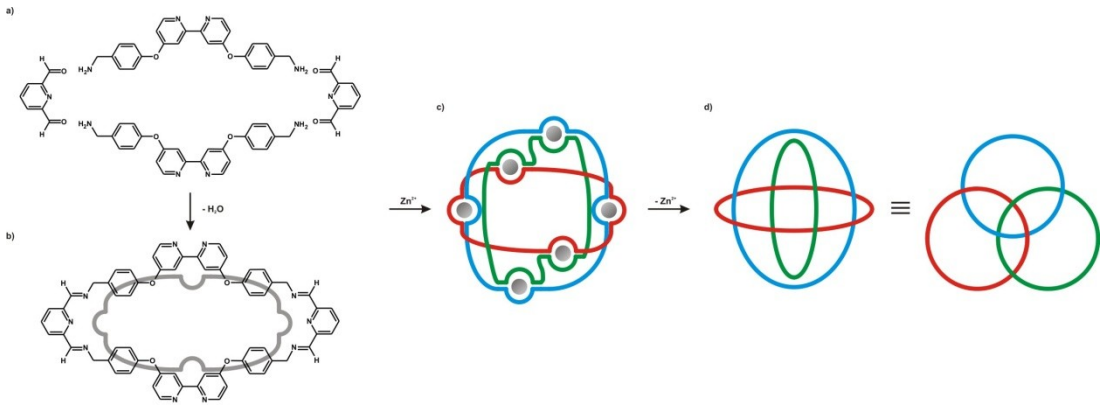

Figure 3: Schematic representation of Stoddart's[18] "one-pot" synthesis of molecular Borromean rings. (a) Structures of the organic components that form a single ring. (b) Chemical and schematic representations of a single ring. (c) Schematic representation showing the role of Zn^{2+} ions (grey spheres) as templates in the self-assembly of the components. (d) Removal of the metal ions leaves three interlinked heterocyclic rings.

Consequently, given their importance, it would seem appropriate to consider some of these different intermolecular forces.

1.2 - Intermolecular interactions

The number of different non-covalent intermolecular interactions is large and the quantity of literature describing and reviewing them is vast. In the interests of brevity, only those interactions relevant to the later discussions will be considered in this section. Consequently interactions with metals and ionic species, although of significance in many supramolecular systems, will be ignored.

1.2.1 - Van der Waals interactions

Van der Waals interactions are a result of dispersive forces between adjacent molecules and are isotropic in nature, meaning that they show no directional selectivity.[19] As a consequence van der Waals interactions are observed between all molecules and, although they are amongst the weakest of the intermolecular forces (they typically have an interaction energy of 2 kJ mol^{-1}), their omnipresence means that their combined effect can be the largest energetic component in an assembly.

Dispersive forces result from electrostatic interactions between a fluctuating multipole on one molecule and a corresponding, mutually induced, multipole on an adjacent molecule. The magnitude of dispersive forces is inversely proportional to r^6 (where r is the distance between the two atoms) and consequently van der Waals interactions are only effective over a short distance.[19, 20] As a result of their ubiquitous nature and short range of interaction, van der Waals forces are unsuitable for directing the assembly of supramolecular systems (i.e. ensuring molecular selectivity). However van der Waals interactions can often provide the energy needed to stabilise a molecular assembly once more directional interactions have aligned the components into the desired orientations.

1.2.2 - Hydrogen bonds

Hydrogen bonds are one of the most widely used interactions in supramolecular chemistry and Desiraju[19] has referred to them as a *"master key for molecular recognition."* As a result they are also one of the most widely studied interactions[14] and there has been much debate about what can be classed as a hydrogen bond and how it should be defined.[19, 21]

Steiner and Saenger[22] proposed the definition that a hydrogen bond is *"any cohesive interaction X-H-Y, where H carries a positive and Y a negative (partial or full) charge, and the charge on X is more negative than on H."* Aakeröy and Seddon[21] help refine the above definition by explaining roles of X and Y. X is an atom or functional group whose role is to reduce the electron density on H, resulting in a partial positive charge. Y (the hydrogen bond acceptor) is a functional group or atom able to donate electron density to the hydrogen bond.

More recently, Steiner[23] has suggested another definition based on that of Pimentel and McCellan:[24] *"an X-H···A interaction is called a 'hydrogen bond', if 1. it constitutes a local bond, and 2. X-H acts as proton donor to A."* These broad definitions allow for both the classic model of a hydrogen bond, where electron density is donated by a lone pair of electrons (such as those on oxygen and nitrogen) to a hydrogen atom bound to an electronegative atom (such as oxygen or nitrogen), and for the weaker interactions where π molecular orbitals act as the hydrogen bond acceptor.

The geometry of a hydrogen bonding interaction is dependent on the nature of both the donor and the acceptor with "stronger" bonds tending to be shorter and more linear. The energy of the interaction is similarly dependent on the functionalities involved but is widely acknowledged to vary between 2 and 40 kJ mol^{-1}, although for some systems (such as those with ionic donors or acceptors) the energy can rise to over 100 kJ mol^{-1}.[19, 21, 23]

In his recent review Steiner[23] explains how, by varying the environment of the donor and/or acceptor, the hydrogen bond can be changed into different types of interaction. The reasoning behind his explanation is that the energy of a hydrogen bond, like most other types of non-covalent interaction,[20] can be considered as being made up of several components. For the hydrogen bond these include electrostatic, dispersive and repulsive forces.

As has already been discussed dispersive forces are isotropic and are only effective over short distances. Electrostatic interactions are directional and effective over a longer range (for interactions between dipoles the energy of the interaction decreases as a function of r^{-3}, and for an interaction between a dipole and a monopole the dependency is proportional to r^{-2}).[23] Thus the character of the hydrogen bond can be altered by varying the contribution of these different forces. For example, if the donor and acceptor atoms are chemically equivalent (i.e. a symmetrical system X-H···X) then it becomes virtually impossible to distinguish X-H from H···X and the hydrogen bond can be considered to be a good approximation to a covalent bond.

Similarly, if the polarity of either the donor or acceptor is reduced, the electrostatic contribution to the overall energy of the hydrogen bond is similarly reduced and the contributions from dispersive and repulsive forces become more significant - the hydrogen bond becomes more like a van der Waals interaction. This example is particularly important when the weakest hydrogen bonds (such as those with C-H donors) are considered.

Steiner also draws the analogy between a hydrogen bond and the transition state of a proton transfer reaction, such as would occur between an acid and a base. Like acids and bases, hydrogen bond donors and acceptors can be considered to be hard or soft and these descriptions are useful in classifying hydrogen bonding interactions.

Strong and moderate hydrogen bonds occur between hard donors and hard acceptors. Like a hard acid, a hard hydrogen bond donor has a hydrogen atom attached to a strongly electronegative atom and, as a result, the X-H

bond is strongly polarised with a δ+ charge on the hydrogen. Similarly, a hard acceptor is a strongly electronegative species.[19]

Strong and moderate hydrogen bonds can encompass a wide range of interactions from those with ionic species or that are largely covalent in character (described by Jeffrey[23, 25] as "strong") to those which are predominantly electrostatic (such as between molecules of water) which Jeffrey has described as being "moderate".

The strong interactions have bond energies of 60-160 kJ mol^{-1} and are typified by very short interaction distances (X···Y = 2.2-2.5 Å) and X-Ĥ···Y angles of between 170 and 180°.[23, 25]

The moderate hydrogen bonds are predominantly electrostatic in character and tend to have interaction energies of 20-40 kJ mol^{-1}. Bond lengths are longer than those seen for the strong interactions, typically X···Y = 2.5-3.0 Å, and their geometries are less rigidly linear; a median X-Ĥ···Y angle of 165° is observed.[19] A consequence of this less stringent geometry is that bifurcated and trifurcated interactions can occur (interactions between one donor and two or three acceptors), as shown by Grossel *et al.*[26] for the binding of sulphate by 2,6-bis(methylguanidinium)pyridine.

The importance of moderate hydrogen bonds is well known in biological systems (for example consider the hydrogen bonding interactions between bases within the double helix of DNA) and a multitude of supramolecular chemists have used the more moderate interactions extensively.[16, 27-30]

Recently, Orola and Veidis[31] have exploited moderate hydrogen bonding interactions between nicotinamide and fumaric acid to form two-dimensional sheets (Figure 4) and three-dimensional networks. Avendaño and Briceño[32] have used hydrogen bonding interactions in the solid-state to assemble ribbons of fumaric acid and *trans*-1,2-bis(2-pyridyl)ethylene. These form stacks which then undergo photocyclisation.

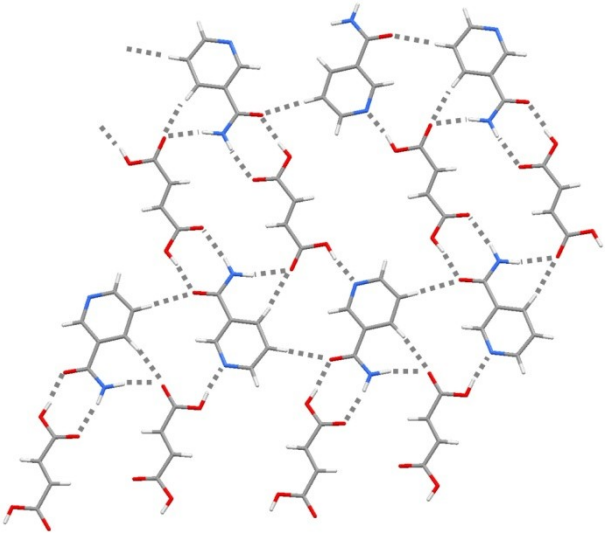

Figure 4: Crystal structure of the two-dimensional hydrogen bonded sheet observed by Orola and Veidis[31] between nicotinamide and fumaric acid; hydrogen bonds are shown as grey-dashed lines.

Weak hydrogen bonds involve soft donors (e.g. C-H) and/or soft acceptors (e.g. π-systems) and generally have interaction energies of between 2 and 16 kJmol^{-1}.[23, 33] Of specific interest to this investigation are those formed with C-H donors. The interactions of C-H donors with hard acceptors will be considered now, whilst the interactions between soft donors and soft acceptors (i.e. C-H···π interactions) will be discussed in the section 1.2.3.

As has already been mentioned, the energy of a hydrogen bond is comprised of both electrostatic and van der Waals components. In a database study of C-H···O interactions between a chloroalkane (acting as the hydrogen bond donor) and an otherwise unspecified oxygen acceptor, Desiraju[34] noticed that changing the acidity of the hydrogen bond donor had a systematic effect on the C···O bond length even at distances above the conventional van der Waals limit (Table 1). This was explained as the result of electrostatic rather than van der Waals interactions, supporting the view that interactions between C-H donors and hard acceptors are genuine hydrogen bonds and not just a consequence of close packing directed by van der Waals forces.

Table 1: Results of a CSD survey on the effect of hydrogen bond donor acidity on C-H···O bond length for interactions between chloroalkane hydrogen bond donors and oxygen atoms from otherwise unspecified molecules.[34]

	Donor	Mean C-H···O distance/Å
More acidic	Cl_3CH	3.32
⇑	RCl_2CH	3.40
	R_3ClCH	3.46
Less acidic	R_3CH	3.59

The electrostatic nature of the interaction was further evident from a preference for certain angles of interaction; the probability that the C-Ĥ···O bond angle would fall in the range 165-180° was found to be 50% for alkynes and 60% for alkenes.[34] Examination of the H···Ô=C angle for carbonyl acceptors showed clustering around 120° with the C-H bond found to be in the plane of the oxygen lone pair.

In a later survey, Steiner and Desiraju[35] compared the lengths and angles of interaction between a variety of hydrogen bond donors and a carbonyl acceptor. As a control group, they also looked at van der Waals-type contacts between an ethyl group and a C-H residue. (The mean H···Y bond lengths and X-H···Y bond angles from the study are presented in Table 2). As with the chloroalkanes, decreasing the acidity of the donor resulted in an increase in the length of the hydrogen bond. When the histograms of angular frequency were examined, the hydroxyl group was found to show a strong preference for interaction angles of 170-180° (in keeping with previous studies). A similar preference was shown by the ethynyl, vinyl and ethyl donors although the extent of the linear preference decreased with the acidity of the donor. In contrast, the angular distribution between 120 and 180° for the interactions between an ethyl group and a C-H residue was virtually isotropic, as would be expected for a van der Waals interaction. Steiner and Desiraju concluded that, despite the weakly acidic nature of the donor, C-H···O interactions are genuine hydrogen bonds.

Table 2: Mean bond lengths and angles from Steiner and Desiraju's survey of C-H···O hydrogen bonding interactions.[35]

Contact	Mean H···Y/Å	Mean X-Ĥ···Y/°
$C(sp^3)$-O-H···O=C	1.974(6)	154.0(4)
C=C-H···O=C	2.36(4)	152(2)
$C=CH_2$···O=C	2.67(1)	143(1)
CH_2-CH_3···O=C	2.761(6)	137.1(7)
CH_2-CH_3···H-C	2.500(2)	128.6(3)

More recently, Janiak and Scharmann[36] studied C-H···O and C-H···N interactions in poly(pyrazolyl)borate ligands. They found that H···O bond lengths varied between 2.47 and 2.89 Å and that C-Ĥ···O contact angles were in the range 110-167°. Plotting bond angle against bond length they observed a direct, inverse correlation that, as bond length increased, so the corresponding angle decreased (in keeping with the results of Steiner and Desiraju[35]). A similar, but significantly weaker, correlation was observed for the C-H···N interactions where H···N was found to vary between 2.42 and 2.96 Å and C-Ĥ···O between 94 and 173°.

These interactions were used to explain the non-ideal geometries seen in the crystal structures of the transition metal complexes formed by the ligands. C-H···N interactions were cited as an influence in the formation of ordered layers in the *bc*-plane of bis(hydrogen tris(triazolyl)borate)-zinc(II) hexahydrate (Figure 5b and c). In diaqua-bis(hydrogen tris(1,2,4-triazolyl)borate)-lead(II) dehydrate (Figure 5a), the deviation of the ligands from an idealised staggered geometry is attributed to C-H···O interactions between the ligand and the coordinated water molecules (one of the triazolyl rings in each ligand is observed to be tilted towards a water molecule).

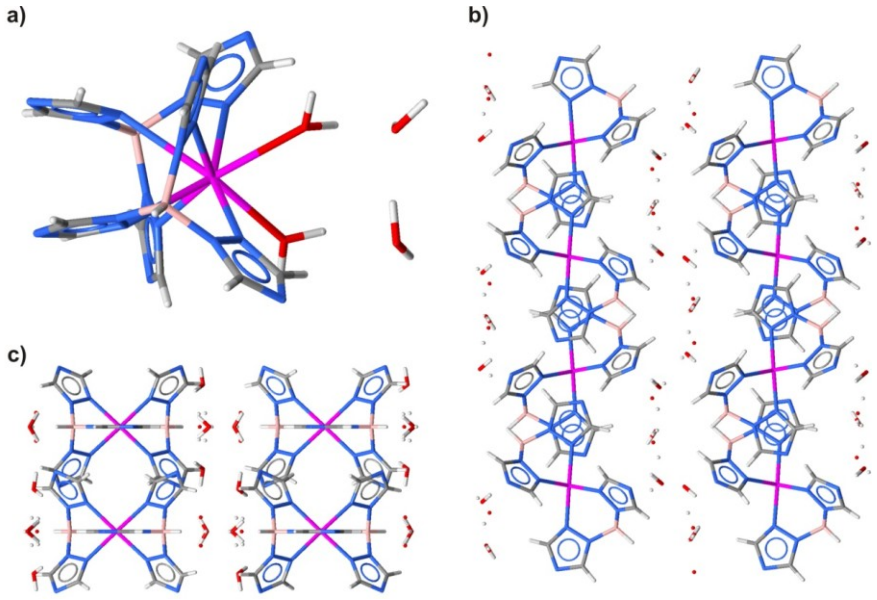

Figure 5: (a) Crystal structure of diaqua-bis(hydrogen tris(1,2,4-triazolyl)borate)-lead(II) dihydrate showing deviation of the ligands from an idealised staggered geometry. (b and c) Crystal structure of bis(hydrogen tris(triazolyl)borate)-zinc(II) hexahydrate viewed along the b- and c-axes respectively, showing the ordered layers formed as a result of C-H···N interactions.[36]

Gatti[37] has studied the occurrence of both intra- and intermolecular C-H···O interactions in the crystal structure of 3,4-bis(dimethylamine)-3-cyclobutene-1,2-dione (**3**) and has observed a range of contacts with H···O bond lengths varying between 2.211 and 2.296 Å with a clustering of the C-Ĥ···O bond angles around 140°. Above bond lengths of 2.7 Å, some of the contacts are observed to have C-Ĥ···O bond angles of around 90°. However, through experimental and theoretical studies of the charge distribution, Gatti has shown that this latter group of contacts are the result of van der Waals, not hydrogen bonding interactions.

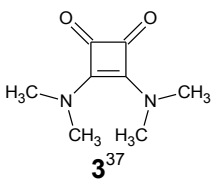

3[37]

Finally, Schmuck and Lex[38] have shown that interactions with a weak donor can be as structurally significant as those with a strong donor. They compared the solid-state behaviour of the chloride salts of compounds **4** and **5**, both of which form dimers linked by two pairs of hydrogen bonds. The outer pair of N^+-H···O bonds observed in **4** are replaced by C-H···O interactions in **5** and computational modelling of the interaction energies for each dimer has shown that the C-H···O interactions are only slightly less stabilising than the "stronger" N^+-H···O interaction.

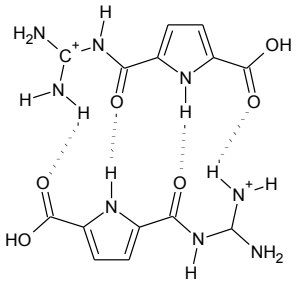

4[38]

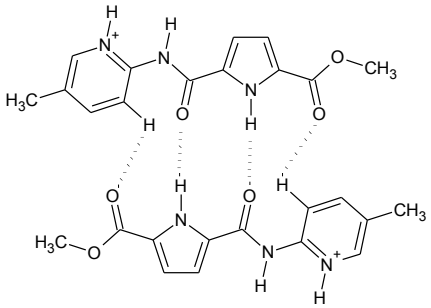

5[38]

These studies have shown that, not only can C-H···O and C-H···N bonding interactions occur beyond the limit of the sum of the van der Waals radii (in keeping with the electrostatic component of the interaction), but that they can also be considered as isostructural replacements for "stronger" interactions.

Whilst C-H···O/N interactions have been shown to be valid hydrogen bonds, the nature of C-H···Cl interactions is dependent on the environment of the acceptor. Thallapally and Nangia[39] have performed an extensive statistical survey of C-H···Cl contacts in which they examined the bond lengths and angles for interactions with Cl^-, Cl-M and Cl-C acceptors. In each case a significant number of contacts were observed above the sum of van der Waals radii and this proportion increased as the acidity of the acceptor decreased. However, whilst the interactions with Cl^- and Cl-M showed a correlation between the H···Cl distance and C-Ĥ···Cl angle, the same was not true for the Cl-C acceptor.

The effect of donor acidity on length of the H···Cl contact for each of the three acceptors was also examined. For the Cl^- and Cl-M acceptors, the contact distance was observed to increase as the donor became less acidic (in keeping with the results of Desiraju and Steiner[35] for C-H···O interactions). For the contacts observed with a Cl-C acceptor, changing the acidity of the donor had no noticeable effect on the length of the contact. Consequently it was concluded that, whilst C-H···Cl^- and C-H···Cl-M interactions show evidence of an electrostatic dependence and can be considered to be hydrogen bonds, C-H···Cl-C interactions appear to be isotropic and are likely to be a result of van der Waals close packing interactions.

1.2.3 - Interactions with π-systems

The nature of interactions between two π systems and between a π system and another functional group has been the subject of much debate and several studies over a number of decades.

Although generally considered to be weak, their importance in the supramolecular chemistry of biological systems has been noted.[33, 40] Burley and Petsko[41] studied the interactions between the aromatic side chains in the crystal structures of 33 proteins. They examined the straight line distance between the centres of the aromatic residues (r in Figure 6), the angle between this line and the normal to the aromatic plane of one of the residues (θ) and the angle between the two aromatic planes (φ). They identified 580 interactions with a centroid separation of less than 10 Å and plotted a histogram of frequency of occurrence as a function of the separation distance. No interaction was found with a centroid separation less than 3.4 Å due to van der Waals repulsions, between 3.4 and 6.5 Å the distribution was observed to vary with the separation distance, above 6.5 Å the distribution remained virtually constant.

An analysis of the contacts between 3.4 and 6.5 Å showed an interesting relationship between the angles θ and ϕ (Table 3). When the residues were either directly above one another or side-by-side (θ = 0 or 90°) an edge-to-face or T-shaped geometry was observed. Approximately half-way between these extremes the residues were found to be either coplanar or only slightly tilted with respect to each other. The frequency distribution of the observed geometries was found to deviate significantly from that expected if the orientation of the two residues was purely random. The T-shaped geometry (ϕ = 90°) was found to be the most frequently observed interaction with coplanar configurations (ϕ = 0°) being rarely observed.

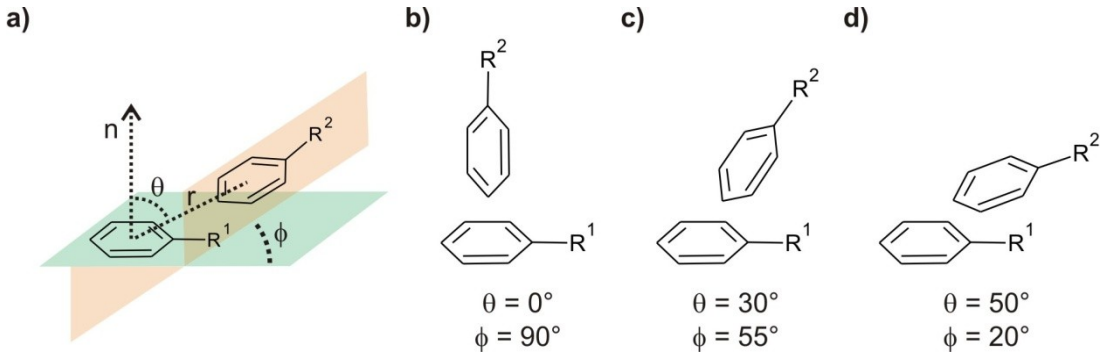

Figure 6: (a) Distances and angles examined by Burley and Petsko[41] in their survey of aromatic interactions in proteins; r denotes the straight line distance between the centres of the aromatic residues, θ denotes the angle between this line and the normal to the aromatic plane of one of the residues (n) and ϕ denotes the angle between the two aromatic planes (shown as green and peach polygons). (b - d) Examples of the relationship between θ and ϕ; examples shown are the optimal geometries identified by Burley and Petsko[41] for benzene (R^1 = R^2 = H) where r = 5.5 Å.

Table 3: Relationship between angles θ and ϕ for interactions between aromatic residues in protein crystals.[41]

θ/°	ϕ/°
0.0-22.5	90
22.5-45.0	45-60
45.0-67.5	5-35
67.5-90.0	45-90

Hunter and Sanders[42] went on to show how the geometries of interactions between π systems can be explained using a simple electrostatic model. They modelled a π system as a positively charged σ framework sandwiched

between two negatively charged π-clouds, and then represented this as a set of simple point charges (Figure 7).

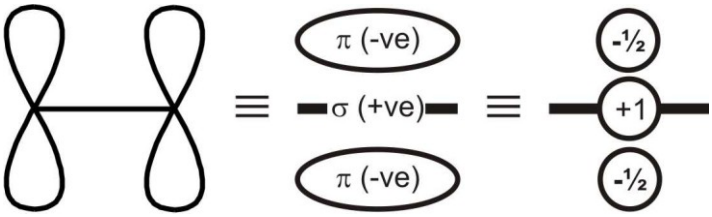

Figure 7: Schematic representation of Hunter's[42] point charge model for a π system.

By calculating the electrostatic energy between two point charges it was found that, although simplistic, the model could be used to explain the interactions observed between porphyrin molecules. Porphyrins have been observed to form aggregates where adjacent molecules are cofacial to each other with a vertical separation of between 3.4 and 3.6 Å. Molecules adjacent to each other in a stack are observed to lie in the same orientation but one molecule is seen to be offset with respect to its neighbour by between 3 and 4 Å along the N-N axis, placing the pyrrole ring of one molecule over the "π-cavity" of the neighbouring molecule (Figure 8a). Using the point-charge model, Hunter and Sanders were able to show that this geometry maximises the interactions between the π-cloud of one molecule and the σ-framework of the neighbouring molecule and minimises π-π repulsion.

The observation that coordination of a metal atom by the porphyrin increased the stabilisation energy of the stack was also explained using the electrostatic model. The metal atom effectively places a positively charged centre in the middle of the porphyrin, directly under the negatively charged π-cloud of the pyrrole ring from a neighbouring molecule (Figure 8b). Coordination of the metal centre by a ligand causes it to be partially displaced from the porphyrin (Figure 8c) thus weakening the electrostatic interaction with the π-system of the molecule above. This is observed as a reduction in the stabilisation energy resulting from metallation.

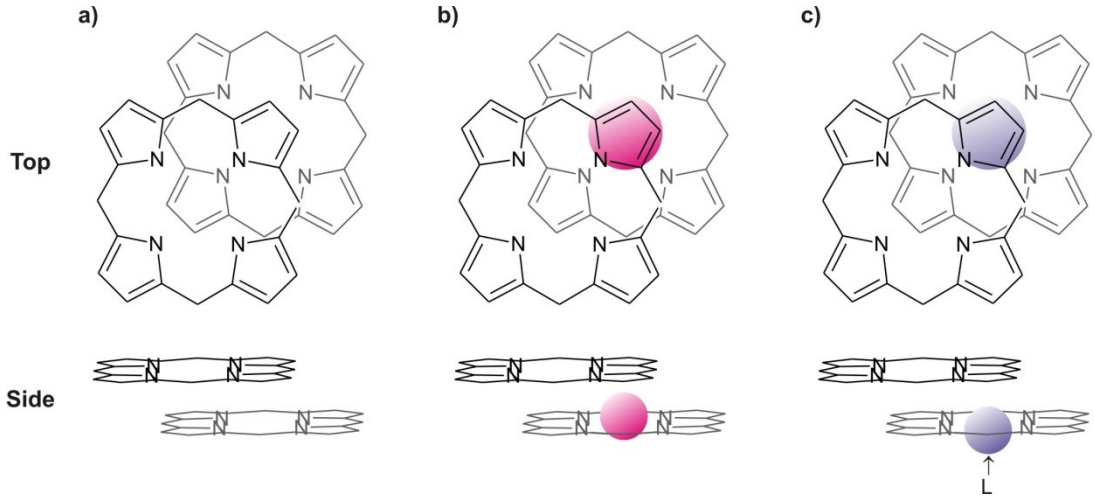

Figure 8: (a) Schematic representation of stacking arrangement shown by a neutral porphyrin - the aromatic pyrrole ring of one molecule is alligned above the π-cavity of its neighbour.[42] (b) Metallation of the porphyrin places the positively charged metal directly under the π-cloud of the pyrrole ring in the adjacent molecule, stabilising the interaction. (c) Addition of a competing ligand alters the geometry of the metal centre in the porphyrin, weakening the electrostatic interaction between the pyrolle π-cloud and the metal centre, reducing the stabilisation provided by metallation.

Using the point charge model,[42] the energy of a generic interaction between two π-systems was calculated for a variety of different offset distances and angles of rotation between the two sets of charges. These were mapped and bands of geometries where the interactions were either favoured or disfavoured were determined. These were simplified to three limiting cases, as shown in Figure 9.

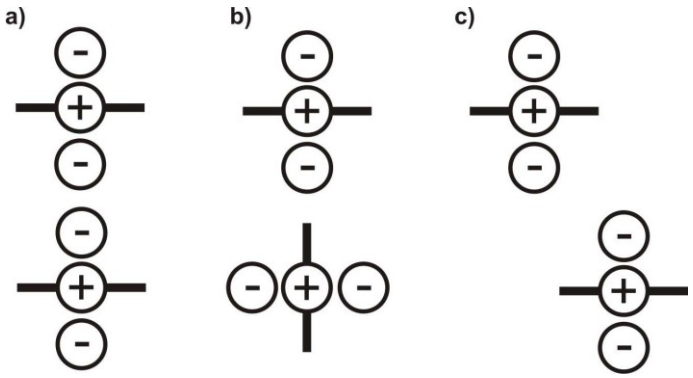

Figure 9: Limiting geometries for interactions between π-systems:[42] (a) face-to-face stacked geometry is dominated by π-π repulsion and the interactions are unfavourable; (b) rotation of one of the π-systems by 90° forms an edge-to-face geometry dominated by favourable π-σ interactions; (c) offsetting the two π-systems by several Ångströms also allows π-σ interactions to occur, as seen for the interactions between porphyrins.

Hunter and Sanders[42] go on to explain the effect of incorporating polarising atoms on the geometry of the interactions and of particular note is that a face-to-face geometry can be stabilised if one of the π-systems is electron deficient or contains a positively charged atom. This theoretical observation was confirmed by Cozzi *et al.*[43] who performed a series of NMR experiments on substituted 1,8-diphenylnaphthalenes (**6**). Steric constraints forced the phenyl rings to adopt a face-to-face geometry and the barrier to rotation of the rings was determined by NMR. In keeping with the model described by Hunter and Sanders,[42] it was anticipated that, if the electron density of the phenyl ring was increased, the π-repulsion between the two rings would increase, destabilising the stacked geometry and thus decreasing the energetic barrier to rotation of the rings. The observations supported the theory with the energy barrier for rotation of the rings found to be lowest for R_1 = OMe and highest for R_1 = NO_2.

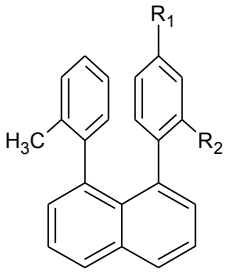

6[43]

R_1 = OMe, Me, H, Cl, CO_2Me, NO_2
R_2 = H, Me

Interactions between electron rich and electron poor aromatic systems to produce assemblies where the molecules are arranged in a face-to-face geometry has been exploited to align molecules for photocyclisation[44] and produce both organic semi-conductors[45] and non-centrosymmetric crystals[46].

It should be remembered that the electrostatic model proposed by Hunter and Sanders[42] is simplistic and that the electrostatic contribution to the overall energy of the π-π interaction is small, with the major component of the stabilisation energy, especially for systems containing no polarising atoms, coming from dispersive interactions. Consequently if the area of overlap

between two molecules is large enough, the dispersive contribution can result in face-to-face π-π assemblies. This was shown empirically by Desiraju[47] who found that the ratio between hydrogen and carbon, as well as the shape of the molecule, could be used to predict the packing mode of planar aromatic hydrocarbons, and in theoretical studies by Grimme[48] where π-π interactions were shown to be *"a special type of electron correlation (dispersion) effect that can only act in large unsaturated systems when they are spatially close, which is only possible in the stacked orientation."* The design of fullerene receptors based around corannulene "Buckybowls" (Figure 10)[49] provides an example of the exploitation of face-to-face π-π interactions.

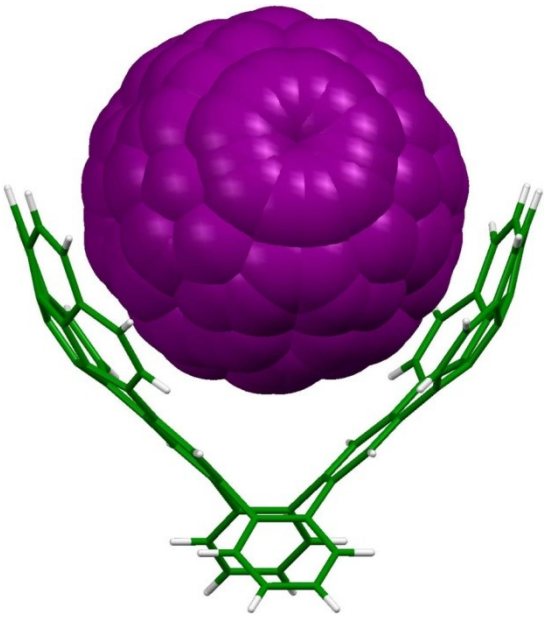

Figure 10: Crystal structure of fullerene receptor designed by Sygula et al.;[49] the fullerene guest is coloured purple and the carbon framework of the corannulene based host green.

Grossel *et al.*[50, 51] observed that the aromatic groups of *cis*-1,4-dihydro-4-tritylbiphenyl (**7**) adopted an edge-to-face geometry in both the solid-state and in solution (Figure 11).

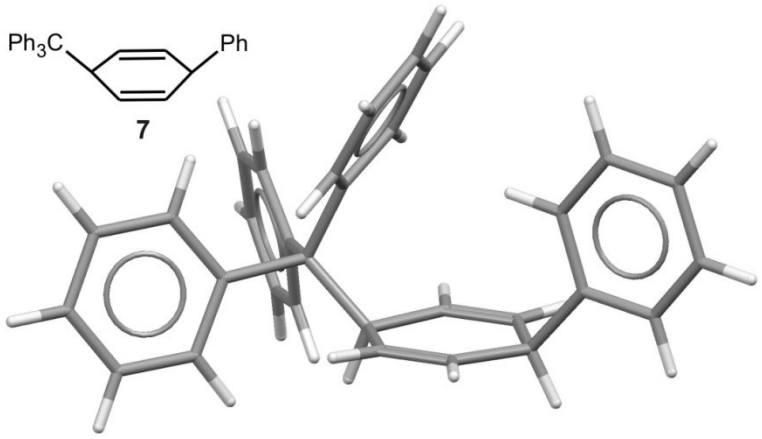

*Figure 11: Edge-to-face conformation observed in the solid-state for **7** by Grossel et al.*[50, 51]

Wilcox *et al.*[52] subsequently used NMR experiments to probe the edge-to-face nature of interactions between aromatic systems. They designed a molecular "balance" (**8**), a molecule which could exist in two states (shown for the phenyl derivative in the lower half of Figure 12). Wilcox investigated the relative populations of these states for a number of different substituents and observed that, for the aromatic substituents with additional functionalities at the *para*-position (**8c**-**h**), the folded conformer was favoured over the unfolded.

Moving the additional functional group to the *meta*-position (**8i**-**j**) reduced the population of the folded state but it was still favoured over the unfolded geometry. When the aromatic substituent was methylated at both *meta*-positions (**8k**) the unfolded geometry was favoured.

The population of the folded state was found to increase when an electron withdrawing substituent was attached to the phenyl ring, although interestingly adding an electron donating substituent did not decrease the population of the folded state. Wilcox[52] also noted that the folded geometry was preferred for alkyl as well as aromatic substituents. Whilst not suggested by Wilcox, it could be inferred from this observation that C-H···π interactions were involved in the stabilisation of the folded conformers and thus that edge-to-face π-π interactions are actually a specific case of C-H···π hydrogen bonding.

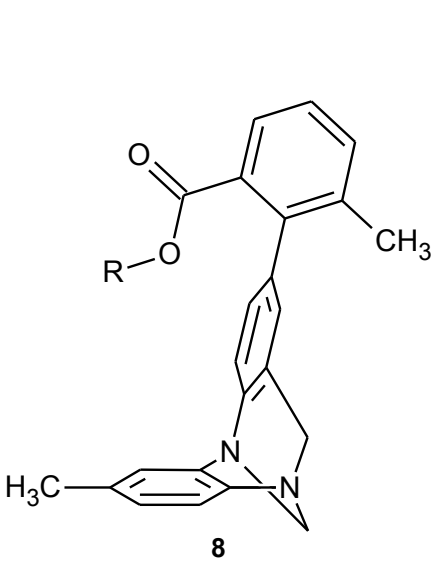

8

R=

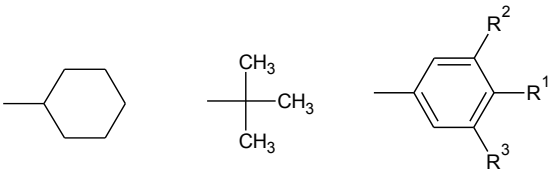

a **b** **c-k**

	R^1	R^2	R^3
c	H	H	H
d	Me	H	H
e	OMe	H	H
f	CN	H	H
g	NO_2	H	H
h	I	H	H
i	H	H	Me
j	H	H	CN
k	H	Me	Me

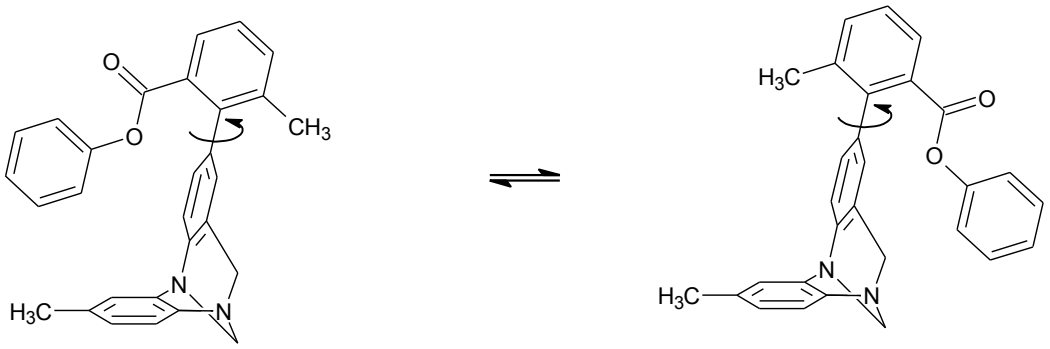

folded state unfolded state

Figure 12: Molecular balance designed by Wilcox et al.[52] to investigate edge-to-face interactions between aromatic systems; the lower half of the diagram shows the two different states that the molecule can adopt.

In a recent study Wantanabe *et al.*[53] have investigated the solid-state behaviour of benzyl ethers. They sought to establish whether these compounds formed the theoretically predicted but sterically disfavoured *gauche*-conformer stabilised by C-H···π interactions, as had been observed for the analogous ketones, sulphides and sulfoxides. The crystal structure of the diether (**9**, Figure 13) showed that one phenyl ring was arranged in a *gauche* conformer, stabilised by intramolecular C-H···π interactions with the alkyl protons of the central core. The other phenyl ring was held in an *anti*-conformer by intermolecular C-H···π contacts with adjacent phenyl groups. The intermolecular C-H···π contacts were observed to be cooperative with

each aromatic ring acting as both a donor and an acceptor, forming a "molecular staircase."[53]

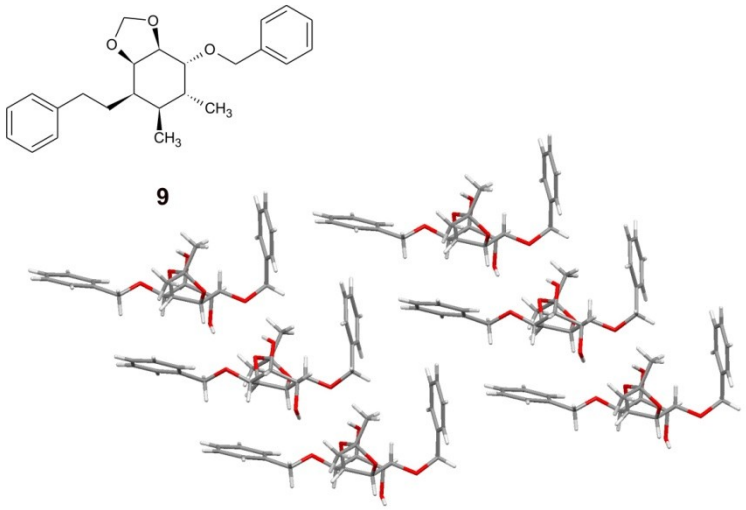

*Figure 13: View along the b-axis of **9**[53] showing the stepped assembly and the gauche- and anti-conformers adopted by the phenyl groups.*

Several reviews[33, 40, 54, 55] have examined the nature of the C-H···π bond. Takahashi *et al.*[54] surveyed the structures deposited in the CSD looking at interactions between C-H groups and aromatic π-systems. They found that, as for other "weak" hydrogen bonding interactions, the distance between the proton and the plane of the π system increases as the hydrogen bond donor becomes less acidic, and that more acidic donors favour a more linear geometry (Table 4).

Table 4: Contact geometry data from the CSD survey of C-H···$\pi_{(Ph)}$ contacts by Takahashi et al.[54]

Donor	D_{pln}/Å	α/°	$\alpha_{(corrected)}$/°
Cl_3CH	2.53±0.17	157±12	169±11
Cl_2CH_2	2.62±0.15	151±13	159±14
(sp)CH	2.62±0.13	152±13	159±13
(sp^2)CH	2.73±0.11	148±11	154±13
CCH_3	2.75±0.10	148±13	157±15

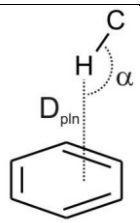

D_{pln} is the straight-line distance between the proton and the plane of the phenyl ring; α is the angle between the C-H bond and this line; the values of α were corrected to compensate for a statistical bias towards less linear geometries using a factor of 1/sin α; values for sp^2 C-H donors are for organic species where the crystal structure had an R-factor of less than 5%, a second survey of sp^2 donors using neutron data and including organometallic species gave values of D_{pln} = 2.70±0.11 Å; α = 146±9°; $\alpha_{(corrected)}$ = 149±11°.

It should be noted that the study only included hydrogen atoms that had a horizontal displacement of less than 1.4 Å from the centre of the ring (*i.e.* the proton was inside the vertical space directly above the carbon skeleton). This was justified using the results of a survey of structures obtained from neutron diffraction data that contained an sp^2 hybridised C-H donor; the raw data showed a relatively even distribution of contacts for horizontal displacements (D_{px1}) between 0.2 and 1.6 Å. The number of observed compounds decreased below this range and increased above it; however once the data was corrected by applying a factor of $1/D_{px1}$, a systematic decrease in the number of contacts was observed with increasing displacement, and this value reached a constant for displacements greater than 1.4 Å from the centre of the aromatic ring.

The preference of donors to sit directly above the π-cloud has been commented on in subsequent reviews. In 2002, Suezawa *et al.*[55] studied C-H···π interactions in the crystal structures of transition metal complexes. They found that in over 72% of the 39570 entries containing a C_6 aromatic ring, the ring acts as an acceptor for an intermolecular C-H···π interaction with H···C distances ranging between 2.5 and 3.2 Å (the mean H···C distance being 2.90 ±0.13 Å). It was noted that the H atom tends to sit above the centre of the aromatic ring and that the C-H bond of the donor is generally aligned towards the ring centroid. Intramolecular C-H···π interactions were also studied and identified as playing an important role in determining the shape of the complex. It was found that the H···C distance increases with the number of covalent bonds between the donor and the acceptor and that, when more than 10 covalent bonds exist between the donor and acceptor, the mean H···C distance is the same as that for intermolecular interactions.

The most recent survey of C-H···π interactions by Nishio *et al.*[33] focussed on interactions where the C-H donor was from an organic methyl group. Again, the tendency of the proton to lie above the centre of the ring was noticed and the average distance between the proton and the aromatic plane of the acceptor was found to be 2.80 ±0.14 Å.

The weak nature of the hydrogen bond-like interaction between C-H donors and π systems means that it is susceptible to influences from other functional groups. A wide range of contact distances have been reported, many of them longer than the sum of the Bondi[56] van der Waals radii (2.77 - 2.97 Å). However, there is a general trend for the proton of the donor to be located above the ring of the π acceptor. The fact that electrostatic forces are a minor component in the overall stabilisation energy of these interactions makes it hard to determine whether the interactions are the causes or consequences of crystal packing.[57] However, it also make them important for supramolecular assembly in solution,[55] and their role in the assembly of proteins and in the formation of complexes between cyclodextrin hosts and aromatic guests is well documented.[33, 40]

1.2.4 - Halogen bonding interactions

Like hydrogen, halogen atoms can accept electrons from atoms such as nitrogen, oxygen and sulfur to form directional intermolecular interactions. These interactions are known as halogen bonds.[58, 59] In their recent review, Metrangolo *et al.*[60] defined a halogen bond as the interaction between an electron donor (the halogen bond acceptor) and the region of positive potential at the end of a C-X bond (the halogen bond donor).

It should be noted that the distribution of electron density around a covalently bound halogen atom has been shown to be anisotropic.[61] Molecular modelling experiments by Clark *et al.*[62] suggest that, in an R-X bond, the unpaired valence electrons of the halogen atom form an electron-rich "belt" around the equator of the halogen atom (orthogonal to the R-X bond), leaving an electron deficient "σ-hole" centred around an axis made by extension of the R-X bond through the halogen. The magnitude and size of this region depends on the nature of the halogen; fluorine, for example, is more electronegative than the other halogens and thus the valence electrons are less polarisable. As a consequence, a region of slightly-less-negative, rather than positive, potential is seen at the end of the halogen atom. In

contrast, the electrons of iodine are notably more polarisable and the "σ-hole" is found to cover a larger area and to have a more positive potential than that of the other halogens. The magnitude of the polarisation is also observed to be dependent on the acidity of the attached R-group. For example, the chlorine atom in $CHCl_3$ is not found to have a σ-hole but the electron withdrawing nature of the R-group in CF_3Cl is sufficient to induce one.

The effect of polarisation on the halogen atom has been noted by Metrangolo *et al.*[63] who have ranked the halogens in order of strength as halogen bond donors I > Br > Cl > F (fluorine is not observed to form halogen bonds[62]). This can be shown empirically by comparison of the melting points of the co-crystals of **10** with either **11** or **12**; the iodo-derivative (**10·12**) is found to have a higher melting point than that of the bromo-analogue (**10·11**). A competitive co-crystallisation experiment between a 1:1:1 mixture of **10**, **12** and **13** in acetone gave pure crystals of **10·12**, also illustrating that iodine is a stronger donor than bromine. (Note that, although **12** and **13** are different configurational isomers, the **10·13** adduct is known.[63])

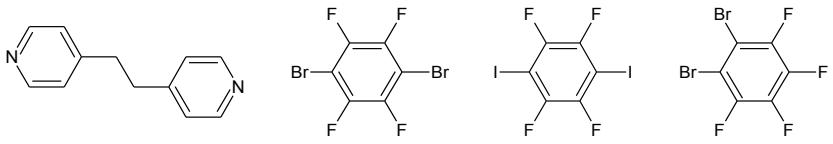

10 **11** **12** **13**

A consequence of the polarisation of the halogen atom is that, like hydrogen bonds, halogen bonds are directional. A survey of the CSD by Parthasarathy *et al.*,[64] found that for halogen contacts with nitrogen or oxygen the majority of contacts occur with C-X···N/O angles between 135 and 180° for chlorine, and between 150 and 180° for bromine and iodine. Subsequent studies[58, 65] have also shown a preference for linear interactions, with contacts to oxygen adopting a greater range of angles than those to nitrogen.

The strength of a halogen bond has been found to vary between 10 and 200 kJ mol^{-1} and the interaction has been shown to compete with hydrogen bonds.[63, 66] A competitive co-crystallisation experiment between a 1:1:1 mixture of **10**, **12** and **14** in acetone gave pure crystals of **10·12** and pure crystals of **12·15** have been obtained from a solution of the components in methanol.[63]

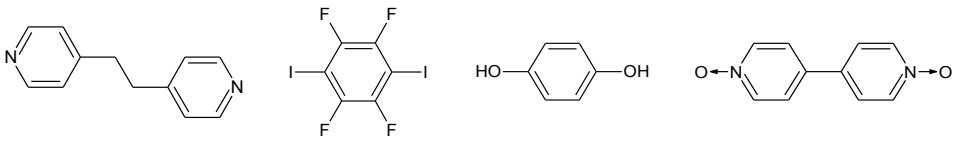

10 **12** **14** **15**

Ho *et al.*[67] have described an assay using conformational isomerisation of a DNA Holliday junction to show that a bromine halogen bond can compete with a "classic" N-H···O$^-$ hydrogen bond.

However, it should be noted that halogen bonding will not always take precedence over hydrogen bonding; Desiraju *et al.*[68] have compared the crystal structures of derivatives of **16** and found that they all form corrugated sheets linked by O-H···O hydrogen bonds (Figure 14).

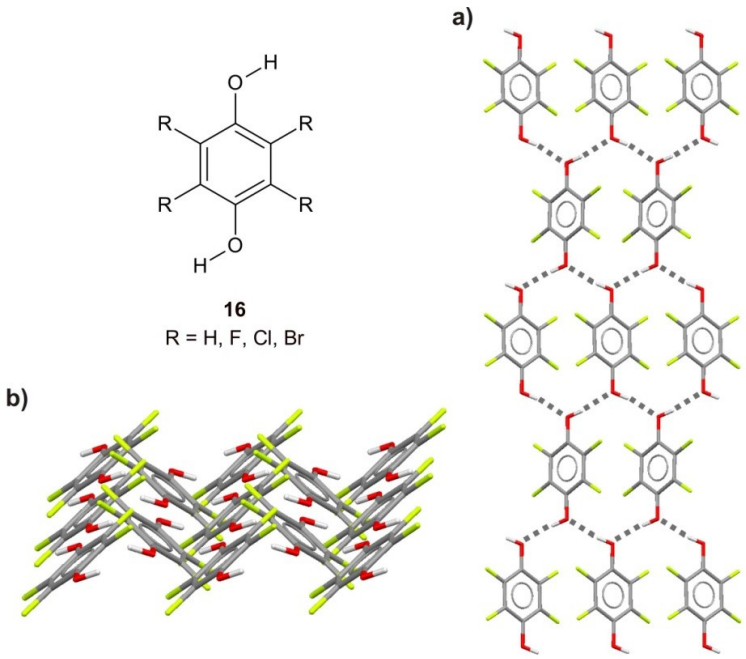

*Figure 14: (a) Top and (b) side views of the hydrogen bonded corrugated sheet formed by the fluoro derivative of **16**;[68] hydrogen bonds are shown in (a) by grey dashed lines.*

It should also be noted that hydrogen and halogen bonds are not mutually exclusive. A recent analysis by Ho *et al.*[59] of the crystal structures of protein-ligand complexes highlighted several examples where the carbonyl oxygen atom of a peptide residue acts as the acceptor for both a hydrogen and a halogen bond. The two interactions were observed to be orthogonal to each other and molecular modelling showed them to be energetically independent.

In a recent review, Rissanen[65] notes that the number of papers reporting halogen bonding interactions has steadily grown over the last decade and that, as a result of work by Metrangolo and Resnati, iodoperfluoro compounds are the donors of choice. Of the interactions with this class of compounds, those with a nitrogen acceptor are the most common and this ties in with observation by Metrangolo, Resnati *et al.*[60, 63] that, of the neutral receptors for perfluoroalkyl and -aryl halides, those with nitrogen atoms make better acceptors than those with oxygen or sulfur atoms. It should be noted that N-oxides are often better acceptors than simple nitrogen containing compounds and anions are better acceptors still. It is also worth commenting that, like hydrogen bonds, interactions with lone pairs of electrons are generally stronger than those with π systems.

As a result of their strength, interactions with iodoperfluorocarbon donors dominate recent reviews of halogen bonding[60, 65] and a few specific examples will be mentioned briefly. As has already been mentioned, halogen bond contacts tend to be linear along the line of the C-X bond and this directionality has been exploited in the design of one-, two- and three-dimensional assemblies; Metrangolo *et al.*[69] have reported the synthesis of a series of interpenetrated rings from diiodoperfluoroalkanes and I^- anions (Figure 15).

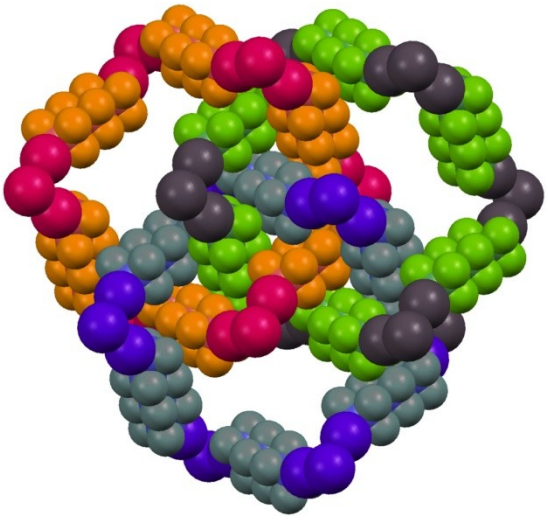

Figure 15: Space-filling representation of the intercalated rings formed by the supramolecular assembly of 1,6-diiodoperfluorohexane and I⁻, viewed along the crystallographic c-axis.[69] For clarity, each ring has been tinted a different colour and the catanane complexes of the sodium counter ion have been hidden.

A combination of C-I···N halogen bonds and π-π interactions were used to assemble molecules of **17** in the solid-state so that the alkene linkers were aligned for photocyclisation to produce **18**.[60] (Recrystallisation of **18** from chloroform was found to give an open framework linked by further C-I···N halogen bonds with molecules of chloroform trapped in the cavities.)

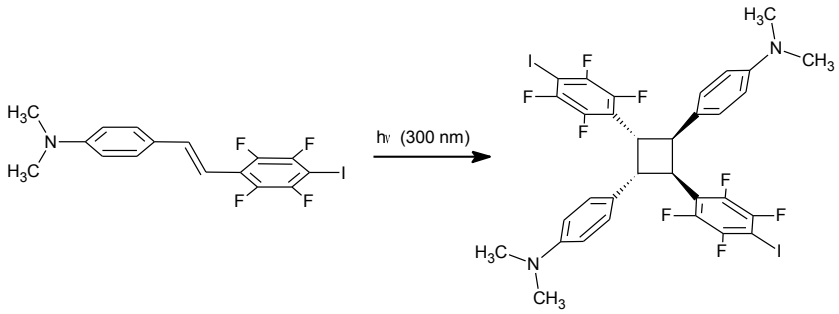

17 **18**

Desiraju *et al.*[70] have used birfucated C-I···O halogen bonding interactions between molecules of 4-iodo-4'-nitrobiphenyl (**19**) to form a crystalline solid containing one-dimensional chains which was found to act as a second harmonic generator.

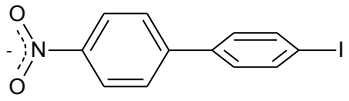

19

In addition to the types of halogen bonds described above, interhalogen contacts can also be formed. These have been classified into two different types based on the geometry of the interaction (Figure 16).[71] Type I contacts occur where the angles θ_1 and θ_2 are approximately equal to each other, whereas type II contacts occur where $\theta_1 \approx 180°$ and $\theta_2 \approx 90°$.

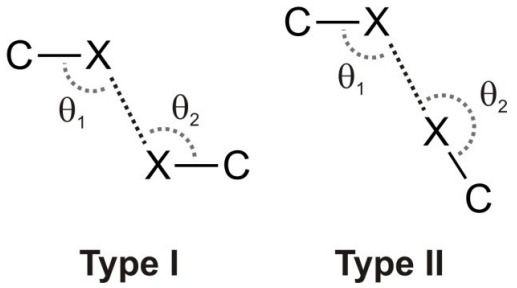

Figure 16: Classifications of interhalogen contacts.[71]

Desiraju *et al.*[71] performed a survey of structures deposited in the CSD and compared the values of θ_1 and θ_2 for Cl···Cl, Br···Br and I···I contacts. The distinction between type I and II contacts was found to become less distinct for the lighter halogens and had disappeared completely for Cl···Cl interactions.

Whilst interhalogen contacts between the more polarisable halogens (Br and I) are accepted as structure directing contacts[15] the evidence for Cl···Cl interactions is less clear. Price *et al.*[72] have examined the structures of chlorinated hydrocarbons containing only carbon, hydrogen and chlorine. Like Desiraju, Price observed that aside from an absence of contacts with a

value of θ less than 90°, there was little evidence of a geometric preference for the angle of interaction.

Price[72] also noted that over 80% of the contacts occur for compounds where the number of hydrogen atoms is less than the number of chlorine atoms even though these account for less than 50% of the structures sampled. In other words, the majority of Cl···Cl interactions are observed in compounds where close packing as a result of van der Waals forces would place chlorine atoms in close proximity to each other. Computer modelling of the interactions between molecules of $ClCH_3$, CCl_4, C_6H_5Cl and C_6Cl_6 suggested that the charge transfer contribution to the Cl···Cl interaction was very small and that the dispersive energy was only weakly dependent on the orientation of the molecules. Both Price[72] and Desiraju[71] concluded that the crystal packing behaviour observed in their studies could best be explained as the result of close packing and repulsion between the anisotropic electron clouds of chlorine atoms rather than as the result of a specific donor/acceptor interaction.

It should be noted that whilst there is no evidence of a specific donor/acceptor-type interaction, the anisotropy of the chlorine atom still has a marked effect on the packing of molecules in the solid-state. Although the volumes of the chloro and methyl-groups in the solid-state are known to be comparable,[56, 73] the literature contains many examples[68, 73, 74] where chloro/methyl exchange results in significant changes to the solid-state behaviour of otherwise analogous compounds. For example, Csöregh *et al.*[74] have observed that the crystals formed by **20** with R = CH_3 have a higher symmetry and are more dense than those formed with R = Cl.

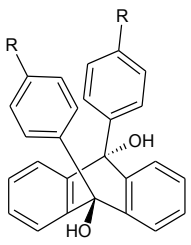

20[74]

1.2.5 - Competition between interactions

Computational modelling is now a routine part of the drug discovery process[75] and freely available software[76] allows the energy of receptor-ligand complexes to be determined. Modelling can be used to evaluate the likelihood of a proposed complex behaving as anticipated and can be used to screen potential candidates so that only the most promising are taken forward for further development. However, the initial design of a supramolecular system relies on a chemist's intuition and an understanding of how different functional groups are likely to interact with each other. Different interactions are often in competition with each other and, for the design of a supramolecular assembly or crystal architecture to be successful, it is important to be able to predict which will dominate.

Etter's rules[77] for hydrogen bonding are a prime example of supramolecular chemists' attempts to do this and the first three rules are generally applicable to a wide range of systems;

> *"1. All good proton donors and acceptors are used in hydrogen bonding.*
> 2. *Six-membered-ring intramolecular hydrogen bonds form in preference to intermolecular hydrogen bonds.*
> 3. *The best proton donors and acceptors remaining after intramolecular molecular hydrogen bond formation form intermolecular hydrogen bonds to one another."*

More recently, Hunter[20] has shown how molecular electrostatic potential (MEP) surfaces can be used to predict which functional groups are likely to form favourable interactions and to rank the interactions between different functional groups on the basis of their energy. Hunter then goes on to show the effect of different solvents on these interactions and how different solvents can compete with other solute molecules to interact with certain functionalities.

Aakeröy *et al.*[78] have since reported the use of MEP surfaces to rank the donor and acceptor properties of different functional groups and have successfully used these rankings to predict the interactions observed in a molecular assembly formed by the cocrystallisation of three different components (Figure 17).

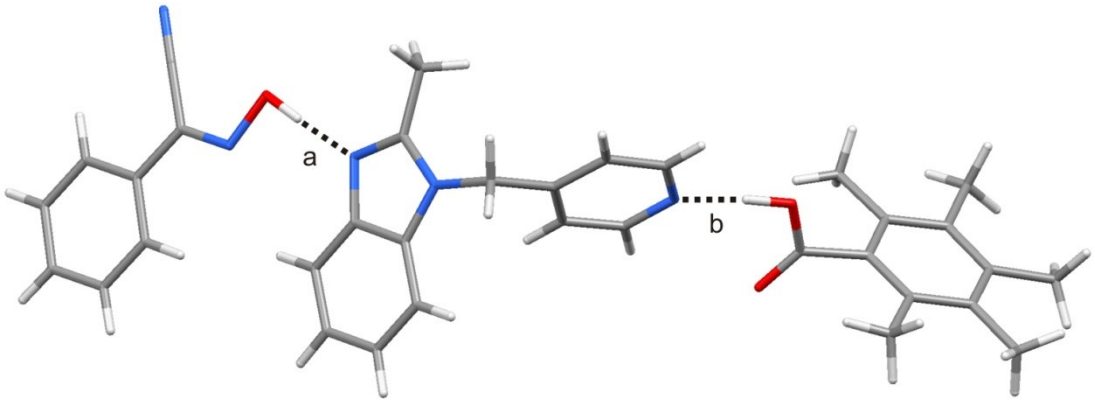

Figure 17: Three component assembly characterised by Aakeroy et al.[78] In accordance with Etter's rules and as predicted from MEP calculations, the best hydrogen donor forms an interaction with the best acceptor (contact a) and the second best donor with the second best acceptor (contact b).

Empirical studies are also still important in helping rank the significance of different interactions. Some examples have already been presented in the preceding section and others can be found in work by Nangia[79] and Aakeröy.[80]

Both empirical and computational studies of different interactions have helped our understanding of how different functional groups compete with each other. They have also shown that the interplay between different interactions is exceptionally complex; interactions that appear strong in one system can be overcome by a "weaker" interaction in another.

1.3 - Designing crystalline systems

As has already been mentioned, crystal engineering is the concept of exploiting molecular recognition in the solid-state with the ultimate aim of controlling the structure and properties of the resultant assembly. As several authors (Davis[81] and Desiraju[14] amongst them) have noted, both chemical and geometric aspects must be considered.

The experiments of Desiraju *et al.* [82] with cubanecarboxylic and phenylpropiolic acids (**21** and **22**) provide an elegant illustration of this. Although the crystal packing of the cubane systems is dominated by the size of the substitutent group and the packing of the phenylpropiolic system by electronic effects, neither system can be purely explained in geometric or electronic terms.

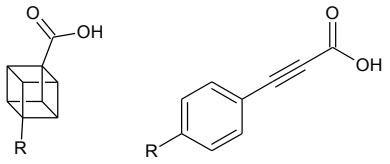

21 **22**

Within crystal engineering, Desiraju[19] has proposed the concept of the "supramolecular synthon" as a means to account for both steric and chemical contributions to molecular recognition. Like Etter's rules,[77] synthons are the product of observation of a large number of systems. Desiraju[19] describes them as *"substructural motifs which incorporate the chemical and geometrical characteristics of intermolecular interactions"* and goes on to say that *"they are spatial combinations of intermolecular interactions which can be recognized clearly as design elements for solid-state architecture."* In essence, a synthon is a set of intermolecular interactions that have been observed to form reliably in a variety of different environments, some examples are shown in Figure 18.

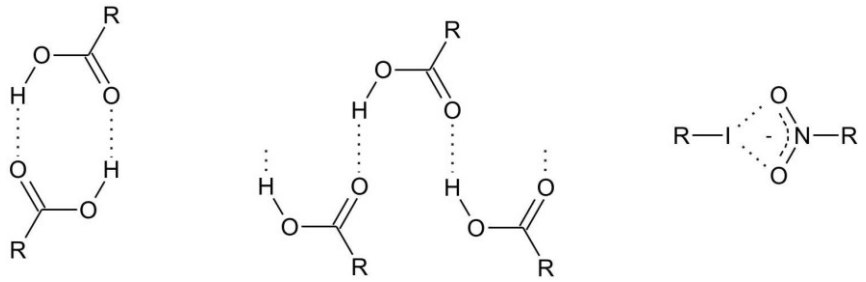

Figure 18: Examples of supramolecular synthons.

The face-to-face interactions observed between a π-electron rich and a π-electron deficient system are a well known and exploited synthon. Desiraju, Sharma *et al.* [44] have employed them in the photochemical synthesis of **25** from **23** and **24**, and Morales-Morales *et al.*[46] have used them to direct the crystallisation of **26** to give a non-centrosymmetric assembly (Figure 19) which is a requirement for a material to exhibit non-linear optical properties.

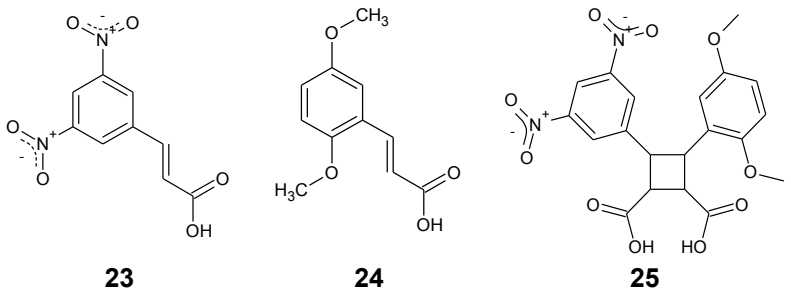

23 **24** **25**

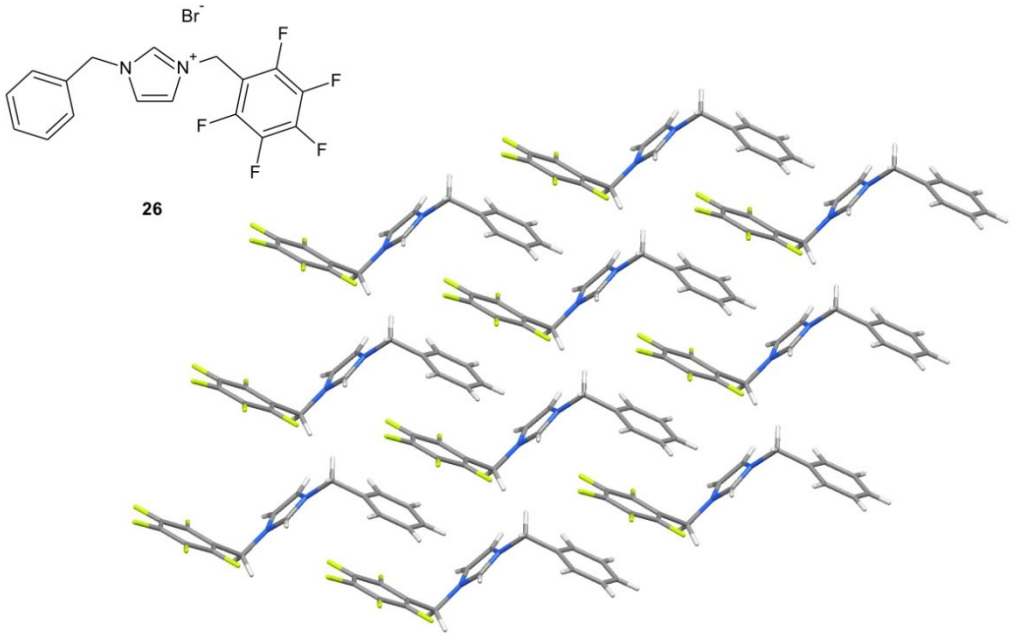

26

*Figure 19: Non-centrosymmetric assembly of **26** directed by π-π synthon.*[46]

Isaacs *et al.*[83] have used synthons based around π-π interactions and hydrogen bonds to form supramolecular grids (Figure 20). A π-π interaction directs the formation of a dimeric node from the basic monomer, and hydrogen bonding interactions between these nodes form the two-dimensional grid.

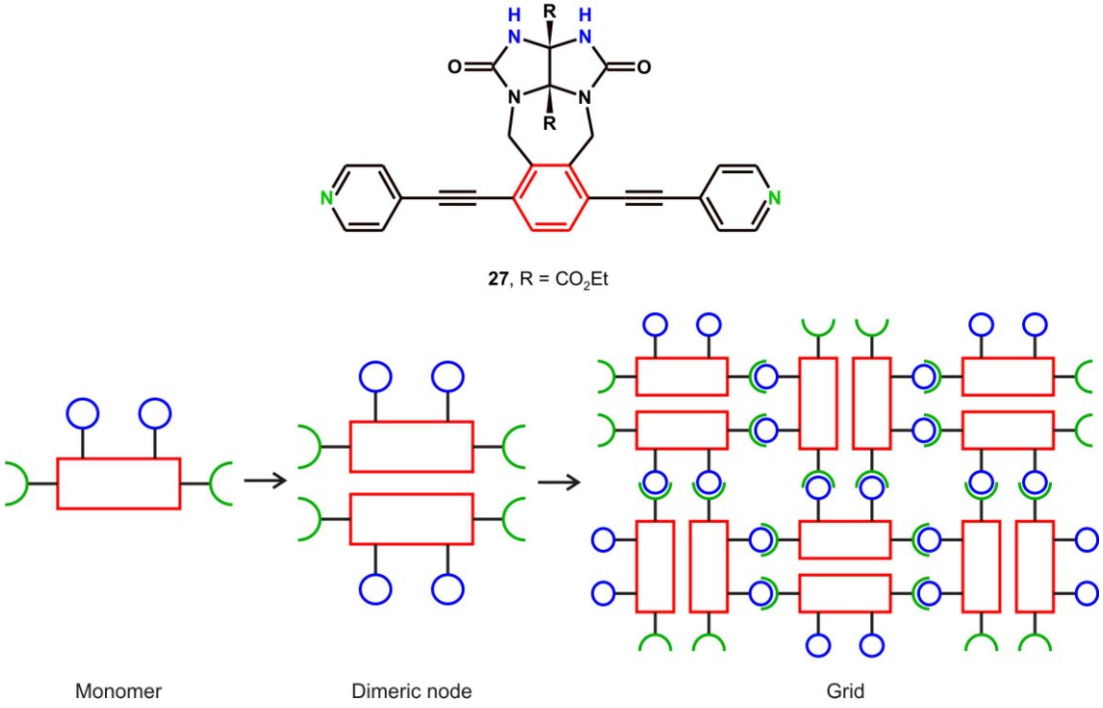

*Figure 20: Schematic illustration of the assembly of **27** into supramolecular grids.*[83]

Wuest[84] has exploited simple synthons based around hydrogen bonds to produce a number of three dimensional, porous structures. One such example is that of spirobifluorene (**28**)[85] which Wuest believes is one of the least dense frameworks built from small molecules with 75% of the volume accessible to guest molecules (Figure 21).

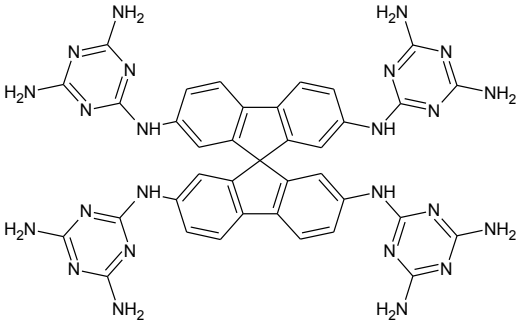

28

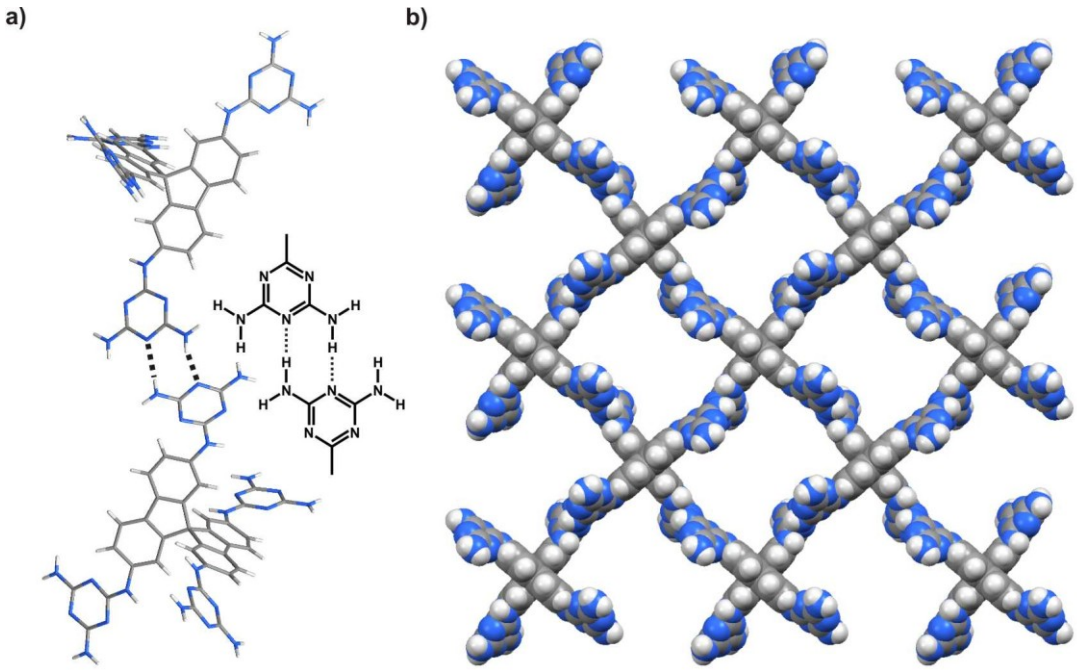

*Figure 21: (a) N-H···N supramolecular synthon observed between molecules of **28**; (b) view along the c-axis of the supramolecular assembly of **28** showing the open framework (guest molecules have been omitted for clarity).*[85]

1.4 - Supramolecular tapes

In a feature article on crystal engineering, Desiraju[13] has highlighted some simple supramolecular synthons based on hydrogen bonds that give rise to one-dimensional linear ribbons (Figure 22).

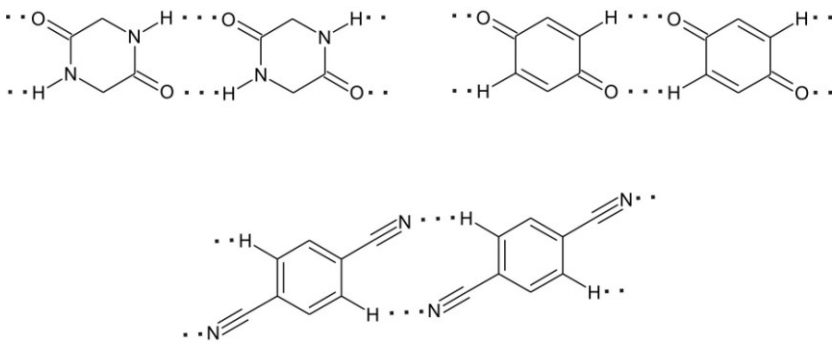

Figure 22: Synthons that form linear ribbons highlighted by Desiraju.[13]

Lehn,[86] Whitesides[87] and Nangia[88] have also employed hydrogen bonding interactions to form tape-like assemblies (Figure 23).

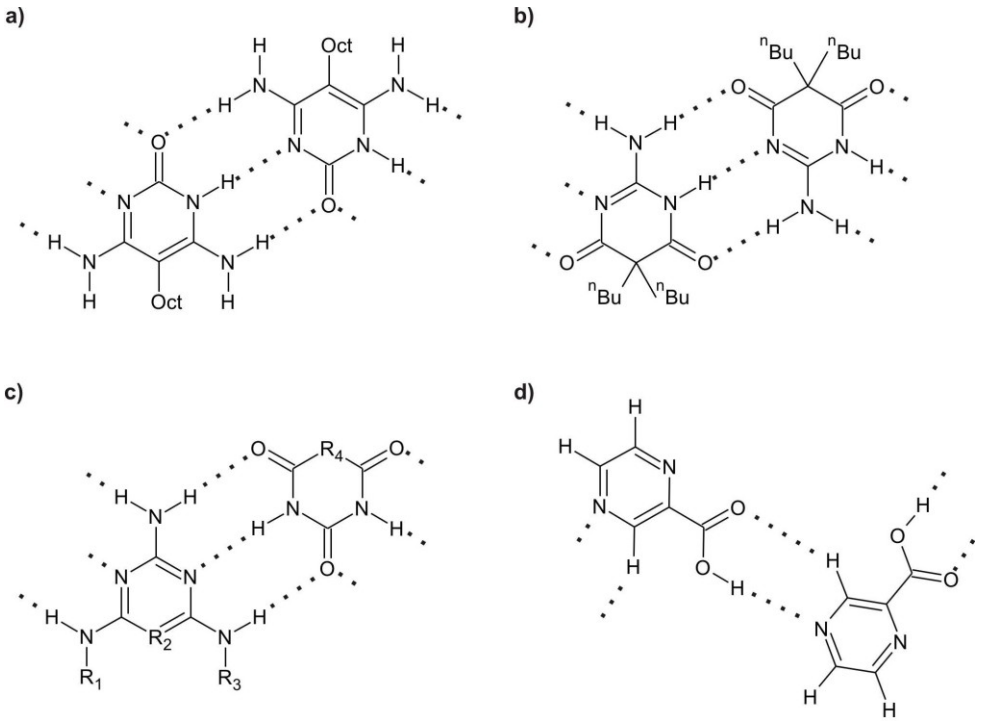

Figure 23: (a) and (b) Lehn's[86] tapes based on 1H-pyrimidine-4,6-dione; (c) generic structure of the tapes described by Whitesides[87] using derivatives of melamine and barbituric acid; (d) an example of a tape prepared by Nangia[88] from pyrazinecarboxylic acids.

The tapes formed by Whitesides[87] employed recognition between two different molecules, whilst the examples highlighted by Desiraju[13] and the tapes prepared by Lehn[86] and Nangia[88] were based on molecular self-recognition.

Self-recognition has also been used by Meijer *et al.*[89] to produce one-dimensional polymeric chains and two-dimensional polymeric networks. In these systems, hydrogen bonding interactions between two self-complimentary ureidopyrimidone units have been exploited (Figure 24).

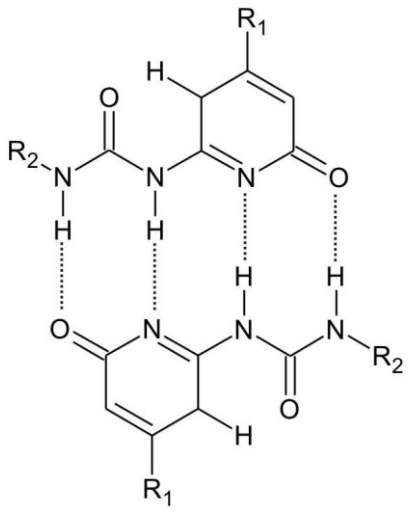

Figure 24: Hydrogen bonding array exploited by Meijer et al.[89] in the formation of polymeric tapes and networks.

Grossel *et al.* [90-95] have examined the self-recognition of a number of pyridinedicarboxylates which have been observed to form one-dimensional assemblies in the solid-state. The following section contains a brief overview of these investigations.

1.5 - Previous investigations into the tape-forming behaviour of pyridine-dicarboxylates

Investigations by Grossel *et al.* into the solid-state behaviour of the pyridine dicarboxylates originated with a study on the application of pyridine diamides with aromatic substituents as pincers to bind azo-dyes.[96] These compounds were found to favour the *trans-trans* conformer (Figure 25). Following a series of molecular modelling experiments on the conformational preference of a number of methyl-diamides with a variety of different heterocyclic cores, Gomm[92] suggested that the conformational preference observed for the pyridine diamides was the result of hydrogen bonding interactions between the protons of the amide and the pyridyl nitrogen.

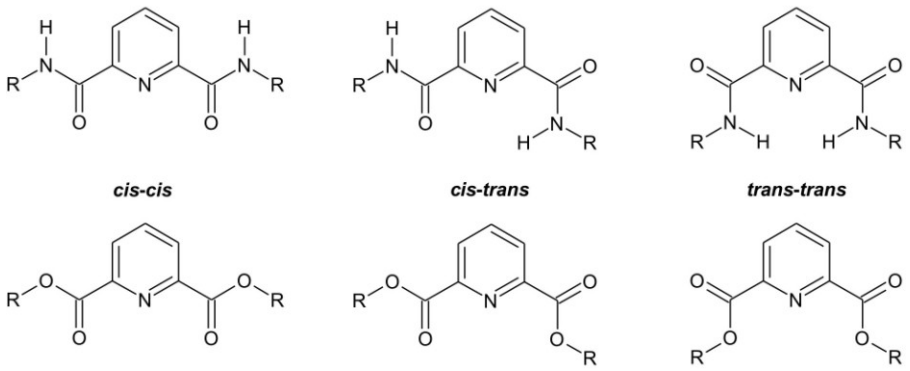

Figure 25: Potential conformers for pyridine-2,6-diamides (top) and -dicarboxylates (bottom); cis *and* trans *refer to the orientation of the carbonyl group with respect to the pyridyl nitrogen.*

As part of a study investigating the effect of preorganisation in the diamide systems, Oszer[95] prepared a number of pyridine-2,6-dicarboxylates which were found to favour the more open *cis-cis* conformer. This observation was in agreement with modelling experiments by Gomm[92] which suggested that, for the methyl diester, the *cis-cis* conformer was more stable than the *trans-trans* conformer by 20.4 kJ mol^{-1}. Additionally, Oszer observed that the *cis-cis* conformation facilitated self-recognition of the dicarboxylates in the solid-state to form a linear, tape-like assembly mediated by a triple hydrogen bond motif (Figure 26).

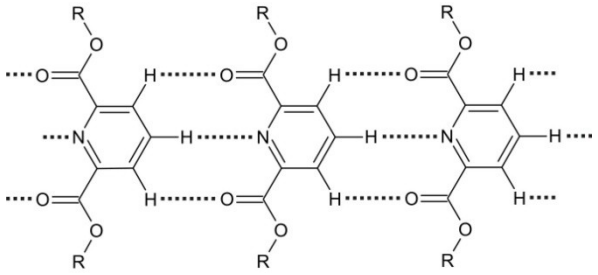

Figure 26: Hydrogen bonding motif observed by Oszer[95] in the solid-state assemblies of the 2,6-pyridinedicarboxylates.

Golden[93] demonstrated that this triple contact could be disrupted by adding a substituent to the 4-position of the pyridine core (**29-31**). For **29**, the crystal structure was found to contain chains of the diester bridged by hydrogen bonds with a tightly bound water molecule. **30** was seen to adopt the *trans-trans* conformer, forming zig-zagged tape-like assemblies which were linked into sheets by interdigitation of the ester groups (Figure 27).

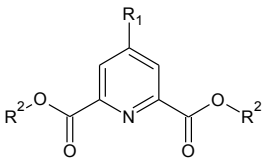

R_1 = OH, R_2 = Me **29**
R_2 = Cl, R_2 = Me **30**
R_1 = Cl, R_2 = Et **31**

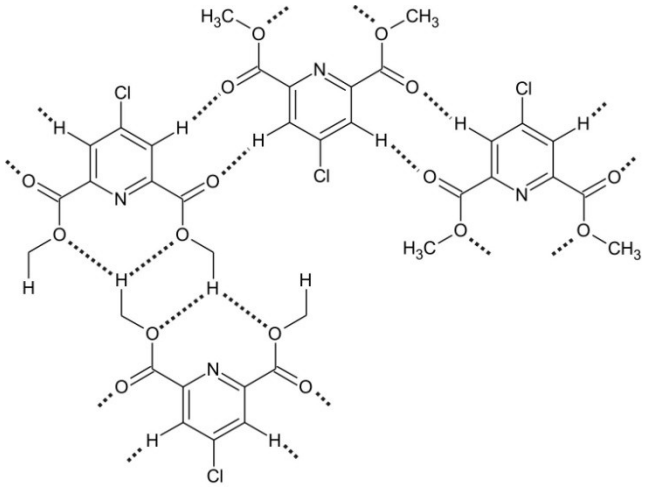

*Figure 27: Hydrogen bond mediated assembly observed by Golden[93] for compound **30**.*

Gomm[92] continued Oszer's investigation of the solid-state behaviour of the pyridine-2,6-dicarboxylates and started to consider the effect of changing the substitution pattern around the pyridine core, examining the behaviour of some structural isomers with 3,5, 2,3 and 2,5 substitution patterns. Orton[91] undertook a comprehensive, systematic study of the solid-state behaviour of the diesters, encompassing the work done by Oszer and Gomm. A brief review of this latter investigation follows, the scope of which is illustrated in Figure 28.

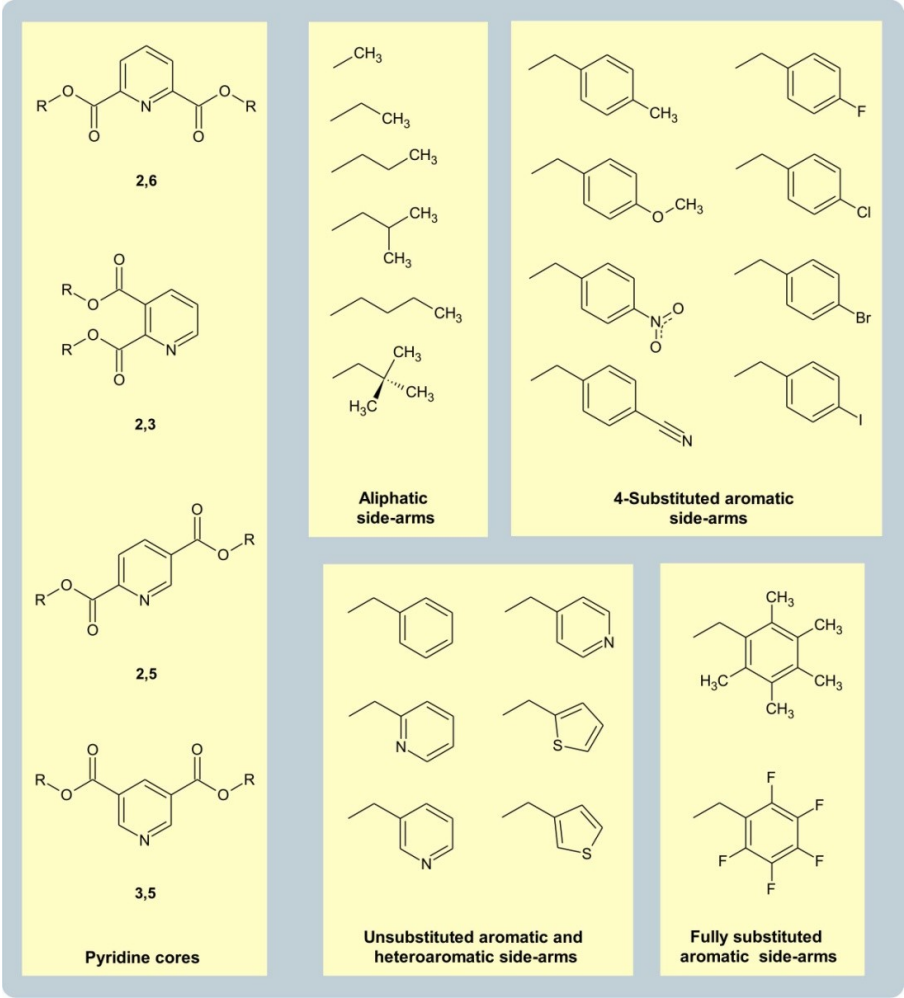

Figure 28: The different pyridine-dicarboxylate cores and range of side-arms that have been studied by Oszer,[95] Gomm[92] and Orton.[91]

The triple hydrogen bond contact between diesters with a 2,6-core has been found to be the most reliable and only a few exceptions have been identified. One is that of the methyl 2,6-diester (**38**); which at first glance appears to form a conventional tape-like assembly in the solid-state. However, closer

examination reveals that the pyridine cores are separated as a result of interdigitation of the methyl side-arms (Figure 29); the solid-state behaviour of this compound will be summarised in more detail in Chapter 2.

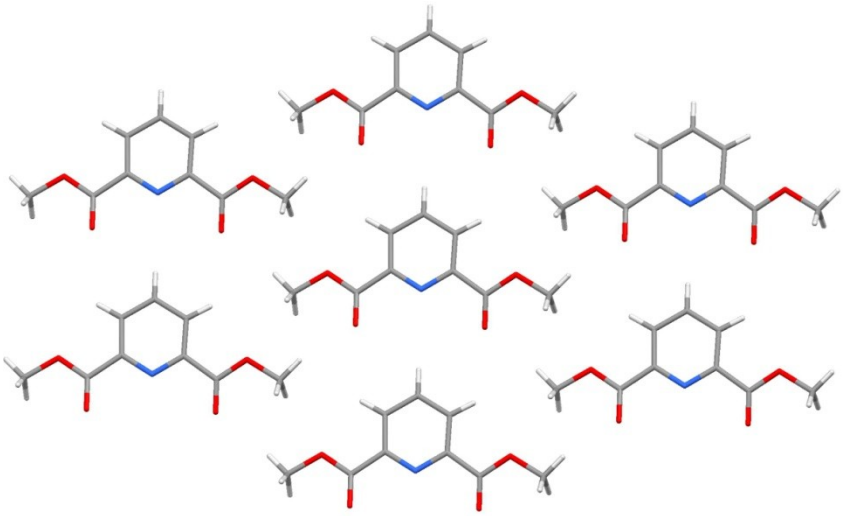

*Figure 29: Top-down view of the primary assembly of bis(methyl) 2,6-pyridinedicarboxylate (**38**)[92] showing the interdigitation of the methyl groups of adjacent tapes.*

Another, and more obvious, exception is that of bis(3-trifluoromethylbenzyl) 2,6-pyridinedicarboxylate (**32**)[92]. Rather than the *cis-cis* conformation displayed by the taping dicarboxylates, **32** adopts a cis-trans conformer, stabilised by C-H···O interactions between the carbonyl oxygen and the protons of the side-arm instead of interactions with the protons of the pyridine core. Gomm[92] suggested that deviation from the expected triple-bond motif may have resulted from an increase in the acidity of these protons as a result of the electron withdrawing nature of the CF_3 group.

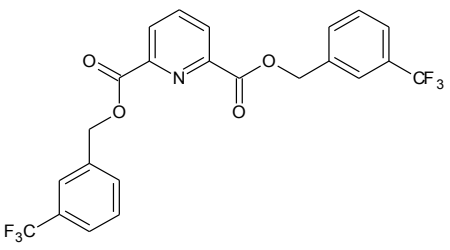

32

Of the other 2,6-dicarboxylates investigated,[91] the propyl derivative was found to form an oil rather than a solid, whilst the 4-cyanobenzyl and pentafluorobenzyl diesters crystallised but failed to form a triple contact. Both of these later derivatives were observed to adopt the *trans-trans* conformer producing a closed, pincer like geometry.

The 4-cyanobenzyl derivative (**33**)[91] was found to form a one-dimensional tape with adjacent molecules linked by C-H···N hydrogen bonds between the nitrogen atom of the side-arm and the protons of the pyridine core (Figure 30). The pentafluoroderivative was observed to adopt a packing arrangement that favoured the formation of slipped face-to-face stacks between the C_6F_5 rings. Orton[91] observed that these are comparable to those seen for hexafluorobenzene.

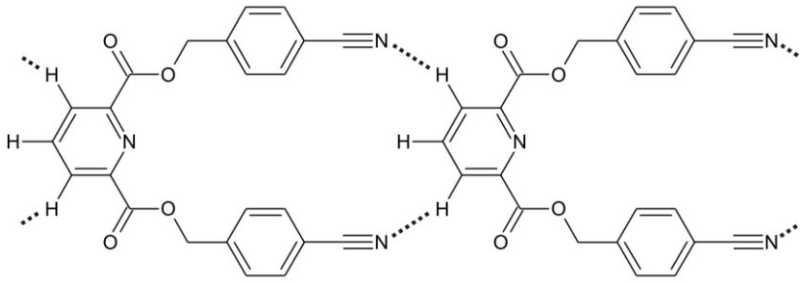

*Figure 30: Hydrogen bonding interactions observed in the tape formed by the 4-cyanobenzyl 2,6-diester (**33**).*[91]

Of the diesters that formed tape-like assemblies, Gomm[92] and Orton[91] noted that the tapes packed with either a planar or a herringbone architecture made up of stacks and layers (Figure 31). They also noted that adjacent tapes could be considered to be aligned either parallel or anti-parallel to each other depending on the relative orientation of the pyridine core.

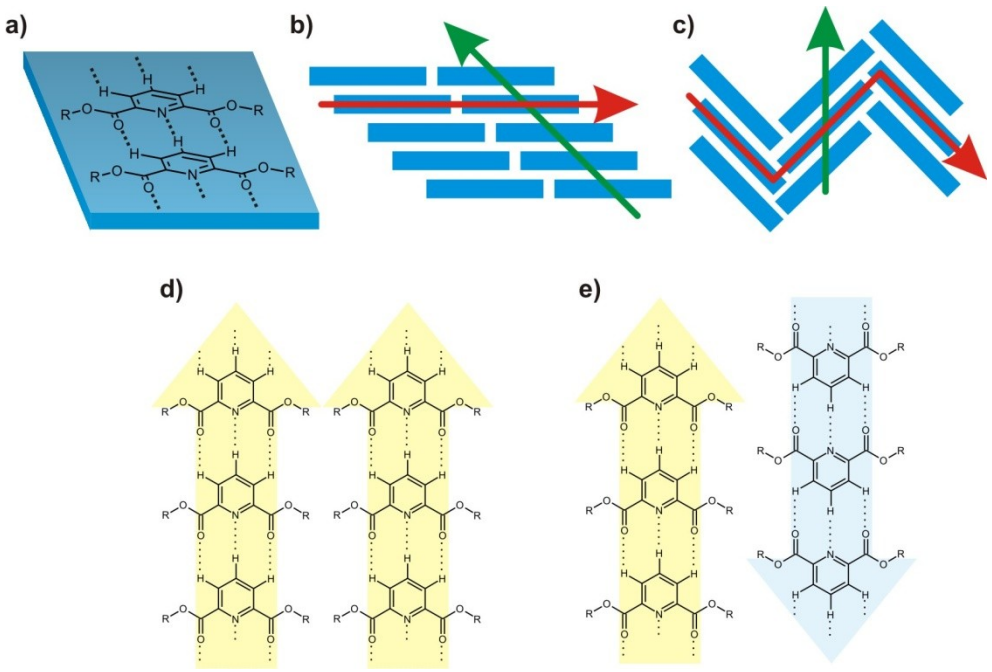

Figure 31: (a) Representation of a tape as a block; view along the direction of the tape showing (b) planar and (c) herringbone packing modes (layers and stacks are indicated by red and green arrows respectively). Illustration of (d) parallel and (e) anti-parallel alignments between adjacent tapes.

In his review of the behaviour of the 2,6-diesters, Orton[91] noted that the packing of tapes is determined by the strongest interactions between the side-arms. In the absence of a directing interaction (such as for the aliphatic derivatives), the packing of tapes is controlled by tessellation of the side-arms so as to maximise the crystal density.

For the tapes formed with aromatic side-arms, Orton[91] observed that variation of the functionality at the 4-position of the benzene ring can alter the observed packing behaviour. Comparing the structures of the benzyl and 4-methylbenzyl derivatives Orton noticed that, although the tapes of both species pack with a planar arrangement, the presence of the methyl group changes the alignment of the tapes adjacent to each other in a layer.

A more significant change in packing behaviour was observed for the 4-nitro-, 4-chloro- and 4-bromobenzyl derivatives which were all found to pack in a herringbone pattern. Orton[91] attributed this to contacts between the halogen and nitro-groups and noted that, within a stack, the side-arms of adjacent tapes were arranged in a slipped face-to-face geometry rather than

the T-shaped arrangement favoured by the benzyl derivative. However, it was unclear whether this was a result of the aromatic rings being electron deficient or simply a geometric consequence of optimising the inter-halogen and inter-nitro contacts.

The effect of the substituent on packing was also seen for the derivatives with a methylpyridine side-arm. The 2- and 3-methylpyridine derivatives were observed to pack in a herringbone pattern with C-H···π interactions present between the side-arms of tapes adjacent to each other in a layer. In contrast, the 4-methylpyridine derivative was found to form planar layers with adjacent tapes linked by C-H···N interactions between the aromatic side-arms. This interaction also changed the alignment of adjacent tapes relative to the benzyl analogue.

Unlike the 2,6-derivatives, where tape formation was generally only observed for the *cis-cis* conformer (the 4-cyanobenzyl derivative being the sole exception), Orton[91] and Gomm[92] found that each of the conformers of the 2,5-diesters can form a tape. Orton referred to these different tape motifs as the “2,5”, “2,5i” and “2i,5i” (Figure 32).

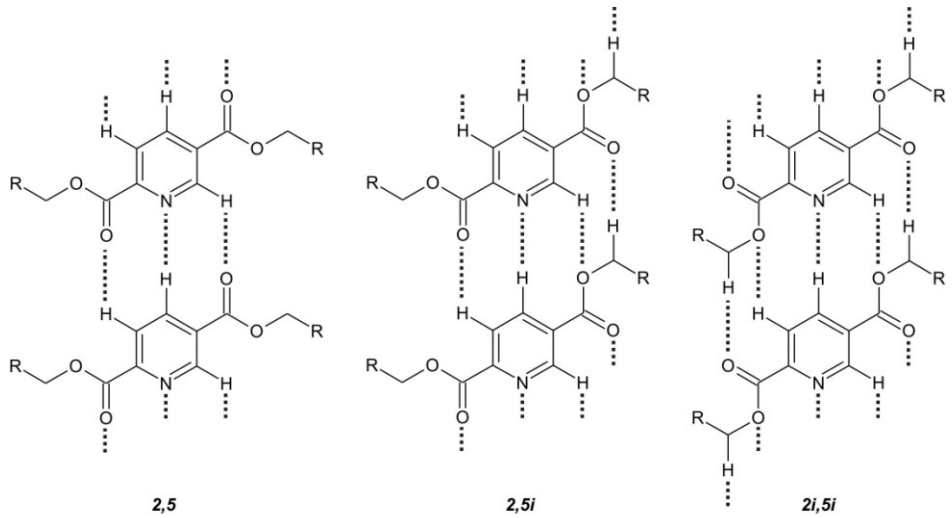

Figure 32: Hydrogen bonding patterns observed in the general structures of the "2,5", "2,5i" and "2i,5i" tape-like assemblies.[91]

As a consequence of the hydrogen bonding patterns observed for the 2,5i and 2i,5i motifs, the side-arm of the inverted carboxylate group is found to fold out of the plane of the pyridine core. This results in the formation of an L-shaped molecule for the 2,5i motif and a Z-shaped molecule for the 2i,5i motif (Figure 33).[91] The tapes formed by the 2,5i molecules are all observed to pack in a head-to-tail manner (Figure 33a) resulting in the formation of anti-parallel stacks. Where derivatives with an aromatic side-arm adopt a 2,5i motif, C-H···π interactions between the side-arms are observed to stabilise the head-to-tail packing arrangement.[91]

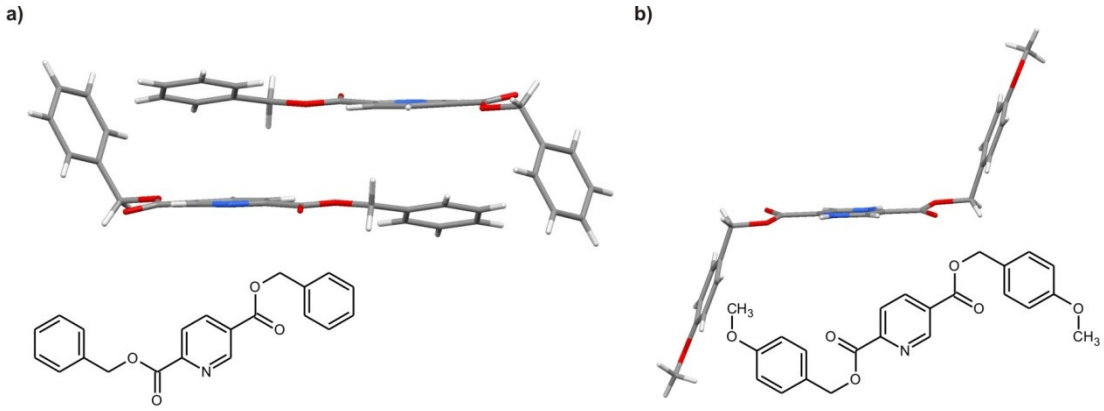

Figure 33: (a) View along the plane of the pyridine core of a molecule observed to form a tape with a 2,5i motif showing the head-to-tail packing behaviour observed for all molecules in this group; (b) an example of the Z-shape adopted by molecules that form a 2i,5i tape.[91]

Inverting one or both of the side-arms increases the number of hydrogen bonds that can be formed between molecules adjacent to each other in a tape relative to the conventional 2,5 conformer. However, the conventional motif was observed to be the most common, particularly for the diesters formed with a 4-substituted benzyl sidearm, while the 2i,5i motif was only seen for two compounds (the methyl and 4-methoxybenzyl diesters).[91]

Orton[91] noted that the symmetry of the 2,5 and 2i,5i tapes meant that structures were often disordered and, with the exception of the 4-iodobenzyl and 4-methylderivatives whose absolute structures could be determined, Orton deduced that the orientation of tapes adopting these motifs was random.

As with the 2,6-derivatives, in the absence of any stronger interactions, the packing of individual tapes was found to be determined by tessellation of the substituents.[91] Where the side-arms contained functional groups capable of forming specific interactions, these interactions directed the packing behaviour. Interestingly, the 2,5-diesters with 4-chloro and 4-bromobenzyl side-arms were observed to pack with a planar arrangement, rather than the herringbone pattern observed for the 2,6-isomers, and type I rather than type II contacts were observed between the halogen atoms.[91]

As with the 2,6-analogue the propyl derivative was found to be a low-melting oil and, although solid, the derivatives with (2-thiophenyl)methyl, 4-fluorobenzyl or penta-substituted benzyl side-arms failed to form tape-like assemblies.[91] For the tape-forming compounds that were directly comparable to the 2,6-analogues, the hydrogen bonds of the triple contact were observed to be between 0.5 and 0.8 Å longer than for the 2,5-derivatives. Orton[91] concluded that the tapes formed by molecules with a 2,5-core are weaker than their 2,6-anaolgues and that the 2,5 motif is less reliable. This was not unexpected since the hydrogen bond array of the 2,5-diesters contains an unfavourable secondary interaction, the theory of which will now briefly be discussed.

In an array of multiple hydrogen bonds, additional interactions can occur diagonally between adjacent donors and acceptors. Jorgensen and Pranata[97] have shown that, for interactions between classical hard donors and acceptors, favourable secondary interactions (i.e. between a hydrogen bond donor and acceptor) can stabilise the array by between 8 and 12 kJ mol^{-1} per contact.

In the case of the pyridine diesters (Figure 34), the donor-acceptor array of the 2,6-core results in two pairs of favourable secondary interactions. The 2,5-core has one pair of favourable and one pair of unfavourable secondary interactions, whilst the 3,5-derivative has two pairs of unfavourable secondary interactions. Consequently Orton[91] and Gomm[92] hypothesised

that the stability of the different motifs is likely to decrease in the order 2,6 > 2,5 > 3,5.

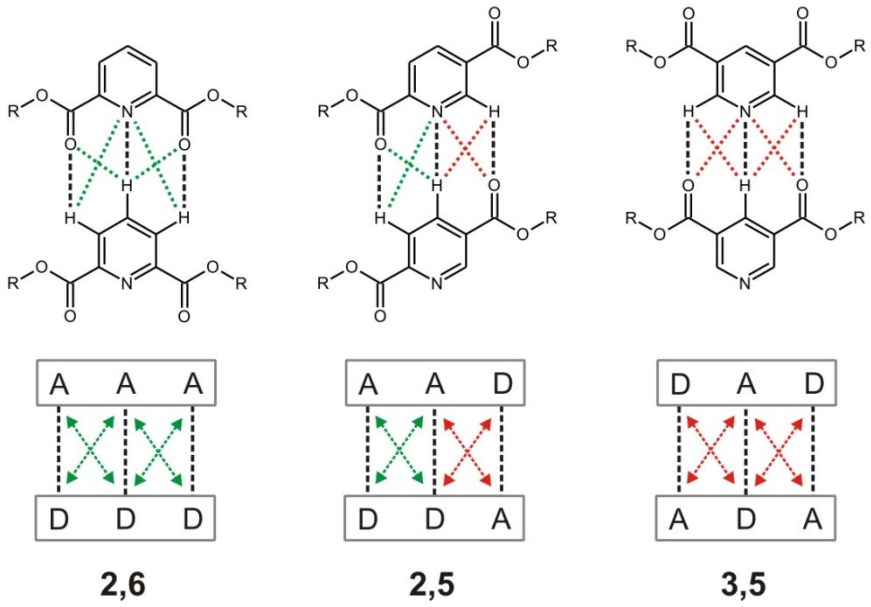

Figure 34: Primary and secondary hydrogen bonding interactions observed between adjacent molecules in the tape-like assemblies of 2,6-, 2,5- and 3,5-pyridinedicarboxylate. Hydrogen bonds are denoted by dashed lines: black for the primary interaction; green for a favourable secondary interaction and red for an unfavourable secondary interaction. In the lower, schematic, representations "D" indicates a hydrogen bond donor and "A" an acceptor.

It was thus unsurprising that, with the exception of the neopentyl derivative, the 3,5-diesters with aliphatic side-arms failed to form a triple hydrogen bond tape-like motif.[91] The n-butyl derivative was observed to be a low-melting oil whilst the methyl derivative formed a dimeric system. The other aliphatic diesters formed a "slipped tape" motif as shown in Figure 35.

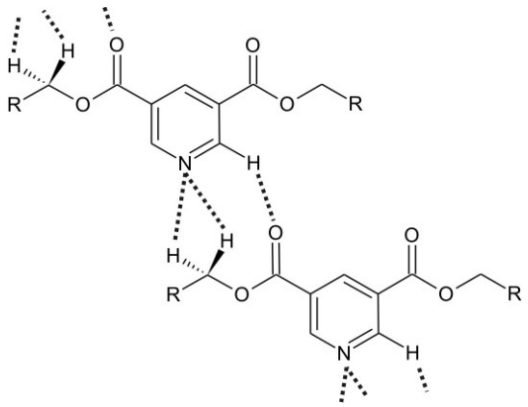

Figure 35: Slipped tape motif observed for the 3,5-pyridinedicarboxylates with an aliphatic side-arm.[91]

The hydrogen bonds observed for this slipped interaction are longer than those of the conventional tape motif suggesting that the slipped tapes are weaker. Orton[91] has suggested that the slipped tape motif is favoured as it allows the molecules to pack more efficiently but that in the 2,6- and 2,5-diesters the stronger triple hydrogen bond motif dominates and thus the more space-efficient slipped tape is not observed.

Considering the expectation for the 3,5-motif to be weaker than the 2,5-analogue, Orton[91] was surprised that, with 4 exceptions (the derivatives with (4-pyridyl)methyl, 4-cyanobenzyl, 4-methoxybenzyl and pentafluorobenzyl side-arms), all of the aromatic diesters formed tape-like assemblies with a conventional triple hydrogen bond motif. Orton[91] speculated that aromatic interactions between the side-arms stabilised the triple hydrogen bond contact for this series of compounds.

The packing of the 3,5-tapes was found to be largely comparable to that of the 2,6- analogues.[91] One notable exception was that of the 4-bromobenzyl derivative, the crystal structure of which was found to be isostructural with that of the 4-iodobenzyl diester.[91] In contrast, the bromobenzyl 2,6- and 2,5-diesters were found to behave in a manner comparable with that of the 4-chlorobenzyl analogues rather than the 4-iodo derivatives. The packing of the 3,5-diester with a 4-chlorobenzyl side-arm was observed to be more comparable to that of the 2,5-isomer rather than the 2,6-analogue.[91]

Like its 2,6-analogue, the side-arms of the pentafluorobenzyl 3,5-diester were rotated into a closed, pincer-like geometry.[91] This same configuration was also seen for the (4-pyridyl)methyl derivative which, like the (4-cyanobenzyl) 2,6-diester (**33**), formed a tape-like assembly. Adjacent molecules were observed to be linked by C-H···N hydrogen bonds between the 2- and 6- protons of the pyridine core and the nitrogen atoms of the pyridine side-arm. The (4-cyanobenzyl) 3,5-diester was not found to form an analogous tape.

The 3,5-diester formed with 4-methoxybenzyl side-arms was found to form a two-dimensional sheet with C-H···O hydrogen bonds observed between the carbonyl oxygen atoms and the methyl protons of the side-arm and between the ester oxygen atoms and the 2- and 6-protons of the pyridine core.

Only a few diesters with a 2,3-substituted core have been examined, and in all cases steric hindrance between the side-arms prevented the formation of conventional tape-like assemblies (Figure 36a).[91] The closest assembly to that of the theoretical tape was observed for the methyl derivative (Figure 36b), other derivatives have also been observed to form extended structures mediated by C-H···O interactions but no general trends have been found.

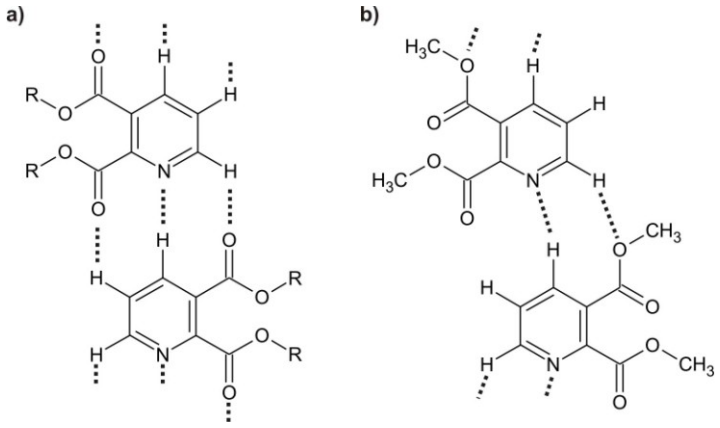

Figure 36: (a) Theoretical triple hydrogen bond tape suggested for the 2,3-pyridinedicarboxylates; (b) tape-like assembly observed for dimethyl 2,3-pyridinedicarboxylate.[91]

In summary, Orton[91] concluded that the triple hydrogen bond motif observed for the 2,6-pyridinedicarboxylates is a robust synthon. The assemblies formed by tapes with a 3,5-substituted pyridine core were noted to be generally less reliable, but the presence of aromatic side-arms appeared to stabilise tape formation. The formation of tapes by the 2,5-derivatives was found to be complicated by the symmetry of the core and Orton[91] noted that the conformational lability of these systems makes them less useful for crystal engineering.

The packing of pyridine-dicarboxylate tapes has been observed to be dictated by the nature of the functional groups at the edges of the tapes. For the tapes formed with aliphatic side-arms and 4-substituted benzyl side-arms where the substituent exerts a steric rather than an electronic influence (for example the 4-methyl benzyl and 4-iodobenzyl derivatives), tessellation of the substituents determines the packing behaviour. It was observed that the presence of functionalities able to form stronger, more directional interactions (for example the derivatives formed with 4-nitrobenzyl, 4-methoxybenzyl and (4-pyridyl)methyl side-arms) causes the triple hydrogen bond contact to lengthen. Orton[91] concluded that this was indicative of the triple hydrogen bonding motif being strained.

Although Orton[91] restricted himself to studying symmetrical systems, some efforts have been made by other members of the research group to develop asymmetric systems. Gomm[92] described the synthesis of four asymmetric systems (**34**) but was unable to explore their solid-state behaviour. Dwyer[94] successfully characterised the solid-state behaviour of the asymmetric methyl 2,6-"monoester" (**75**), which will be discussed in more detail in Chapter 4.

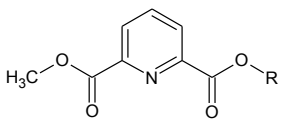

34

Where R =

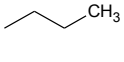

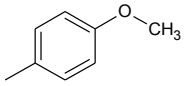

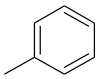

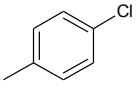

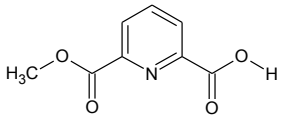

75

1.6 - Introduction to the current study

Li *et al.*[98] observed that derivatives of bi-dihydrazine (**35**) self-assemble to form dimers mediated by a quadruple hydrogen bond motif. They used this synthon in the design of a liquid crystalline molecule and observed its behaviour in solution using ^{1}H NMR. The chemical shift of the N-H protons was found to move downfield as the concentration of the sample was increased. Li *et al.*[98] suggested that this provided evidence of molecular aggregation in solution. During his investigations, Gomm[92] observed differences between the solid-state and solution phase ^{13}C NMR spectra of the pyridine dicarboxylates. In light of these results it was decided to investigate the solution-phase behaviour of the pyridine dicarboxylates.

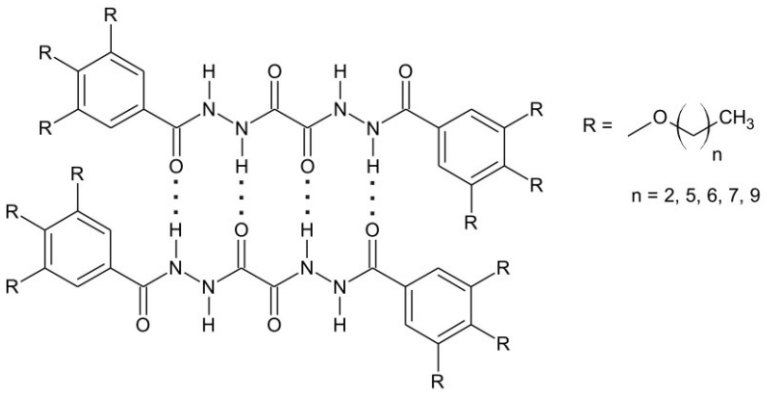

35

To date, no consideration has been given to the effect on tape formation of introducing polyaromatic side-arms or to altering the length of the alkyl spacer between the aromatic group and the pyridine dicarboxylate core. To this end a number of derivatives with naphthyl and anthryl side-arms have been prepared and their solid-state behaviour explored.

Both Gomm[92] and Orton[91] expressed the view that asymmetric systems would be worthy of further study. In this investigation five additional monoesters have been synthesised. The solid-state behaviour of three of these has been determined and is discussed in conjunction with that of both the methyl-2,6-monoester characterised by Dwyer[94] (**75**), and the analogous

diesters. The thermal behaviour of the monoesters is also considered and compared with that of the diester analogues.

In his conclusions, Orton[91] noted that it might be possible to use the tapes formed by the pyridinedicarboxylates as a framework for the synthesis of functional materials. Studies by Wudl *et al.*[99-101] have shown that TTF (**36**) can act as an organic semiconductor upon oxidation by a halogen. Derivatives of TTF are still of interest to chemists and have been incorporated into a number of supramolecular systems.[102, 103] Wallis *et al.*[104] have described the synthesis of a number of TTF derivatives, including one with a 2,6-pyridinedicarboxylate core (**37**). Consequently, it was decided to attempt the synthesis of a number of functional diesters using side-arms containing TTF derivatives.

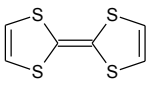

36

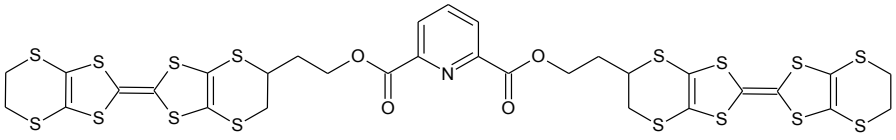

37[104]

The following discussions of the solid-state behaviour of the compounds under study are based upon examination of structures obtained from single crystal X-ray diffraction experiments. Intermolecular interactions in the solid-state have been examined both by looking at close contacts (i.e. where the distance between a pair of atoms is less than the sum of their van der Waals radii) using the Mercury software application,[105, 106] and by analysis of the Hirshfeld surface using CrystalExplorer.[107]

The Hirshfeld surface defines the region of crystal space around a molecule where the ratio of the electron density attributable to the molecule, relative to that of the crystal as a whole, is greater than 50%. (I.e. within the surface, the electron density of the molecule dominates that of the bulk crystal.)

The distance between a given point on the surface and the closest atoms inside and outside the surface can be measured (D_i and D_e respectively). McKinnon[108] states that mapping these parameters onto the surface allows for an analysis of intermolecular interactions *"while maintaining a whole-of-molecule approach"* ignoring *"biases inherent in focussing on a limited number of short atom contacts that are assumed to be important."*

"Fingerprint plots" of D_i against D_e allow the information from these three-dimensional surfaces to be displayed in two dimensions and certain types of interactions can be observed as characteristic patterns. Figure 37 shows an example for the benzyl 2,6-diester (**44**).[92]

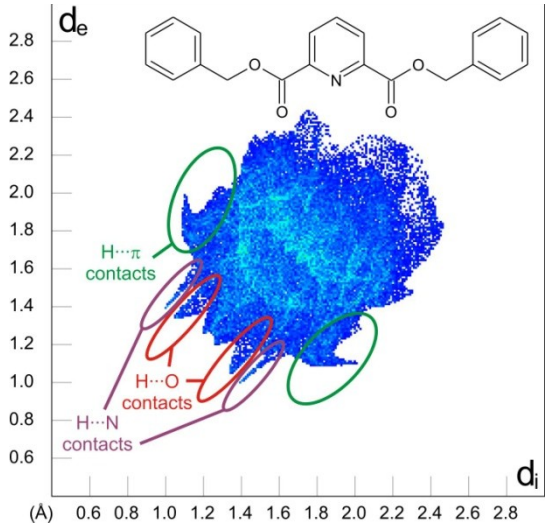

*Figure 37: Fingerprint plot for bis(benzyl) 2,6-pyridinedicarboxylate (**44**).[92] Selected features corresponding to certain types of intermolecular interaction are highlighted to illustrate how fingerprint plots can be used in structural analysis.*

The fingerprint plots for all of the compounds discussed in the following chapters are presented in Appendix D. CIF files and tables of crystallographic data for those structures that have not been collected in other studies are included on the data CD at the back of this thesis. This CD also contains pdb files corresponding to the figures used in the discussions of each compound.

In the following chapters, certain key distances and angles will be examined. These are defined below for systems that form conventional tapes and are generally in keeping with those parameters used by Orton[91].

The triple hydrogen bond contact that forms the primary tape is described using the bond distances and angles shown in Figure 38.

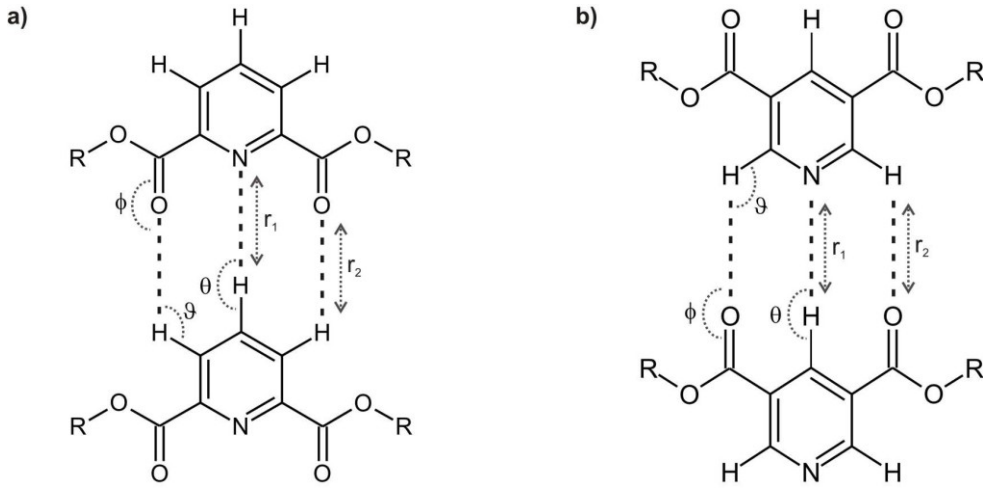

Figure 38: Distances and angles used to describe the triple hydrogen bond contact for (a) the 2,6-pyridinedicarboxylates and (b) the 3,5-pyridinedicarboxylates.

For tapes with an aromatic substituent a further parameter is considered; the fold angle (Figure 39) is defined as the angle between the mean plane of the pyridine core (shown in green) and the mean plane of the substituent aromatic ring (shown in pink).

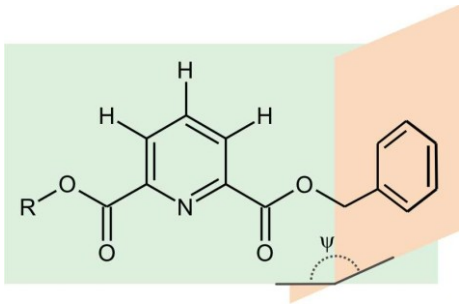

Figure 39: Schematic illustration of the fold angle measured for systems with an aromatic substituent.

The packing and relative alignment of adjacent tapes (see Figure 31) will be described using the notation introduced by Orton.[91] The geometry of packing

can either be denoted as planar (P) or herringbone (H) and this designation is followed by notation of the relative alignment of adjacent tapes in a stack (S) and a layer (L). Thus, $PS_{\uparrow\downarrow}L_{\uparrow\uparrow}$ denotes a planar assembly where tapes adjacent to each other in a stack are aligned anti-parallel whilst those in a layer show parallel alignment. Similarly, $HS_{\uparrow\uparrow}L_{\uparrow\uparrow}$ indicates a herringbone packing motif where all tapes are aligned in the same direction.

Tapes in a stack are rarely found to be aligned completely vertically and the parameters S_S, S_T and T_O have been defined to help establish the degree to which a stack deviates from a perfectly vertical column. The stack separation (S_S) is defined as the distance between the planes of two adjacent tapes (shown in blue in Figure 40). The angle S_T measures the degree of slip orthogonal to the direction of the tape and is defined by the angle between the plane of the tape and a plane that bisects the N-N axis of each tape in the stack (shown in yellow in Figure 40). Finally, the angle T_O measures the degree of slip parallel to the direction of the tape and is defined as the angle between the plane of the tape and a plane that links the C2 and C4 atoms of the reference molecule with either, the C2 and C4 atoms of the molecule below for a parallel stack (shown in pink Figure 40) or, the C3 and C5 atoms of the molecule below for an anti-parallel stack. The angles S_T and T_O should both equal 90° if tapes are arranged in a perfect stack (*i.e.* looking down the normal to the plane of the tape, the atoms of lower tapes would all be perfectly eclipsed by the atoms of the top layer).

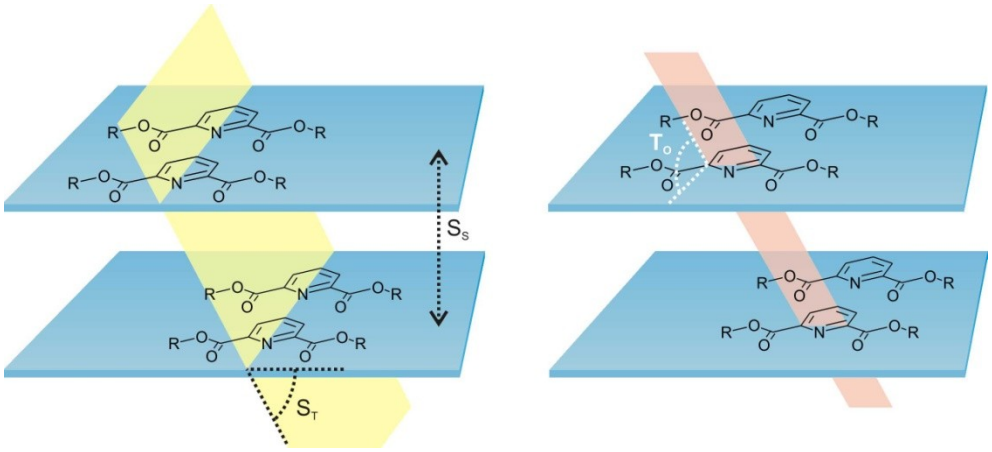

Figure 40: Definition of angles used to define stack geometries.

2 - Spectroscopic studies

2.1 - Introduction

Gomm[92] has previously compared the solution and solid-state ^{13}C NMR spectra of a number of pyridine dicarboxylates. It was observed that transition between the solution and solid phases corresponded to a change in the chemical shift of the pyridyl carbon atoms associated with the protons that formed intermolecular contacts in the solid-state. Gomm noted that, in general, the signal corresponding to the γ-carbon shifted downfield by between 4.2 and 5.8 ppm between the solution and solid-state spectra. A corresponding upfield shift of between 0.7 and 1.9 ppm was observed for the signals of the β-carbon atoms. However, Gomm[92] found that there was no clear correlation between the change in the magnitude of the shift and the lengths and bond angles of the corresponding interactions.

It was therefore to investigate further to determine whether NMR spectroscopy could be used to study the possible aggregation of the pyridine dicarboxylates in solution. A series of titration experiments were performed and the effect of sample concentration on the chemical shifts of the pyridyl protons was examined. It was suggested that, as the concentration of the sample was increased, weak hydrogen bonding interactions would form tape-like aggregates. Hydrogen bond formation would deshield the protons involved, consequently it would be expected that the formation of tape-like assemblies in solution would be indicated by a concentration-dependant downfield change in the chemical shift of the pyridyl protons involved.

Gomm[92] and Turner[109] used Raman spectroscopy to investigate the behaviour of the dimethyl 2,6- and 3,5-pyridinedicarboxylates and observed a temperature dependant change in the spectra of these compounds. Orton[110] obtained DSC data for the methyl diesters which showed that the heat of melting was greater for the 2,6-isomer than for the 3,5-analogue.

In the present work, compounds (**38** - **45**) were chosen to be the subject of solution NMR, Raman and DSC studies. Diethyl 2,6-pyridinedicarboxylate (**40**) was chosen for investigation as it represents the simplest system that forms a conventional tape-like assembly in the solid-state. Although the 3,5-analogue (**41**) does not tape, it was included in the study to help establish whether any observed spectroscopic changes were related to the solid-state behaviour. The neopentyl and benzyl diesters (**42** - **45**) were also chosen as they represent the simplest alkyl and aromatic systems where both the 2,6- and 3,5-derivatives crystallise with a conventional tape-like motif. It was hoped that study of these compounds would allow the effect of the substitution pattern around the pyridine ring to be considered.

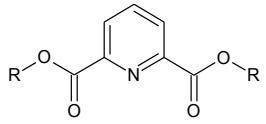

38[92]	R = CH_3	(methyl)
40[91]	R = CH_2CH_3	(ethyl)
42[91]	R = $CH_2C(CH_3)_3$	(neopentyl)
44[92]	R = CH_2Ph	(benzyl)

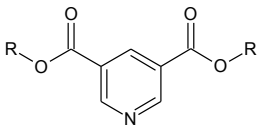

39[91]	R = CH_3	(methyl)
41[91]	R = CH_2CH_3	(ethyl)
43[91]	R = $CH_2C(CH_3)_3$	(neopentyl)
45[91]	R = CH_2Ph	(benzyl)

2.2 - Solid-state behaviour

The crystal structures of all the compounds discussed in this chapter have been previously described by Orton[91] and only a brief summary of their solid-state behaviour will be given here as an aid to the discussion of the spectroscopic results that follow.

The neopentyl and benzyl diesters (**42** - **45**) and the ethyl 2,6-diester (**40**) all appear[91] to form conventional tape-like assemblies in the solid-state and the primary contact parameters are presented in Table 5. The unit cell of bis(benzyl) 3,5-pyridinedicarboxylate (**45**) contains two different molecules, one symmetrical and one asymmetrical and this is reflected in the primary assembly parameters.

Table 5: Primary tape parameters for compounds forming tape-like architectures.

	R	r_1/Å	r_2/Å	θ/°	ϕ/°	ϑ/°	ψ/°
38[92]	CH_3	3.02	2.88	180.0	170.3	124.8	-
40[91]	CH_2CH_3	2.58	2.53	180.0	160.5	127.8	-
42[91]	$CH_2C(CH_3)_3$	2.54	2.48	180.0	167.2	128.5	-
43[91]	$CH_2C(CH_3)_3$	2.47	2.50	180.0	160.1	135.0	-
44[92]	R = CH_2Ph	2.48	2.48	180.0	163.8	127.0	28.3
45[91]	R = CH_2Ph	2.41	2.45	180.0	159.2	135.4	25.9
		2.48	2.54, 2.48	163.9	155.5, 151.9	134.6, 131.2	19.0, 13.9

As has already been mentioned (Chapter 1), the tape-like assembly of dimethyl 2,6-pyridinedicarboxylate (**38**)[92] is slightly unconventional. The triple bond contact distances are observed to be longer than normal and this is attributed to interdigitation of the methyl side-arms of tapes adjacent to each other in a layer. This interdigitation is stabilised by C-H···O hydrogen bonds between the methyl substituents of the molecules in one tape and the oxygen atoms of the molecules in a neighbouring tape (Figure 41, orange contacts).[91]

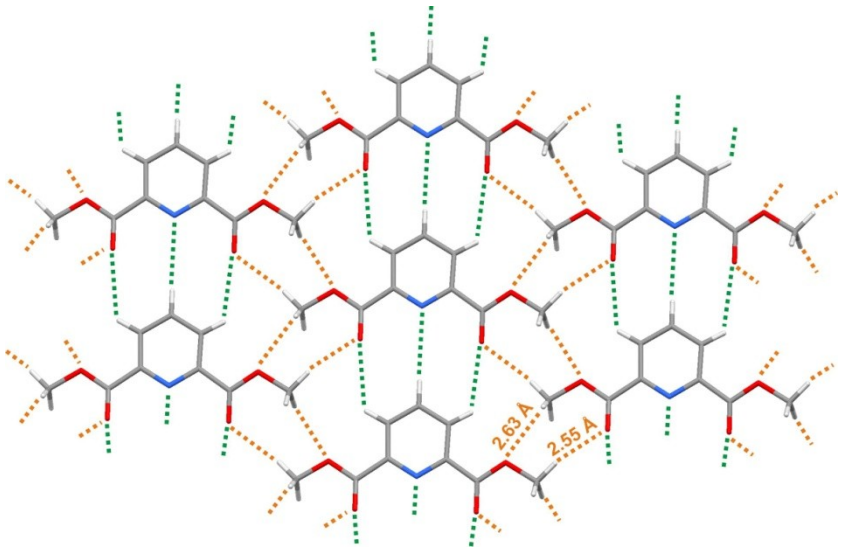

*Figure 41: Interactions in the primary assembly of dimethyl 2,6-pyridinedicarboxylate (**38**);[92] intermolecular contacts are shown as dashed lines, those of the conventional triple bond are shown in green, and the C-H···O contacts stabilising the interdigitation of the methyl groups are coloured orange.*

Orton[91] has also described the unconventional solid-state behaviour of the 3,5-diesters with methyl and ethyl side-arms (**39** and **41**). The methyl diester (**39**) is found to form dimers linked by a pair of $C\text{-}H_{(Me)}\cdots N$ and $C\text{-}H_{(Py)}\cdots O$ hydrogen bonds which are then assembled into a two dimensional sheet by

further C-H···O interactions (Figure 42a). C-H···N interactions between the protons of the alkyl substituent and the pyridyl nitrogen are also observed in the "slipped-tapes" formed by the ethyl diester (**41**), although in this case the contacts are bifurcated (pale blue contacts in Figure 42b). Further bifurcated C-H···O contacts are observed between the tapes (red contacts in Figure 42b), although whether these are structure directing or simply the result of close packing is uncertain.

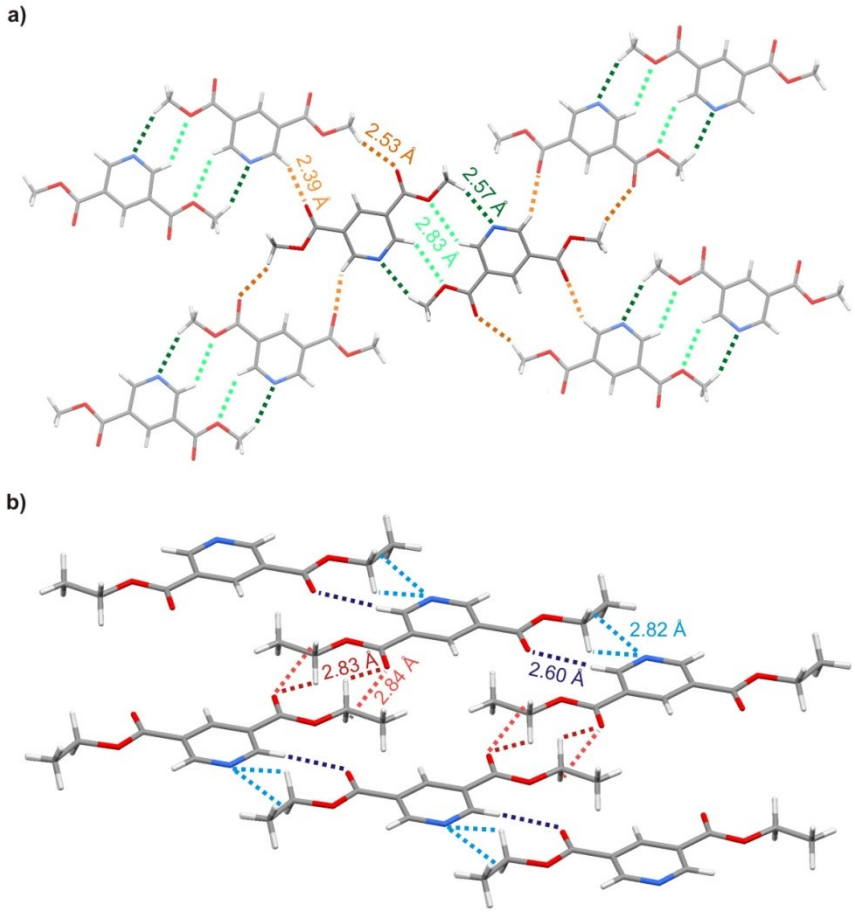

*Figure 42: (a) Solid-state behaviour of dimethyl 3,5-pyridinedicarboxylate (**39**);[91] hydrogen bonds forming dimers are shown in green and those linking dimers into sheets in orange. (b) Solid-state behaviour of diethyl 3,5-pyridinedicarboxylate (**41**);[91] hydrogen bonds forming slipped tapes are shown in blue and those linking the tapes into sheets are shown in red.*

In his analysis Orton[91] notes that the packing of the tape-like assemblies formed by the diesters with aliphatic side-arms is largely the result of close-packing and minimisation of free space. The packing of the diesters with benzyl side-arms (**44** and **45**) is directed by edge-to-face aromatic

interactions. All of the tape-like assemblies involved in the present discussion are observed to pack with a planar geometry with the exception of the 3,5-neopentyl derivative which adopts a herringbone pattern.

2.3 - Examination of solution phase behaviour using ^{1}H NMR

A series of proton spectra were obtained for solutions of each compound in deuterated chloroform at 27 °C (stacked plots of the spectra are included in Appendix A). The range of concentrations varied from approximately 50 mM to the room temperature saturation point of the compound under study.

2.3.1 - Solution phase behaviour of the 2,6-diesters

Figure 43 shows the plot of peak position as a function of concentration for the pyridyl protons. The results of analysis on the data by linear regression are presented in Table 6.

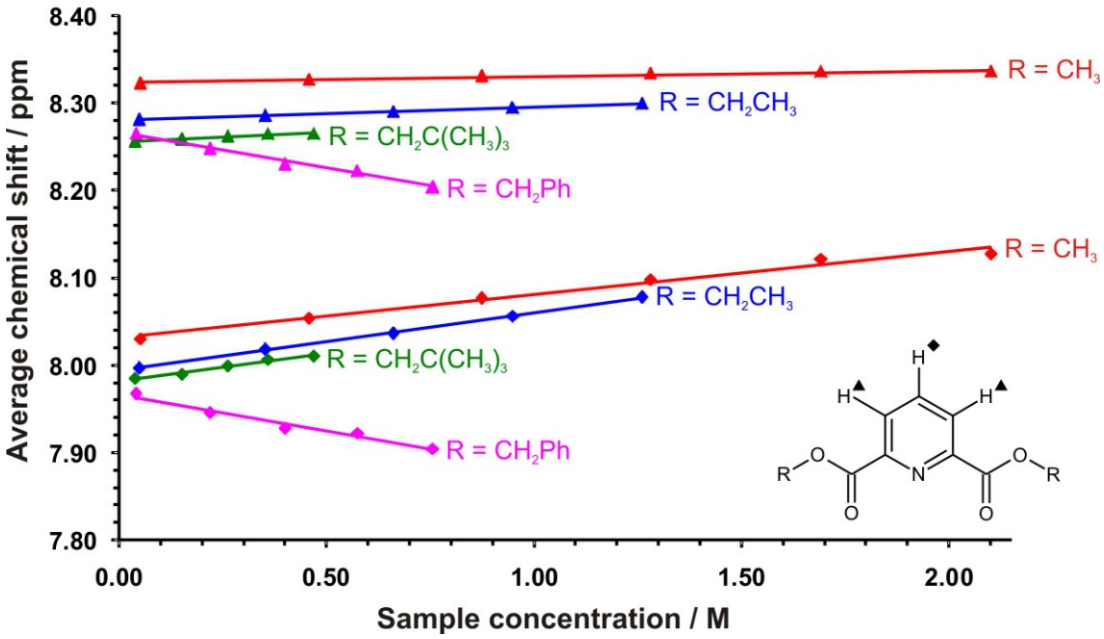

Figure 43: Plot of chemical shift as a function of sample concentration for the pyridyl protons of the 2,6-pyridinedicarboxylates; gradients for the lines of linear regression are given in Table 6.

Table 6: Rates of change in the chemical shift of the pyridyl protons as a function of the sample concentration for the 2,6-diesters; the standard error for the linear regression is given in brackets.

	R		γ-proton (H$^{\blacklozenge}$)/ppm M^{-1}	β-proton (H$^{\blacktriangle}$)/ppm M^{-1}
38	CH_3	(methyl)	+ 0.050 (0.0035)	+ 0.007 (0.0009)
40	CH_2CH_3	(ethyl)	+ 0.066 (0.0017)	+ 0.015 (0.0002)
42	$CH_2C(CH_3)_3$	(neopentyl)	+ 0.063 (0.0053)	+ 0.023 (0.0033)
44	CH_2Ph	(benzyl)	- 0.084 (0.0083)	- 0.083 (0.0050)

For the compounds with an aliphatic side-arm (**38**, **40** and **42**), a concentration dependant increase in the chemical shift of the pyridyl protons is observed. Significantly, the rate of change is different for the γ- and β-protons suggesting that the observed changes are not simply a solvation effect.

A similar concentration dependant deshielding effect is also observed for the methyl protons of the 2,6-methyl diester (**38**, Table 7). Considering the observed interactions with these protons in the solid-state this is not unexpected, however the magnitude of this change is relatively small. One possible explanation, assuming that tape-like assemblies are formed in the solution phase, would be that the methyl groups only interdigitate upon crystallisation; consequently, the solution phase interactions with the methyl groups are weak and the change in chemical shift with concentration is small.

Table 7: Rates of change in the chemical shift of the alkyl protons as a function of the sample concentration for the 2,6-pyridinedicarboxylates; the standard error for the linear regression is given in brackets.

	R		CH_2/ppm M^{-1}	CH_3/ppm M^{-1}
38	CH_3	(methyl)	-	+ 0.005 (0.0005)
40	CH_2CH_3	(ethyl)	+ 0.000 (0.0002)	- 0.003 (0.0001)
42	$CH_2C(CH_3)_3$	(neopentyl)	+ 0.014 (0.0013)	+ 0.013 (0.0032)
44	CH_2Ph	(benzyl)	- 0.051 (0.0032)	-

The alkyl protons of neither the ethyl (**40**) nor the neopentyl (**42**) derivatives have previously been implicated in solid-state intermolecular interactions.[91] Consequently, although a change in the chemical shift of these shift protons is noted, the fact that the rate of change is comparable between the different

proton environments within the molecule suggests that it is a consequence of solvation rather than the result of aggregation.

The upfield shift observed for all of the protons in the benzyl diester (**44**) was particularly surprising. Considering that the rate of change in chemical shift for both of the pyridyl protons is essentially identical, it is probable that the observed behaviour is the result of solvation rather than the formation of tape-like aggregates. Thus it appears that whilst the 2,6-diesters with an aliphatic side-arm may form aggregates in solution similar to those observed in the solid-state, the molecules of the benzyl derivatives are isolated from each other by interactions with the solvent.

2.3.2 - Solution phase behaviour of the 3,5-diesters

Of the 3,5-derivatives studied, only the pyridyl protons of the neopentyl diester (**43**) exhibited a concentration dependant deshielding effect (Table 8, Figure 44). Whether this is indicative of tape-like aggregation as opposed to a solvation effect is harder to say as the differences between the rates of change are much smaller than those seen for the 2,6-isomers.

Table 8: Rates of change in the chemical shift of the pyridyl protons as a function of the sample concentration for the 3,5-pyridinedicarboxylates; the standard error for the linear regression is given in brackets.

	R		γ-proton ($H^{\blacklozenge}$)/ppm M^{-1}	α-proton ($H^{\blacktriangle}$)/ppm M^{-1}
39	CH_3	(methyl)	- 0.034 (0.0017)	- 0.020 (0.0010)
41	CH_2CH_3	(ethyl)	- 0.028 (0.0042)	- 0.017 (0.0027)
43	$CH_2C(CH_3)_3$	(neopentyl)	+ 0.009 (0.0030)	+ 0.011 (0.0030)
45	CH_2Ph	(benzyl)	- 0.025 (0.0005)	- 0.016 (0.0007)

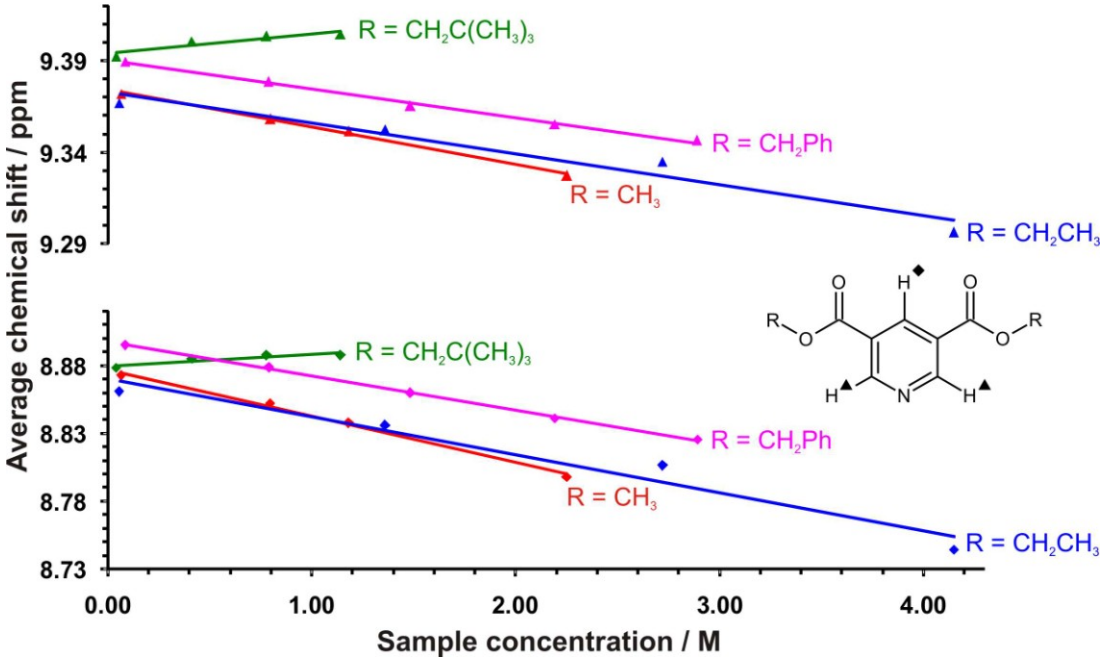

Figure 44: Plot of chemical shift as a function of sample concentration for the pyridyl protons of the 3,5-pyridinedicarboxylates; gradients for the lines of linear regression are given in Table 8.

If, as appears to be the case for the aliphatic 2,6-diesters, the solid-state behaviour of the 3,5-isomers is reflected in solution, then a downfield shift would be expected for the α-protons of the methyl and ethyl derivatives (**39** and **41**). Additionally, the CH_2 protons of the ethyl derivative and the CH_3 protons of the methyl analogue would also be expected to shift downfield as the concentration of the solution is increased. As has already been mentioned, the pyridyl protons for both **39** and **41** were observed to show an upfield shift. The alkyl protons of both **39** and **41** are found to move downfield (Table 9) as the sample concentration is increased but the magnitudes of these shifts, particularly for **41**, are quite small.

Table 9: Rates of change in the chemical shift of the alkyl protons as a function of the sample concentration for the 3,5-pyridinedicarboxylates; the standard error for the linear regression is given in brackets.

	R		CH_2/ppm M^{-1}	CH_3/ppm M^{-1}
39	CH_3	(methyl)	-	+ 0.010 (0.0006)
41	CH_2CH_3	(ethyl)	+ 0.003 (0.0019)	+ 0.009 (0.0016)
43	$CH_2C(CH_3)_3$	(neopentyl)	+ 0.016 (0.0022)	+ 0.020 (0.0018)
45	CH_2Ph	(benzyl)	- 0.030 (0.0022)	-

Like the 2,6-benzyl diester, the protons of the 3,5-isomer are all observed to move upfield as the concentration of the solution is increased. Whilst the difference between the rates of change for the pyridyl protons is greater than for the 2,6-analogue, the magnitudes of the changes are significantly lower.

2.3.3 - Conclusions

In conclusion, the data for the 2,6-diesters with aliphatic side-arms suggests that tape-like assemblies may be formed in solution. The evidence for solution phase aggregation of the 3,5-analogues is less convincing although this is unsurprising considering that the contact for these isomers is considered to be less favourable. The benzyl derivatives, whilst both forming tape-like assemblies in the solid-state show no evidence of tape-formation in solution. Further investigations would be required to determine whether this is generally true or whether tape-like aggregation is seen in other solvent systems or for solutions of other aromatic diesters.

2.4 - Variable temperature Raman studies

Samples were prepared by dry loading a cut-down NMR tube (approximately 1cm long) with the crystalline material and the tube was placed in an electronically controlled heating cell inside the spectrometer. Raman spectra were collected between 100 and 3500 cm^{-1} at (i) 25 ºC, (ii) the melting point of the sample, (iii) 5 °C above the melting point and (iv) a number of intervals between the melting point and room temperature. A broad absorption was observed above 2000 cm^{-1} for the spectra collected at higher temperatures. Since the absorptions of greatest interest were found to occur at lower wave numbers, data points above 2000 cm^{-1} were discarded.

2.4.1 - Raman studies on the 2,6-diesters

For the compounds with a 2,6-pyridinedicarboxylate core, the shape and positions of the peaks corresponding to the carbonyl stretching and pyridine ring stretching modes are observed to change as the sample melts.

The changes are most apparent for diethyl 2,6-pyridinedicarboxylate (**40**, Figure 45). As the temperature is raised above the melting point (42 °C), the sharp carbonyl peak at 1737 cm^{-1} splits into two broader, overlapping peaks at 1722 and 1742 cm^{-1}. The peak for the pyridine ring stretching mode at 1573 cm^{-1} shifts to a slightly higher energy (1576 cm^{-1}) and broadens with a slight shoulder appearing at 1586 cm^{-1}. Changes are also observed for the absorptions corresponding to the alkyl C-H deformation at 1445 cm^{-1} and the aromatic C-H deformation at 1278 cm^{-1}; as the sample melts, both groups of peaks are observed to broaden and shift to a higher wave number. There is little change in the absorption corresponding to the trigonal ring breathing mode of the pyridine ring at 995 cm^{-1}.

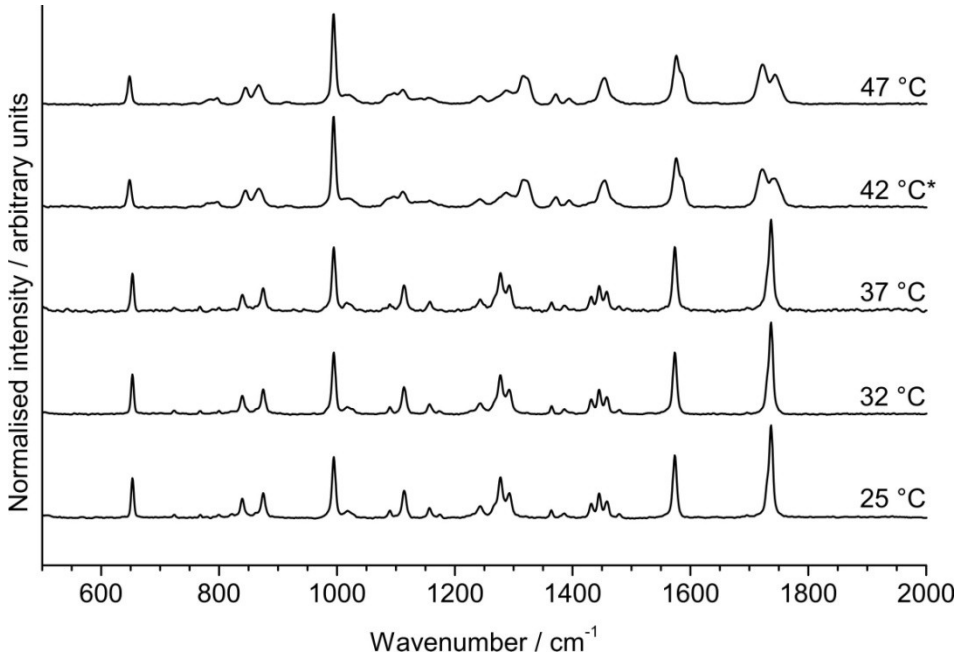

*Figure 45: Raman spectra for diethyl 2,6-pyridinedicarboxylate (**40**; mpt = 42 °C).*

Similar changes are seen for the other compounds in the series (Table 10 and Table 11), although the changes in the pyridyl absorption are not seen for the benzyl derivative. The temperature at which such changes occur (τ) is also observed to vary between the samples; for the methyl and benzyl diesters (**38** and **44**), the change is seen 5 ºC above the melting point, whilst for the neopentyl derivative (**42**), the change is observed 5 ºC below the melting point.

*Table 10: Key data for thermal changes observed in the Raman-active carbonyl absorption of the 2,6-diesters (**38-44**).*

	R	mpt/ °C	τ/ °C	$C=O_{vib}$ (25°C)/ cm^{-1}	$C=O_{vib}$ (τ)/ cm^{-1}	$C=O_{sdr}$ (τ)/ cm^{-1}
38	Methyl	115	120	1737	1728	1747
40	Ethyl	42	42	1737	1722	1742
42	Neopentyl	192	187	1735	1726	1752
44	Benzyl	117	122	1746	1726	1746

τ denotes the temperature at which spectral changes are observed; $C=O_{vib}$ denotes the position of the carbonyl vibration at the temperature indicated; $C=O_{sdr}$ denotes the position of the second, smaller carbonyl peak.

*Table 11: Key data for thermal changes observed in other Raman absorptions of the 2,6-diesters (**38-44**).*

	mpt/ °C	τ/ °C	Py_{vib} (25°C)/ cm^{-1}	Py_{vib} (τ)/ cm^{-1}	Py_{sdr} (τ)/ cm^{-1}	CH_{vib} (25°C)/ cm^{-1}	CH_{vib} (τ)/ cm^{-1}
38	115	120	1572	1575	1584	1299	1323
40	42	42	1573	1576	1586	1278	1316
42	192	187	1576	1572	1585	1281	1318
44	117	122	1607	1607	-	1293	1316

τ denotes the temperature at which spectral changes are observed; Py_{vib} denotes the position of the pyridine ring stretching vibration at the temperature indicated; Py_{sdr} denotes the position of the shoulder observed on the pyridine ring stretching absorption at elevated temperatures; CH_{vib} denotes the position of the most dominant aromatic C-H deformation absorption at the temperature indicated.

As the sample melts, the rigid framework of intermolecular interactions that assemble molecules in the solid-state breaks down. The molecules in the resultant liquid-phase have an increased freedom of movement and this is observed as a broadening of the spectral peaks.

The most obvious spectral change is observed for the carbonyl absorptions. The carbonyl stretch observed for the solid-state sample is thought to be an in-phase stretching mode and is believed to move to a higher energy as the

sample melts. The second, lower, absorption seen in the molten sample is thought to be the consequence of an out-of-phase stretching mode which is suppressed by the rigid framework of the crystal at lower-temperatures.

2.4.2 - Raman studies on the 3,5-diesters

The spectra for the compounds with a 3,5-pyridinedicarboxylate core also show changes around the melting point of the sample. Like the spectra of the 2,6-derivatives, most peaks broaden as the sample melts (the spectra of the ethyl 3,5-diester (**41**) is shown in Figure 46).

However, unlike the spectra of the 2,6-derivatives, whilst the carbonyl peak is observed to shift to a higher energy as the sample melts (Table 12), it is not seen to split. The carbonyl peak of the molten sample is observed to be broader than that of the solid and it is suggested that for the 3,5-diesters the in-phase and out-of-phase stretching modes occur at a similar energy and that the corresponding peaks overlap.

Whilst the absorptions for pyridine ring stretching and aromatic C-H deformation (Table 13) are not found to change position significantly, the absorptions are observed to broaden at or above the melting point.

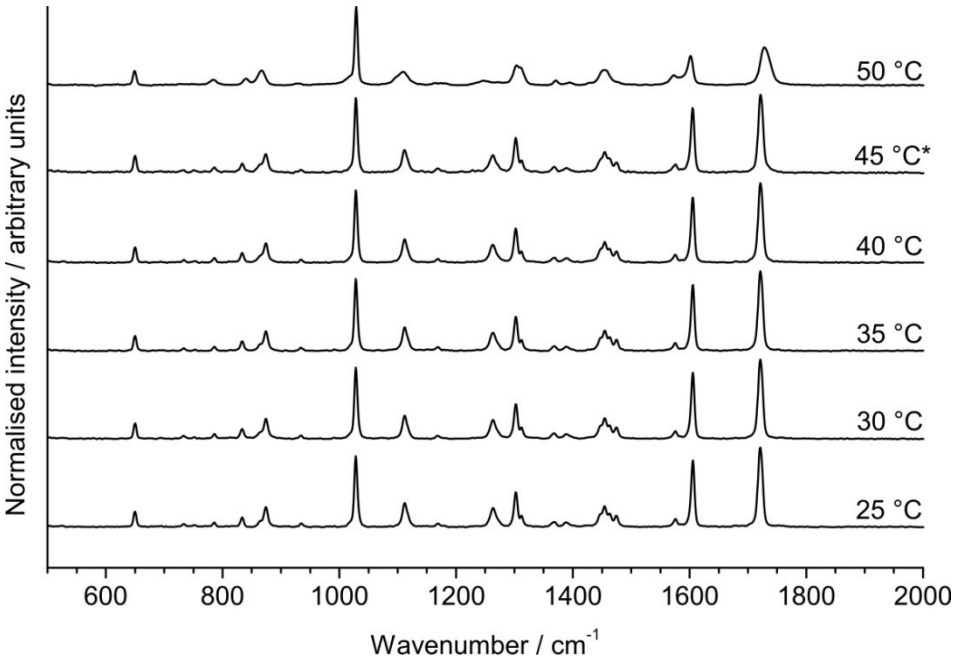

*Figure 46: Raman spectra for diethyl 3,5-pyridinedicarboxylate (**41**; mpt = 45 °C).*

*Table 12: Key data for thermal changes observed in the Raman-active carbonyl absorption of 3,5-pyridinedicarboxylates **39** - **45**.*

	R	mpt/°C	τ/°C	$C=O_{vib}$ (25°C)/cm^{-1}	$C=O_{vib}$ (τ)/cm^{-1}
39	Methyl	82	82	1723	1730
41	Ethyl	45	50	1721	1728
43	Neopentyl	140	145	1720	1736
45	Benzyl	72	72	1724	1730

τ denotes the temperature at which spectral changes are observed; $C=O_{vib}$ denotes the position of the carbonyl vibration at the temperature indicated.

*Table 13: Key data for thermal changes observed in other Raman absorptions of 3,5-pyridinedicarboxylates **39** - **45**.*

	mpt/ °C	τ/ °C	Py_{vib} (25°C)/ cm^{-1}	Py_{vib} (τ)/ cm^{-1}	Py_{sdr} (τ)/ cm^{-1}	CH_{vib} (25°C)/ cm^{-1}	CH_{vib} (τ)/ cm^{-1}
39	82	82	1606	1601	1470	1316	1314
41	45	50	1606	1602	1454	1302	1304
43*	140	145*	1599	1600	1459	1299	1301
45	72	72	1599	1602	-	1304	1300

τ denotes the temperature at which spectral changes are observed; Py_{vib} denotes the position of the pyridine ring stretching vibration at the temperature indicated; Py_{sdr} denotes the position of the shoulder observed on the pyridine ring stretching absorption at elevated temperatures; CH_{vib} denotes the position of the most dominant aromatic C-H deformation absorption at the temperature indicated.

* The high temperature spectrum for **43** was found to have a poor signal to noise ratio, attempts to subsequently recollect the data were unsuccessful.

2.4.3 - Conclusions

It has been shown that the Raman spectroscopy can be used to observe the disruption of the crystal architecture in both the 2,6- and the 3,5-diesters. Further work should be undertaken to see whether this technique can be used to help understand the solution-phase behaviour of the diesters.

2.5 - Differential scanning calorimetry experiments

The role of secondary hydrogen bonding interactions between the donors and acceptors of the triple hydrogen bond motif has been used[91, 92] to explain the prevalence of the triple hydrogen bond tape-like motif in the solid-state for samples with a 2,6-core as compared to their 3,5-analogues. It has been hypothesised[91, 92] that these secondary interactions stabilise the triple hydrogen bond contact in the 2,6-substituted compounds, making their formation more energetically favourable. Consequently it is to be expected that the enthalpy of melting should be greater for the 2,6-derivatives than for their 3,5 counterparts. Table 14 gives the heats of melting for compounds **38**-**45** as determined by DSC.

*Table 14: DSC data for compounds **38** - **45**.*

		2,6-core			3,5-core		
R			$\Delta H_{melting}$/ J g^{-1}	$\Delta H_{melting}$/ kJ mol^{-1}		$\Delta H_{melting}$/ J g^{-1}	$\Delta H_{melting}$/ kJ mol^{-1}
CH_3	(methyl)	**38**	172.52	33.67	**39**	137.25	26.79
CH_2CH_3	(ethyl)	**40**	110.17	24.59	**41**	125.63	28.04
$CH_2C(CH_3)_3$	(neopentyl)	**42**	168.23	51.71	**43**	136.97	42.10
CH_2Ph	(benzyl)	**44**	131.38	45.64	**45**	102.55	35.62

As expected, the 2,6-diesters with methyl, neopentyl and benzyl substituents show a higher heat of melting than their 3,5-analogues, although this comparison is less valid for the methyl derivatives as the two isomers do not form directly comparable assemblies in the solid-state. For the neopentyl and benzyl systems, where both isomers form tape-like assemblies, the heat of melting is approximately 10 kJ mol^{-1} greater for the 2,6-diester than for the 3,5-analogue.

It is surprising that the ethyl 3,5-diester (**41**) shows a higher enthalpy of melting than the 2,6-analogue (**40**). One possible, although somewhat contrived, explanation may be found in Orton's[91] suggestion that the slipped tape motif allows for more efficient close packing. This would increase the number of dispersive contacts and the sum of these may account for the observed increase in enthalpy of melting.

2.6 - Conclusions and further work

Gomm[92] and Orton[91] have observed that the 2,6-synthon is more robust than the 3,5-analogue and they have suggested that this is the result of a stronger triple hydrogen bond motif owing to the presence of favourable secondary hydrogen bonding interactions in the 2,6-isomer. DSC analysis of compounds **38** - **45** has confirmed that the tapes formed with a triple hydrogen bond motif by the 2,6-pyridinedicarboxylates are often stronger than those formed by their 3,5-analogues.

The NMR titration experiments have shown that, for the 2,6-diesters with aliphatic side-arms, there is evidence of supramolecular assembly in solution. The evidence for solution-phase assembly of the 3,5-isomers is less conclusive, and this may be a reflection of the weaker solid-state interactions. The solution behaviour of the benzyl derivatives seems to be dominated by interactions with the solvent as no evidence of aggregation has been seen. Aggregation may be observed for these benzyl diesters in a different solvent system and examination of other diesters with substituted aromatic side-arms should be considered.

Finally, it has been shown that Raman spectroscopy can be used to observe disruption of the crystalline framework. It would be worth investigating the behaviour of the alkyl-substituted diesters in solution using this technique to verify the conclusions drawn from the NMR titration experiments. It may also be possible to use Raman titration experiments to probe the interactions between the benzyl diesters and the solvent.

3 - Solid-state behaviour of pyridinedicarboxylates with polyaromatic side-arms

3.1 - Compounds under study and synthesis

Previous studies[91, 92, 95] within the research group have examined the solid-state behaviour of a number of pyridinedicarboxylates with aromatic side-arms. However, these studies have been limited to systems with 5- or 6-membered aromatic rings. The present work aims to examine the effect of the presence of side-arms with larger aromatic groups on the solid-state behaviour of the diesters. The effects of changing the length of the alkyl linker or the position of attachment to the polynuclear aromatic ring will also be considered.

The bis(phenyl)pyridine-dicarboxylate diesters (**46** and **47**) were prepared as shown in Scheme 1. The synthesis of the diesters with polyaromatic side-arms (**48** - **59**) was performed by two undergraduate project students, R. Parker[111] and S. Twiddy,[112] by reaction of the appropriate acid chloride with the required alcohol in the presence of triethylamine (Scheme 2).

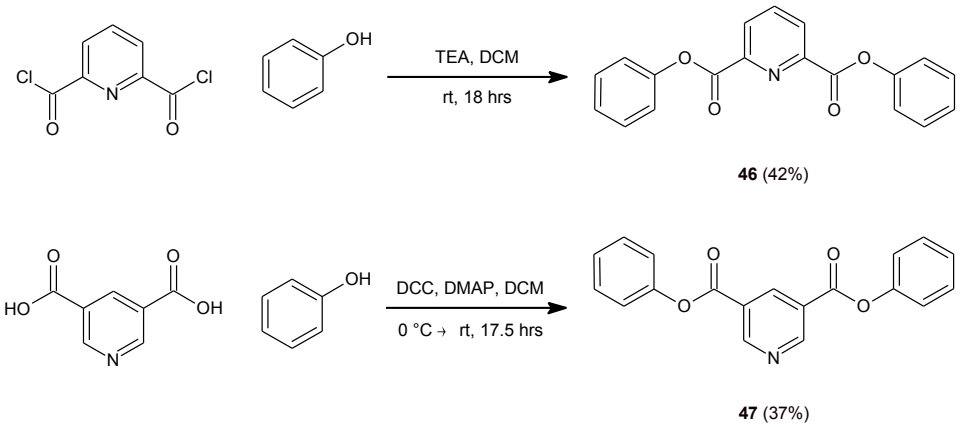

*Scheme 1: Outline of the synthetic routes used to prepare the phenyl diesters **46** and **47**.*

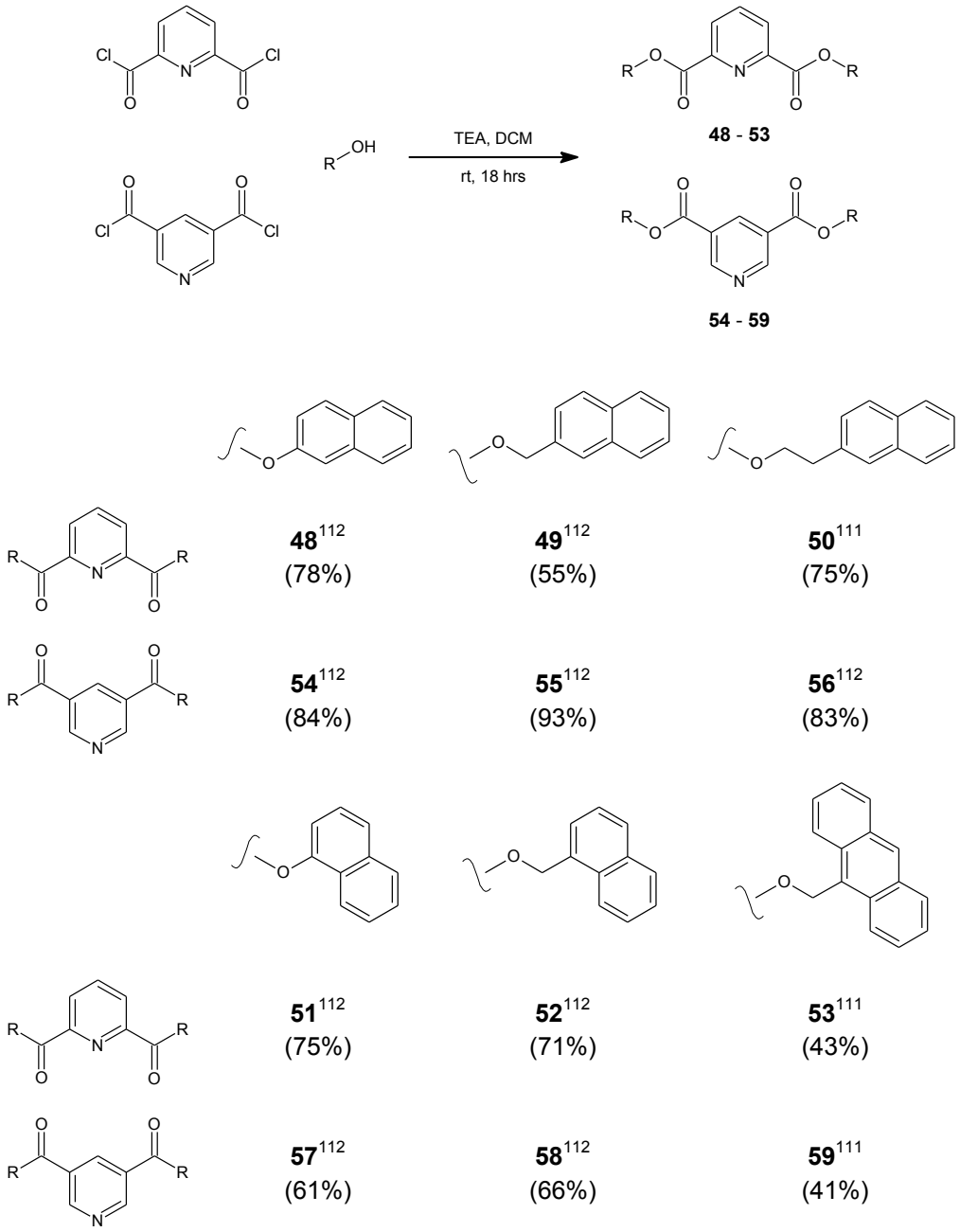

Scheme 2: Summary of the diesters prepared with polyaromatic side-arms.

The naphthyl and anthryl diesters were found to be less soluble than the phenyl or benzyl derivatives, making purification of the samples and growth of crystals suitable for diffraction more complicated. Crystals suitable for study by single crystal diffraction could not be obtained for the 2-naphthyl 2,6-diester (**48**), or the 3,5-diesters with (2-naphthyl)ethyl or (1-naphthyl) side-arms (**56** and **57**). The crystals obtained for the (2-naphthyl)methyl diester (**55**) were of very poor quality and data had to be collected by the EPSRC NCS using the high flux X-ray source at the Daresbury synchrotron.

3.2 - Solid-state behaviour of the 2,6-diesters

3.2.1 - Primary assembly

With the exception of the 1-naphthyl-derivative (**51**), all of the 2,6-diesters studied formed conventional tapes (Table 15).

Table 15: Primary assembly parameters for 2,6-diesters with aromatic side-arms.

	Side-arm	r_1/Å	r_2/Å	θ/°	ϕ/°	ϑ/°	ψ/°
44[92]	Benzyl	2.48	2.48	180.0	163.8	127.0	28.3
46	Phenyl	2.62	2.60	180.0	145.5	121.8	30.0
49	(2-Naphthyl)methyl	2.48	2.40	180.0	164.4	125.9	25.5
50	(2-Naphthyl)ethyl	2.52	2.54	180.0	157.9	128.1	74.7
52	(1-Naphthyl)methyl	2.66	2.50	180.0	172.7	123.7	70.5
53	(9-Anthryl)methyl	2.58	2.50	180.0	173.6	123.5	71.6

The phenyl and (2-naphthyl)methyl 2,6-diesters (**46** and **49**) both adopt a primary assembly comparable to that of the benzyl analogue (**44**[92]). The aromatic rings of the side-arms are observed to rotate slightly out of the plane of the pyridine ring (Figure 47). Comparing the parameters for the benzyl and (2-naphthyl)methyl derivatives (**44**[92] and **49**) suggests that increasing the size of the side-arm orthogonal to the direction of the tape has a negligible effect on the formation of a tape-like assembly.

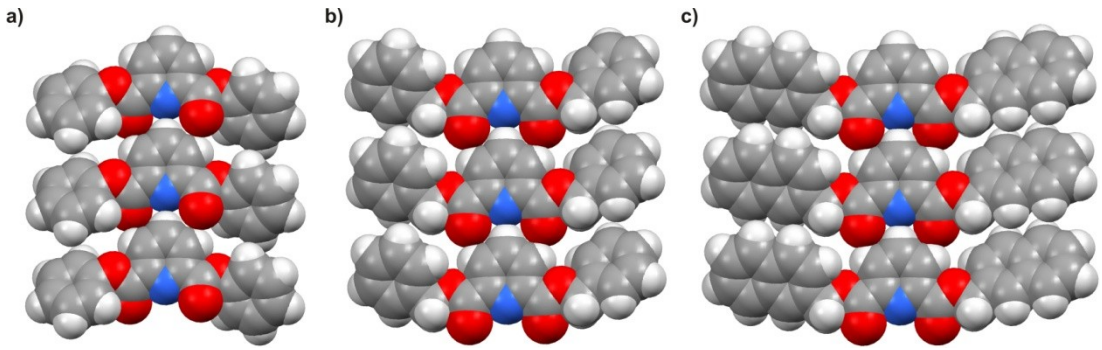

*Figure 47: Space filling representations of the primary tape-like assemblies formed by the 2,6-diesters with: (a) phenyl; (b) benzyl and (c) (2-naphthyl)methyl side-arms (**46**, **44**[92] and **49** respectively).*

Removal of the alkyl linker limits the rotation of the aromatic substituent. In the phenyl diester (**46**), the aromatic side-arm is observed to sit in front of the pyridine ring, rather than alongside it as is observed for the benzyl derivative

(**44**[92]). Additionally, the carbonyl groups are found to rotate out of the pyridyl plane.

Increasing the length of the alkyl spacer from one to two carbons in length (**50**) allows the aromatic substituent to fold out the plane of the pyridine ring (Figure 48a). A consequence of this geometry is that the naphthalene ring is unable to twist to minimise the steric interference between adjacent molecules in the tape, consequently the hydrogen bonds of the primary contact are lengthened in comparison to those of the (2-naphthyl)methyl derivative (**49**).

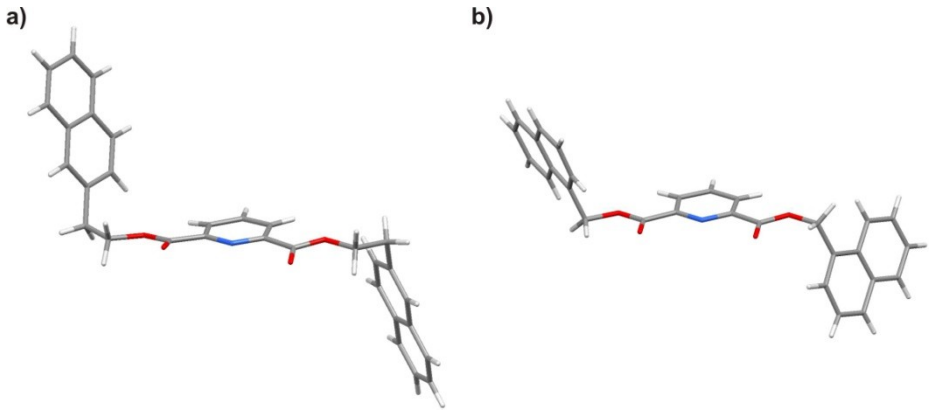

*Figure 48: Conformations of the 2,6-diesters formed with: (a) (2-naphthyl)ethyl and; (b) (1-naphthyl)methyl side-arms (**50** and **52** respectively).*

The effect on solid-state behaviour of moving the point of attachment from the 2- to the 1-position on the naphthalene ring is highly dependent on the presence of an alkyl spacer. Where the naphthalene ring is directly bound to the oxygen atom of the ester (*i.e.* there is no spacer, **51**), the substituent is unable to rotate and tape formation is inhibited (this will be discussed later). Addition of a single CH_2 spacer (**52**) allows the substituent to fold out of the pyridyl plane (Figure 48b) and the formation of a tape-like assembly is observed.

Unlike the tapes formed with phenyl, benzyl or 2-naphthyl substituents, the tape formed with a (1-naphthyl)methyl side-arm (**52**) shows evidence of overlap between the substituents of molecules adjacent to each other in the tape. However, the overlap is eclipsing rather than slipped (Figure 49a) and

this could explain the increase in the length of the C-H···N bond (r_1); direct overlap of the π-clouds of adjacent molecules would lead to electrostatic repulsion, forcing the molecules apart.

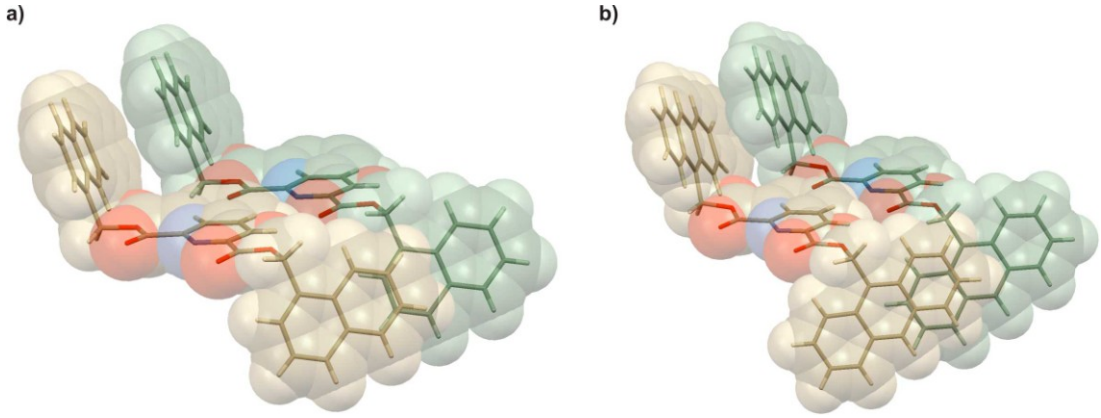

*Figure 49: Space-filling and wire-frame illustrations of the different degrees of overlap between the side-arms of the (a) (1-naphthyl)methyl and (b) (9-anthryl)methyl 2,6-diesters (**52** and **53** respectively). The inter-planar separations for the side-arms were found to be 3.40 and 3.34 Å for **52** and **53** respectively.*

The overlap between the adjacent side-arms of molecules in the same tape increases on going from the (1-naphthyl)methyl diester (**52**) to the (9-anthryl)methyl analogue (**53**). However, despite the increase in π overlap, the C-H···N bond of the tape formed by anthryl diester (**53**) is shorter than that of naphthyl analogue (**52**). Examination of the structures shows that, whilst the overlap between the aromatic side-arms of **52** is eclipsing, the anthracene side-arms in **53** are slightly slipped relative to each other (Figure 49b). It is suggested that the resulting electrostatic repulsion is less for the slipped interaction than for the eclipsing one, consequently molecules adjacent to each other in the tape can pack closer together. It should also be noted that the C-H···N bond is still longer for **53** than for the benzyl or 2-naphthyl diesters (**44**[92], **49** and **50**) where there is no face-to-face overlap of the side-arms indicating that this interaction is still repulsive. Apart from this, increasing the steric bulk of the substituent group from naphthalene to anthracene is observed to have little effect on the primary assembly.

In the case of the 1-naphthyl diester (**51**), the *trans-trans* conformer is adopted in the solid-state. The naphthalene rings sit in front of the pyridine

core, forming a pincer-like molecule and inhibiting the formation of tape-like assemblies. Instead, molecular dimers are observed, one of the naphthyl groups of each molecule sits in the "cleft" formed by the naphthalene rings of the other (Figure 50). This arrangement is in some ways similar to that of the hermaphrodite dimers described by Gomm[92] for the pyridinediamides with methylpyridine side-arms. The dimer appears to be stabilised by two C-H···O interactions (contact i in Figure 50). A slipped, face-to-face π-π interaction is also observed (contact ii in Figure 50).

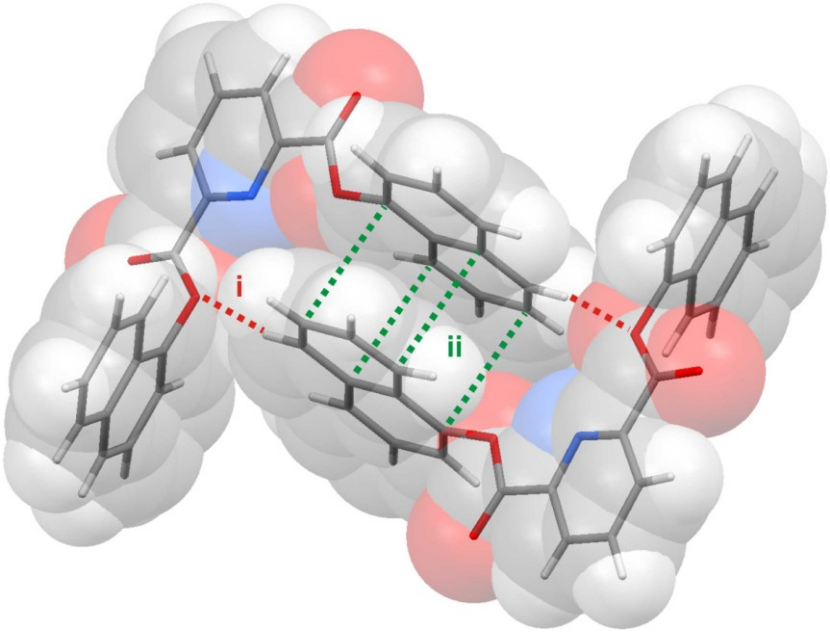

*Figure 50: Close contacts observed within the molecular dimers formed by the 1-naphthyl diester (**51**). Contact i (red lines): H···O = 2.46 Å, C-Ĥ···O = 168.7°. Contact ii: slipped π-π interaction (interplanar separation = 3.37 Å), green dashed lines show the points of closest contact between the carbon skeletons of the two naphthyl rings.*

3.2.2 - Secondary assembly

All of the compounds that adopt tape-like assemblies also form planar secondary assemblies with anti-parallel stacks (Table 16). In all cases, stack formation appears to be directed by C-H···π interactions. Between adjacent stacks there are few specific interactions and assembly is primarily determined by close-packing between the aromatic substituents.

Table 16: Secondary assembly parameters for the 2,6-pyridine dicarboxylates.

	Side-arm	Assembly	S_S/Å	S_T/°	T_O/°
44[92]	Benzyl	$PS_{\uparrow\downarrow}L_{\uparrow\downarrow}$	3.32	52.1	48.9
46	Phenyl	$PS_{\uparrow\downarrow}L_{\uparrow\uparrow}$	3.40	74.0	70.3
49	(2-Naphthyl)methyl	$PS_{\uparrow\downarrow}L_{\uparrow\downarrow}$	3.31	51.8	50.2
50	(2-Naphthyl)ethyl	$PS_{\uparrow\downarrow}L_{\uparrow\uparrow}$	3.35	48.9	72.8
52	(1-Naphthyl)methyl	$PS_{\uparrow\downarrow}L_{\uparrow\uparrow}$	3.06	37.3	54.9
53	(9-Anthryl)methyl	$PS_{\uparrow\downarrow}L_{\uparrow\downarrow}$	2.92	29.2	59.2

As with the primary assemblies, the intermolecular contacts observed between tapes formed by the benzyl and (2-naphthyl)methyl diesters (**44**[92] and **49**) are almost identical. In each case, one of the methylene protons is observed to form a η^6 C-H···π contact with the aromatic side-arm of a molecule in a neighbouring layer (Figure 51).

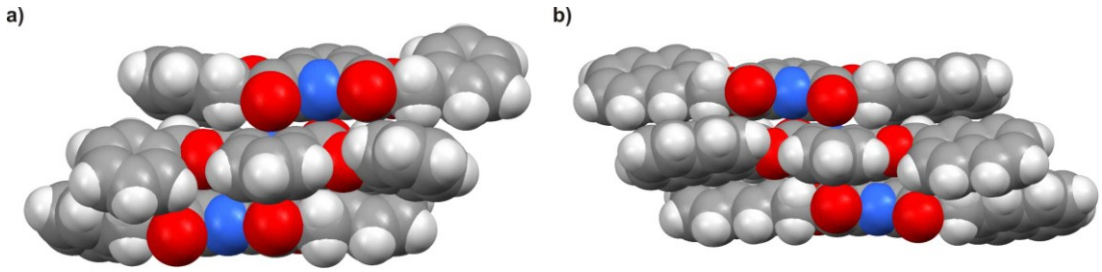

*Figure 51: Space filling representations of the stacks formed by (a) the benzyl diester (**44**[92]) and (b) the (2-naphthyl)methyl analogue (**49**) showing the C-H···π contacts observed between the methylene protons and the aromatic side-arms of neighbouring molecules (H···centroid = 2.68 and 2.53 Å, C-Ĥ···centroid = 164.8 and 160.3° for **44**[92] and **49** respectively).*

In both derivatives (**44**[92] and **49**), the aromatic side-arms of tapes adjacent to each other in the stack are aligned with an edge-to-face geometry. However, a specific interaction is only seen between the larger rings of the (2-naphthyl)methyl diester. The 5-proton of one naphthalene ring is observed

to form a η^3 C-H···π interaction with the 1-, 2- and 9-carbon atoms of a naphthalene ring in an adjacent tape (black dashed lines in Figure 52).

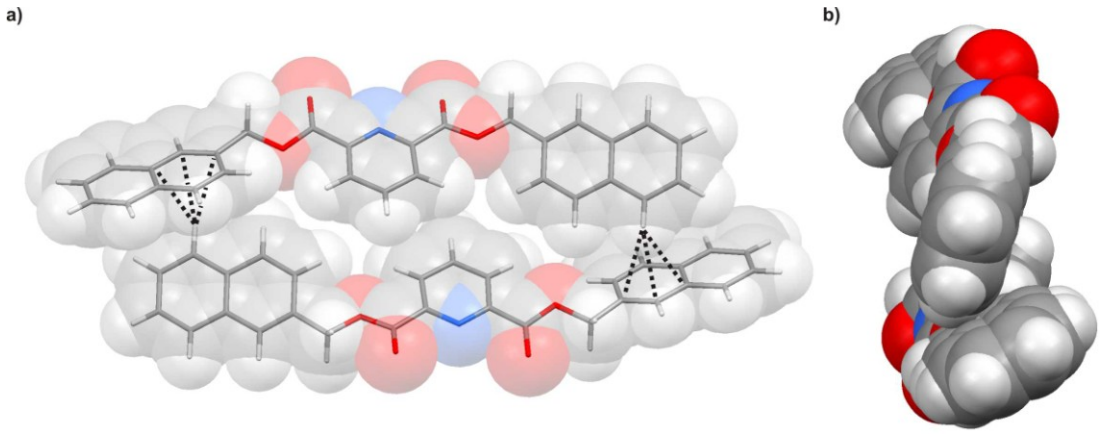

*Figure 52: (a) Front and (b) side views of two molecules of bis(2-naphthyl)methyl 2,6-pyridinedicarboxylate (**49**) showing the η^3 C-H···π interactions between the naphthalene rings of adjacent tapes (black dashed lines; H···centroid$_{(C1\text{-}C2\text{-}C9)}$ = 2.71 Å, C-Ĥ···centroid = 144.1°).*

Similar interactions are seen within the stacks formed by the (2-naphthyl)ethyl diester (**50**), with both the 5-naphthyl and the methylene protons forming η^6 C-H···π contacts with the naphthalene rings of neighbouring tapes.

The aromatic rings of the phenyl diester (**46**) are also aligned in an edge-to-face geometry and η^6 C-H···π contacts are seen between the side-arms of tapes adjacent to each other in the stack (contacts i and iii in Figure 53). These replace the CH_2···π contacts observed in the benzyl analogue (**44**[92]).

As has already been mentioned, the carbonyl oxygen atoms in the phenyl diester (**46**) are slightly twisted out of the pyridyl plane. A consequence of this geometry is the formation of an additional intra-stack interaction between the phenyl protons and the carbonyl oxygen atoms (contact ii in Figure 53).

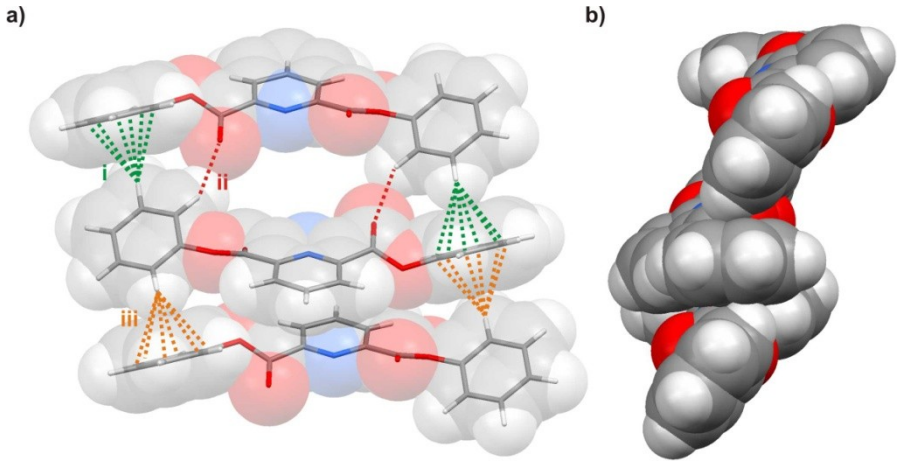

*Figure 53: (a) Front and (b) side views of a stack formed by the tapes of the phenyl diester (**46**). Close contacts are shown by dashed lines; contact i (green): H···centroid = 2.69 Å, C-Ĥ···centroid = 141.5°; contact ii (red): H···O = 2.35 Å, C-Ĥ···O = 150.4°, C=Ô···H = 149.0°; contact iii (orange): H···centroid = 2.67 Å, C-Ĥ···centroid = 131.7°.*

Changing the position of attachment of the alkyl spacer on the aromatic substituent, changes the geometry of the intra-stack edge-to-face interactions. For the (2-naphthyl)alkyl diesters (**49** and **50**) these occur between the long edges of the aromatic ring. However, for the (1-naphthyl)methyl and (9-anthryl)methyl diesters (**52** and **53**) they are observed to occur between the short edges of the rings (Figure 54).

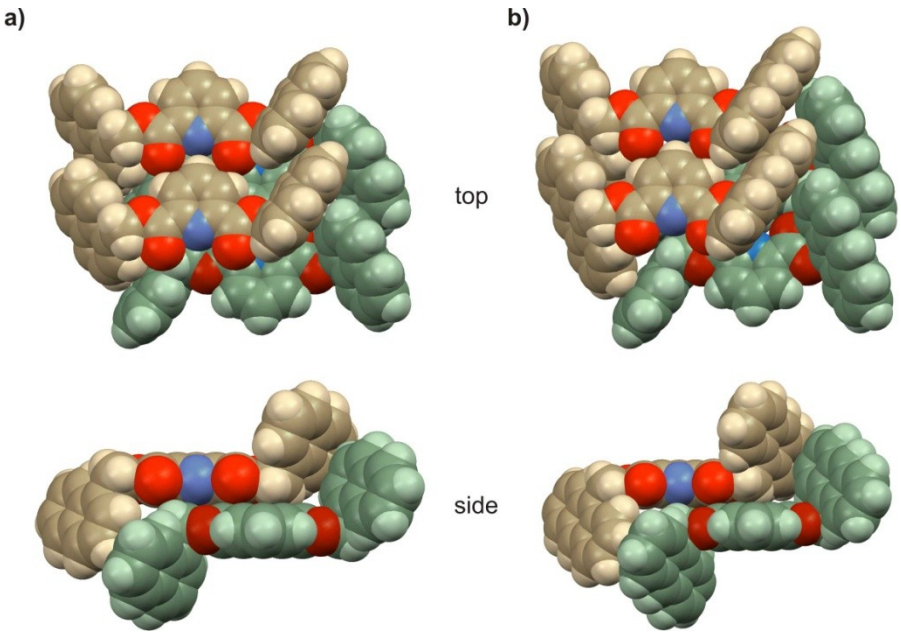

*Figure 54: Space-filling views from above the tape looking down and from the side looking along the tape of: (a) the (1-naphthyl)methyl and; (b) the (9-anthryl)methyl diesters (**52** and **53**), showing the edge-to-face packing between the side-arms.*

It should be noted that although the side-arms of both **52** and **53** are aligned for edge-to-face interactions, the observed close contacts are different in the two systems. The geometry of the close contact observed between adjacent tapes of the anthryl derivative (**53**, H···centroid = 2.54 Å, C-Ĥ···centroid = 142.6°) indicates the existence of a genuine C-H···π interaction. In contrast, the closest C-H···π type contact between neighbouring tapes of the naphthyl derivative (**52**, H···centroid = 3.00 Å, C-Ĥ···centroid = 143.0°) is much longer than the sum of the van der Waals radii.

3.2.3 - Conclusions

Comparing the benzyl and (2-naphthyl)methyl diesters (**44**[92] and **49**), it can be seen that increasing the size of the substituent along the length of the molecule has a negligible effect on their solid-state behaviour.

The effect of changing the length of the alkyl spacer is dependent on the point of attachment to the aromatic substituent. For the phenyl or 2-naphthyl derivatives, tape-like assemblies were observed in all of the systems studied and it is suggested that the effect of changing the length of the spacer on tape formation is relatively small. When the point of attachment is moved to the 1- or 9- position of a larger aromatic substituent, the aromatic side-arm is observed to fold out of the plane of the tape. If the alkyl spacer is removed this flexibility is lost and the diester is forced into a *trans-trans* conformation, inhibiting the formation of a tape-like assembly.

For all of the diesters that formed tape-like assemblies, the association of tapes into stacks is dominated by C-H···π interactions between the aromatic side-arms. The packing of stacks is determined by close-packing forces.

3.3 - Solid-state behaviour of the 3,5-diesters

3.3.1 - Primary assembly

As has already been discussed, the triple hydrogen bond motif of the 3,5-substituted diesters is weaker and consequently less robust than that of the 2,6-analogues. This is demonstrated by their solid-state behaviour. Of the seven derivatives under study, only three formed conventional tape-like assemblies; those with 2-naphthyl, (2-naphthyl)methyl and (9-anthryl)methyl side-arms (**54**, **55**, **59**). Of the other four, the (2-naphthyl)ethyl and 1-naphthyl derivatives (**56** and **57**) failed to form crystals suitable for X-ray diffraction. Lastly the phenyl diester (**47**) formed what appears to be a corrugated tape, whilst the (1-naphthyl)methyl analogue (**58**) was found to form a stepped "tape" of dimers.

Table 17: Primary assembly parameters for the 3,5-diesters with aromatic side-arms.

		r_1/Å	r_2/Å	θ/°	ϕ/°	ϑ/°	ψ/°
45[91]	Benzyl	2.41	2.45	180.0	159.2	135.4	25.9
		2.48	2.54, 2.48	163.9	155.5, 151.9	134.6, 131.2	19.0, 13.9
54	2-Naphthyl	2.34	2.51	180.0	139.5	132.7	29.8
55	(2-Naphthyl)methyl	2.07	2.59, 2.41	179.4	153.4, 153.8	139.5, 135.5	40.8, 34.6
59	(9-Anthryl)methyl	2.45	2.46	180.0	166.2	132.6	71.0

As was observed for the 2,6-diesters, the primary assemblies of the benzyl and (2-naphthyl)methyl derivatives (**45**[91] and **55**) are essentially comparable to one another (Figure 55a and b). A few differences are observed; the benzyl derivative (**45**[91]) contains two crystallographically unique molecules, whilst the naphthyl analogue (**55**) contains only one. This molecule is observed to be asymmetric (i.e. the bond lengths and angles of the two C-H···O=C bonds are not equal) however, this is probably a reflection of the low quality of the data set than of the true nature of the molecule. The C-H···N bond is observed to be substantially shorter in the tape formed by the naphthyl derivative (**55**) than in the tapes formed by the benzyl analogue, and consequently the aromatic side-arm is observed to fold out of the pyridyl plane to a greater degree.

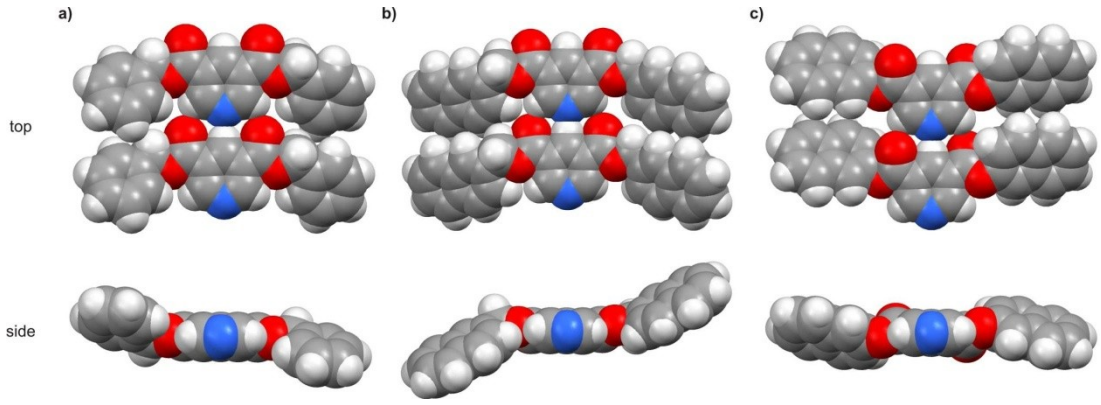

*Figure 55: Space-filling representations of the primary tape-like assemblies formed by the 3,5-diesters with: (a) benzyl; (b) (2-naphthyl)methyl and; (c) 2-naphthyl side-arms (**45**[91], **55** and **54** respectively). For clarity only the tape formed by the A-type molecules of **45** have been shown.*

Removing the CH_2 linker from the (2-naphthyl)methyl diester (**55**) to give the 2-naphthyl analogue (**54**), forces the aromatic group to sit in front of the pyridine ring rather than alongside it (Figure 55b and c). This results in a lengthening of the C-H···N bond (r_1) and the carbonyl groups are also seen to rotate slightly out of the pyridyl plane. This behaviour is comparable to that observed between the benzyl and phenyl 2,6-diesters (**44**[92] and **46**) and it would be expected that the phenyl 3,5-diester (**47**) would also form a conventional tape-like assembly in the solid-state.

Instead, the phenyl diester (**47**) forms a corrugated "tape" where the angle between the pyridine cores of adjacent molecules is 50.0° (Figure 56). Only a C-H···N close contact is observed between adjacent molecules in the same "tape" and the length and angle of this "interaction" (H···N = 2.64 Å, C-Ĥ···N = 114.8°) suggests that it is more likely to be a consequence of other packing forces. Adjacent tapes form close-packed, parallel stacks with adjacent pyridine rings separated by 3.45 Å and phenyl rings by 3.39 Å. Although adjacent phenyl rings are aligned in an edge-to-face geometry the close-contacts between the protons and the carbon skeleton do not indicate the existence of significant C-H···π interactions. Consequently it is concluded that the solid-state behaviour of the phenyl 3,5-diester is the result of close-packing by dispersive forces, possibly influenced by very weak edge-to-face aromatic interactions.

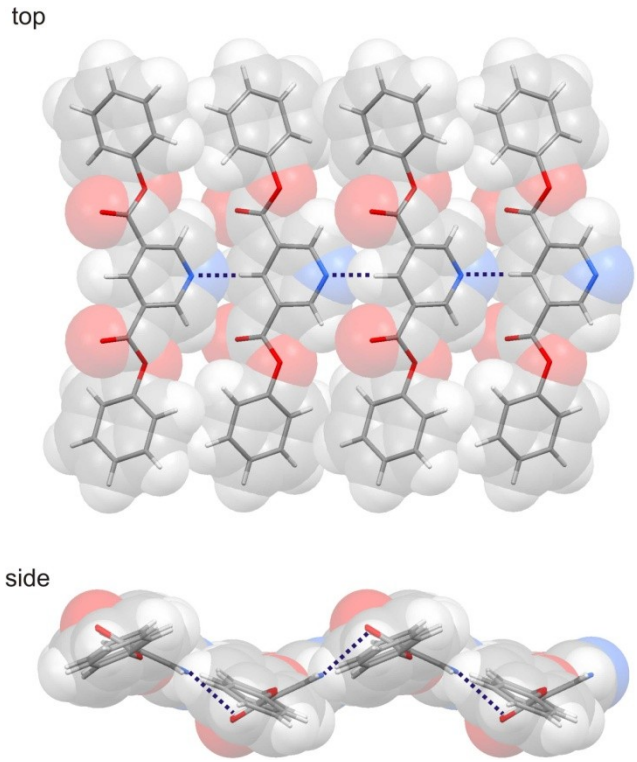

*Figure 56: Top and side views of the corrugated "tape" formed by the phenyl 3,5-diester (**47**); C-H···N close contacts are shown as dark blue dashed lines.*

As with the 2,6-analogue (**53**), the aromatic side-chains of adjacent molecules of bis(anthryl-5-methyl)pyridine-3,5-dicarboxylate (**59**) overlap and slipped, face-to-face π···π interactions are observed between them.

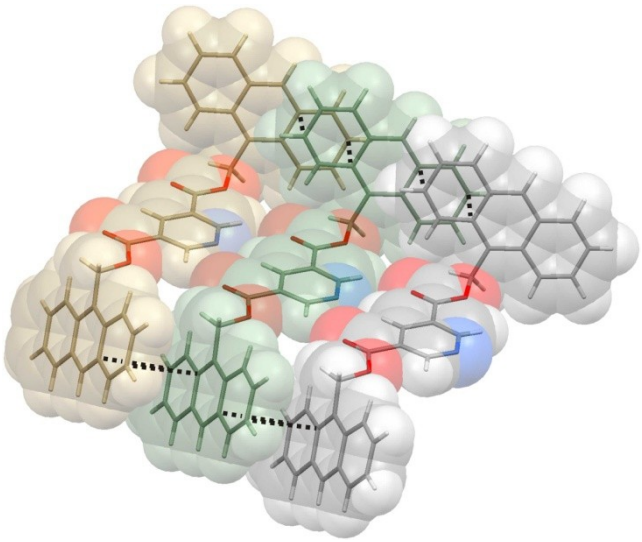

*Figure 57: Tape-like assembly formed by the (9-anthryl)methyl 3,5-diester (**59**). The close-contacts between eclipsing carbon atoms of adjacent side-arms are indicated by black dashed lines. The interplanar separation of adjacent side-arms is 3.36 Å.*

The solid-state behaviour of the (1-naphthyl)methyl 3,5-diester (**58**) is significantly different from that of its 2,6-analogue (**52**). Whilst **52** is symmetrical about an axis running through the centre of the pyridine ring, **58** is asymmetrical. One of the naphthalene side-arms lies almost parallel to the plane of the pyridine ring (ψ = 4.4°) whilst the other is folded so that it sits almost perpendicular to the pyridine core (ψ = 76.9°).

The solid-state behaviour can be described in terms of the tape-like assembly of molecular dimers, an example of which is shown in Figure 58. Close contacts are observed between the molecules (shown as black, dashed lines) which are suggestive of C-H···π interactions. The H···C distances of these contacts vary between 2.60 and 2.89 Å and the C-H···C bond angles range from 150.7 to 172.9°.

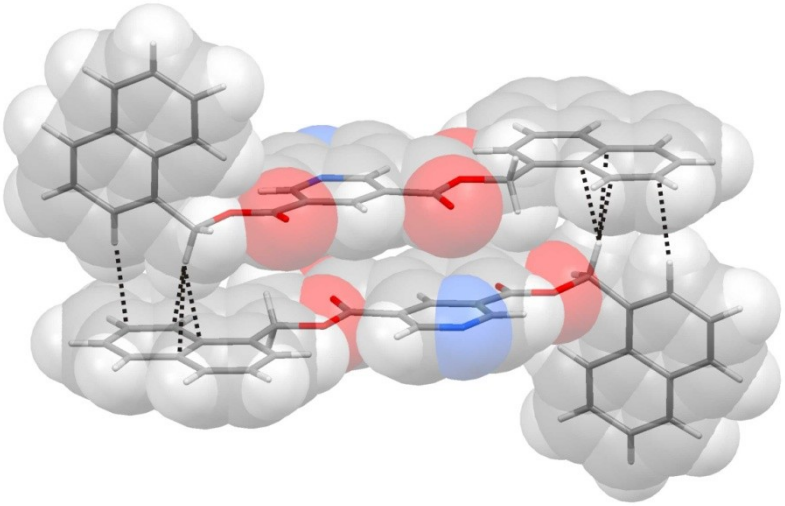

*Figure 58: Illustration of a molecular dimer formed by (1-naphyl)methyl 3,5-diester (**58**); close contacts are shown as black, dashed lines.*

Figure 59 illustrates the packing of the molecular dimers of **58** into a tape-like assembly. Although close contacts are observed between adjacent dimers (contacts i and ii), it is likely that the predominant force in the assembly of the tapes is close-packing.

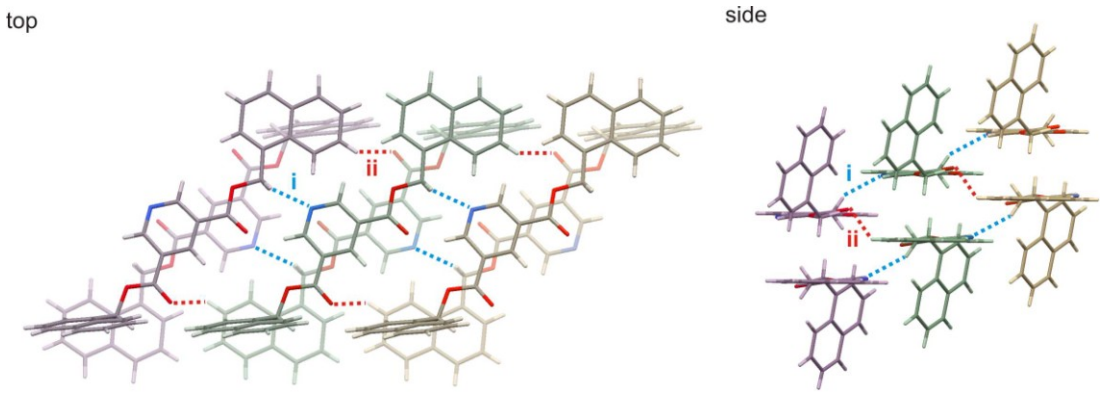

*Figure 59: Views from above and from the side of the tape-like assembly formed by dimers of the (1-naphyl)methyl 3,5-diester (**58**). Each dimer has been tinted with a different colour and close contacts are shown as either red or blue dashed lines. Contact i (blue): H···N = 2.57 Å, C-Ĥ···N = 150.8°; contact ii (red): H···O = 2.56 Å, C-Ĥ···O = 129.7°, H···Ô=C = 111.6°.*

3.3.2 - Secondary assembly

Of the 3,5-diesters that form conventional tape-like assemblies in the solid-state, planar secondary assemblies are observed. Like the 2,6-derivatives, the interactions between stacks of the tape-forming 3,5-diesters appear to be the result of close-packing and tessellation of the side-arms. Unlike the 2,6-diesters there is no common alignment between tapes adjacent to each other within a stack. Table 18 describes the secondary tape parameters for compounds **54**, **55** and **59**.

Table 18: Secondary assembly parameters for the 3,5-diesters with aromatic side-arms.

	Side-arm	Assembly	S_S/Å	S_T/°	T_O/°
54	2-Naphthyl	$PS_{\uparrow\downarrow}L_{\uparrow\uparrow}$	3.51	76.8	72.2
55	(2-Naphthyl)methyl	$PS_{\uparrow\uparrow}L_{\uparrow\downarrow}$	3.13	57.8	45.7
			3.14		45.8
59	(9-Anthryl)methyl	$PS_{\uparrow\downarrow}L_{\uparrow\downarrow}$	2.92	28.8	57.7

As Orton[91] has discussed, description of the secondary assembly of the tapes formed by the benzyl 3,5-diester (**45**[91]) is complicated by the presence of two crystallographically distinct molecules. Although the formal description[91] of the packing behaviour of **45**[91] ($PS^{ABBABB}_{\uparrow\uparrow\downarrow\downarrow\downarrow\uparrow}L^{ABBABB}_{\uparrow\uparrow\downarrow\downarrow\downarrow\uparrow}$) suggests a complicated set of interactions, Orton has noted that the forces influencing the packing behaviour are comparable to those seen for the 2,6-analogue (*i.e.* a combination of C-H···π and dispersive interactions).

The asymmetry of the (2-naphthyl)methyl diester (**55**) means that, within a stack, the observed close-contacts and the distance to the neighbouring molecules is slightly different above and below each tape. However, as has already been mentioned, this is most likely attributable to the quality of the data set. Looking at the packing of tapes in a stack (Figure 60), the side-arms are seen to be aligned in an edge-to-face geometry, although the distances and angles for the contacts between the aromatic protons and the carbon skeleton suggest that any interaction is likely to be weak (H···C = 2.8-3.1 Å, C-Ĥ···O = 127-135°).

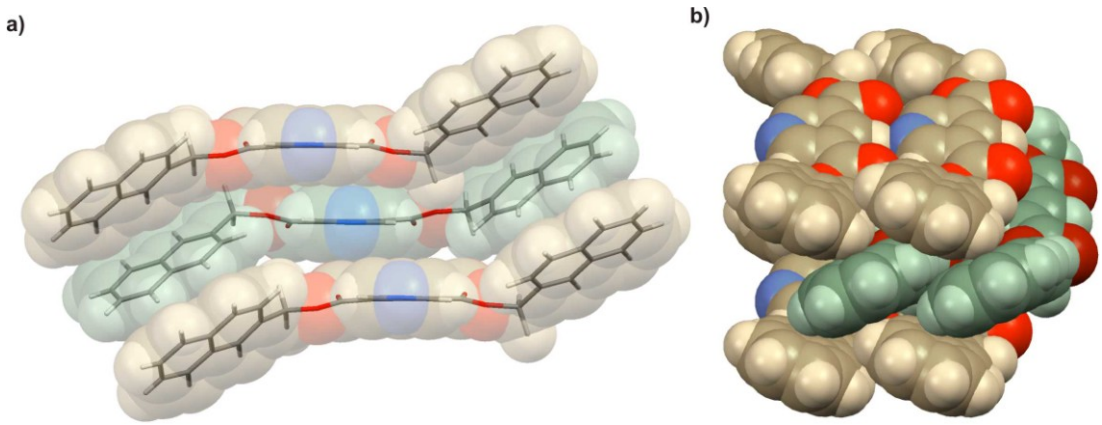

*Figure 60: Edge-to-face arrangement of the aromatic side-arms in a stack of tapes formed by the (2-naphthyl)methyl 3,5-diester (**55**) viewed (a) along the direction of the tape and (b) from the side of the tape.*

In the stacks formed by the 2-naphthyl diester (**54**) the aromatic side-arms also pack with an edge-to-face geometry (Figure 61). The contacts between the aromatic protons and the neighbouring ring are shorter than those observed in **55** and are comparable to those seen within the stacks of the 2,6-diesters (H···centroid = 2.67-2.74 Å, C-Ĥ···centroid = 133.5-139.1°). As with the phenyl 2,6-diester an extra contact is observed between one of the naphthyl protons and the carbonyl oxygen atom (contact i in Figure 61).

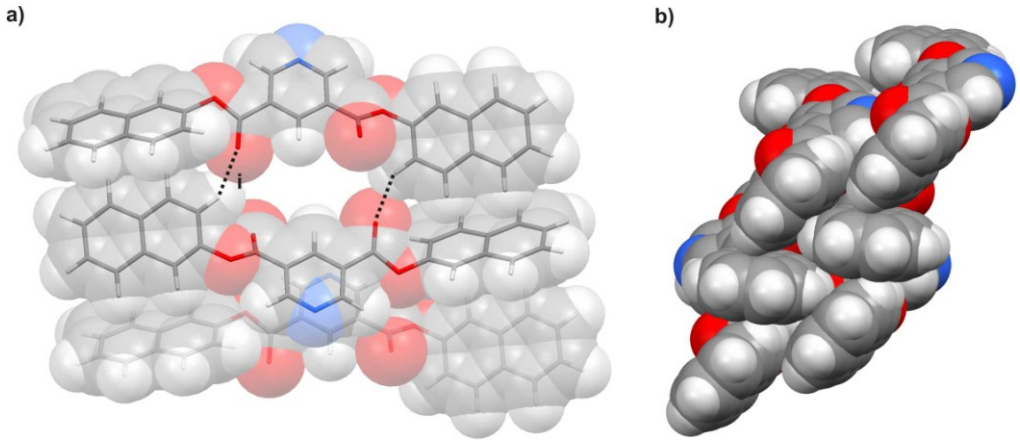

*Figure 61: (a) Front and (b) side views of a stack formed by the tapes of the 2-naphthyl diester (**54**). The C-H···O close contact is shown by black dashed lines (contact i: H···O = 2.33 Å, C-Ĥ···O = 148.1°, C=Ô···H = 153.7°).*

Like its 2,6-analogue the (9-anthryl)methyl 3,5-diester (**59**) also forms edge-to-face interactions along the short edge of the anthracene ring (Figure 62). The length of the C-H···centroid contacts indicate the presence of genuine C-H···π interactions (H···centroid = 2.62 Å, C-Ĥ···centroid = 142.1-143.9°).

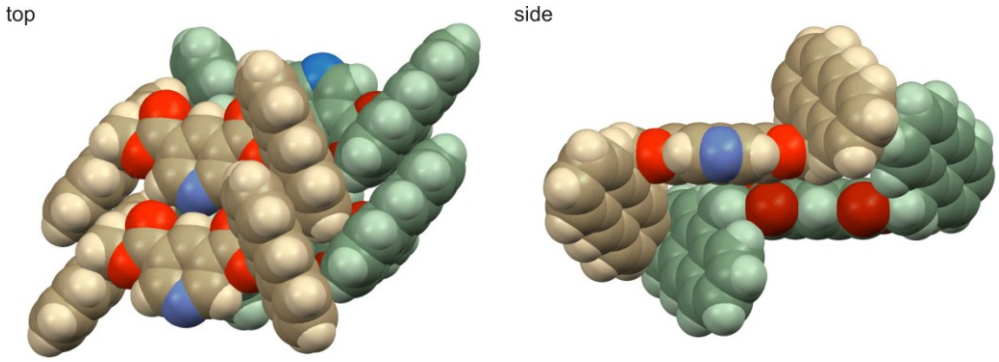

*Figure 62: Space-filling views of a stack formed by the (9-anthryl)methyl 3,5-diester (**59**).*

The assembly of the dimer "tapes" formed by the (1-naphthyl)methyl diester (**58**) is primarily the result of close-packing (Figure 63) although a couple of edge-to-face close contacts are observed (H···C = 2.84-2.97 Å, C-Ĥ···C = 135.9-162.4°).

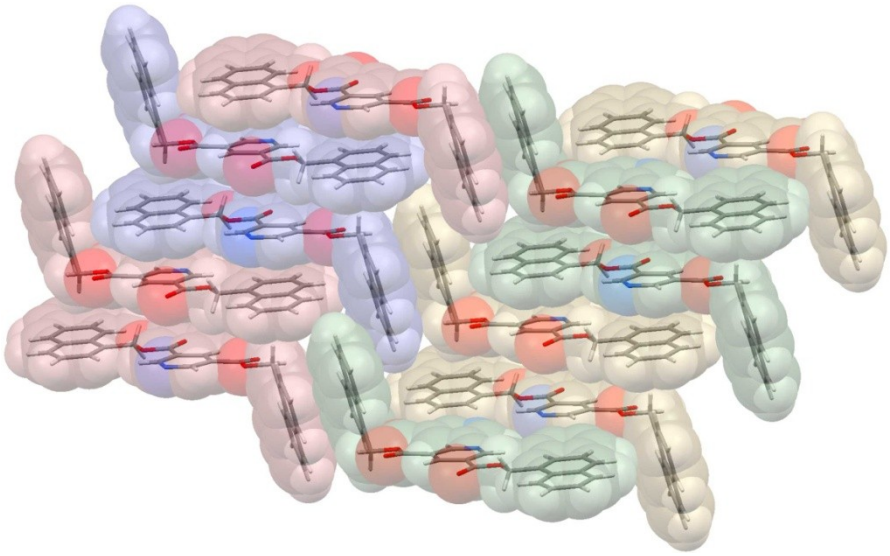

*Figure 63: Solid-state assembly formed by the (1-naphthyl)methyl 3,5-diester (**58**) viewed along the line of the dimer "tapes" showing close packing. Dimers are differentiated by coloured tinting.*

3.3.3- Conclusions

The formation of tape-like assemblies mediated by a triple hydrogen bond motif is less common for the 3,5-pyridinedicarboxylates than for their 2,6-analogues. Where conventional tapes are formed, like the 2,6-diesters, stack formation is influenced by edge-to-face interactions between the aromatic side-arms.

3.4 - Conclusions and further work

Both the 2,6- and 3,5- diesters show tape-formation with relatively large polyaromatic substituents, although a general observation has been that increasing the size of the substituent has had an adverse effect on the solubility of the samples. Whether a tape is formed in the solid-state appears to be more dependant on the orientation of the substituent relative to the pyridine core and this is in turn dependant on both the length of the alkyl spacer and the point of attachment to the aromatic substituent.

Attachment of the aromatic side-arm via the 2-position appears to have the smallest effect on solid-state behaviour compared to the benzyl derivatives. In contrast, attachment of the spacer to the 1- or 9-positions of the aromatic group forces the substituent to rotate out of the plane of the pyridyl ring. In some instances this has been found to disrupt the formation of a conventional tape-like assembly, particularly for the diesters where there is no alkyl spacer between the ester functionality and the aromatic substituent.

Once again the triple hydrogen bond synthon has been shown to be more robust for the diesters with a 2,6-substituted core than their 3,5-analogues.

Current investigations have been limited to extending the length of the polyaromatic side-arm. Further investigations with larger groups such as pyrene would enable the effect on tape formation of changing the width as well as the length of the substituent to be examined. Investigations with anthracene attached at the 1- and 2- positions would also be worthwhile to verify the trends observed with the naphthalene derivatives.

4 - Comparison of the solid-state behaviour of pyridine diesters with chloro- and methyl-substituted side-arms

4.1 - Introduction

Orton[91] has described the solid-state behaviour of pyridine diesters with 4-chlorobenzyl, 4-methylbenzyl and pentamethylbenzyl side-arms (**60**, **62**, **63**, **65**, **66**, and **68**). It was observed[91] that, in the solid-state, the conformation of the diesters with mono- and pentamethyl substituted side-arms (**60**, **62**) were significantly different. Whilst the aromatic ring of **62** was found to fold out of the plane of the pyridyl core, the side-arm of the 4-substituted derivative remained in the pyridyl plane. Orton noted that folding the pentamethyl side-arm removed the steric barrier to tape formation and that both derivatives formed comparable tape-like assemblies. For the 2,6-deriviatives, tessellation of the 4-methyl groups resulted in a similar packing mode for the tapes formed by both **60** and **62**. The packing of the tapes formed by the analogous 3,5-diesters (**63** and **65**) was also dominated by close packing between the substituents. However, changing the steric bulk of the side-arm from 4-methylbenzyl to pentamethylbenzyl was found to completely reverse the relative alignments of adjacent tapes (from PS↑↑L↑↑ in **63** to PS↑↓L↑↓ in **65**).

In the present study, it was decided to prepare the 2,6- and 3,5-diesters with a 2,4,6-trimethylbenzyl sidearm (**61** and **64**) as an intermediate case between Orton's[91] two extremes of fully substituted and mono-substituted.

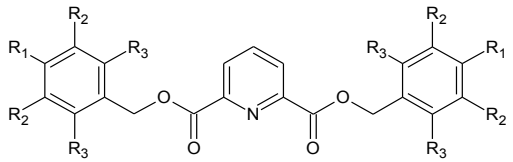

R_1 = Me, R_2 = R_3 = H **60**[95]
R_1 = R_3 = Me, R_2 =H **61**
R_1 = R_2 = R_3 = Me **62**[91]

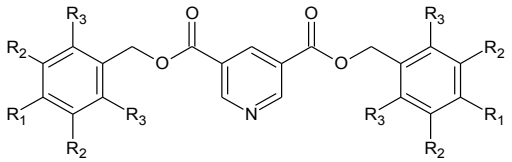

R_1 = Me, R_2 = R_3 = H **63**[91]
R_1 = R_3 = Me, R_2 =H **64**
R_1 = R_2 = R_3 = Me **65**[91]

As was mentioned in Chapter 1, although chloro and methyl groups are comparable in terms of their crystallographic volume, they have very different effects on how molecules pack in the solid-state. When Orton[91] compared the solid-state behaviour of the 4-chlorobenzyl diesters (**66** and **68**) to those of the 4-methylbenzyl diesters (**60** and **63**), he found that the tapes formed by the chlorinated esters adopted a herringbone packing motif rather than the planar motif observed for the methyl analogues. To date, no other chlorinated aromatic diesters have been examined and it was decided to attempt the synthesis and characterisation of the 2,6- and 3,5-diesters with a 2,4,6-trichlorobenzyl side-arm (**67**, **69**) to see how their behaviour compared with that of the methyl analogues.

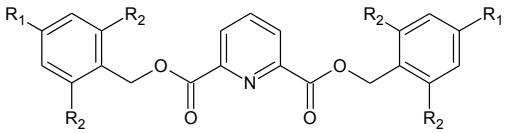

R_1 = Cl, R_2 = H **66**[92]
R_1 = R_2 = Cl **67**

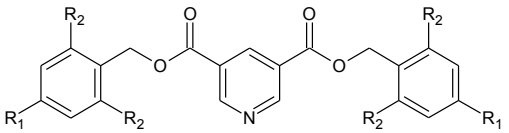

R_1 = Cl, R_2 = H **68**[91]
R_1 = R_2 = Cl **69**

4.2 - Synthesis

The novel diesters with 2,4,6-trisubstituted benzyl side-arms (**61**, **64**, **67**, **69**) were synthesised from the appropriate benzyl alcohol and the corresponding *bis*-acid chloride (Scheme 3).

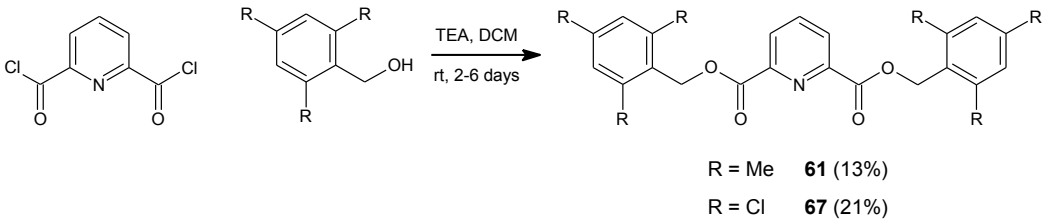

*Scheme 3: Synthetic route to the diesters with 2,4,6-trimethylbenzyl and 2,4,6-trichlorobenzyl side-arms (**61**, **64**, **67** and **69**).*

4.3 - Comparison of the solid-state behaviour of the 2,6-diesters formed with substituted aromatic side-arms

Crystals of **61** and **67** were grown from DCM. As was observed for the 4-methyl and 4-chlorobenzyl derivatives (**60**[95] and **66**[92]), the chlorinated compound (**67,** mpt = 220-223 °C) was found to have a higher melting point than the methylated analogue (**61**, mpt = 120-123 °C). Interestingly the melting point of **61** was found to be significantly lower than that of the previously characterised methylated diesters (**60**[95] and **62**,[91] mpt = 149 and 244 °C respectively).

4.3.1 - Primary assemblies

Both the trimethyl and the trichloro diesters were observed to form tape-like assemblies mediated by the expected triple hydrogen bond motif. The primary assembly parameters for these novel compounds are presented in Table 19 alongside those for the previously characterised materials.

Table 19: Primary assembly parameters for the tape-like assemblies formed by the 2,6-diesters with chloro- or methyl-substituted benzyl side-arms.

	R	r_1/Å	r_2/Å	θ/°	ϕ/°	ϑ/°	ψ/°
60[95]	4-Me	2.56	2.50	180.0	164.6	123.7	24.7
61	2,4,6-Me	2.43	2.50	180.0	143.0	126.5	67.5
62[91]	2,3,4,5,6-Me	2.55	2.46	180.0	169.6	127.6	64.4
66[92]	4-Cl	2.63	2.65	180.0	150.5	128.5	23.6
67	2,4,6-Cl	2.44	2.46	180.0	161.2	132.0	73.8

Whilst Orton[91] observed that the tapes formed by the derivatives having 4-methylbenzyl and pentamethylbenzyl side-arms (**60** and **62**) were comparable to each other, the C-H···N (r_1) contact of the tape formed by the 2,4,6-trimethyl analogue (**61**) is notably shorter than that seen for **60** or **62**.

The fold angles (ψ) for the tri- and pentamethyl derivatives (**61** and **62**[91]) are comparable with each other, and both are significantly larger than that observed for the 4-methyl analogue **60**.[95] This indicates that it is the

increased steric bulk at the *ortho* position of the phenyl ring that acts as an inhibitor to tape formation when the side-arm is coplanar with the pyridine core. As Orton[91] observed, this can be alleviated by folding the substituent out of the plane of the core.

Within the tapes of both the tri- and pentamethyl substituted derivatives (**61** and **62**[91]) there is evidence of C-H···π type contacts between the side-arms of molecules in the same tape. The methyl groups of one molecule are observed to overhang the phenyl ring of a neighbour; in **61** (Figure 64a) one of the protons is directed towards a single carbon atom and a clear close contact is observed (H···C = 2.70 Å, C-Ĥ···C = 160.6°).

The contacts between neighbouring molecules of the pentamethyl analogue (**62**[91]) are less distinct. The methyl proton appears to form a η^2 contact (Figure 64b, for clarity only the shorter contact of each pair is shown, the second contact is approximately 0.1 Å longer) and, although the contacts for **62** are longer than the sum of the van der Waals radii, examination of the Hirshfeld surface suggests that they are real but weak.

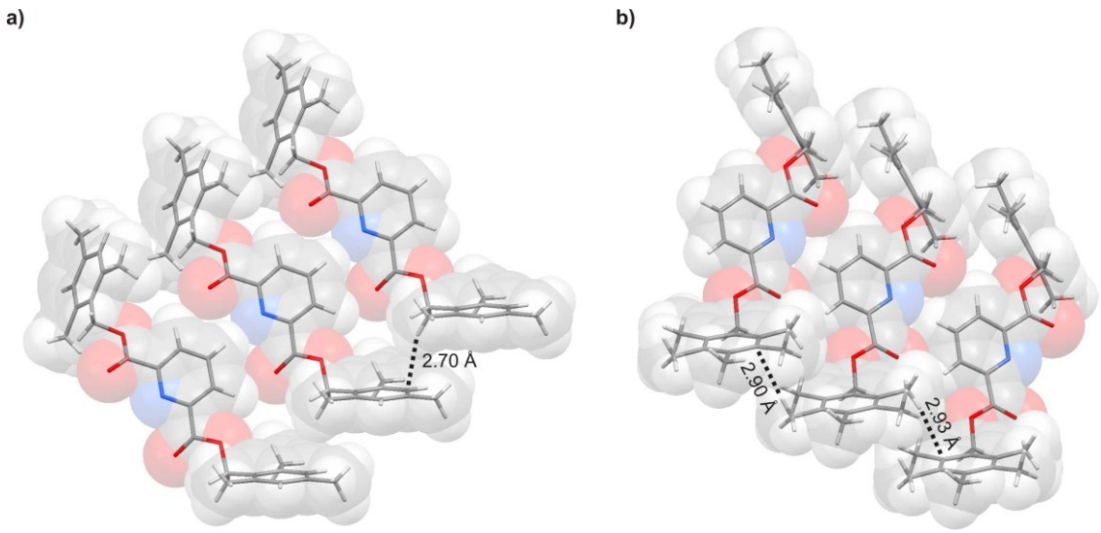

*Figure 64: Intra-tape contacts between neighbouring molecules within tapes formed by the (a) trimethylbenzyl, and (b) pentamethylbenzyl 2,6-diesters (**61** and **62**[91]); only the shorter contact of each pair has been shown for **62**, the second contact is approximately 0.1 Å longer.*

Whilst replacement of the methyl group by a chloro group results in a lengthening of the C-H···O and C-H···N contact distances for the tapes formed with a 4-substituted benzyl side-arm (**60**[95] and **66**[92]), the contact distances in the tapes formed by the trimethylbenzyl (**61**) and trichlorobenzyl (**67**) derivatives are comparable to each other. Consequently the lengths of the triple contact for **67** are significantly shorter than those observed for **66**.[92] As with the trimethyl and pentamethyl derivatives, the trichlorobenzene ring of **67** is found to fold out of the plane of the pyridine core. However, the angle of folding (ψ) is greater for **67** that for any of the methyl derivatives and this may be attributable to the increased proximity of the adjacent pyridine cores.

The reason for the closer contact between the cores is unclear. Examination of the Hirshfeld surface indicates that there may be a weak interaction between the CH_2 spacer and the phenyl ring (Figure 65) but the geometry of the interaction is far from ideal (the alkyl proton only just overlaps the phenyl ring and the closest H···C contact is 3.31 Å with a C-Ĥ···C angle of 134.3°). Consequently if the suggested contact does exist it is unlikely to be strong enough to explain the contraction of the tape.

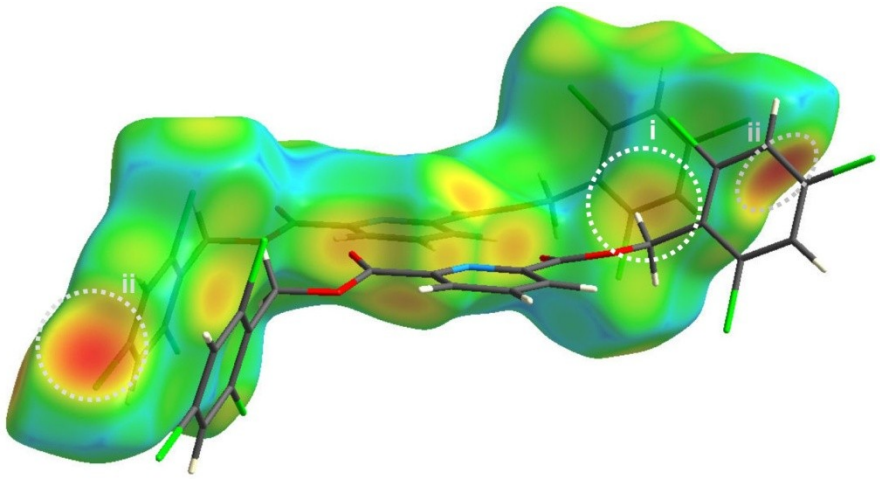

*Figure 65: Hirshfeld surface for the trichlorobenzyl 2,6-diester (**67**) showing the suggested close contact between the CH_2 spacer and the phenyl ring (indicated by a broken white circle, marked i). The surface colouring indicates the distance from the surface to the nearest external atom (d_e), the shortest contacts are shown in red and the longest in blue (the dark red areas, indicated by broken grey circles marked ii, correspond to C-H···Cl close contacts).*

4.3.2 - Secondary architecture of the methylated derivatives

In analysing the packing behaviour of the 4-methyl and pentamethyl derivatives (**60**[95] and **62**[91]), Orton[91] noted that packing was determined by tessellation of the side-arms (particularly of the 4-methyl group). Thus it is not entirely surprising to see that the trimethylbenzyl analogue (**61**) also packs with a $PS_{\uparrow\downarrow}L_{\uparrow\uparrow}$ pattern (Table 20). What is surprising is that the spacing of layers within a stack (S_S) is more than double that seen for the other compounds.

Table 20: Secondary assembly parameters for tape-like assemblies of the 2,6-diesters with methyl-substituted aromatic side-arms.

	Substitution pattern	Assembly	S_S/Å	S_T/°	T_O/°
60[95]	4	$PS_{\uparrow\downarrow}L_{\uparrow\uparrow}$	3.35	50.0	49.5
61	2,4,6	$PS_{\uparrow\downarrow}L_{\uparrow\uparrow}$	7.04	39.5	77.9
62[91]	2,3,4,5,6	$PS_{\uparrow\downarrow}L_{\uparrow\uparrow}$	3.05	36.1	59.5

In stacks of both the mono- and pentamethyl diesters (**60**[95] and **62**[91]), adjacent layers of tapes are observed to be offset with respect to each other so that the bulk of the molecule overlaps that of its neighbour. The side-arms of adjacent tapes are observed to be angled in an edge-to-face manner (Figure 66a-b) and analysis of the Hirshfeld surface shows the alkyl protons of the molecules in one-tape to be sited over the centres of the aromatic side-arms of the molecules in an adjacent layer (Figure 66c-d).

In contrast, adjacent tapes of the trimethylbenzyl analogue (**61**) are slipped so that the side-arms of tapes in one layer are sited above and below the pyridine cores of tapes in a neighbouring layer. Close contacts are observed between the pyridine ring and both the aromatic and methyl protons (Figure *67*). As a consequence of this different mode of interaction, the side-arms of molecules in adjacent tapes lie coplanar with an interplanar separation of 3.75 Å. This unexpected geometry of interaction explains the large value of S_S although why this mode of assembly is adopted is still not clear.

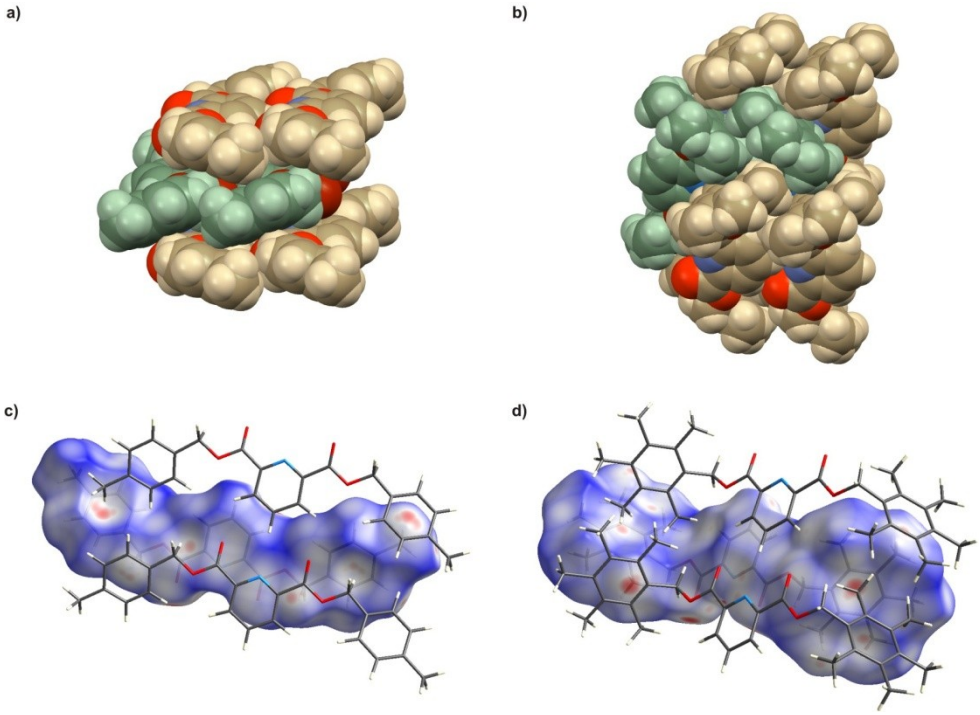

*Figure 66: (a & b) Side-on views showing the edge-to-face alignment of the side-arms in adjacent layers of the 4-methylbenzyl and pentamethyl benzyl 2,6-diesters (**60**[95] and **62**[91]) respectively; for clarity alternate layers have been shaded green and gold. (c & d) Looking down onto tapes of **60**[95] and **62**[91] respectively; a Hirshfeld surface is shown for the molecule in the lower layer (the surface is coloured so that short contacts are shaded red and longer contacts blue).*

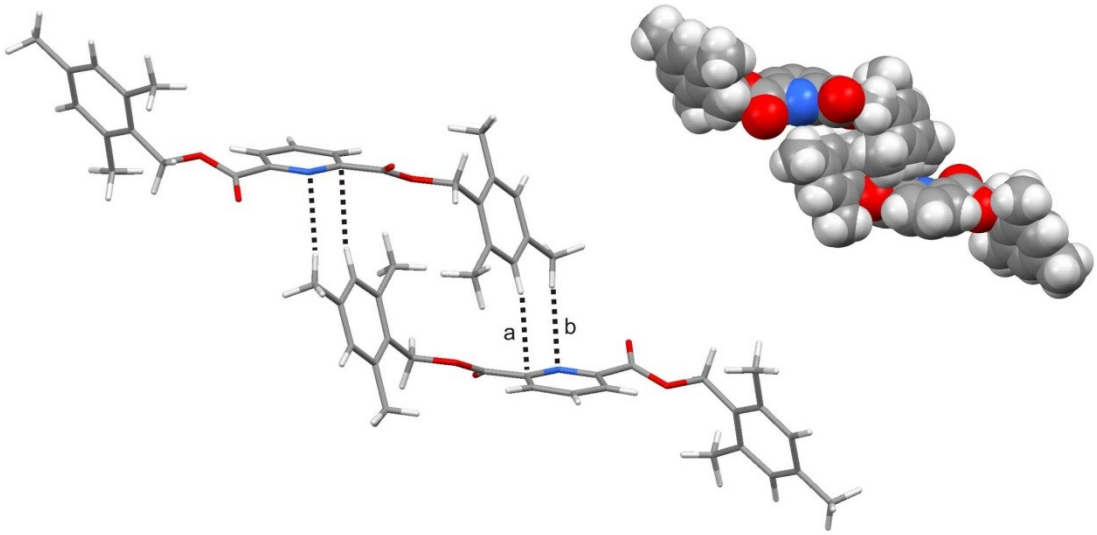

*Figure 67: View along the direction of the tapes formed by the trimethylbenzyl 2,6-diester (**61**) showing the face-to-face, interlocking arrangement of the side-arms of molecules in adjacent tapes within a stack. Close contacts between the protons of the side-arm and the skeleton of the pyridine core in an adjacent layer are shown by broken lines (contact a: H···C = 2.83 Å, C-Ĥ···C = 160.0°; contact b: H···C = 2.73 Å, C-Ĥ···C = 167.4°).*

Whilst the packing of the mono- and pentamethyl tapes (**60** and **62**) within a layer is directed by tessellation of the side-arms,[91] the packing of tapes within layers of the trimethylbenzyl diester (**61**) results in the side-arms of adjacent tapes being aligned in an edge-to-face geometry (Figure 68). A single close contact is observed between a methyl proton of one molecule and the benzyl ring of a neighbouring molecule. However, it is unclear whether the alignment of tapes in the layer is the result of C-H···π interactions or whether, like **60** and **62**, close-packing is the dominant force.

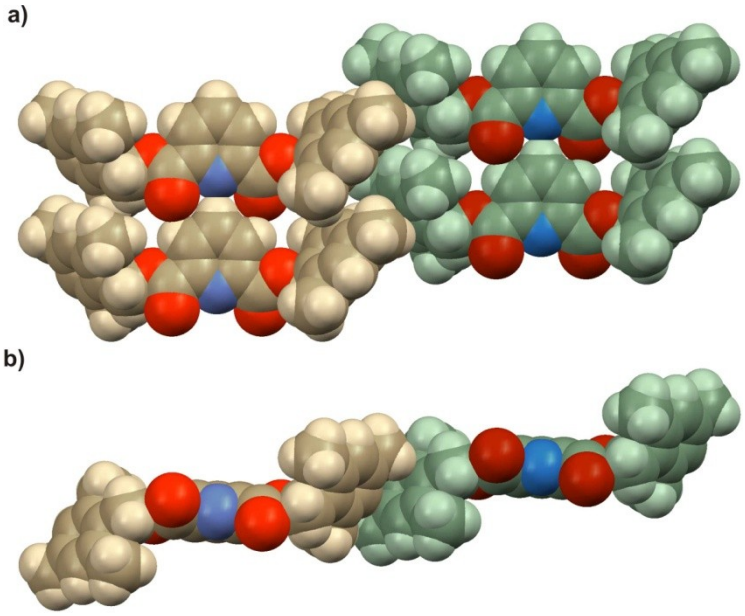

*Figure 68: (a) Top and (b) side views of a layer formed by the trimethylbezyl 2,6-diester (**61**) showing the edge-to-face geometry of the side-arms; tapes have been shaded green and gold for clarity.*

4.3.3 - Secondary architecture of the chlorinated derivatives

Although the interactions between tapes of the trimethyl derivatives are different to those of the mono- and pentamethyl analogues, the overall packing mode is the same. In contrast, the packing of the trichlorobenzyl derivative (**67**) is significantly different to that of the 4-chlorobenzyl analogue (**66**[92]), adopting a parallel rather than a herringbone packing mode (Table 21). Despite this apparently large difference, certain similarities can be seen between the packing behaviours of the two systems.

Table 21: Secondary assembly parameters for tape-like assemblies of 2,6-diesters with chloro-substituted aromatic side-arms.

	Substitution Pattern	Assembly	S_S/Å	S_T/°	T_O/°
66[92]	4	$HS_{\uparrow\uparrow}L_{\uparrow\downarrow}$	3.57	50.0	90.0
67	2,4,6	$PS_{\uparrow\uparrow}L_{\uparrow\downarrow}$	6.32	36.8	63.7

Stacks of the 4-chlorobenzyl diester (**66**[92]) are slipped perpendicular to the tape direction, allowing the chlorine atoms of the molecules in one layer to sit over the centre of the phenyl rings in adjacent layers (Figure 69a). Within stacks of the trichlorobenzyl analogue (**67**), the tapes of adjacent layers are also offset so that the 4-chloro group is sited over the centre of an adjacent aromatic ring. However, owing to the folded conformation of the side-arms, the chlorine atoms are found to sit over the centre of the pyridine rather than the benzene ring (Figure 69b). Examination of the Hirshfeld surface shows no evidence of a specific interaction between the chlorine atom and the π-cloud and it is assumed that the observed alignment is likely to be the result of close packing and minimisation of the repulsive forces between the electrons of the chlorine atom and the π-cloud.

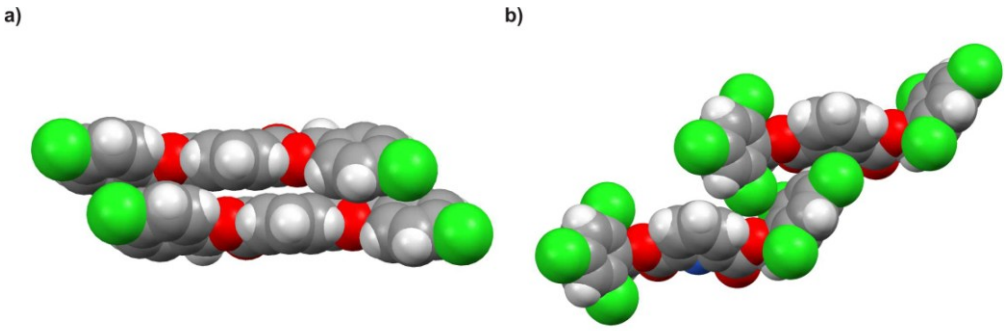

Figure 69: Space filling views along the direction of the tape for (a) the 4-chlorobenzyl[92] *and and (b) the trichlorobenzyl 2,6-diesters (**66** and **67**), showing alignment of the 4-chloro substituent over the centre of the phenyl or pyridyl aromatic ring respectively. Cl···centroid = 3.62 and 3.32 Å for **66** and **67** respectively.*

Whilst the side-arms of adjacent molecules are aligned coplanar with each other in the trimethyl derivative (**61**), in the chlorinated analogue (**67**) an interplanar angle of 66.2° is observed. The C-Cl bond is directed towards the carbon of the CH_2 spacer, minimising the electrostatic interactions between the two groups.

Whilst Orton[91] has observed that the interactions between layers of the 4-chlorobenzyl diester (**66**) are a result of type II inter-halogen contacts, the packing of layers of the trichloro-analogue (**67**) is best described as being mediated by H···Cl interactions (Figure 70a-b, H···Cl = 2.81 Å, C-Ĥ···Cl = 168.3°, H···Ĉl-C = 110.4°). The angles of interaction around both the hydrogen and chlorine atoms correlate with those expected for an interaction directed by electrostatic forces between those two centres. Although the H···Cl contact is found to be slightly longer than the sum of the Bondi van der Waals radii (Cl = 1.77 Å, H = 1.00 Å),[56] examination of the Hirshfeld surface (Figure 70c) indicates the existence of a strong contact.

However, as has been discussed in Chapter 1, the evidence for C-H···Cl-C hydrogen bonds is weak at best and it is equally possible that the observed close contacts are simply the result of close packing between the substituents. The side-arms of adjacent tapes in a layer are coplanar with each other (Figure 70c, interplanar separation = 3.39 Å) and the anti-parallel alignment of adjacent tapes means that the chlorine atoms of facing rings are staggered, reducing the repulsion between them.

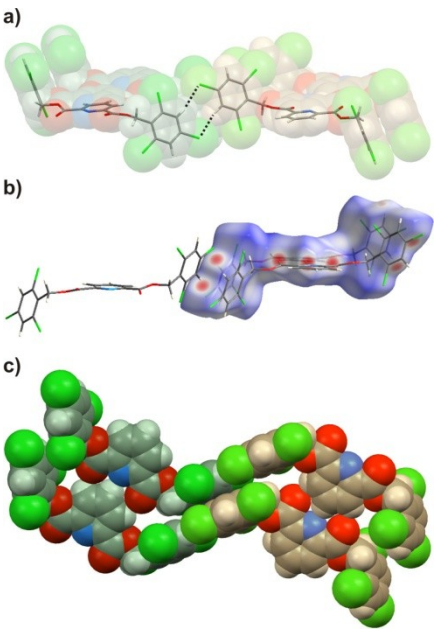

*Figure 70: Layers formed by tapes of the trichlorobenzyl 2,6-diester (**67**): (a) view along the direction of the tapes with C-H···Cl-C close contacts shown by dashed lines; (b) view along the direction of the tapes showing the Hirshfeld surface evidence for an H···Cl interaction; (c) view from above the plane of the tapes showing the coplanar alignment of adjacent side-arms;.*

4.3.4 - Conclusions

The primary assembly of the 2,6-pyridinedicarboxylates with aromatic side-arms appears largely unaffected by chloro-methyl exchange, indicating that the hydrogen bonding interactions responsible for directing tape formation are isolated from the electronic characteristics of the substituent. However, chloro-methyl exchange is observed to have an effect on the secondary assembly of the tapes, reflecting the differences in the electronic characteristics of the substituents.

Altering the degree of substitution on the aromatic side-arm also has a notable effect on the secondary assembly of the tapes, especially for the chlorinated derivatives. However, closer examination suggests that close packing of the substituents is important in determining the secondary assembly of all of the systems, and it seems likely that the observed differences in behaviour can be attributed to changes in the steric bulk and anisotropy of the substituent groups.

4.4 - Comparison of the solid-state behaviour of the 3,5-diesters formed with substituted aromatic side-arms

Crystallisation of the trimethylbenzyl diester (**64**) from acetonitrile and the trichlorobenzyl diester (**69**) from toluene resulted in the formation of needle-like crystals for both samples. Whilst X-ray structural data was obtained relatively easily for **64**, crystals of **69** were found to be poorly diffracting and data was collected by the EPSRC NCS using the high-flux source at the Diamond synchrotron.

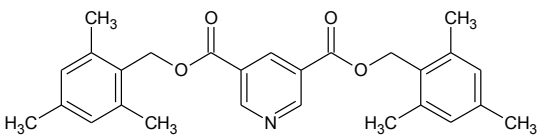

64

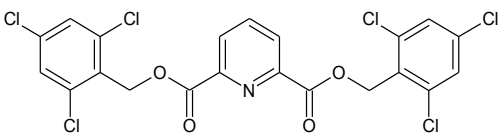

69

Whereas the 3,5-diesters with 4-chlorobenzyl (**68**),[91] 4-methylbenzyl (**63**)[91] and pentamethylbenzyl (**65**)[91] side-arms were found to form conventional tape-like assemblies, neither of the tri-substituted analogues behaved in a similar manner. Rather than the standard conformer, both of the side-arms of the trimethylbenzyl diester (**64**) are inverted (Figure 71a), and one of the ester groups of the chlorinated analogue (**69**) is found behave similarly (Figure 71b).

a) **b)**

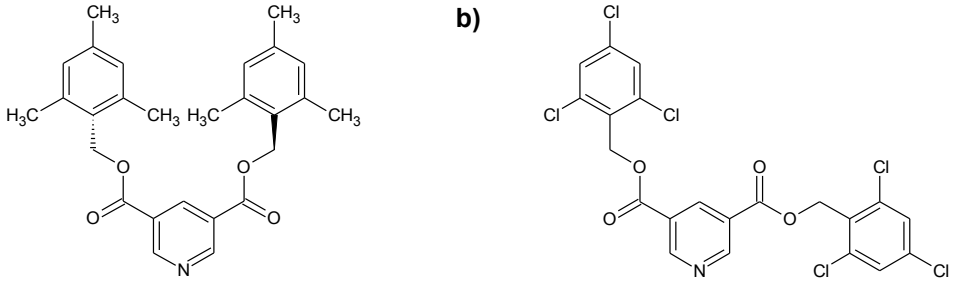

64 **69**

*Figure 71: Conformers observed in the solid-state for the 3,5-diesters formed with (a) trimethylbenzyl and (b) trichlorobenzyl sidearms (**64** and **69**).*

Whilst the side-arms of other dicarboxylates previously observed to adopt the fully inverted conformation are arranged parallel to each other in a pincer-like geometry[91] (see Figure 30 in Chapter 1), the side-arms of the trimethylbenzyl 3,5-diester (**64**) rotate away from each other to sit above and below the plane of the pyridine core (Figure 72a). Molecules are observed to form a corrugated two-dimensional sheet (Figure 72c-e) by a combination of C-H···O hydrogen bonds (shown as dashed lines in Figure 72c) and dispersive forces.

Orthogonal to the sheet, molecules of **64** are observed to form tessellated stacks (Figure 72b) with the pyridine and phenyl planes of one molecule coplanar with those of the molecules above and below them and separated by between 3.4 and 3.5 Å. Although close contacts are observed between one of the protons of the 4-methyl group and the 4-carbon of an adjacent phenyl group (C···H = 2.84 and 2.94 Å), they are most likely a consequence, rather than a cause of close packing.

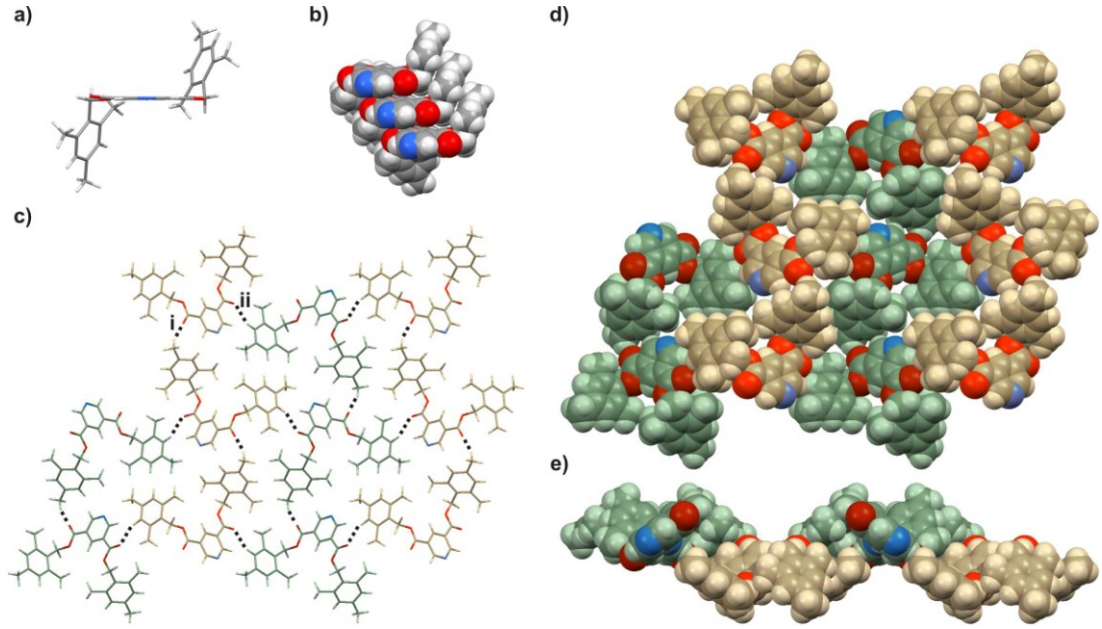

*Figure 72: (a) View along the pyridine plane of a single molecule of the trimethylbenzyl 3,5-diester (**64**) showing the orientation of the side-arms. (b)Space-filling view of a tessellated stack formed by **64**. (c) View along the a-axis of **64** showing the C-H···O contacts observed in the corrugated sheet (contact i: H···O = 2.49 Å, C-Ĥ···O = 154.9°, H···Ô=C = 176.4°; contact ii: H···O = 2.59 Å, C-Ĥ···O = 160.4°, H···Ô=C = 140.9°). (d) Space-filling representation of the sheet depicted in (c). (e) Side-on view of the corrugated sheet shown in (c) and (d).*

A complex array of interactions assemble molecules of the trichlorobenzyl analogue (**69**) into a three dimensional structure. To understand the interactions within the assembly, it helps to consider an individual stack of molecules. Stacks are formed along the *b*-axis of the crystal and can be compared to those of **64** in that the molecules lie parallel to each other with the aromatic rings separated by 3.4-3.5 Å.

Each stack is linked to two adjacent stacks by a pair of H···N interactions on one side and a pair of Cl···O contacts on the other (Figure 73a), forming a "block." Whilst the Cl···O contacts occur between discrete pairs of molecules, the N···H interactions bridge molecules in adjacent layers (Figure 73b).

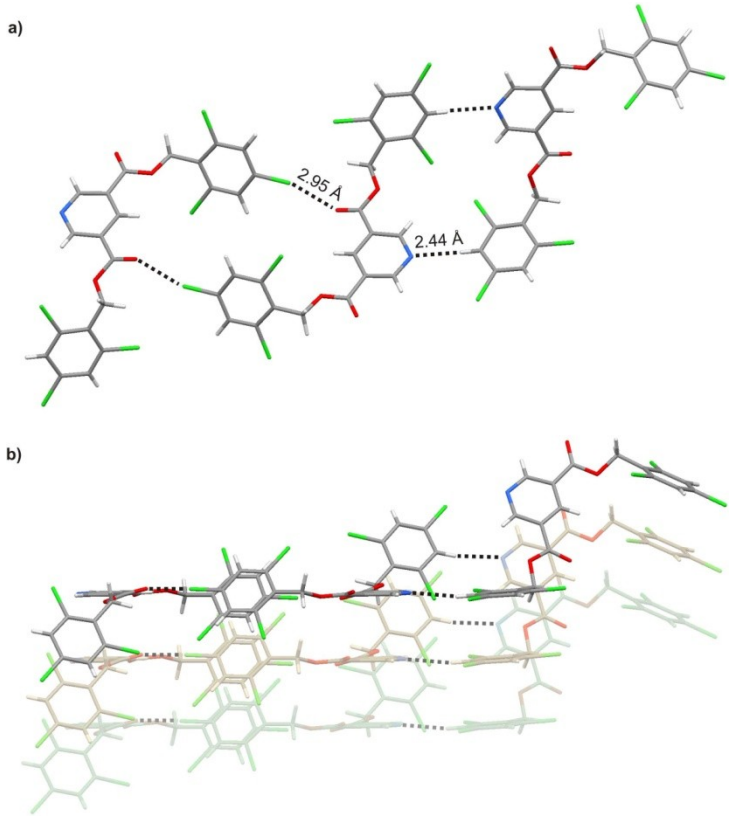

*Figure 73: (a) View down the b-axis showing pairs of Cl···O and N···H interactions formed between molecules of the trichlorbenzyl 3,5-diester (**69**); (b) side view showing how N···H interactions link different layers; the bottom layer is tinted green, the middle layer orange and the uppermost layer is untinted.*

The forces directing the assembly of blocks into the final packed structure are unclear. The Hirshfeld surface indicates the existence of C-H···O contacts between the carbonyl oxygen atoms and phenyl protons not involved in forming other interactions (Figure 74). However, these contacts are approximately the same length as the sum of the van der Waals radii and the angle of interaction about the carbonyl oxygen is not ideal (H···Ô-C = 176.9°). Consequently the observed contacts may simply be an artefact of close packing by dispersive forces.

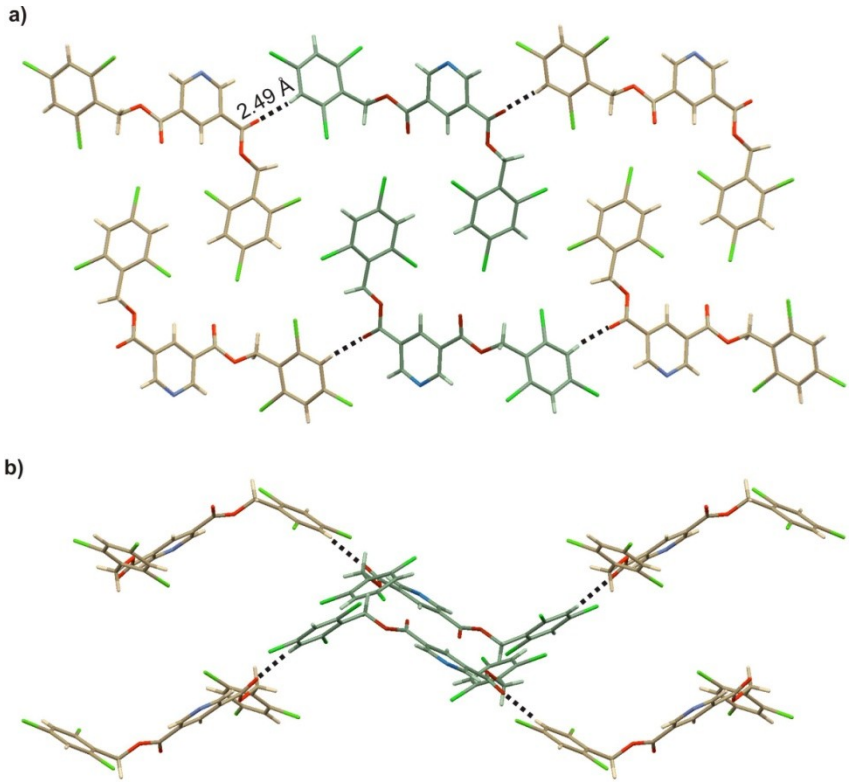

*Figure 74: (a) View down the b-axis showing three "blocks" of the trichlorobenzyl diester (**69**, tinted green and gold); (b) side view of the assembly shown in (a). For clarity, only a single layer of the green block has been shown and only molecules produced as a result of H···O interactions within that layer have been shown in the gold blocks. H···O interactions are shown by broken black lines (H···O = 2.49 Å, C-Ĥ···O = 170.1 Å, H···Ô=C = 176.9 Å).*

In summary, neither of the 3,5-pyridinedicarboxylates with a 2,4,6-substitued side-arms forms a conventional tape-like assembly. Instead, extended networks are formed with individual molecules linked by hydrogen and, in the case of **69**, halogen bonds.

4.5 - Solid-state behaviour of 3,5-diacetyl pyridine (73)

4.5.1 - Introduction

Grossel *et al.*[113] have described the structures of the acid chlorides (**70** and **71**). The synthesis of both of the corresponding dimethyl ketones (**72** and **73**) has been reported in the literature[114, 115] but the solid-state behaviour has only been published for the 2,6-derivative (**72**)[114]. Once again, these compounds provide a potentially attractive target for exploring the effect of chloro/methyl exchange on the solid-state behaviour of these pyridine derivatives.

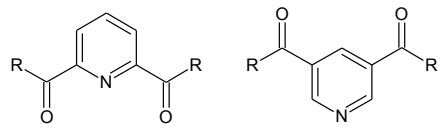

R = Cl **70** R = Cl **71**
R = Me **72** R = Me **73**

Neither the ketone (**72**)[114] nor the acid chloride (**70**)[113] form conventional tape-like assemblies, in both cases C-H···O=C hydrogen bonds favour the formation of molecular dimers (red dashed lines in Figure 75a and b). In the ketone further C-H···O=C hydrogen bonds (blue dashed lines in Figure 75a) link the dimers into ribbons (Figure 75c) which then pack with a herringbone pattern (Figure 75d). The dimers of the acid chloride also pack with a herringbone pattern. However, when viewed along the *a*-axis (Figure 75e), the packing motif is observed to be analogous to the sandwich packing of pyrene.[47]

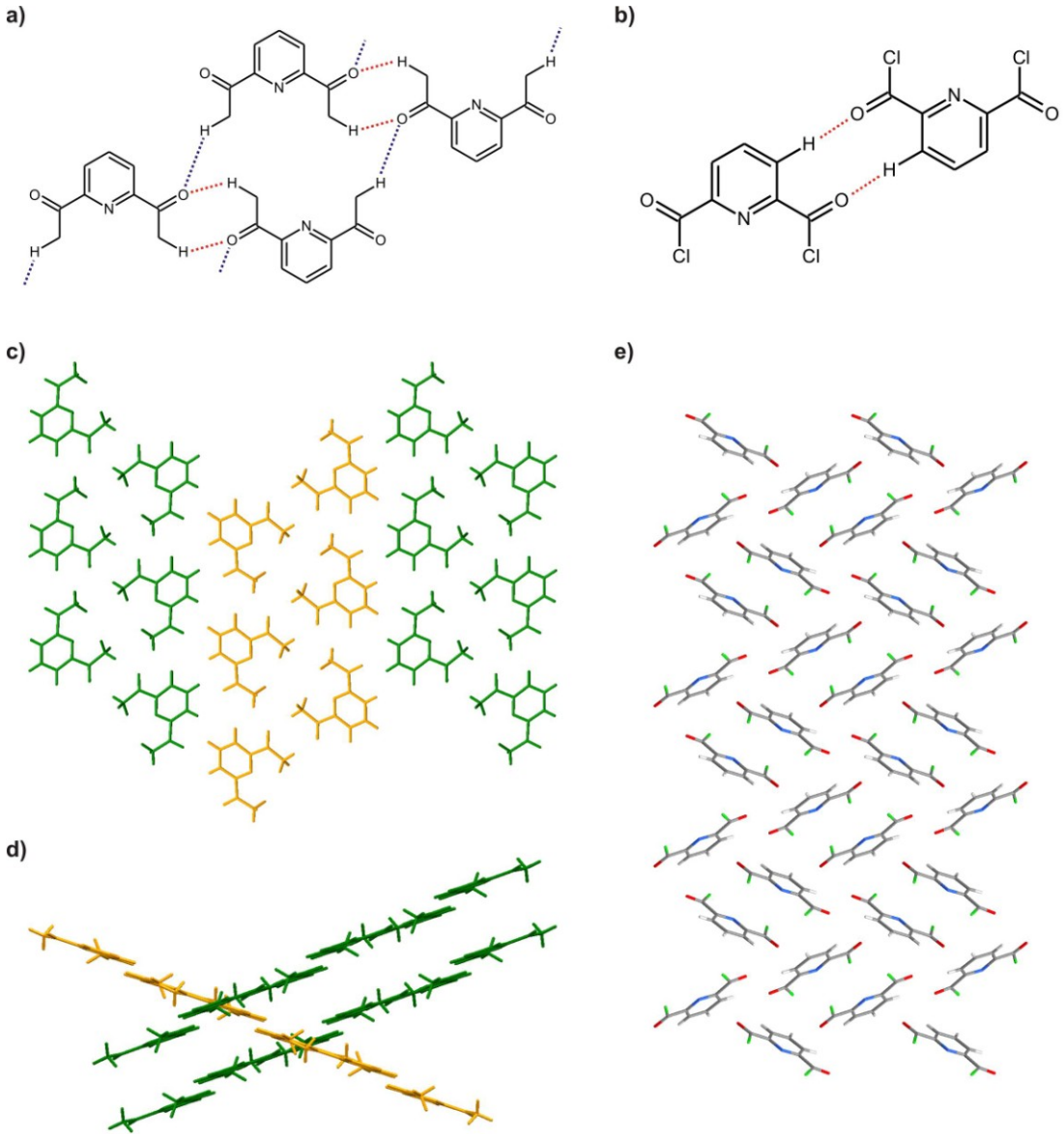

*Figure 75: (a) Hydrogen bonds forming dimers (red dashed lines) and ribbons (blue dashed lines) in the 2,6-dimethylketone (**72**);[114] (b) Hydrogen bonds forming dimers (red dashed lines) in the 2,6-bis(acid chloride) (**70**);[113] (c) view along the a-axis of **72**[114] showing three different ribbons (coloured green and yellow); (d) side view of the ribbons of **72**,[114] illustrating the herringbone pattern; (e) view along the a-axis of **70**[113] showing the sandwich-herringbone packing pattern.*

Unlike its 2,6-disubstituted analogue (**70**[113]), the pyridine-3,5-dicarbonyl dichloride (**71**[113]) was found to form a tape-like assembly mediated by a conventional triple hydrogen bond motif. In view of the difference in behaviour of the 2,6- and 3,5-acid chlorides, it was decided to synthesise and investigate the solid-state behaviour of the 3,5-dimethyl ketone (**73**).

4.5.2 - Synthesis

3,5-Diacetyl pyridine (**73**) was prepared following the procedure described by West *et al.*[115] (Scheme 4). Crystalline needles were grown from chloroform and light petroleum ether.

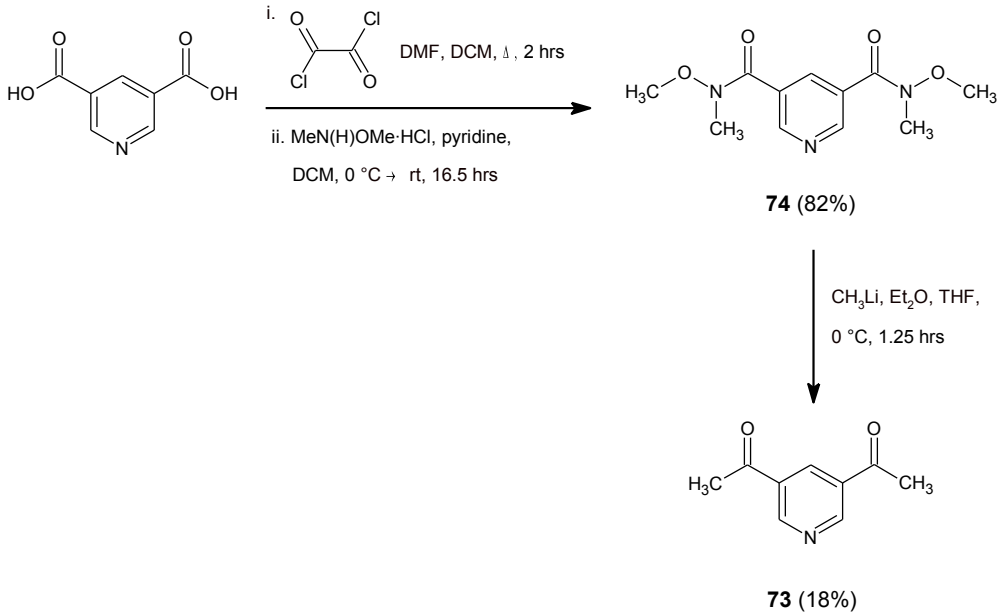

*Scheme 4: Synthetic route to 3,5-diacetyl pyridine (**73**).*

4.5.3 - Solid-state behaviour

Whilst the 3,5-acid chloride (**71**) forms a conventional tape,[113] the corresponding dimethyl ketone (**73**) does not. Instead a zig-zag tape is formed with adjacent molecules linked by pairs of either C-H···O or C-H···N hydrogen bonds (Figure 76, contacts i and ii). Further C-H···O interactions assemble these tapes into a slipped stack (Figure 76, contact iii). These stacks are found to pack in a herringbone pattern (Figure 77a) and close contacts are observed between the carbonyl oxygen atoms and methyl protons of molecules in adjacent sheets (Figure 77b, contacts iv and v).

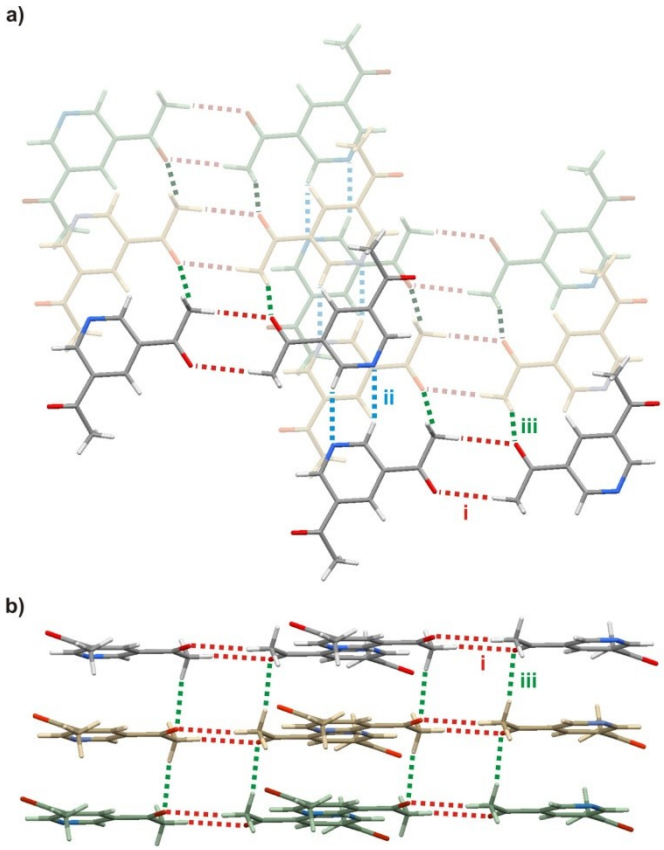

*Figure 76: Sheets of zig-zagged tapes formed by 3,5-diacetyl pyridine (**73**) viewed from: (a) above the tape looking down and; (b) from the side of the tape looking along the H···N contact. Layers have been tinted different colours to aid distinction and hydrogen bonding contacts are indicated by broken coloured lines: contact i (red) H···O = 2.57 Å, C-Ĥ···O = 174.9°, H···Ô=C = 129.2°; contact ii (blue) H···N = 2.54 Å, C-Ĥ···N = 155.1°; contact iii (green) H···O = 2.52 Å, C-Ĥ···O = 167.0°, H···Ô=C = 126.3°.*

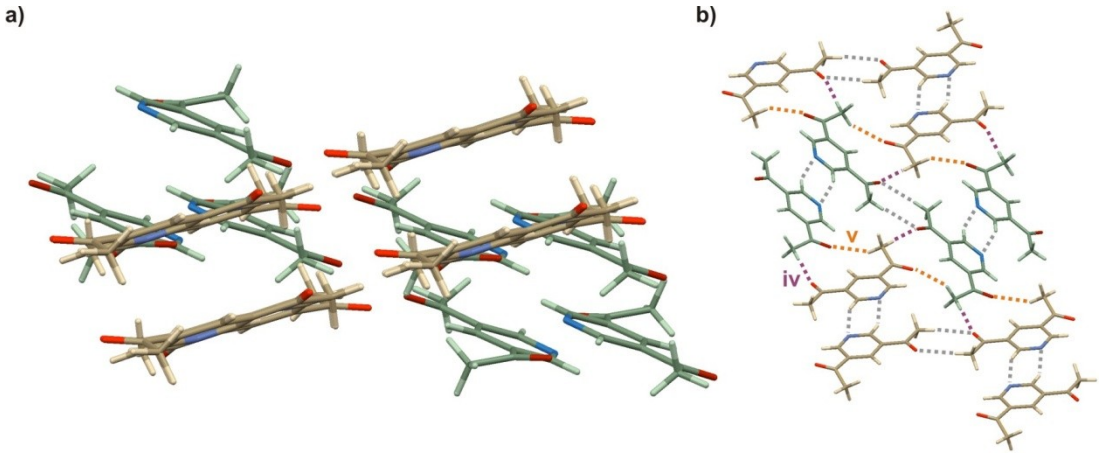

*Figure 77: (a) Side view of tapes formed by 3,5-diacetyl pyridine (**73**) showing the herringbone arrangement between them, anti-parallel tapes are distinguished by green and gold tinting; (b) top view showing intermolecular close contacts; grey dashed lines indicate hydrogen bonds between molecules in the same tape (see Figure 76), close contacts between sheets are shown as orange or purple dashed lines: contact iv (purple) H···O = 2.49 Å, C-Ĥ···O = 179.1°, H···Ô=C = 164.9°; contact v (orange) H···O = 2.64 Å, C-Ĥ···O = 152.0°, H···Ô=C = 160.5°.*

4.6 - Conclusions

The degree of substitution and the electronic characteristics of the substituent were observed to alter the conformations of individual molecules of the 2,6-diesters with substituted benzyl side-arms. None the less, all of the systems studied were found to form tape-like assemblies with a triple hydrogen bond contact and the packing of these tapes was largely influenced by tessellation of the side-arms and minimisation of repulsive forces.

The increased strength of the 2,6-synthon relative to that of the analogous 3,5-contact is observed by comparison of trimethylbenzyl and trichlorobenzyl 2,6- and 3,5-diesters. Whilst those with a 2,6-substituted core form tapes mediated by the triple bond synthon, one or both of the carboxylate groups of the 3,5-derivatives is seen to invert and these compounds prefer to form extended networks.

Inversion of one of the side groups is also seen for 3,5-diacetyl pyridine (**73**) which forms a sheet containing zig-zagged tapes assembled by two different double hydrogen bond motifs. The fact that the acid chloride (**71**) is observed to form a tape mediated by the triple hydrogen bond synthon could be a reflection of the different electronic characteristics of the molecule or simply a consequence of a lack of other hydrogen bond-donors to interact with the carbonyl oxygen and pyridyl nitrogen.

It has also been shown that, although the chloro and methyl groups are similar in terms of their crystallographic size, the differences in their electronic characteristics can dramatically alter the solid-state behaviour of otherwise analogous structures.

5 - Monoesters

5.1 - Introduction

Within our research group, Dwyer[94] has previously reported the crystal structure for 6-methoxycarbonyl-2-pyridinecarboxylic acid (**75**). In the solid-state this asymmetric system was found to form carboxylic acid dimers which then formed a tape-like assembly.

Unlike the corresponding diester (**38**) which crystallised as the *cis-cis* conformer, the monoester characterised by Dwyer[94] adopted the *cis-trans* conformation (Figure 78a). The dimers were observed to form a tape-like assembly but this was found to be mediated by a double, rather than a triple, hydrogen bond motif (purple lines in Figure 78a). Whilst the carboxylic acid groups were observed to lie in the plane of the tape, the pyridine rings were slightly rotated out of the plane (Figure 78b and c).

Although the synthesis of other monoesters has been reported in the literature,[116-121] the solid-state behaviour of these compounds has not, as yet, been determined. In light of the interesting interplay observed between the different supramolecular synthons in the crystal architecture of **75**, it was decided to investigate the solid-state behaviour of some other simple monoesters. The 2,6-ethyl and benzyl monoesters (**76** and **77**) were chosen as targets since both of the corresponding diesters form conventional tape-like assemblies in the solid-state. It was also decided to investigate the analogous 3,5-monoesters (**78** - **80**) to see what the effect of changing the substitution pattern around the pyridine core would be.

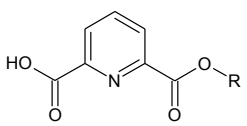

75	R = CH_3	(methyl)
76	R = CH_2CH_3	(ethyl)
77	R = CH_2Ph	(benzyl)

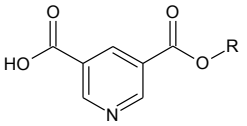

78	R = CH_3	(methyl)
79	R = CH_2CH_3	(ethyl)
80	R = CH_2Ph	(benzyl)

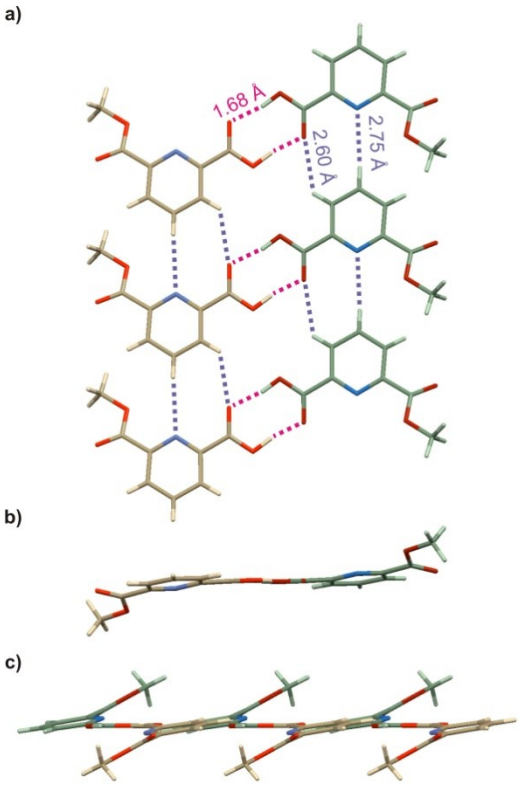

*Figure 78: Structure of the tape-like assembly formed by carboxylic acid dimers of the methyl 2,6-monoester (**75**),[94] molecules have been tinted green and gold for clarity. (a) View from above the tape showing the hydrogen bonds forming the carboxylic acid dimer (pink dashed lines) and the tape (purple dashed lines); (b) view along the direction of the tape and (c) side view of the tape showing the out-of-plane alignment of the pyridine cores.*

5.2 - Synthesis

Dwyer[94] synthesised the 2,6-methyl monester (**75**) by hydrolysis of the corresponding diester. The 3,5-isomer (**78**) and both ethyl analogues (**76** and **79**) were prepared using the same basic method; the reaction scheme for the synthesis of **76** is outlined in Scheme 5.

The benzyl-substituted monoesters (**77** and **80**) were synthesised directly from benzyl alcohol and the corresponding pyridinedicarboxylic acid using the procedure described by Reddy *et al.*[121] (shown for compound **77** in Scheme 6).

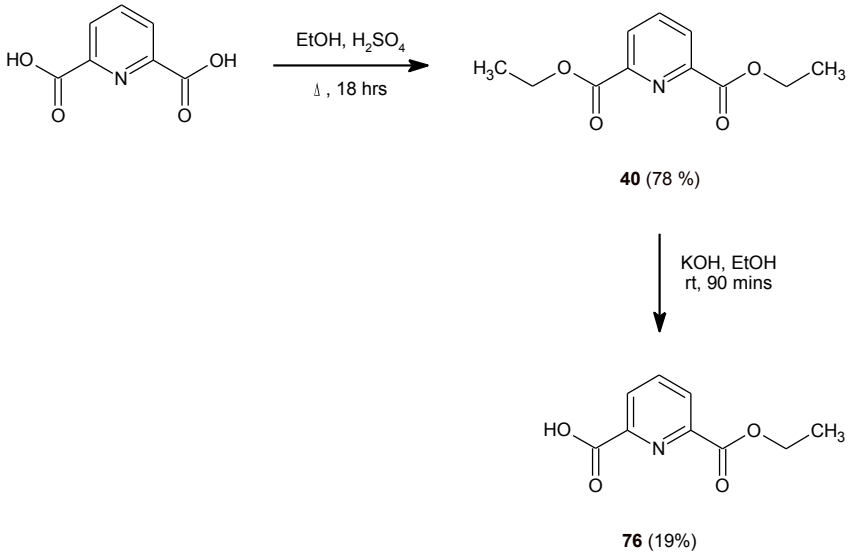

*Scheme 5: Outline of the synthetic route to 6-ethoxycarbonyl-2-pyridinecarboxylic acid (**76**); the same basic method was used to prepare the ethyl diesters (**78** and **79**).*

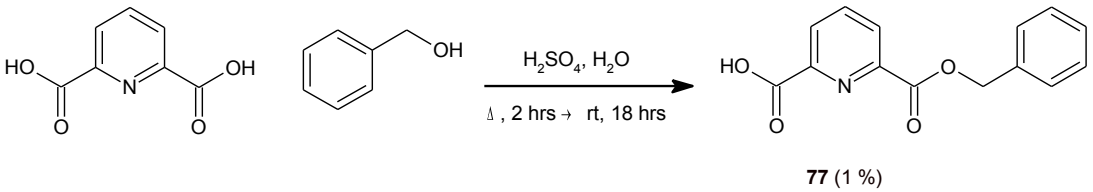

*Scheme 6: Outline of the synthetic route to 6-benzyloxycarbonyl-2-pyridinecarboxylic acid (**77**); the 3,5-isomer (**80**) was prepared in the same way.*

In all cases the crude reaction mixture was filtered to remove any diacid. Base was then added and any diester was removed by organic extraction. Finally the aqueous phases were carefully acidified and the target monoester was isolated by extraction into an organic solvent. The overall yield for total synthesis of the target compounds from the corresponding dicarboxylic acid was generally poor (Table 22).

*Table 22: Overall yields for synthesis of monoesters (**76**-**80**); the yield quoted is for the synthesis of the monoester from the corresponding pyridinedicarboxylic acid.*

	Pyridine substitution	Ester substituent	% Yield*
76	2,6	Ethyl	15
77	2,6	Benzyl	1
78	3,5	Methyl	27
79	3,5	Ethyl	3
80	3,5	Benzyl	22

5.3 - Solid-state behaviour of the 2,6-monoesters

Crystals of the ethyl monoester (**76**) were grown from toluene and light petroleum ether. The benzyl derivative (**77**) was crystallised from a mixture of toluene and chloroform. Whilst the unit cell of **76** contained one crystallographically unique molecule, the asymmetric unit of **77** was found to include both molecules of the carboxylic acid dimer.

5.3.1 - Primary assembly

In the solid-state, each of the 2,6-monoesters under discussion is observed to adopt a different conformation (Figure 79). As already mentioned, the methyl-monoester (**75**)[94] adopts the *cis-trans* conformer. The ethyl derivative (**76**) crystallises in the *cis-cis* conformation and the benzyl analogue (**77**) favours a *trans-cis* arrangement.

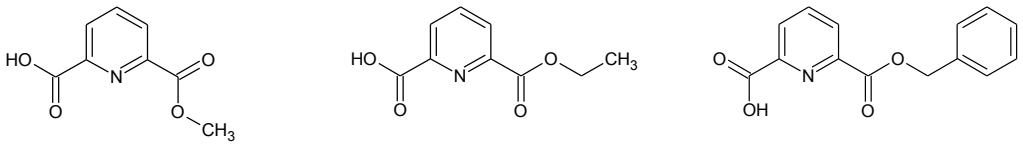

75[94] **76** **77**

cis-trans *cis-cis* *trans-cis*

*Figure 79: Conformational behaviour of the 2,6-monoesters (**75**-**77**).*

Like the methyl-monoester (**75**),[94] both the ethyl and benzyl derivatives are observed to form carboxylic acid dimers (Table 23). Since the molecules that form the dimer are crystallographically equivalent for the methyl and ethyl derivatives (**75** and **76**), the bond angles and lengths are the same for both O-H···O contacts. The contacts observed in the benzyl dimer (**77**) occur between two crystallographically distinct molecules and consequently the hydrogen bond parameters are subtly different from each other.

The H···O contacts of the benzyl monoester dimers (**77**) are also seen to be substantially longer than those seen for the methyl or ethyl derivatives but the O···O contact distances are similar in all three examples. One possible explanation for this is that the acidic protons in compound **77** (particularly for

the B-type molecules) are observed to rotate slightly out of the carbonyl plane.

Table 23: Bond lengths and angles for carboxylic dimers formed by the 2,6-monoesters.

	R		H···O/Å	O···O/Å	O···Ĥ-O/º	C=Ô···H/º
75[94]	Methyl		1.68	2.62	169.7	116.0
76	Ethyl		1.67	2.64	174.6	120.5
77	Benzyl	A	1.78	2.61	169.5	119.2
		B	1.81	2.62	162.3	120.0

The carboxylic acid dimers of the ethyl and benzyl monesters are also observed to form tape-like assemblies. However, whilst the methyl derivative only forms a double hydrogen bond, the tapes formed by the ethyl and benzyl derivatives are both mediated by a triple hydrogen bond motif. The tapes formed by the ethyl derivative are mediated by a "conventional" motif, comparable to that seen for the diesters. In contrast, in the benzyl derivative the hydrogen bond with the carboxylic acid group is formed to the hydroxyl, rather than the carbonyl, oxygen atom. A second, diagonal, close contact is also observed between the hydroxyl oxygen atom and the γ-proton of the pyridyl ring (orange lines in Figure 80).

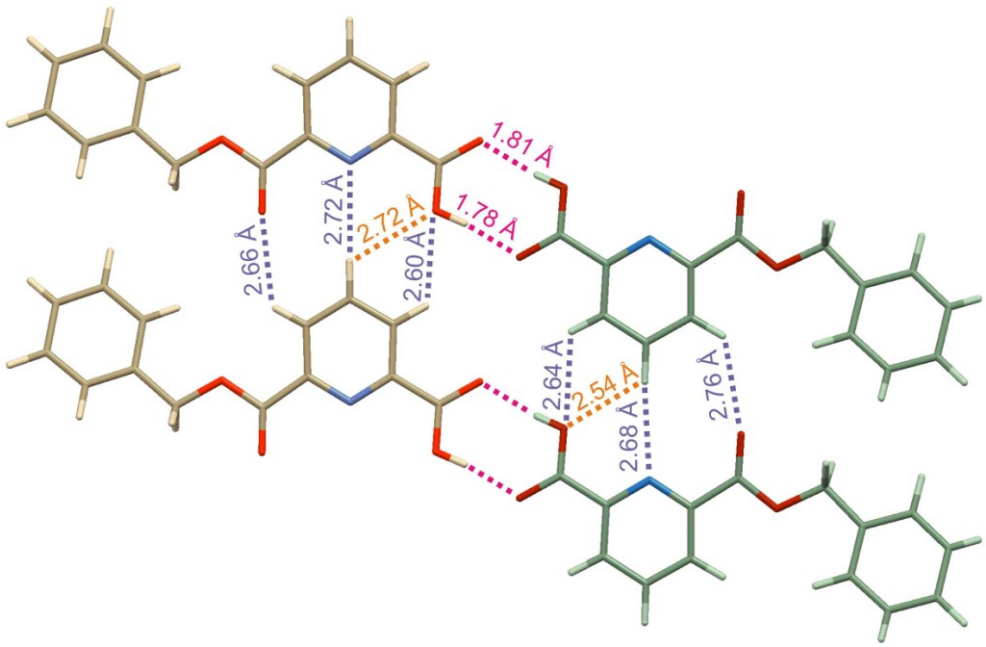

*Figure 80: Tape-like assembly formed by carboxylic acid dimers of the benzyl 2,6-monoester (**77**); A-type molecules are tinted gold and B-type, green. Dashed lines indicate hydrogen bonding interactions and are coloured pink for those forming carboxylic acid dimers and purple or orange for those forming the tape-like assembly.*

The contacts that direct the tape formation of the ethyl monoester (**76**) are notably shorter than those observed for the methyl or benzyl derivatives (Table 24). **76** is also the only compound that adopts a conventional *cis*-*cis* conformation, thus the longer contacts seen for **75** and **77** are likely to be a consequence of the inversion of the side-arms.

*Table 24: Primary assembly parameters for the 2,6-monoesters (**75**-**77**).*

	R		r_1/Å	r_2/Å	r_2'/Å	θ/°	ϕ/°	ϕ'/°	ϑ/°	ϑ'/°	ψ/°
75[94]	Methyl		2.75	-	2.60	159.0	-	168.7	-	127.9	-
76	Ethyl		2.61	2.56	2.55	178.2	166.9	165.5	126.5	125.2	-
77	Benzyl	A	2.72	2.66	2.60	174.7	169.9	174.8	126.2	125.2	13.9
		B	2.68	2.76	2.64	170.6	157.3	179.9	129.1	121.6	13.9

r_2, ϕ and ϑ parameters have been measured for contacts with the ester group.
r_2', ϕ' and ϑ' parameters have been measured for contacts with the acid group.

When the primary assembly parameters of the monoesters are compared with those of the analogous diesters (Table 25) it can be seen that the tape forming contacts of the ethyl monoester (**76**) are comparable with those of the analogous diester (**40**)[91]. The contact distances observed for the benzyl monoester (**77**) are significantly longer than those of the corresponding diester (**44**[92]), again this is attributed to the inversion of the acid group.

Although the tape-forming contacts of the methyl monoester (**75**[94]) are notably shorter than those of the diester (**38**[92]), it should be remembered that the two systems are not directly comparable. Whereas the methyl groups of adjacent "tapes" in the diester interdigitate, those of the monoester do not.

*Table 25: Primary assembly parameters for the 2,6-diesters (**38**, **40**, **44**).*

	R	r_1/Å	r_2/Å	θ/°	ϕ/°	ϑ/°	ψ/°
38[92]	Methyl	3.02	2.88	180.0	170.3	124.8	-
40[91]	Ethyl	2.58	2.53	180.0	160.5	127.8	-
44[92]	Benzyl	2.48	2.48	180.0	163.8	127.0	28.3

5.3.2 - Secondary assembly

The tape-like assembly of the carboxylic acid dimers can be thought of as a wider version of the tapes formed by the diesters and the periphery of both "tapes" is dependent on the ester substituent. Consequently it was anticipated that the secondary assemblies of the monoesters would be comparable to those of the diesters. As can be seen from Table 26, this did not prove to be the case.

Table 26: Secondary assembly parameters for the 2,6-diesters and monoesters

		R	Assembly	S_S/Å	S_T/°	T_O/°
38[92]	Diester	Methyl	$PS_{\uparrow\downarrow}L_{\uparrow\uparrow}$	3.47	34.0	64.4
75[94]	Monoester	Methyl	$PS_{\uparrow\uparrow}L_{\uparrow\uparrow}$	3.19	66.8	62.3
40[91]	Diester	Ethyl	$PS_{\uparrow\downarrow}L_{\uparrow\uparrow}$	3.21	33.1	51.7
76	Monoester	Ethyl	$HS_{\uparrow\uparrow}L_{\uparrow\downarrow}$	3.16	30.2	85.6
44[92]	Diester	Benzyl	$PS_{\uparrow\downarrow}L_{\uparrow\downarrow}$	3.32	52.1	48.9
77	Monoester	Benzyl	$HS_{\uparrow\downarrow}L_{\uparrow\uparrow}$	3.21	-	-

On paper, the most comparable systems are those with methyl side-arms (**38**[92] and **75**[94]) where both the monoester and the diester form planar assemblies. However, and as has already been mentioned, unlike the diester[92], the methyl groups of **75**[94] do not interdigitate. Instead the packing of the monoester appears to be determined by close packing of the side-arms.

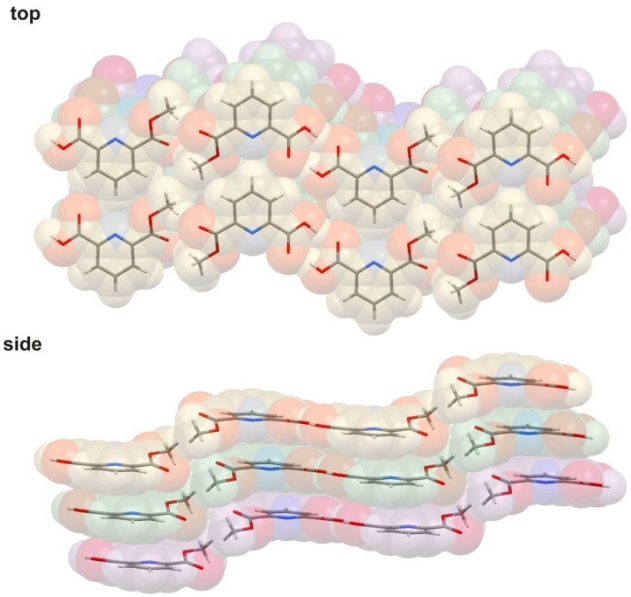

*Figure 81: Top and side views of the 2,6-methyl monoester (**75**[94]); different layers are tinted in gold, green and purple.*

Whilst the packing mode of the ethyl-monoester (**76**) is significantly different from that of the analogous diester (**40**[91]), like the diester the packing in **76** appears to be determined by dispersive forces and the minimisation of free space (Figure 82).

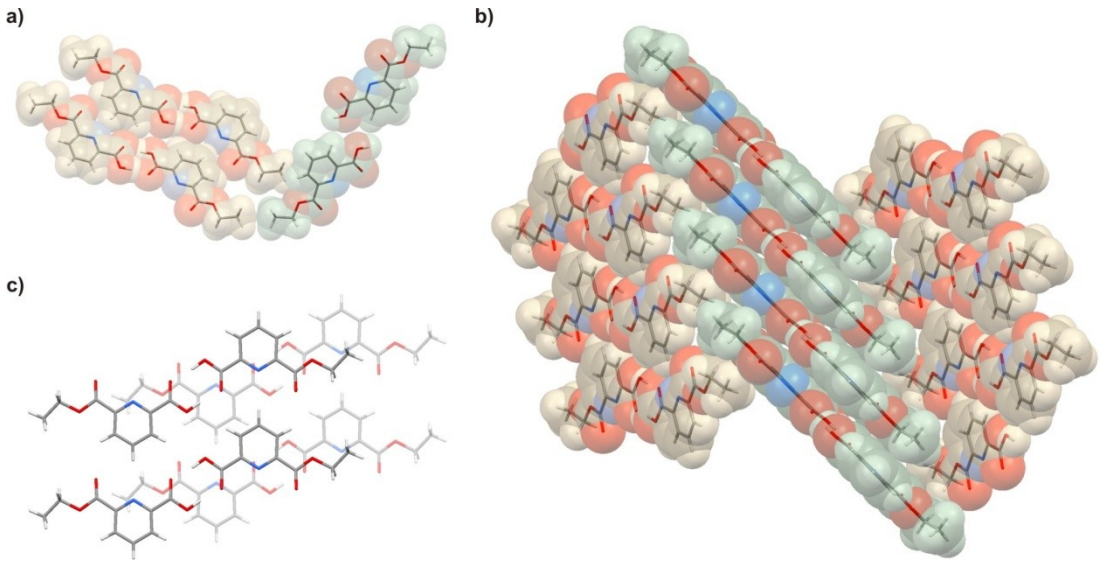

*Figure 82: Packing behaviour of the 2,6-ethyl monoester (**76**): (a & b) close packing of ethyl groups between adjacent tapes; (c) top-down view showing two different layers.*

Like the ethyl monoester, the benzyl derivative (**77**) also packs in a herringbone pattern (Figure 83c and d), rather than the planar motif adopted by the analogous diester (**44**[92]). Unlike the ethyl monoester, tapes in

adjacent stacks point in the same direction. Looking down onto a stack (Figure 83a) it also appears that the dimers in alternate layers are rotated slightly with respect to each other. However, whether the observed packing behaviour is directed by close packing and the maximisation of dispersive interactions or is the result of specific intermolecular forces is hard to determine. The Hirshfeld surface shows a number of weak contacts (Figure 83, contacts i-iii) but it is questionable whether they alone are sufficiently strong to account for the observed behaviour.

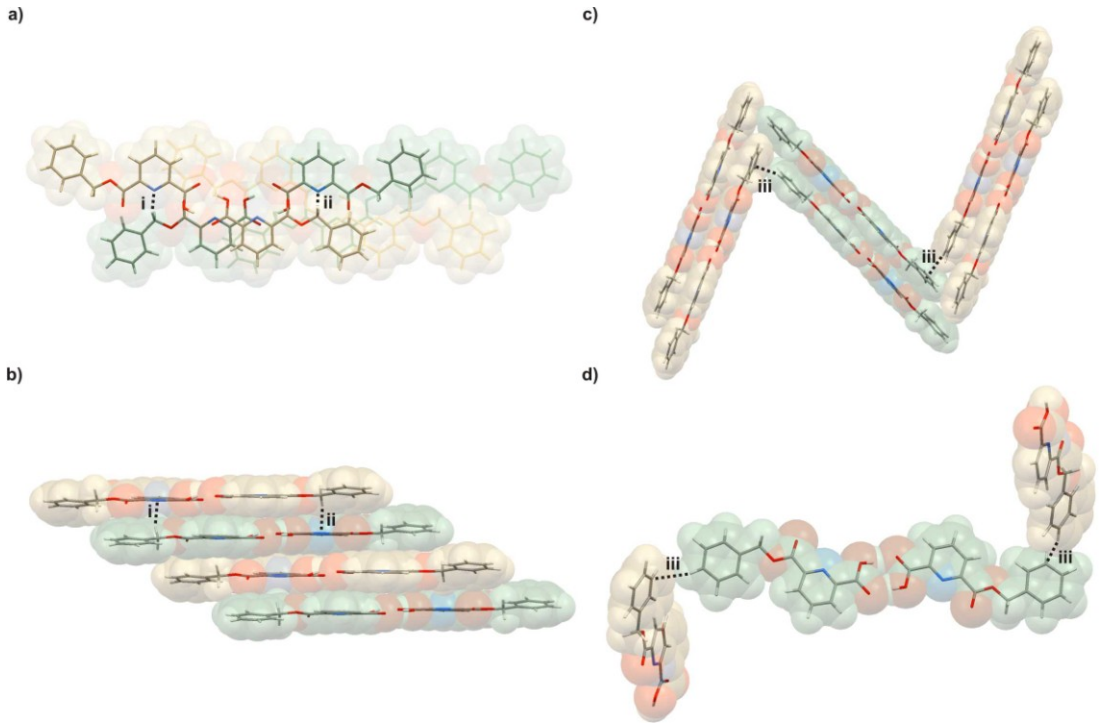

*Figure 83: (a) Top-down view of a stack of the 2,6-benzyl monoester (**77**) showing how alternate layers are rotated at a slight angle to each other; (b) side-on view of the same stack looking along the plane of the tapes; alternate layers are tinted green and gold. (c) Side-on view of three stacks of **77** (alternately coloured green and gold) showing herringbone packing; (d) close up-view of inter-tape edge-to-face C-H···C close contacts. (Contact i: H···N = 2.77 Å, C-Ĥ···N = 165.3°; contact ii: H···N = 2.65 Å, C-Ĥ···N = 170.9°; contact iii H···C = 2.85 Å, C-Ĥ···C = 152.4°.)*

5.3.3 - DSC

DSC data was collected for the ethyl and benzyl monoesters and is presented in Table 27 along-side the data for the corresponding diesters.

Table 27: DSC data for mono- and diesters with a pyridine-2,6-substituted core

		R	$\Delta H_{melting}/Jg^{-1}$	$\Delta H_{melting}/kJmol^{-1}$
40	Diester	Ethyl	110.17	24.59
76	Monoester	Ethyl	157.55	30.75
44	Diester	Benzyl	347.364	45.64
77	Monoester	Benzyl	150.76	38.78

The heats of melting for the monoesters were expected to be higher than those of the corresponding diester owing to the presence of a carboxylic acid dimer in addition to the tape-forming contacts. This hypothesis was observed to hold true for the ethyl derivative where the heat of melting of the monoester (**76**) was approximately 6 kJ mol^{-1} greater than that of the diester (**40**).

In contrast, the heat of melting of the benzyl monoester (**80**) is almost 7 kJ mol^{-1} lower than that of the corresponding diester (**44**). This correlates with the differences observed between the lengths of the taping contacts for the monoester and the diester. These are much longer for the monester than for the diester and so are expected to be weaker, consequently it is less surprising that the heat of melting is greater for the diester than for the monoester.

A broad, shallow endotherm was observed in the cooling phase for both the ethyl and the benzyl monoesters (the curve for the ethyl monoester is shown in Figure 84) and it is possible that this may correspond to a transition between polymorphs. This suggestion is partially supported by evidence in the literature for the existence of polymorphs of the methyl ester (**75**). Whilst the melting point of **75** is most commonly reported as being in the region of 148-150 °C,[120, 122, 123] one report[124] gives it as 119-120 °C. Further investigation by variable temperature powder X-ray diffraction may offer a further explanation.

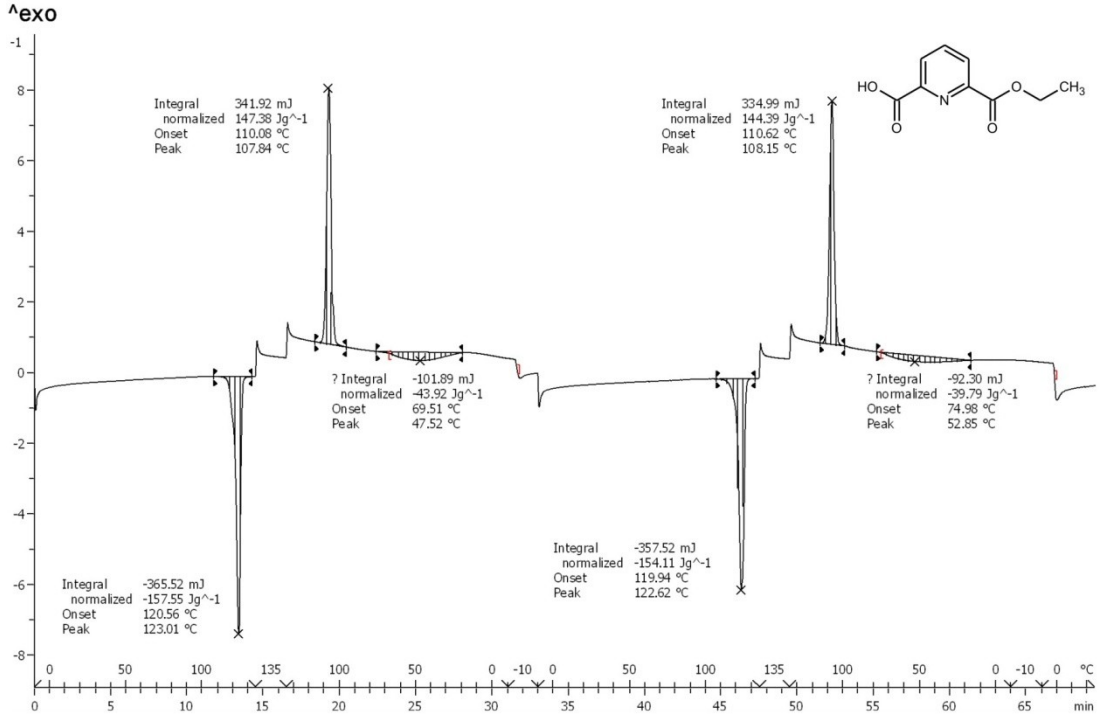

*Figure 84: DSC curve for the 2,6-ethyl monoester (**76**).*

5.3.4 - Conclusions

Investigation of the ethyl and benzyl 2,6-monoesters and comparison of their solid-state behaviour with that of both the methyl monoester[94] and the analogous diesters[91, 92] has shown that this class of compounds is conformationally labile. However, all of the monoesters form carboxylic acid dimers and all form tape-like assemblies similar to those formed by the diesters.

Only the ethyl derivative (**76**) adopts the conventional *cis*-*cis* conformer and the primary assembly of this compound has been shown to be stronger than that of the analogous diester (**40**). In contrast, inversion of the side-arms appears to weaken the primary assembly of the benzyl monoester (**77**) in comparison with the analogous diester (**44**).

Despite the external functional groups being the same, the packing modes of the tapes formed by the monoester dimers is substantially different to those

of the corresponding diesters. Further investigation with a wider range of ester substituents is needed before the secondary assemblies of these systems can be properly understood.

5.4 - Solid-state behaviour of the 3,5-monoesters

The 3,5-monoesters (**78** - **80**) were found to be significantly less soluble than their 2,6-substituted analogues. A crystal of 5-benzyloxycarbonyl-3-pyridinecarboxylic acid (**80**) was eventually obtained from acetonitrile, however attempts to grow crystals of both the methyl and ethyl 3,5-monoesters were unsuccessful and resulted in the formation of fine powders.

5.4.1 - 5-Benzyloxycarbonyl-3-pyridinecarboxylic acid (80)

As has been mentioned, this class of compound proved difficult to crystallise and the data set collected for **80** showed some evidence of disorder. Although a centre of inversion is likely to be present, the best refinement was obtained in the P1 space group.

The asymmetric unit of **80** contains four molecules. Like the 2,6-derivative a *trans*-*cis* conformer is present but the asymmetric unit also contains the *cis*-*trans* conformer (i.e. in some molecules the acid group is inverted but in others the acid group is in the expected orientation and the ester group is found to invert). Unlike the 2,6-substituted derivatives which form carboxylic acid dimers, molecules of **80** are observed to form chains mediated by hydrogen bonds between the carboxylic acid and the pyridine core (contacts i - viii, indicated by orange and green broken lines, in Figure 85a). The chains are observed to pack into corrugated sheets and close contacts are observed between the protons of the benzene ring and the oxygen atoms of the carboxylic acid group (contacts ix - xiv, indicated by purple dashed lines, in Figure 85a).

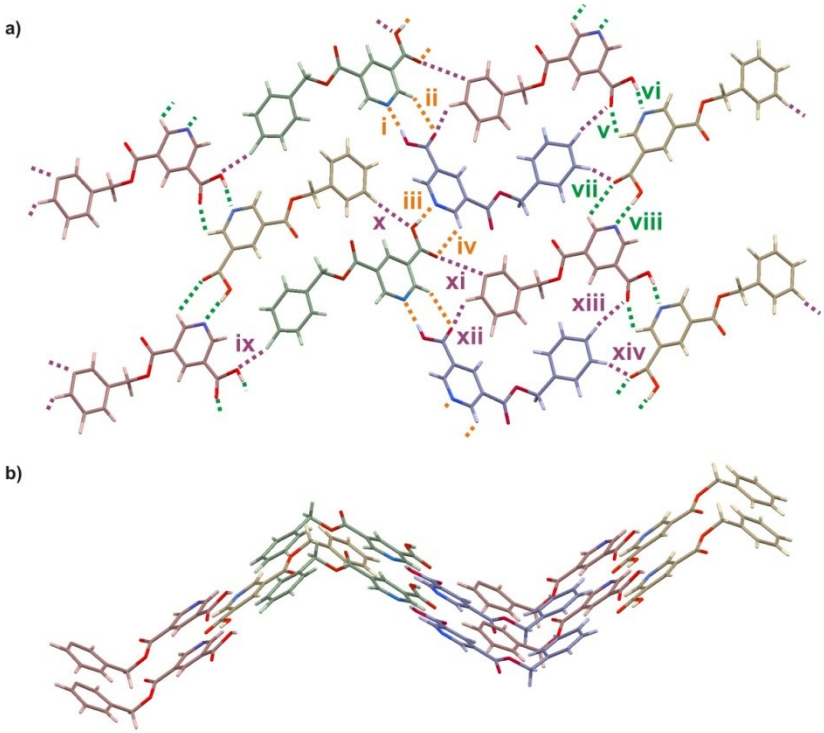

*Figure 85: View from (a) above and (b) from the side of a corrugated sheet formed by the benzyl 3,5-monoester (**80**). Crystallographically unique molecules are differentiated by red, green, gold and blue tinting. Hydrogen bonds forming chains are shown as either green or orange lines and the close contacts between chains are shown as purple lines; contact lengths and angles are detailed in Table 28.*

*Table 28: Bond distances and angles for the acid/pyridine hydrogen bond chains observed in compound **80**.*

		A···H-D distance/Å	**A···H-D angle/°**	**C-O···H angle/°**
i	N···H-O	1.81	176.7	-
ii	C=O···H-C	2.65	128.2	116.5
iii	N···H-O	1.79	178.6	-
iv	C=O···H-C	2.78	121.0	118.1
v	C=O···H-C	2.47	112.3	143.4
vi	N···H-O	1.70	169.8	-
vii	C=O···H-C	2.60	111.3	143.3
viii	N···H-O	1.69	174.4	-
ix	C-O···H-C	2.23	159.0	155.0
x	C-O···C	2.66	152.2	147.4
xi*	C=O···H-C	3.15	-	157.2
xii	C=O···H-C	2.37	140.4	172.4
xiii	C=O···H-C	2.44	147.6	136.5
xiv	C=O···H-C	2.48	168.0	133.1

* No hydrogen could be identified from the data set thus the contact reported is C=O···$C_{(bn)}$.

The absence of carboxylic acid dimers was initially surprising. However the CSD[125, 126] contains other examples of a similar contacts in the structures of molecules containing both a 3,5-substituted pyridine ring and a carboxylic

acid group.[127-130] Nangia *et al.*[131] have reported the presence of the synthon in co-crystals of di- and tricarboxylic acids with substituted pyridines.

One possible explanation as to why this synthon is not observed for the 2,6-monoesters is in the relative basicities of the pyridyl nitrogen atoms. Several authors[132, 133] have shown that the basicity of the nitrogen atom for the structural isomers of picolinic acid is dependent on the position of the acid group; and that the nitrogen atoms are more basic for nicotinic acid (acid group at the 3 position) than for picolinic acid (acid group at the 2-position). Thus, applying Etter's rules,[77] in the 2,6-monoesters the nitrogen atom of the pyridine ring is a significantly weaker hydrogen bond acceptor than the carbonyl oxygen of the acid group and a carboxylic acid dimer is formed. In the 3,5-monoester, the nitrogen atom is more basic and is able to compete with the carbonyl oxygen. In the 3,5-derivative there is also an acidic proton ortho to the nitrogen which can form a second hydrogen bond with the carbonyl oxygen, thus ensuring that bonds are formed with both of the strongest acceptors.

5.4.2 - DSC

The thermal behaviour of all three 3,5-monoesters was investigated by DSC (Table 29). It was found that no heat flow was observed after the initial heating step had been completed. Examination of the traces showed the presence of two peaks - the first corresponded to the melting point of the sample and the second was assumed to be a decomposition step.

*Table 29: DSC data for 3,5-monoesters (**78**-**80**).*

			$\Delta H_{melting}$/ Jg^{-1}	$\Delta H_{melting}$/ $kJmol^{-1}$	$\Delta H_{decomposition}$/ Jg^{-1}	$\Delta H_{decomposition}$/ $kJmol^{-1}$
78	Me	Monoester	310.78	56.30	316.58	57.35
79	Et	Monoester	173.29	33.82	455.51	88.90
80	Bn	Monoester	181.13	46.59	61.32	15.77

The DSC experiments were repeated for the ethyl and benzyl samples (**79** and **80**), but the maximum temperature of the first cycle was reduced to a value below the onset temperature of the second endotherm. The sample

was then cooled and reheated to the same maximum temperature used in the first experiment.

The behaviour of **80** was unchanged from the first experiment, suggesting that it decomposed upon melting. However, for the ethyl-derivative (**79,** Figure 86), a small exotherm corresponding to crystallisation was observed in the first cooling step and a double endotherm was seen in the second heating cycle. The integral of the second melting peak was significantly smaller than that seen for the first scan, suggesting that the ethyl derivative also decomposes as it melts.

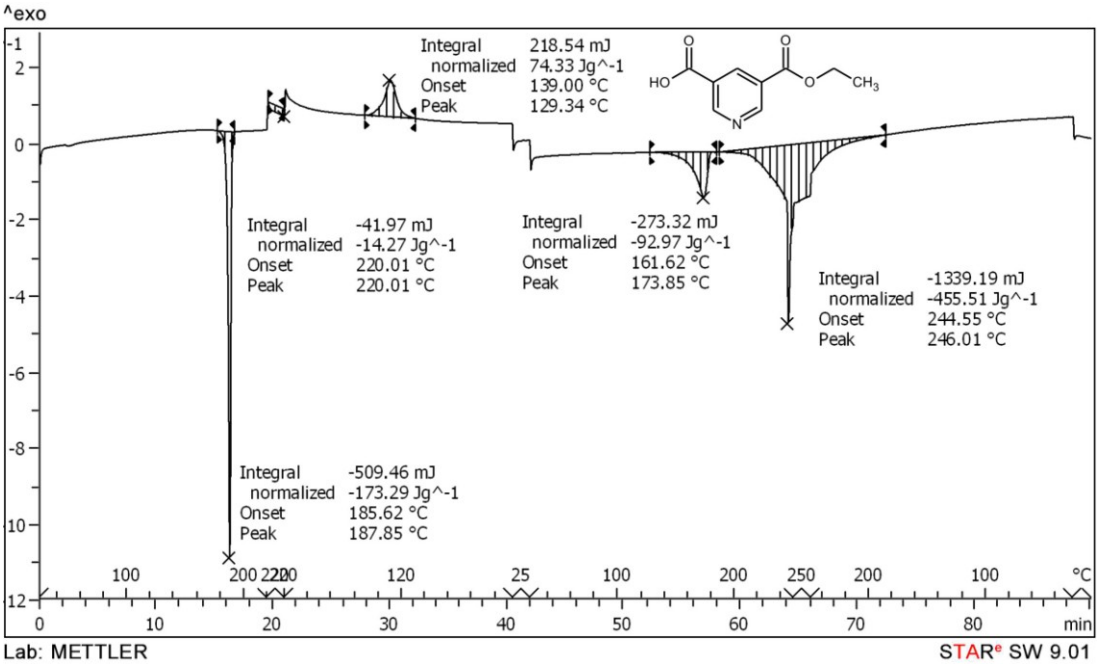

*Figure 86: DSC curve for **79** showing the initial melting of the sample, partial crystallisation, partial melting and decomposition.*

The method of decomposition is unknown and may warrant further investigation, although a likely route might involve decarboxylation. However, if this is the case, then it is surprising that the 2,6-monoesters are not observed to decompose since decarboxylation at the 2-position is known to occur more readily than that at the 3-position.[134]

5.5 - Conclusions and further work

The solid-state behaviour of the monoesters has shown them to be conformationally labile and there is no obvious relationship between the molecular structure and the observed conformer. However the range of samples investigated thus far has been small and a larger, systematic investigation would be needed to draw a firm conclusion.

Carboxylic acid dimers have been observed for the 2,6-monoesters which then form tape-like assemblies. The strength of these assemblies has been observed to be disrupted by inversion of the side-arms. The factors affecting the packing of these tapes are currently unclear and a systematic study of additional compounds is required.

Changing the pattern of substitution around the pyridine ring results in the formation of a completely different assembly mediated by a carboxylic acid-pyridine dimer. Although it has only been possible to examine the solid-state behaviour of a single 3,5-monoester, the prevalence of similar motifs in the literature suggests that it is likely that other 3,5-monoesters would assemble in a similar manner.

DSC results indicate that, contrary to expectations, the 3,5-monoesters are more susceptible to decarboxylation than the 2,6-derivatives. Further analysis of the thermal behaviour of the monoesters should be considered, and TGA-MS analysis of the decomposition of the 3,5-isomers would be particularly worthwhile.

6 - Functionalised systems

During the course of this investigation, initial attempts have been made to use the supramolecular tapes formed by the pyridine-dicarboxylate diesters as a molecular scaffold. It was intended to exploit the general robustness of the triple hydrogen bond motif, particularly that of the 2,6-substituted systems, to control the position of the substituent functionalities in the solid-state and to observe the interactions between them.

6.1 - Progress towards a system with the potential for photocyclisation

It was of interest to see if photocyclisation could be used to convert the tape-like assemblies formed by the pyridine dicarboxylates into a covalent network. Desiraju[44] and Schmidt[12] have reported the successful photocyclisation of supramolecular assemblies containing substituted cinnamic acids, consequently cinnamyl alcohol was chosen as the substituent for this experiment. Bis(cinnamyl)pyridine-2,6-dicarboxylate diester (**81**) was synthesised from pyridine-2,6-dicarbonyl dichloride as shown in Scheme 7. Crystals suitable for X-ray structural study were obtained by crystallisation from DCM and light petroleum ether.

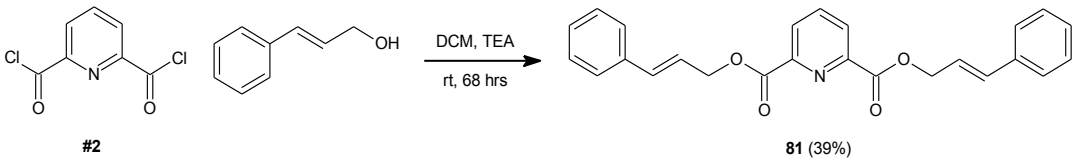

#2 **81** (39%)

*Scheme 7: Synthetic route to the cinnamyl 2,6-diester (**81**).*

The diester is found to form a conventional tape-like assembly in the solid-state, with the expected triple hydrogen bond motif observed between adjacent pyridine dicarboxylate cores (Table 30). Molecules adjacent to each other in the tape are sufficiently close together that the secondary bonding interactions between the γ-proton and the carbonyl oxygen atoms can be seen as close contacts (H···O = 2.72 Å, C-Ĥ···O 116.8°, C=Ô···H = 115.2°).

*Table 30: Primary assembly parameters for bis(cinnamyl)pyridine-2,6-dicarboxylate diester (**81**).*

	r_1/Å	r_2/Å	θ/°	ϕ/°	ϑ/°	ψ/°
81	2.56	2.53	180.0	167.1	126.7	47.8

The tapes formed by **81** are observed to form a planar assembly (Table 31). Within an anti-parallel stack, close contacts are observed between one of the protons of the CH_2 spacer and the pyridyl nitrogen in an adjacent layer (contact i in Figure 87a). Adjacent stacks are observed to pack so that neighbouring phenyl rings are aligned in an edge-to-face geometry. However, even the shortest contacts (contacts ii and iii in Figure 87a) are observed to be significantly longer than the sum of the van der Waals radii and it is hard to determine whether C-H···π type interactions are the primary force in directing the observed behaviour.

*Table 31: Secondary assembly parameters for bis(cinnamyl)pyridine-2,6-dicarboxylate diester (**81**).*

	Assembly	S_S/Å	S_T/°	T_O/°
81	$PS_{\uparrow\downarrow}L_{\uparrow\uparrow}$	2.99	31.7	61.5

As can be seen from the crystal structure data, the alkene groups are isolated from each other within the crystal architecture. Consequently, formation of a covalent network was not possible.

Increasing the length of the saturated spacer between the pyridine core and the alkene/phenyl ring might allow the alkene groups to adopt a more favourable conformation. Another possible approach would be to prepare two different esters where the benzene ring of the cinnamyl moiety had been functionalised to make it either electron rich or electron poor. Co-crystallisation of these two different molecules would hopefully form stacks where the alkenes were aligned as a result of π-π interactions between the phenyl rings. No attempt was made to perform the cyclisation in solution and this should be investigated in the future.

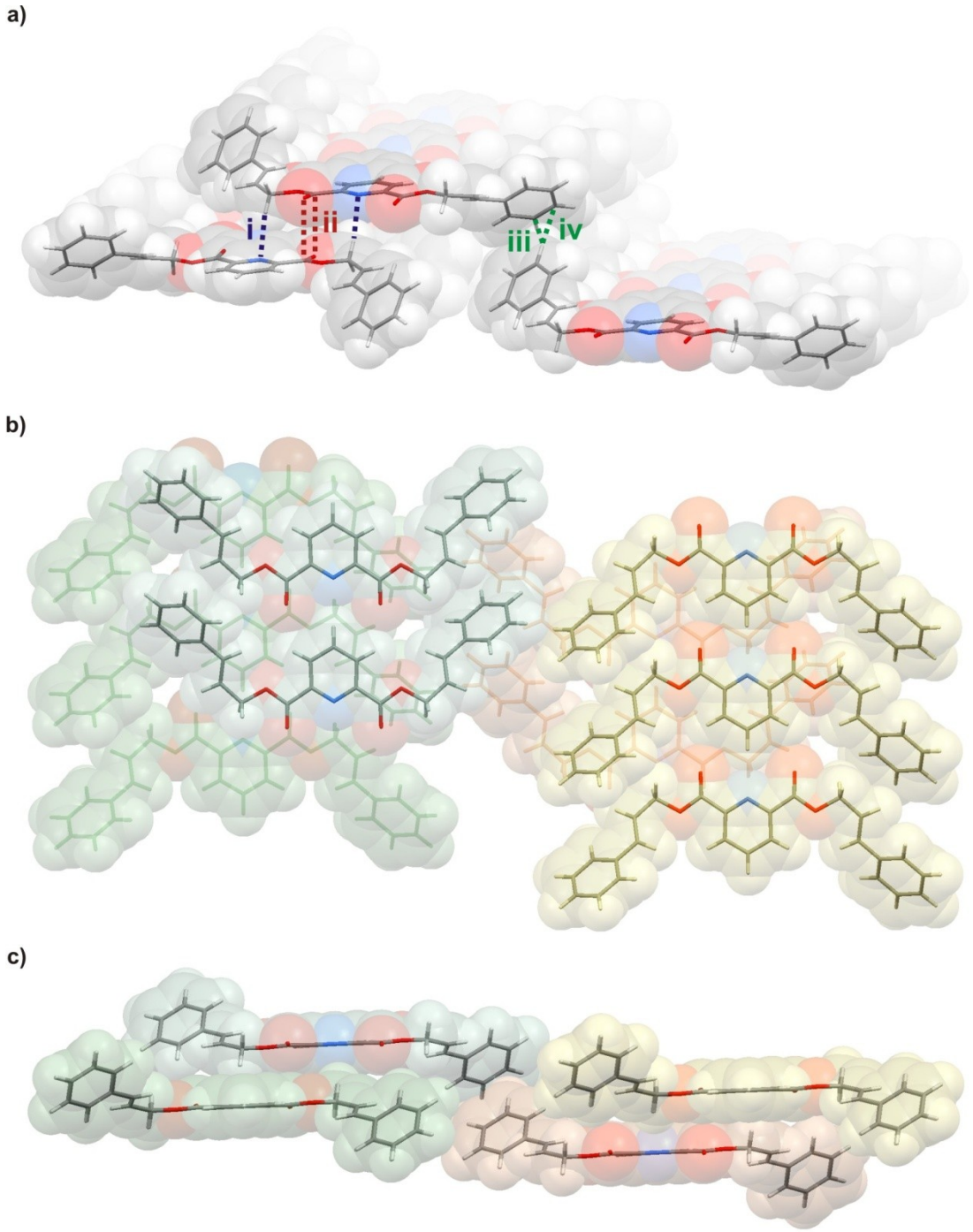

*Figure 87: (a) Close contacts present in the solid-state assembly of the bis(cinnamyl) 2,6-pyridinedicarboxylate diester (**81**); contact i (blue) H···N = 2.60 Å, C-Ĥ···N = 166.2°; contact ii (red): C···O = 3.20 Å, C=O···C = 94.2°, O=Ĉ···O = 85.8°; contact iii (green): H···C = 2.96 Å, C-Ĥ···C = 137.3°; contact iv (green): H···C = 2.95 Å, C-Ĥ···C = 162.1°. (b) View of an assembly of **81** looking from above the tape. (c) View of the same assembly looking along the tape.*

6.2 - Progress towards the formation of pyridine-dicarboxylate diesters with tetrathiafulvalene substituents

As has been mentioned in Chapter 1, derivatives of TTF can be partially oxidised to produce materials with interesting electrochemical properties. It was intended to combine derivatives of TTF with a pyridinedicarboxylate core. It was expected that the triple hydrogen bond motif would form tape-like assemblies, the packing of which would be directed by the propensity of TTF to self-stack. It was then intended to investigate the solid-state and redox behaviour of these systems.

The attempted route to the synthesis of bis(4-methyl-TTF) 2,6-pyridinedicarboxylate (**84**) is shown in Scheme 8. Synthesis of intermediate **83** from TTF was performed in good yield following the procedure described by Garin *et al.*[135] Despite a literature precedent for the reaction of TTF-derivatives with acid chlorides to form esters[104, 136] and repeated attempts at the synthesis, isolation of the purified product was unsuccessful; attempts at purification of the crude material by column chromatography resulted in the degredation of the product.

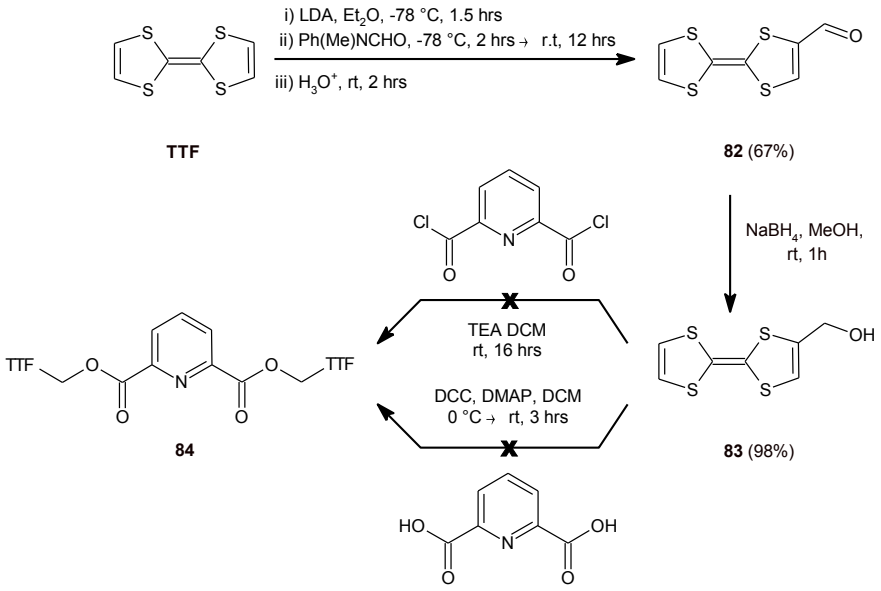

*Scheme 8: Synthetic route for the attempted synthesis of the TTF 2,6-diester (**84**).*

An attempt to prepare **84** using DCC coupling of the alcohol (**83**) with pyridine dicarboxylic acid was also unsuccessful. The crude product was dominated by an impurity exhibiting ^{1}H NMR signals at low chemical shift. Five distinct multiplets were also observed in the aromatic region of the NMR spectrum which were attributed to pyridyl protons, although the integrals of these were very small. It was concluded that the reaction had been largely unsuccessful and that where esterification had occurred, a mixture of the monoester and diester had been formed. Given the expected low yield of the product and previous problems with purification, the experiment was not continued.

Working in collaboration with the Batail research group at the University of Angers, further attempts were made to synthesise **84**. The synthesis of an EDT-TTF substituted diester (**87**) was also attempted, as shown in Scheme 9.

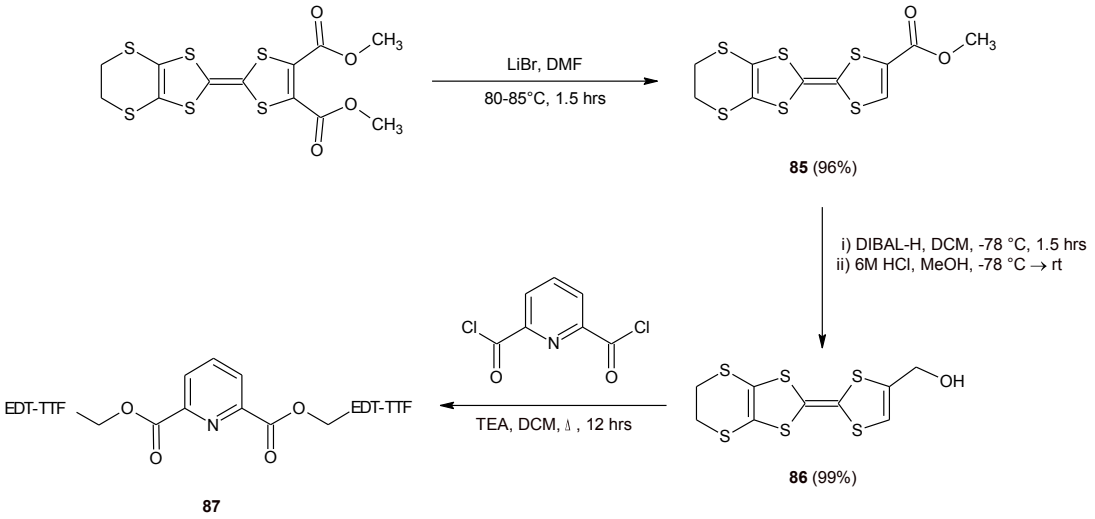

*Scheme 9: Synthetic route to the EDT-TTF 2,6-diester (**87**).*

Unfortunately although both diesters were identified in the crude reaction mixture, restrictions on the time available to work with the Batail group prevented the samples from being purified and attempts to repeat the reactions in the UK were unsuccessful.

Investigations by the Batail group had suggested that the esterification reaction could be improved if a solution of the acid chloride was added to a suspension of the alcohol and TEA and the reaction mixture was heated at reflux. However, an attempt to prepare the diester of dimethyl-TTF (**89**) using this strategy (Scheme 10) was also unsuccessful. NMR analysis of the crude product showed no evidence of TTF; the expected single peak at 6 ppm was not observed.

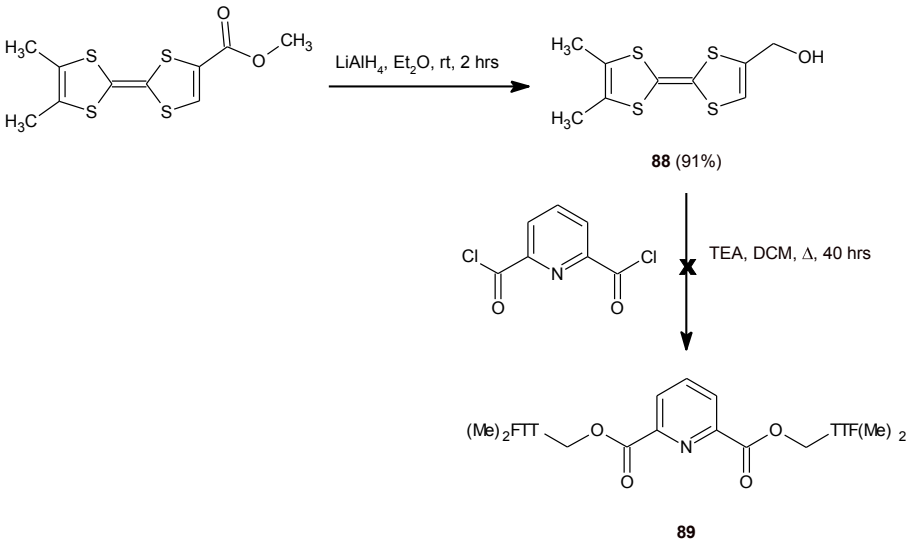

*Scheme 10: Synthetic route for the attempted synthesis of the dimethyl-TTF 2,6-diester (**89**).*

Although isolation of the TTF-substituted pyridine dicarboxylate diesters and subsequent investigation of their solid-state and electrochemical behaviour has not been possible, progress has been made towards the successful preparation of these compounds. Further work is required to understand why the TTF moiety appears to decompose during the ester formation and to develop a successful strategy for purification of the final compound.

7 - Other investigations

7.1 - Pyridinedicarbaldehydes

Of the simple pyridine-dicarboxy derivatives, the solid-state behaviour of the carboxylic acids[128, 137], acid chlorides[113] and methyl ketones[114] is known for both the 2,6- and 3,5-structural isomers. However, although the preparation of the dialdehydes (**90**, **91**) has been reported[138, 139] as intermediates in the synthesis of macrocycles, their solid-state behaviour has not been explored.

7.1.1 - Synthesis of the pyridinedicarbaldehydes

Synthesis was attempted by oxidation of the corresponding dimethylpyridine with selenium dioxide. Pyridine-2,6-dicarboxaldehyde (**90**) was successfully synthesised in this way but, despite a literature precedent for the use of this method,[139] the 3,5-derivative could not be prepared. Several attempts were made but in each instance NMR analysis of the crude product showed it to be unreacted starting material.

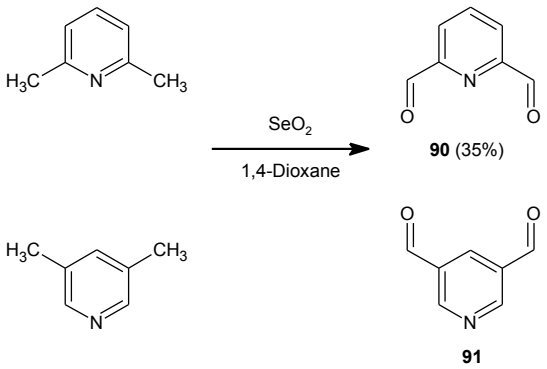

*Scheme 11: Outline of the synthesis of pyridinedicarbaldehydes **90** and **91**.*

7.1.2 - Solid-state behaviour of pyridine-2,6-dicarbaldehyde (90)

Like the methylketone (**72**)[114] and acid chloride (**70**)[113] analogues, the 2,6-dialdehyde (**90**) crystallises in a *trans-trans* conformation. Despite this, the solid-state assembly resembles that of a conventional tape with a single C-H···N hydrogen bond observed between the pyridyl nitrogen of one molecule and the γ-proton of an adjacent pyridine ring (contact i in Figure 88a).

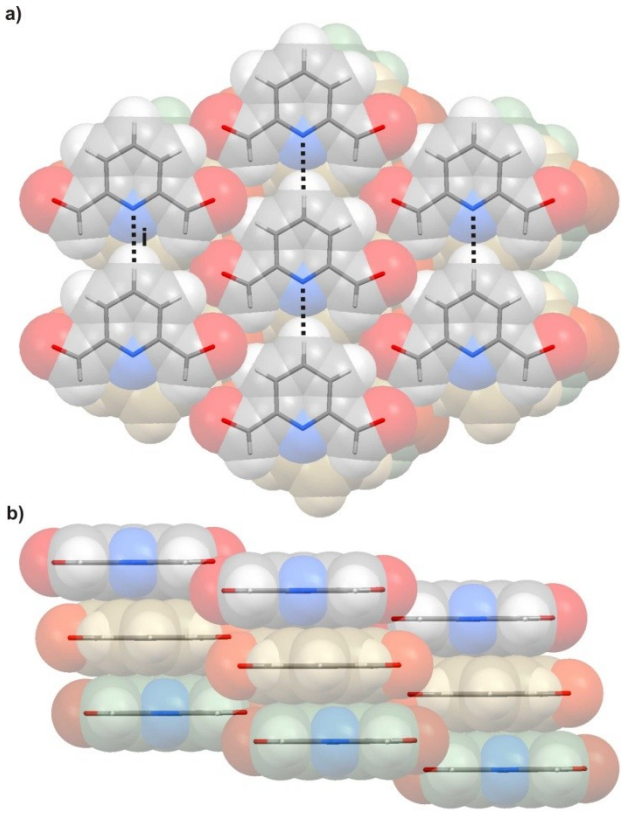

*Figure 88: (a) Top-down view of the solid-state assembly formed by pyridine-2,6-dicarbaldehyde (**90**) showing the H···N hydrogen bonds as dashed lines (contact i: H···N = 2.69 Å, C-H···N = 177.98°). (b) Side-view of the same assembly looking along the direction of the tapes; the molecules in different layers have been tinted for clarity.*

Tapes are observed to assemble into anti-parallel stacks (the observed packing mode is PS↑↓L↑↑) with adjacent tapes separated by 3.32 Å. Alternate layers are slightly out of register with each other and the carbonyl oxygen atoms are observed to sit in a "proton pocket" made by four protons from molecules in the neighbouring stack. The corresponding H···O contact distances are observed to vary between 2.54 and 2.77 Å and the C-H···O angles range from 119.3 to 149.7°. Consequently it is unclear whether the

observed packing behaviour is the result of electrostatic interactions directing the formation of a “proton pocket” or whether this arrangement simply allows for the best tessellation of neighbouring tapes.

7.2 - Pyridinediamides

As part of the current study four pyridine diamides (**92** - **95**) were prepared, originally for use as intermediates in the synthesis of the diacetylpyridines. Examination of the structures deposited in the CSD showed that solid-state behaviour of these compounds had not been characterised previously and a crystallographic study was undertaken.

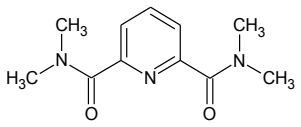

92

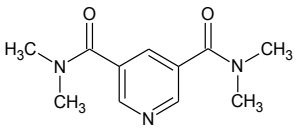

93

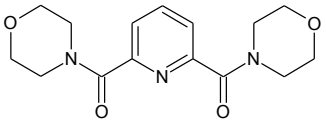

94

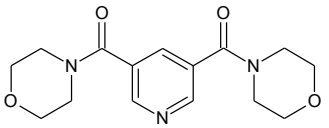

95

7.2.1 - bis(Dimethyl) pyridinediamides

The dimethyl diamides (**92** and **93**) were synthesised from dimethylamine and the corresponding acid chloride as shown in Scheme 12. Crystallisation of both compounds from ethyl acetate gave multi-domain blocks for the 2,6-isomer and platelets for the 3,5-derivative.

The platelets of the 3,5-diamide were found to be unsuitable for study by X-ray diffraction. Recrystallisation, again from ethyl acetate, produced crystalline needles which were suitable for crystallographic study, although the quality of the refined structure was not as good as had been hoped.

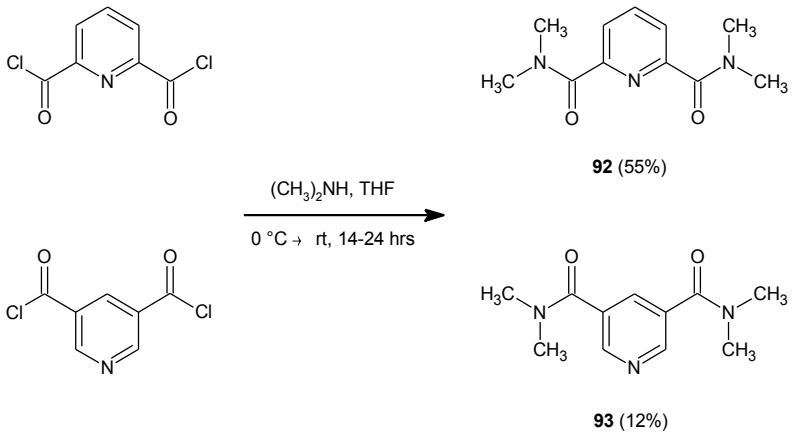

*Scheme 12: Synthetic route used in the preparation of dimethyl diamides **92** and **93**.*

In the solid-state, the carbonyl groups of both compounds rotate out of the plane of the pyridine ring (Figure 89). The 2,6-isomer (**92**) is symmetrical about a mirror plane passing through the nitrogen and 4-carbon atoms of the pyridine ring, whilst the 3,5-anaolgue (**93**) is asymmetric. However, the arrangement of the side-arms in **93** can be crudely approximated by rotation about a C_2 axis passing through the 4-carbon and nitrogen atoms of the pyridine ring.

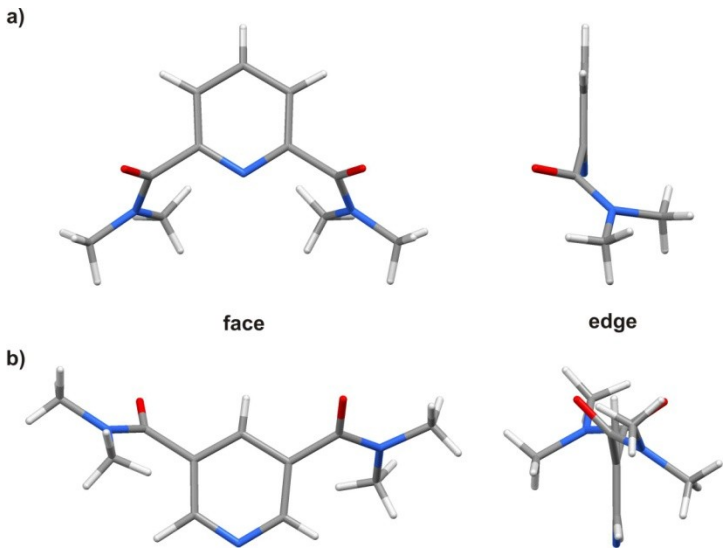

*Figure 89: Face-on and edge-on views of (a) bis(dimethyl) 2,6-pyridinediamide (**92**) and (b) bis(dimethyl) 3,5-pyridinediamide (**93**).*

Both derivatives are observed to form tape-like assemblies (Figure 90) but, unlike those seen for the diesters, the tapes formed by the dimethyl diamides are stepped with adjacent cores angled at 83.4° to each other in the 2,6-isomer (**92**) and at 56.9° in the 3,5-analogue (**93**).

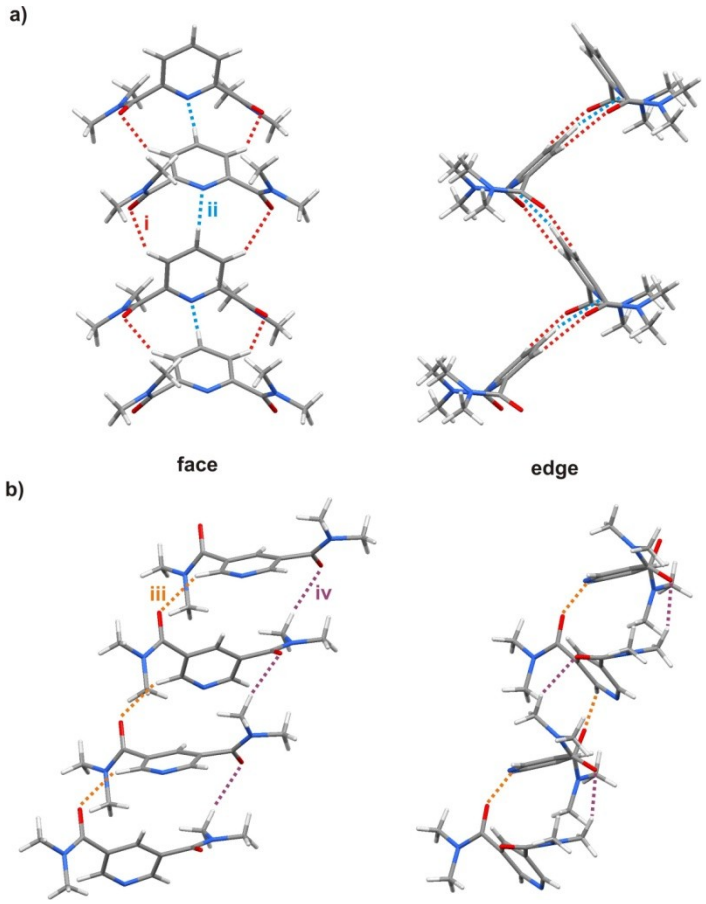

*Figure 90: Face-on and edge-on views of the stepped, tape-like assemblies formed by (a) the 2,6-diamide (**92**) and (b) the 3,5-diamide (**93**). Close-contacts implicated in tape formation are shown as dashed lines and the geometries of these interactions are given in Table 32.*

*Table 32: Lengths and angles for the close contacts observed within tapes of **92** and **93,** as shown in Figure 90.*

	D-H···A-Y Contact	H···A/Å	C-Ĥ···A/º	H···Â-Y/°
92	i	2.50	170.6	-
	ii	2.63	140.4	124.4
93	iii	2.40	146.5	129.0
	v	2.55	156.9	109.1

As can be seen from Figure 90 and Table 32, the tape formed by the 2,6-isomer (Figure 90a) is essentially just a corrugated version of that formed by the 2,6-diesters. In contrast, the 3,5-isomer (Figure 90b, contacts iii and iv)

is more strained and the geometries of the contacts observed are far from those of ideal hydrogen bonds. It is entirely possible that the tape-like assembly observed for **93** is as much the result of close packing as it is of specific interactions. In both isomers, the packing of the "tapes" in the bulk crystal appears to be determined by close packing.

7.2.2 - bis(Morpholino) pyridinediamides

The morpholino derivatives were synthesised from the corresponding pyridine-dicarboxylic acid by forming the acid chloride *in situ* and reacting this with morpholine (Scheme 13). Crystalline blocks were obtained for both compounds by crystallisation from chloroform and ethylacetate.

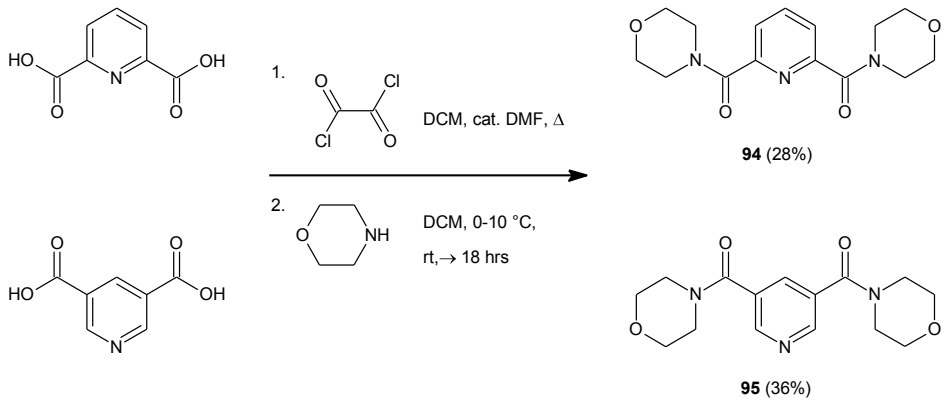

*Scheme 13: Outline of the synthesis of the bis(morpholino) pyridinediamides **94** and **95**.*

Like the dimethyl analogue (**92**), the carbonyl groups are rotated out of the plane of the pyridine ring (Figure 91a). However, unlike **92**, the morpholino derivative (**94**) is not symmetrical and does not form a tape-like assembly; instead a three-dimensional network is formed as a result of dispersive close-packing forces and C-H···O interactions.

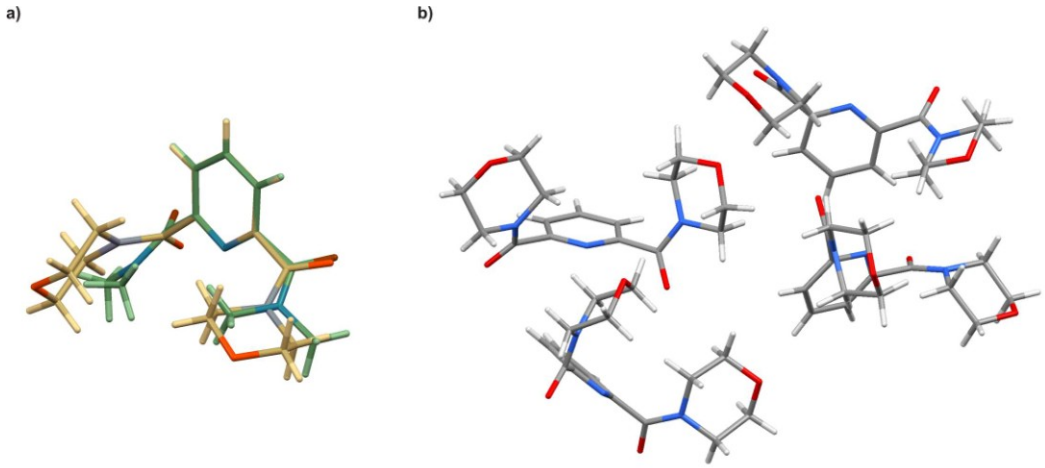

*Figure 91: (a) Overlay of the crystal structures of the bis(dimethyl) (**92**, green tint) and the bis(morpholino) (**94**, gold tint) 2,6-pyridinediamides. (b) Unit cell of **94** showing the arrangement of close-packed molecules.*

The side-arms of the 3,5-analogue are orientated in a pincer-like geometry (Figure 92). Tape-like assemblies similar to those observed in crystals of the 4-cyanobenzyl 2,6-diester (**33**), are formed along the crystallographic *b*-axis by C-H···O interactions between the oxygen atoms of the morpholine side-arm and the α-protons of the pyridine ring.

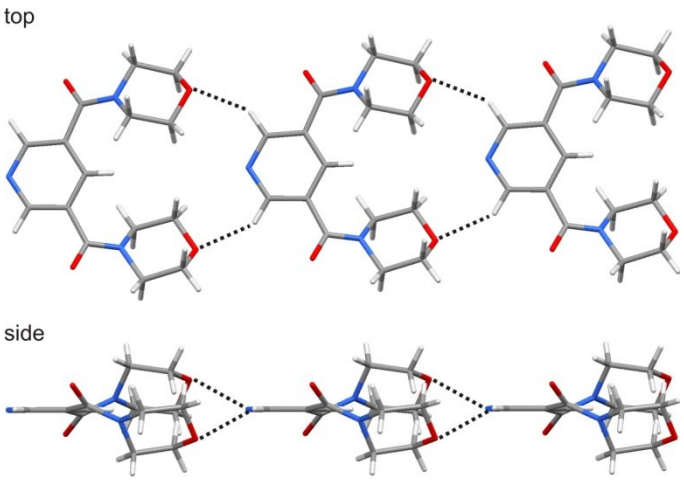

*Figure 92: Top-down and side-on views of the tape-like assembly formed by bis(morpholino) 2,6-pyridinediamide (**95**); tape-forming C-H···O hydrogen bonds are shown as black dashed lines (H···O = 2.61 Å, C-H···O = 138.1°).*

Anti-parallel stacks are assembled as a result of a C-H···O interactions between the carbonyl group of one molecule and one of the CH_2 protons of the morpholine ring beneath it (contact i in Figure 93). There is also

evidence of a possible weak C-H···π type contact with the γ-carbon of the pyridine ring (contact ii in Figure 93).

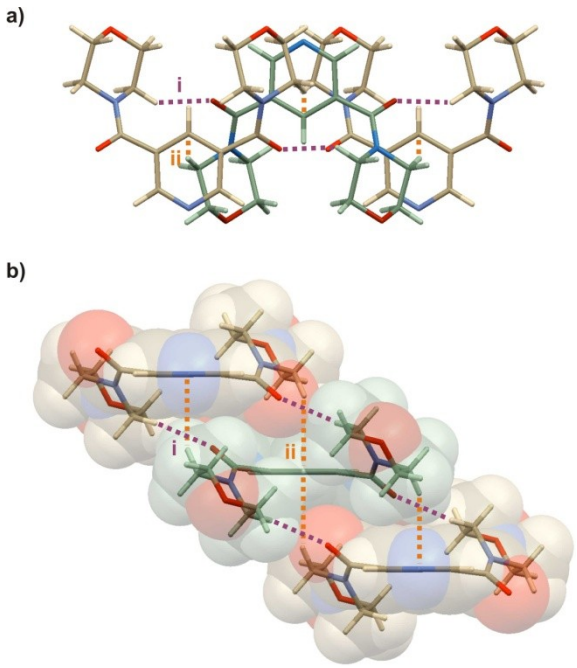

*Figure 93: Representations of a stack of the bis(morpholino) 2,6-pyridinediamide (**95**) viewed from: (a) above, looking down onto the tape and; (b) the side, looking along the direction of the tape. Alternate layers have been tinted green and gold and the contacts potentially involved in directing the formation of stacks are shown as orange and purple dashed lines. Contact i (purple lines): H···O = 2.35 Å, C-Ĥ···O = 145.3°, H···Ô-C = 147.9°; contact ii (orange lines): H···C = 2.99 Å, C-Ĥ···C = 156.9°.*

Lastly, stacks are assembled in a herringbone pattern by dispersive forces and interdigitation of the morpholine side-arms (Figure 94).

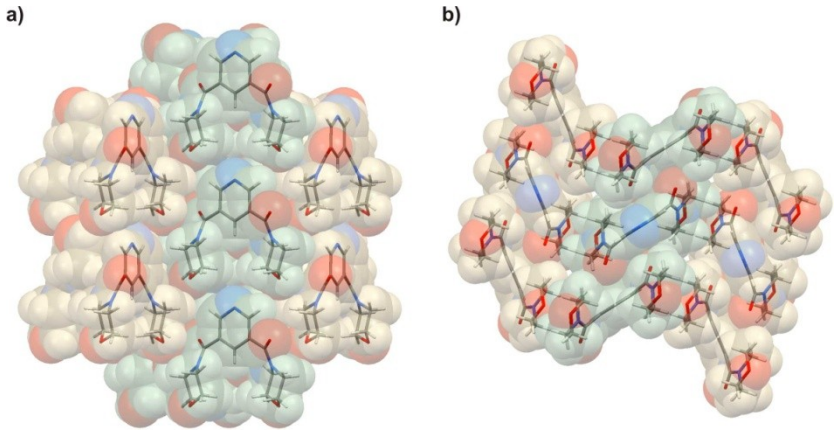

*Figure 94: Representations of the herringbone array formed by **95** showing tessellation of the morpholine side-arms. (a) View from above looking down onto the tape. (b) View from the side, looking along the direction of the tape. Alternate stacks have been tinted green and gold.*

8 - Conclusions and further work

This investigation has built on the work of Gomm,[92] Orton[91] and others[93-95] in exploring and characterising the supramolecular behaviour of the pyridine dicarboxylate synthon. Analysis of the thermal behaviour of a number of simple diesters by DSC has provided quantitative evidence that the triple hydrogen bond motif of the pyridine-2,6-dicarboxylates is stronger than that of the 3,5-substituted analogues.

The strength of the 2,6-synthon is evidenced by ^{1}H NMR titration studies on some aliphatic derivatives which appear to form tape-like assemblies in solution as well as in the solid-state. Similar studies on the analogous 3,5-isomers were inconclusive, but suggest that similar associations do not occur in solution for this weaker motif. Studies on the solution phase behaviour of the benzyl-diesters have also shown no evidence of tape formation in solution. It is suggested that the interactions that direct self-assembly in these derivatives are not strong enough to compete with the interactions between the solute and the solvent.

Examination of the carbonyl absorption by variable temperature Raman spectroscopy for the same group of compounds has been used to show the disruption of the crystal architecture as the sample is melted. It has been suggested that this technique may be applicable to the study of the diesters in solution, and additional experiments should be considered with the aim of confirming or refuting the formation of tape-like assemblies in solutions of the aliphatic diesters.

Continuing Orton's[91] systematic survey, diesters with 2,4,6-trimethylbenzyl and 2,4,6-trichlorobenzyl side-arms were prepared and their solid-state behaviour was investigated. The folded conformation of the methyl derivatives was similar to that of the analogous pentamethylbenzyl diesters.[91] This conformation is also adopted by the trichlorobenzyl-diesters and it is suggested that it is a consequence of steric interference between the side-arm and the pyridine core, resulting from substitution at the 2- and 6-positions of the benzene ring.

The 2,6-diesters with trimethylbenzyl and trichlorobenzyl side-arms were both observed to form tape-like assemblies in the solid-state, mediated by the triple hydrogen bond synthon. Like the 4-methylbenzyl and pentamethylbenzyl derivatives,[91] the packing behaviour of the trimethylbenzyl system was found to be determined by tessellation of the side-arms. Although the packing mode of tapes formed by the trichlorobenzyl 2,6-diester was significantly different from that of the 4-chlorobenzyl analogue,[91] the intermolecular forces directing packing appear to be similar in both cases.

Unlike the tri-substituted benzyl 2,6-diesters or the 4-chlorobenzyl and 4-methylbenzyl 3,5-diesters,[91] the side-arms of trichlorobenzyl and trimethylbenzyl 3,5-diesters were observed to invert. This resulted in the formation of extended networks in the solid-state, rather than tape-like assemblies. Further investigations using DSC and powder X-ray diffraction techniques should be conducted to determine whether this is the only behaviour displayed by these systems or whether these compounds are polymorphic.

Whilst previous work has only considered the solid-state behaviour of aromatic side-arms containing a 5- or 6-membered aromatic ring, this study has examined the behaviour of diesters with larger naphthyl and anthryl side-arms. This series of compounds, together with the phenyl-diesters, has allowed the effect of changing both the length of the alkyl linker and its position of attachment to the polyaromatic to be considered.

Tape-like assemblies were observed for both the 2,6- and the 3,5-isomers but the 2,6-motif was found to be more robust. Where tapes were formed, edge-to-face C-H···π type interactions were observed to direct the assembly of stacks. The packing of these stacks in the bulk crystal appeared to be the result of close-packing.

Tape formation appears to be affected by the orientation of the polyaromatic side-arm relative to the pyridine ring, rather than being dependent on the size of the substituent alone. The length of the spacer and the point of attachment to the aromatic substituent are important factors in determining the observed geometry. Attachment at the 1- or 5-positions of the aromatic substituent results in the side-arm folding out of the plane of the pyridine ring. Increasing the length of the alkyl-spacer from one to two CH_2 units has a similar effect.

Progress has also been made towards the synthesis and solid-state characterisation of some asymmetric systems. The 2,6- and 3,5- "monoesters" with ethyl and benzyl side-arms have been synthesised, as has the methyl 3,5-monoester.

The solid-state behaviour of the 2,6-ethyl and benzyl monoesters has been determined and discussed in comparison with the solid-state behaviour of the methyl 2,6-monoester described by Dwyer.[94] Each compound is found to crystallise with a different conformation about the pyridine core. The ethyl derivative adopts the conventional *cis*-*cis* conformer whilst the acid group of the benzyl analogue is observed to invert, forming the *cis*-*trans* conformer. The methyl derivative also adopts a *cis*-*trans* conformer but in this case the ester, rather than the carboxylic acid, is seen to invert. All three 2,6-monoesters form carboxylic acid dimers which associate to form tape-like arrays mediated by a similar hydrogen bonding pattern to the diesters. However, the packing modes of these dimer tapes are significantly different to their diester analogues.

The poor solubility of the 3,5-diesters has meant that only the solid-state behaviour of the benzyl derivative has been determined. Rather than the linear tape-like assemblies formed by the carboxylic acid dimers, this compound is found to form a zig-zagged tape in which adjacent molecules are linked by an O-H···N, C-H···O dimer.

Examination of the DSC curves for the ethyl and benzyl 2,6-monoesters suggests that both species may be polymorphic. The data for the 3,5-monoesters shows that the samples decompose upon melting. This is surprising considering that the pyridine-2-carboxylic acids are generally known to decarboxylate more easily than the pyridine-3-carboxylic acids.[134]

A tape-like assembly is observed for the bis(*N*,*N'*-dimethyl) 2,6-pyridinediamide. However, unlike the tapes-formed by the diesters, the pyridine cores of adjacent molecules are observed to the lie at almost 90° to each other, forming a stepped assembly. Although the 3,5-analogue packs with an apparently similar geometry, the interactions appear much weaker and the observed behaviour is thought to be the result of close-packing.

A tape-like assembly is also observed for the bis(morpholino) 3,5-pyridine-diamide. Here, the side-arms are observed to adopt a pincer-like conformation and planar tapes are formed by a pair of hydrogen bonds between the α-protons of the pyridine ring and the oxygen atoms of the morpholine group. The lower acidity of the β-pyridyl protons in the 2,6-analogue means that a comparable assembly is not observed. Instead the crystal architecture is predominantly the result of close-packing.

Attempts to form functional systems based on the pyridine dicarboxylate core have thus far been unsuccessful, however this is likely to be an area of great interest for future studies. Attempts to attach a TTF derivative to the pyridine core have been partially successful and further investigations should be carried out into the synthesis and characterisation of these systems.

The credibility of the pyridine-2,6-dicarboxylate core as a supramolecular synthon has now been firmly established and the characterisation of the 2,6-monoesters has shown that it can be used in conjunction with other established synthons. Further work along this avenue with both symmetric and asymmetric systems is likely to produce some interesting results. A few potential targets are shown in Figure 95.

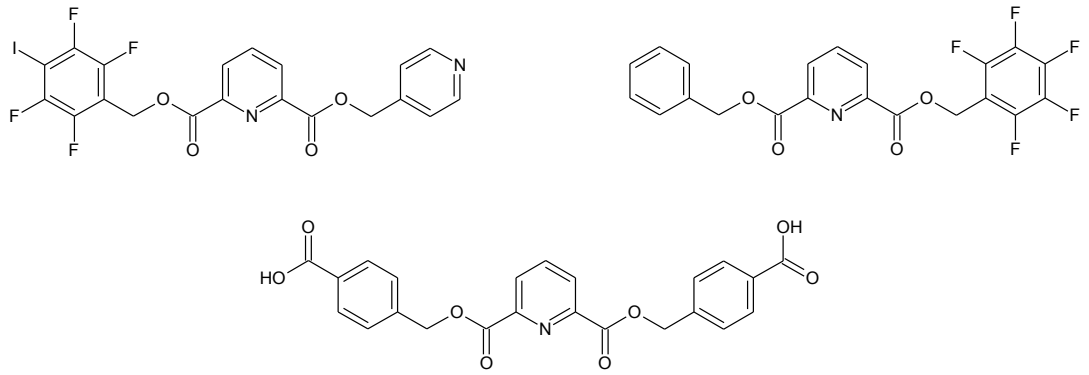

Figure 95: Ideas for 2,6-pyridinedicarboxylates with the potential to form multi-dimensional networks.

The success in forming tapes using diesters with an anthracene substituent opens the possibility of using the pyridine dicarboxylate motif in the design of materials capable of acting as sensors. Two possible scenarios could be envisaged for these systems. In the first a single, asymmetric diester is used; one side-arm would incorporate a chromophore or fluorophore whilst the other would include a switchable receptor. (The receptor would be capable of quenching the optical behaviour of the optically active group in either the bound or unbound state.) The second scenario would require a co-crystal of two different, symmetrical diesters to be prepared; one with photo-active side-arms and the other with the receptor.

Lastly, as more complex systems are prepared, a greater understanding of the factors leading up to and influencing crystal formation will be required. Since crystals are generally grown from the solution-phase, an understanding of how the molecules interact with each other and with the solvent may aid the crystal design process. Consequently, further

spectroscopic investigations into the behaviour of the pyridine dicarboxylates using NMR and Raman spectroscopy should be considered.

9 - Experimental

9.1 - General notes

Commercially available compounds were obtained from Sigma Aldrich or Fisher. All reagents and solvents were reagent grade or better and were used as supplied without further purification. Where the use of dry solvents was required, DCM was dried over calcium hydride and distilled. Diethyl ether and THF were both dried over sodium wire.

TLC analysis was performed using aluminium plates coated with a layer of silica gel 60 treated with fluorescent agent F_{254} obtained from Merck. Column chromatography was performed using chromatography grade silica 60A with a particle size of between 35 and 70 microns obtained from Fisher.

Melting points were measured using either an Electrothermal, or a Gallenkamp melting point apparatus and are uncorrected.

Electrospray mass spectra were recorded using a Micromass Platform II single quadrapole mass spectrometer. High resolution spectra were collected by the School of Chemistry Mass Spectrometry Service using a Bruker Apex III FT-ICR mass spectrometer fitted with an Apollo electrospray ionisation source.

NMR spectra were collected using either a Bruker AV300 spectrometer, or a Bruker DPX400 spectrometer; operating at 300 or 400 MHz respectively for ^{1}H NMR experiments and at 75 MHz or 100 MHz respectively for ^{13}C and Dept-135 NMR experiments. ^{13}C NMR spectra were collected fully decoupled. ACD Labs software[140] was used to process and analyse the spectral data. Chemical shift data are given in ppm. Multiplicities are denoted as follows: s, singlet; d, doublet; dd, double doublet; t, triplet; q, quartet; m, multiplet.

NMR titration data was collected at 400 MHz in deuterated chloroform containing 1% TMS as an internal standard. Spectra were calibrated so that the TMS peak occurred at a chemical shift of 0.00 ppm. Samples were prepared at a range of concentrations between 50 mM and the room temperature saturation point of the compound under study. The average chemical shift for each multiplet was calculated from the mean average of the individual positions of peaks in that multiplet. The rate of change of chemical shift as a function of concentration ($\Delta\delta$) was determined by linear regression analysis. Stacked plots of the titration spectra are presented in Appendix A.

A Thermo Nicolet 380 FT-IR spectrometer with a SmartOrbit Golden Gate Attenuated Total Reflection (ATR) attachment was used to collect IR spectra. Spectra were collected over 32 scans between 370 and 3700 cm^{-1} with a resolution of 4 cm^{-1} and a data spacing of 1.929 cm^{-1}. The spectral data was processed using the Omnic software suite.[141]

Raman IR spectra were collected using a Perkin Elmer System 2000 NIR FT-Raman spectrometer with a Perkin Elmer diode pumped Nd:YAG laser operating at 300 mW. Samples were prepared by dry loading a cut-down NMR tube (approximately 1cm long) with the crystalline material which was then placed in an electronically controlled heating cell inside the spectrometer. Spectra were collected over 64 scans between 3500 cm^{-1} and 100 cm^{-1} with a resolution of 4 cm^{-1} and a data interval of 1 cm^{-1}. Data collection was managed using the Spectrum software package[142] and baseline correction was performed manually using Origin.[143] The relative intensities of the absorptions are denoted as: s, strong; m, medium; wk, weak; br, broad. The stacked spectra are shown in Appendix B.

A Mettler Toledo DSC821^{e} low temperature differential scanning calorimeter was used to collect DSC data using aluminium pans. Data was processed using the Star^{e} software suite.[144] DSC curves are reproduced in Appendix C.

UV-visible spectra were collected using Shimadzu UV-1601 UV-visible spectrophotometer and a path length of 1 cm. Data collection was managed using the UVPC Personal Spectroscopy Software application.[145]

Elemental analysis was performed by Medac Ltd. results are accurate to ±0.30%.

Apart from compounds **55** and **69**, where data sets were collected by the EPSRC NCS at the Diamond and Daresbury synchrotron light sources, single crystal X-ray diffraction patterns were collected using either a Bruker-Nonius KappaCCD or Bruker-Nonius Apex II CCD detector. X-rays were generated with a Bruker-Nonius FR591 rotating anode X-ray generator using a molybdenum target, all data collections were performed at 120 K. Data was processed using COLLECT,[146] Denzo,[147] DirAx,[148, 149] HKL,[147] SADABS[150, 151] and XPREP[152] software applications. Structures were solved and refined using the SHELX-97[153, 154] and WinGX[155] suite of programs, including PLATON.[156] Crystal structures were analysed using Mercury[105, 106] and CrystalExplorer[107]. The ellipsoid plots included in this section were produced using ORTEP-3 for Windows.[157] A summary of the crystallographic data for each compound has been included in this chapter and electronic copies of the full crystallographic tables of data and CIF files are included on the CD at the end of this thesis. Fingerprint plots produced by CrystalExplorer are shown for all of the compounds previously discussed in Appendix D.

9.2 - Dimethyl 2,6-pyridinedicarboxylate (38)

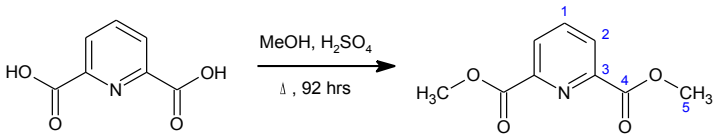

$C_7H_5NO_4$
Fw = 167.12

38
$C_9H_9NO_4$
Fw = 195.17

Concentrated H_2SO_4 (15 drops) was added to a suspension of pyridine-2,6-dicarboxylic acid (3.10 g, 18.5 mmol) in methanol (75 mL). The reaction mixture was heated at reflux for 92 hours after which the solvent was removed *in vacuo*.

The resulting white solid was dissolved in DCM (50 mL) and partitioned against a saturated aqueous solution of $NaHCO_3$ (50 mL). The phases were separated and the aqueous phase was washed with further portions of DCM (2 x 50 mL). The combined organic phases were washed with brine (2 x 50 mL) and dried over Na_2SO_4. Removal of the solvent *in vacuo* gave a crystalline solid (1.37 g, 38%).

Mpt: 119-123 °C (lit.[158] 121-124 °C (H_2O)).

^{1}H NMR (400 MHz, $CDCl_3$): **4.01** (6H, s, **H5**); **8.02** (1H, t, J = 8.0 Hz, **H1**); **8.30** (2H, d, J = 8.0 Hz, **H2**).
Lit.[94] (300 MHz, $CDCl_3$): 4.0 (6H, s); 8.0 (1H, t, J = 8.1 Hz); 8.3 (2H, d, J = 8.1 Hz).

^{1}H NMR titration:

Concentration/M	δ(H1)/ ppm	δ(H2)/ ppm	δ(H5)/ ppm
2.100	8.127	8.336	4.044
1.690	8.121	8.336	4.044
1.280	8.097	8.333	4.041
0.874	8.076	8.331	4.039
0.458	8.053	8.326	4.037
Δδ/ppm M^{-1}	0.050	0.0069	0.0051
R^2	0.98	0.93	0.97

MS ES+ M/Z: **196** (25%, M+H$^+$); **218** (100%, M+Na$^+$); **413** (45%, 2M+Na$^+$).

FTIR ν_{max} cm^{-1}: **(solid-state, selected)** **3063** (wk, aromatic C-H stretch); **2970** (wk, alkyl C-H stretch); **1738** (s, ester C=O stretch); **1570** (m, aromatic C=C stretch).

Raman FTIR: Spectra were collected at 25, 90, 100, 105, 110, 115 and 120 °C. Selected data from the 25 °C spectrum (ν_{max} cm^{-1}): **1737** (s, ester C=O stretching); **1572** (m, pyridine C=C stretching); **1450** (wk, alkyl C-H deformation); **1300**, **1283** (m, aromatic C-H deformation); **993** (s, pyridyl ring breathing); **814** (m, ester C-O-C stretching).

DSC: 2 cycles were performed between -10 and 140 °C using a 3.00 mg sample. Heating and cooling rates of 20 °C min^{-1} were used and end-point temperatures were held for 2 minutes.

Cycle	Onset temperature/°C	Peak temperature/°C	Integral/mJ
1 - heating	122.15	124.66	-517.56
1 - cooling	111.38	108.00	462.75
1 - cooling	103.12	102.00	15.64
1 - cooling	98.90	98.00	11.48
2 - heating	121.88	125.33	-515.21
2 - cooling	114.05	111.33	473.70
2 - cooling	102.00	101.00	31.04

9.3 - Dimethyl 3,5-pyridinedicarboxylate (39)

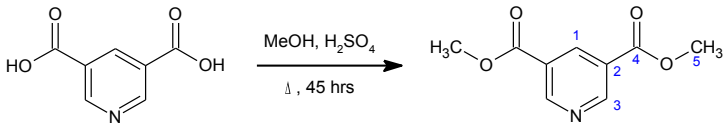

$C_7H_5NO_4$
Fw = 167.12

39
$C_9H_9NO_4$
Fw = 195.17

Concentrated H_2SO_4 (25 drops) was added to a suspension of pyridine-3,5-dicarboxylic acid (2.08 g, 12.4 mmol) in methanol (40 mL). The reaction mixture was heated at reflux for 45 hours during which time a clear, colourless solution was formed.

The reaction mixture was cooled to room temperature and poured into a 1:1 mixture of DCM and water (80 mL) and basified to pH 7-8 using a saturated solution of $NaHCO_3$ in water. The resulting emulsion was separated and the aqueous phase was washed with further portions of DCM (3 x 30 mL). The combined organic phases were dried over Na_2SO_4 and removal of the solvent *in vacuo* gave a pale yellow solid (1.43 g, 59%) which was crystallised from chloroform and light petroleum ether (bpt 60-80 °C).

Mpt: 77-79 °C (lit.[159] 84-85 °C (EtOH/light petroleum ether)).

^{1}H NMR (400 MHz, $CDCl_3$): **4.00** (6H, s, **H5**); **8.88** (1H, t, J = 2.0 Hz, **H1**); **9.37** (2H, d, J = 2.0 Hz, **H3**).
Lit:[92] 3.90 (6H, s); 8.80 (1H, t, J = 2.01 Hz); 9.30 (2H, d, J = 2.01 Hz).

^{13}C NMR (100 MHz, $CDCl_3$): **52.67** (**C5**); **125.97** (**C2**); **138.00** (**C1**); **154.18** (**C3**); **164.87** (**C4**).
Lit:[92] 54.2-53.2; 125.0; 136.9; 155.9-152.1; 165.2.

^{1}H NMR titration:

Concentration/M	δ(H1)/ ppm	δ(H3)/ ppm	δ(H5)/ ppm
2.250	8.798	9.328	4.017
1.180	8.838	9.352	4.007
0.795	8.852	9.359	4.003
0.064	8.873	9.372	3.994
Δδ/ppm M^{-1}	-0.034	-0.020	0.010
R^2	1.00	1.00	0.99

MS ES+ M/Z: **196** (100%, $M+H^+$).

FTIR ν_{max} cm^{-1}: **(solid-state, selected)** **3088**, **3010** (wk, aromatic C-H stretch); **2961** (wk, alkyl C-H stretch); **1716** (s, ester C=O stretch).

Raman FTIR: Spectra were collected at 25, 57, 67, 72, 77, 82, and 87 °C. Selected data from the 25 °C spectrum (ν_{max} cm^{-1}): **1723** (s, ester C=O stretching); **1606** (m, pyridyl C=C stretching); **1470** (alkyl C-H deformation); **1316** (aromatic C-H deformation); **1028** (pyridyl trigonal ring "breathing"); **812** (m, ester C-O-C stretching).

DSC: 2 cycles were performed between -10 and 110 °C using a 3.90 mg sample. Heating and cooling rates of 20 °C min^{-1} were used and end-point temperatures were held for 2 minutes.

Cycle	Onset temperature/°C	Peak temperature/°C	Integral/mJ
1 - heating	84.00	87.67	-535.29
1 - cooling	71.46	69.67	510.14
1 - cooling	52.00	51.00	9.66
2 - heating	83.75	87.33	-531.80
2 - cooling	70.68	69.00	518.63
2 - cooling	45.04	43.67	8.69

9.4 - Diethyl 2,6-pyridinedicarboxylate (40)

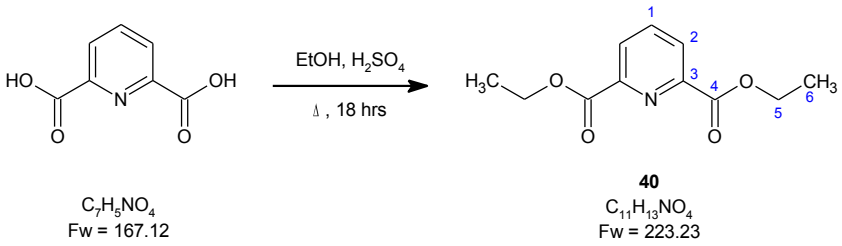

$C_7H_5NO_4$
Fw = 167.12

40
$C_{11}H_{13}NO_4$
Fw = 223.23

Concentrated H_2SO_4 (15 drops) was added to a suspension of pyridine-2,6-dicarboxylic acid (5.04 g, 30.2 mmol) in ethanol (70 mL). The reaction mixture was stirred at reflux for 18 hours.

Removal of the solvent *in vacuo* produced an oil which was dissolved in DCM (50 mL) and partitioned against a saturated aqueous solution of $NaHCO_3$ (50 mL). The phases were separated and the aqueous phase was washed with further portions of DCM (3 x 30 mL). The combined organic phases were then washed with brine (50 mL) and dried over Na_2SO_4. Removal of the solvent *in vacuo* gave a white solid (5.20 g, 78%) which was crystallised from DCM.

Mpt: 38-40 °C (lit.[160] 41-42 °C).

^{1}H NMR (400 MHz, $CDCl_3$): **1.44** (6H, t, J = 7.2 Hz, **H6**); **4.47** (4H, q, J = 7.2 Hz, **H5**); **7.99** (1H, t, J = 7.7 Hz, **H1**); **8.26** (2H, d, J = 7.7 Hz, **H2**).
Lit.[91] (400 MHz, $CHCl_3$): 1.39 (6H, t, J = 7.2 Hz); 4.42 (4H, q, J = 7.2 Hz); 7.94 (1H, t, J = 8.0 Hz); 8.21 (2H, d, J = 8.0 Hz).

^{1}H NMR titration:

Concentration/M	δ(H1)/ ppm	δ(H2)/ ppm	δ(H5)/ ppm	δ(H6)/ ppm
1.260	8.078	8.300	4.496	1.459
0.948	8.056	8.295	4.496	1.460
0.661	8.036	8.290	4.496	1.461
0.352	8.018	8.286	4.496	1.462
0.049	7.994	8.281	4.495	1.463
Δδ/ppm M^{-1}	0.068	0.015	0.0003	-0.0031
R^2	1.00	1.00	0.50	0.99

MS ES+ M/Z: **224** (23%, $M+H^+$); **246** (100%, $M+Na^+$); **469** (100%, $2M+Na^+$).

FTIR ν_{max} cm^{-1}: **(solid-state, selected)** **3062** (m, aromatic C-H stretch); **2985**, **2944**, **2907** (m, alkyl C-H stretch); **1743** (s, ester C=O stretch); **1575** (m, aromatic C=C stretch).

Raman FTIR: Spectra were collected at 25, 32, 37, 42 and 47 °C. Selected data from the 25 °C spectrum (ν_{max} cm^{-1}): **1740** (s, ester C=O stretching); **1575** (s, pyridine C=C stretching); **1460**, **1450**, **1435** (m, alkyl C-H deformation); **1278**, **1293** (m, aromatic C-H deformation); **1000** (s, pyridine ring breathing); **875**, **840** (m, ester C-O-C stretching).

DSC: 2 cycles were performed between -10 and 65 °C using a 3.00 mg sample. Heating and cooling rates of 20 °C min^{-1} were used and end-point temperatures were held for 2 minutes.

Cycle	Onset temperature/°C	Peak temperature/°C	Integral/mJ
1 - heating	43.29	46.00	-330.52
1 - cooling	8.77	4.00	279.36
2 - heating	41.81	45.33	-328.34
2 - cooling	21.27	16.67	314.27

9.5 - Diethyl 3,5-pyridinedicarboxylate (41)

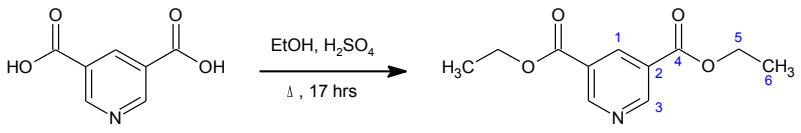

$C_7H_5NO_4$
Fw = 167.12

41
$C_{11}H_{13}NO_4$
Fw = 223.23

Concentrated H_2SO_4 (30 drops) was added to a suspension of pyridine-3,5-dicarboxylic acid (1.00 g, 6.00 mmol) in ethanol (50 mL). The reaction mixture was stirred at reflux for 17 hours.

The resulting solution was cooled to room temperature and poured into DCM (40 mL). The mixture was basified to pH 9 with a saturated solution of $NaHCO_3$ in water (50 mL). The mixture was separated and the aqueous phase was washed with further portions of DCM (3 x 30 mL). The organic phase was washed with a 1:1 mixture of brine and water (50 mL) and dried over Na_2SO_4. Removal of the solvent *in vacuo* gave a yellow solid (1.08 g, 81%) which was crystallised from DCM and light petroleum ether (bpt 60-80 °C) to give off-white crystals (382 mg, 29%).

Mpt: 45-47 °C (lit.[161] 45-47 °C).

^{1}H NMR (400 MHz, $CDCl_3$): **1.42** (6H, t, J = 7.1 Hz, **H6**); **4.44** (4H, q, J = 7.1 Hz, **H5**); **8.84** (1H, t, J = 2.1 Hz, **H1**); **9.35** (2H, d, J = 2.0 Hz, **H3**).
Lit.[91] (400 MHz, $CHCl_3$): 1.43 (6H, t, J = 7.2 Hz); 4.45 (4H, q, J = 7.2 Hz); 8.86 (1H, t, J = 2.0 Hz); 9.35 (2H, d, J = 2.0 Hz).

^{1}H NMR titration:

Concentration/M	δ(H1)/ ppm	δ(H3)/ ppm	δ(H5)/ ppm	δ(H6)/ ppm
4.150	8.744	9.297	4.468	1.472
2.720	8.807	9.335	4.471	1.464
1.360	8.836	9.353	4.468	1.456
0.056	8.861	9.367	4.455	1.436
Δδ/ppm M^{-1}	-0.028	-0.017	0.003	0.0085
R^2	0.96	0.95	0.56	0.94

MS ES+ M/Z: **224** (100%, $M+H^+$)

FTIR ν_{max} cm^{-1}: **2987**, **2933**, **2902** (m, alkyl C-H stretch); **1717** (s, ester C=O stretch); **1604** (m, aromatic C=C stretch)
(solid-state, selected)

Raman FTIR: Spectra were collected at 25, 30, 35, 40, 45, 50 °C. Selected data from the 25 °C spectrum (ν_{max} cm^{-1}): **1721** (s, ester C=O stretching); **1606** (m, pyridyl C=C stretching); **1454** (br, m, alkyl C-H deformation); **1302**, **1263** (m, aromatic C-H deformations); **1028** (s, pyridyl ring breathing); **874** (m, ester C-O-C stretching)

DSC: 2 cycles were performed between -10 and 65 °C using a 2.70 mg sample. Heating and cooling rates of 20 °C min^{-1} were used and end-point temperatures were held for 2 minutes.

Cycle	Onset temperature/°C	Peak temperature/°C	Integral/mJ
1 - heating	49.13	52.67	-339.19
1 - cooling	22.28	14.33	318.63
2 - heating	48.34	51.33	-338.21
2 - cooling	28.20	24.33	322.09

9.6 - *bis*(Neopentyl) 2,6-pyridinedicarboxylate (42)

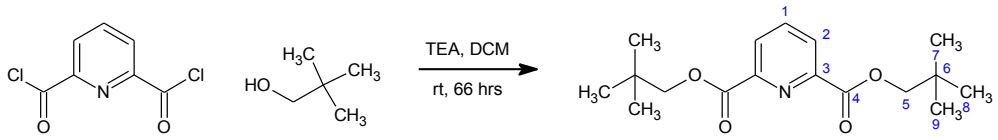

$C_7H_3Cl_2NO_2$
Fw = 204.01

$C_5H_{12}O$
Fw = 88.15

42
$C_{17}H_{25}NO_4$
Fw= 307.38

A solution of 2,6-pyridinedicarbonyl dichloride (1.26 g, 6.17mmol) in DCM (25 mL) was added to a suspension of neopentyl alcohol (1.07 g, 12.1 mmol) and TEA (1.72 mL, 12.3 mmol) in DCM (30 mL). The reaction mixture was stirred at room temperature for 66 hours after which a clear, pale yellow solution had been formed.

The solvent was removed *in vacuo* to give a pale yellow solid which was dissolved in DCM (50 mL) and partitioned against a saturated solution of $NaHCO_3$ in water (100 mL). The phases were separated and the aqueous phase was washed with further portions of DCM (2 x 50 mL). The organic phases were combined and washed with brine (100 mL). Removal of the solvent *in vacuo* gave an off-white solid (2.07 g) which was purified by flash column chromatography using an eluent of diethyl ether (30% v/v) in light petroleum ether (bpt 40-60 °C), to yield a white solid (0.91 g, 48%, R_f = 0.22). White needle crystals (463 mg, 24%) were obtained by crystallisation from DCM and light petroleum ether (bpt 40-60 °C).

Mpt: 181-183 °C (lit. [92] 188-190 ºC).

^{1}H NMR (400 MHz, $CDCl_3$): **1.07** (18H, s, **H7**, **H8**, **H9**); **1.70** (1H, s, H_2O); **4.12** (4H, s, **H5**); **7.99** (1H, t, J = 8.0 Hz, **H1**); **8.26** (2H, d, J = 8.0 Hz, **H2**).
Lit:[92] 1.1 (18H, s); 4.1 (4H, s,); 8.0 (1H, t, J = 8.03 Hz); 8.3 (2H, d, J = 8.03 Hz).

^{1}H NMR titration:

Concentration/M	δ(H1)/ ppm	δ(H2)/ ppm	δ(H5)/ ppm	δ(H7)/ ppm
0.469	8.010	8.265	4.120	1.072
0.359	8.006	8.265	4.119	1.073
0.263	7.998	8.262	4.118	1.071
0.152	7.989	8.258	4.116	1.069
0.040	7.984	8.256	4.114	1.067
Δδ/ppm M^{-1}	0.063	0.023	0.014	0.013
R^2	0.98	0.94	0.98	0.85

MS ES+ M/Z: **308** (37%, M+H$^+$); **330** (100%, M+Na$^+$); **637** (55%, 2M+Na$^+$).

FTIR ν_{max} cm^{-1}: **(solid-state, selected)** **3061** (m, aromatic C-H stretch); **2952**, **2902**, **2867** (m, alkyl C-H stretch); **1737** (ester C=O stretch); **1577** (aromatic C=C stretch).

Raman FTIR: Spectra were collected at 25, 60, 110, 162, 182, 187, 192, 197 and 202 °C. Selected data from the 25°C spectrum (ν_{max} cm^{-1}): **1735** (s, ester C=O stretching); **1576** (m, pyridine C=C stretching); **1461**, **1449** (br, m, alkyl C-H deformation); **1295**, **1281** (aromatic C-H deformation); **997** (m, pyridine ring breathing); **828** (m, ester C-O-C stretching).

DSC: 2 cycles were performed between 25 and 230 °C using a 3.29 mg sample. Heating and cooling rates of 20°C min^{-1} were used and end-point temperatures were held for 2 minutes.

Cycle	Onset temperature/°C	Peak temperature/°C	Integral/mJ
1 - heating	191.08	194.67	-553.48
1 - cooling	163.00	162.00	516.94
2 - heating	190.83	195.00	-548.36
2 - cooling	163.00	161.67	560.22

9.7 - *bis*(Neopentyl) 3,5-pyridinedicarboxylate (43)

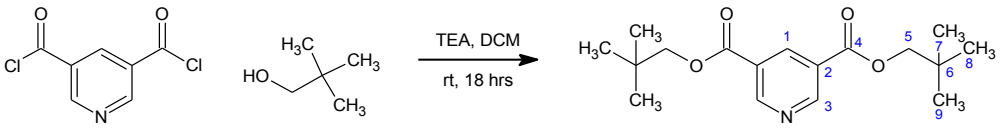

$C_7H_3Cl_2NO_2$
Fw = 204.01

$C_5H_{12}O$
Fw = 88.15

43
$C_{17}H_{25}NO_4$
Fw= 307.38

The compound was prepared and spectroscopic data collected in collaboration with an undergraduate project student, W. Mothersole.[162]

A solution of 3,5-pyridinedicarbonyl dichloride (1.89 g, 9.26 mmol) in DCM (30 mL) was added to a suspension of neopentyl alcohol (1.633 g, 18.5 mmol) and TEA (2.6 mL, 19 mmol) in DCM (40 mL). The reaction mixture was stirred at room temperature for 18 hours.

Removal of the solvent *in vacuo* gave an off-white solid which was dissolved in DCM (50 mL) and partitioned against a saturated aqueous solution of $NaHCO_3$ (40 mL). The phases were separated and the organic phase was washed with a further portion of saturated $NaHCO_3$ (40 mL). The combined aqueous phases were washed with DCM (3 x 30 mL). The organic phases were combined, washed with brine (2 x 40 mL) and dried over $MgSO_4$. The organic solvent was removed *in vacuo* and the crude product was purified (R_f = 0.36) by flash column chromatography using an eluent of diethyl ether (30% v/v) in light petroleum ether (bpt 40-60). Removal of the solvent *in vacuo* gave a white crystalline product (1.34 g, 47%).

Mpt: 139-140 °C (lit.[91] 137 °C).

^{1}H NMR (400 MHz, $CDCl_3$): **1.06** (18H, s, **H7**, **H8**, **H9**); **4.09** (4H, s, **H5**); **8.88** (1H, t, J = 2.0 Hz, **H1**); **9.39** (2H, d, J = 2.0 Hz, **H3**).
Lit.[91] (400 MHz, $CHCl_3$): 0.99 (18H, s, J = 7.2 Hz); 4.02 (4H, s); 8.81 (1H, t, J = 1.8 Hz); 9.32 (2H, d, J = 1.8Hz).

^{1}H NMR titration:

Concentration/M	**δ(H1)/ ppm**	**δ(H3)/ ppm**	**δ(H5)/ ppm**	**δ(H7)/ ppm**
1.140	8.888	9.405	4.107	1.082
0.776	8.888	9.404	4.103	1.076
0.411	8.885	9.401	4.098	1.070
0.040	8.878	9.393	4.089	1.060
$\Delta\delta$/ppm M^{-1}	0.0087	0.011	0.016	0.020
R^2	0.81	0.86	0.96	0.98

MS ES+ M/Z: **308** (100%, $M+H^+$).

FTIR ν_{max} cm^{-1}: **(solid-state, selected)** **3029**, **3008** (wk, aromatic C-H stretch); **2953**, **2900** **2867** (m, alkyl C-H stretch); **1717** (s, ester C=O stretch); **1598** (m, aromatic C=C stretch).

Raman FTIR: Spectra were collected at 25, 115, 120, 125, 130, 135, 140 and 145 °C. Selected data from the 25°C spectrum (ν_{max} cm^{-1}): **1720** (s, ester C=O stretching); **1599** (s, pyridine C=C stretching); **1459** (br, m, alkyl C- H deformation); **1299** (m, aromatic C-H deformation); **1022** (s, pyridine ring breathing); **823** (m, ester C-O-C stretching).

DSC: 2 cycles were performed between -10 and 160 °C using a 2.50 mg sample. Heating and cooling rates of 20 °C min^{-1} were used and end-point temperatures were held for 2 minutes.

Cycle	Onset temperature/°C	Peak temperature/°C	Integral/mJ
1 - heating	143.11	145.66	-342.44
1 - cooling	110.00	108.66	347.86
2 - heating	142.32	145.66	-318.40
2 - cooling	107.01	105.66	330.33

9.8 - *bis*(Benzyl) 2,6-pyridinedicarboxylate (44)

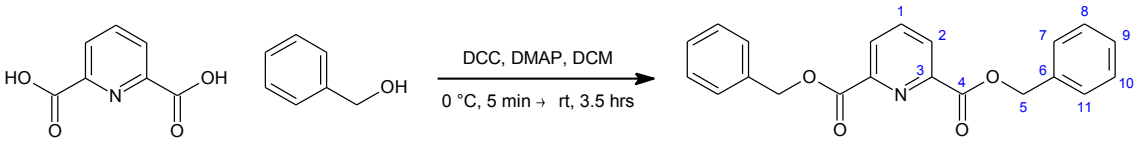

$C_7H_5NO_4$
Fw = 167.12

C_7H_8O
Fw = 108.14

44
$C_{21}H_{17}NO_4$
Fw = 347.36

DMAP (105 mg, 0.86 mmol) was added to a suspension of pyridine-2,6-dicarboxylic acid (1.37 g, 8.19 mmol), benzyl alcohol (1.7 mL, 16 mmol) and DCC (3.40 g, 16.5 mmol) in DCM (50 mL) at 0 °C. The reaction mixture was stirred at 0 °C for 5 minutes before warming to room temperature and stirring for a further 3.5 hours.

The solvent was removed *in vacuo* to give a white solid which was dissolved in DCM (80 mL) and filtered. The filtrate was washed sequentially with aqeuous solutions of HCl (1M, 50 mL), $NaHCO_3$ (saturated, 50 mL) and brine (50 mL). The organic phase was then dried over Na_2SO_4 before removal of the solvent *in vacuo* yielded a yellow crystalline powder (3.12 g). This was crystallised from DCM and chloroform with light petroleum ether (bpt 40-60°C) to give off-white crystalline platelets (1.77 g, 62%)

Mpt: 114-116 °C (DCM/$CHCl_3$/light petroleum ether); lit. 119 °C (acetone).[90]

^{1}H NMR (400 MHz, $CDCl_3$): **5.39** (4H, s, **H5**); **7.22**-**7.32** (6H, m, **H8**, **H9**, **H10**); **7.41** (4H, d, J = 7.3 Hz, **H7**, **H11**); **7.89** (1H, t, J = 7.9 Hz, **H1**); **8.19** (2H, d, J = 7.9 Hz, **H2**).

Lit.[90] ($CHCl_3$): 5.45(4H,s); 7.37(5H,m); 7.50(4H,d, J 7.5Hz); 7.98 (1H,t, J 8.0Hz); 8.27(2H,d, J 8.0Hz).

^{1}H NMR titration:

Concentration/M	δ(H1)/ppm	δ(H2)/ppm	δ(H5)/ppm
0.754	7.904	8.204	5.423
0.573	7.922	8.223	5.435
0.399	7.928	8.231	5.44
0.219	7.945	8.248	5.450
0.040	7.967	8.265	5.461
Δδ/ppm M^{-1}	-0.084	-0.083	-0.051
R^2	0.97	0.99	0.99

MS ES+ M/Z: **370** (19%, $M+Na^+$); **717** (100%, $2M+Na^+$).

FTIR ν_{max} cm^{-1}:
(solid-state, selected) **3323**, **3060**, **3030** (m, aromatic C-H stretch); **2927**, **2850** (m, alkyl C-H stretch); **1742** (m, ester C=O stretch); **1624** (phenyl aromatic C=C stretch); **1573** (pyridyl aromatic C=C stretch).

Raman FTIR: Spectra were collected at 25, 93, 102, 107, 112, 117 and 122 °C. Selected data from the 25 °C spectrum (ν_{max} cm^{-1}): **1746** (s, ester C=O stretch); **1607** (m, phenyl aromatic C=C stretch); **1584**, **1574** (m, pyridyl aromatic C=C stretch); **1212** (m, aromatic C-H deformation); **1030** (m, benzyl ring breathing), **1000** (s, pyridyl ring breathing); **877** (m, ester C-O-C stretching).

DSC: 2 cycles were performed between -10 and 140 °C using a 3.20 mg sample. Heating and cooling rates of 20 °C min^{-1} were used and end-point temperatures were held for 2 minutes.

Cycle	Onset temperature/°C	Peak temperature/°C	Integral/mJ
1 - heating	123.64	127.00	-420.42
1 - cooling	98.13	91.33	388.60
2 - heating	123.57	127.00	-417.33
2 - cooling	98.93	91.66	385.97
2 - cooling	85.51	84.66	1.17

9.9 - *bis*(Benzyl) 3,5-pyridinedicarboxylate (45)

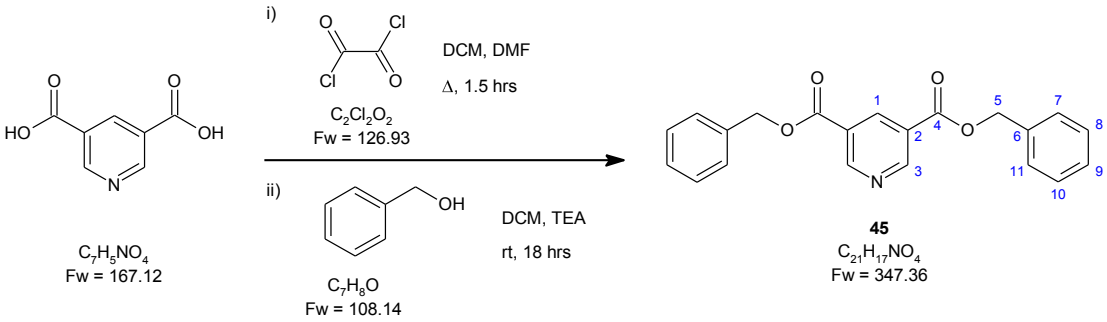

DMF (10 drops) was added to a suspension of pyridine-3,5-dicarboxylic acid (2.09 g, 12.5 mmol) in a solution of oxalyl chloride (2.2 mL, 26 mmol) and DCM (40 mL). The reaction mixture was stirred at reflux under nitrogen for 90 minutes during which time a pale yellow solution was formed. Removal of the solvent *in vacuo* gave an off-white solid which was dissolved in DCM (50 mL).

Benzyl alcohol (2.6 mL, 25 mmol) and TEA (3.5 mL, 25 mmol) were added to the resulting solution causing a violent reaction. Additional TEA (2 mL, 14.3 mmol) was added and the reaction mixture was stirred at room temperature for 18 hours producing a suspension of white precipitate in a brown solution.

Removal of the solvent *in vacuo* gave a white and brown solid which was dissolved in DCM (40 mL) and partitioned against a mixture of water (20 mL) and a saturated solution of $NaHCO_3$ (40 mL). The aqueous phase was

washed with further portions of DCM (2 x 40 mL). The combined organic phases were washed with brine (40 mL) and dried over Na_2SO_4. Removal of the solvent *in vacuo* gave a dark brown oil which solidified on standing.

This crude solid was purified by crystallisation and subsequent crystallisation from DCM and light petroleum ether (bpt 60-80°C) to give white needles (2.74 g, 63%).

Mpt: 68-70 °C (lit.[91] 69 °C (DCM/heptane)).

^{1}H NMR (400 MHz, $CDCl_3$): **5.43** (4H, s, **H5**); **7.32**-**7.54** (10 H, m, **H7**-**H11**); **8.91** (1H, t, J = 2.1 Hz, **H1**); **9.40** (2H, d, J = 2.1 Hz, **H3**).
Lit.[91] (400 MHz, $CHCl_3$): 5.43 (4H, s); 7.44 (10H, m); 8.91 (1H, t, J = 2.2 Hz); 9.40 (2H, d, J = 2.2 Hz).

^{1}H NMR titration:

Concentration/M	δ(H1)/ppm	δ(H3)/ppm	δ(H5)/ppm
2.890	8.825	9.347	5.331
2.190	8.841	9.355	5.345
1.480	8.860	9.366	5.364
0.786	8.879	9.379	5.386
0.082	8.895	9.390	5.414
Δδ/ppm M^{-1}	-0.025	-0.016	-0.030
R^2	1.00	0.99	0.98

MS ES+ M/Z: **348** (62%, M+H$^+$); **717** (22%, M+Na$^+$).

FTIR ν_{max} cm^{-1}: **(solid-state, selected)** **3061**, **3032** (m, aromatic C-H stretch); **2943** (wk, alkyl C-H stretch); **1724** (s, ester C=O stretch); **1597** (s, aromatic C=C stretch).

Raman FTIR: Spectra were collected at 47, 57, 62, 67, 72 and 77 °C. Selected data from the spectrum collected at 47 °C (ν_{max} cm^{-1}): **1724** (s, ester C=O stretch); **1599** (br, s, aromatic C=C stretching); **1460** (m, alkyl C-H deformation); **1214** (m, aromatic C-H deformation); **1024** (s, benzyl ring breathing); **1001** (s, pyridyl ring breathing); **880** (br. m, ester C-O-C stretching).

DSC: 2 cycles were performed between -10 and 90 °C using a 3.50 mg sample. Heating and cooling rates of 20 °C min^{-1} were used and end-point temperatures were held for 2 minutes.

Cycle	Onset temperature/°C	Peak temperature/°C	Integral/mJ
1 - heating	71.86	75.33	-358.92
2 - heating	37.68	50.00	337.59
2 - heating	69.29	73.67	-337.67

9.10 - *bis*(Phenyl) 2,6-pyridinedicarboxylate (46)

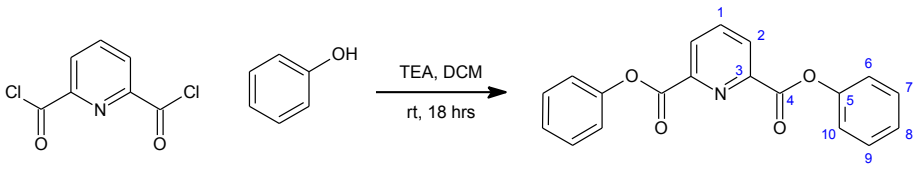

$C_7H_3Cl_2NO_2$
Fw = 204.01

C_6H_6O
Fw = 94.11

46
$C_{19}H_{13}NO_4$
Fw = 319.31

Addition of triethylamine (1.4 mL, 10.0 mmol) to a suspension of 2,6-pyridinedicarbonyl dichloride (1.05 g, 5.12 mmol) and phenol (968 mg, 10.3 mmol) in DCM (60 mL) caused the reaction mixture to turn purple. The reaction mixture was stirred at room temperature for 18 hours, during which time the coloured suspension was observed to clear to form a colourless solution.

The solvent was removed *in vacuo* and the resulting solid was dissolved in DCM (50 mL) and partitioned against an aqeuous solution of NaOH (2 M, 50

mL). The aqueous phase was separated and washed with further portions of DCM (3 x 30 mL), the combined organic phases were dried over Na_2SO_4 and the solvent was removed *in vacuo* to give an off-white solid (1.7294 g).

Crystallisation of this from chloroform and light petroleum ether (bpt 60-80 °C) gave white, plate-like crystals (680 mg, 42%). These were unsuitable for single crystal X-ray diffraction so a second crystallisation from chloroform and heptane was performed.

Mpt: 180 °C (lit.[163] 179 °C).

^{1}H NMR (400 MHz, $CDCl_3$): **7.28**-**7.36** (6H, m, **H7**, **H8**, **H9**); **7.40**-**7.54** (4H, m, **H6**, **H10**); **8.15** (1H, t, J = 8.0 Hz, **H1**); **8.50** (2H, d, J = 8.0 Hz, **H2**).
Lit:[92] 7.20 (5H, m); 7.35 (4H, dd, J = 6.6, 5.3 Hz); 8.05 (1H, t, J = 8.1 Hz); 8.45 (2H, d, J = 8.1 Hz).

^{13}C NMR (100 MHz, $CDCl_3$): **121.59** (**C7**, **C9**); **126.23** (**C2**); **128.87** (**C18**); **129.51** (**C6**, **C10**); **138.53** (**C1**); **148.24** (**C5**); **150.86** (**C3**); **163.15** (**C4**).
Lit:[92] 122.0; 126.7; 129.3; 130.0; 139.0; 148.7; 151.3; 163.6.

MS ES+ M/Z: **320** (20%, $M+H^+$); **342** (100%, $M+Na^+$); **661** (30%, $2M+Na^+$).

FTIR ν_{max} cm^{-1}: (solid-state, selected) **3063** (m, aromatic C-H stretch); **1757** (s, ester C=O stretch).

DSC: 2 cycles were performed between 0 and 200 °C using a 2.07 mg sample. Heating and cooling rates of 10 °C min^{-1} were used and end-point temperatures were held for 2 minutes.

Cycle	Onset temperature/°C	Peak temperature/°C	Integral/mJ
1 - heating	182.04	182.42	-314.45
1 - cooling	154.91	156.86	303.36
2 - heating	181.71	182.49	-310.57
2 - cooling	167.41	167.90	299.88

Elemental analysis: Found: C, 71.36%; H, 4.04%; N, 4.25%
Calculated: C, 71.47%; H, 4.10%; N, 4.38%

X-ray diffraction: All atoms were found from the electron density map.

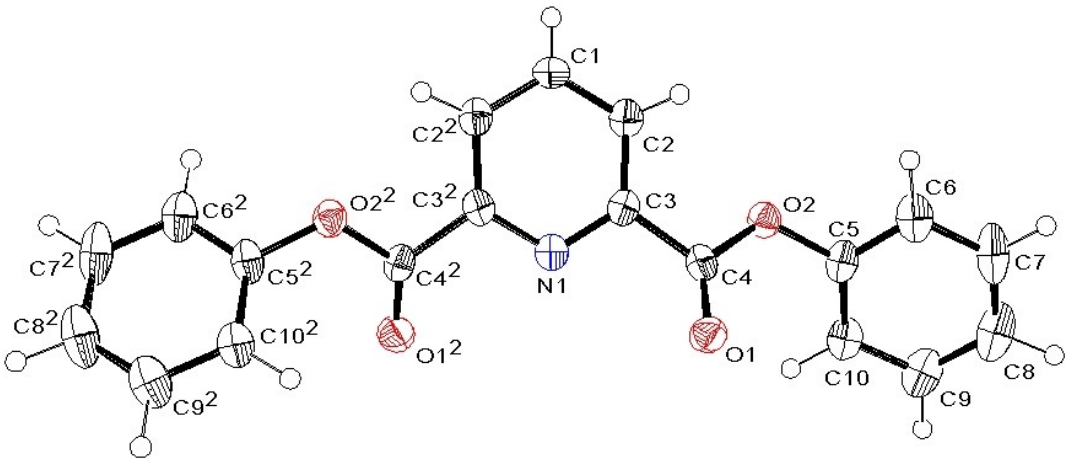

$C_{19}H_{13}NO_4$	a = 34.437 (4) Å	T 120 K
Monoclinic C2/c	b = 6.2697 (7) Å	λ = 0.71073 Å
V = 1518.05 (19) $Å^3$	c = 7.0743 (7) Å	D_c = 1.40 g cm^{-3}
Z = 4	α = 90.000 (0)°	μ = 0.099 mm^{-1}
R_1 = 7.7%	β = 96.341 (11)°	0.14 x 0.08 x 0.01 mm^3
R_{all} = 9.5%	γ = 90.000 (0)°	Clear, colourless plate

9.11 - *bis*(Phenyl) 3,5-pyridinedicarboxylate (47)

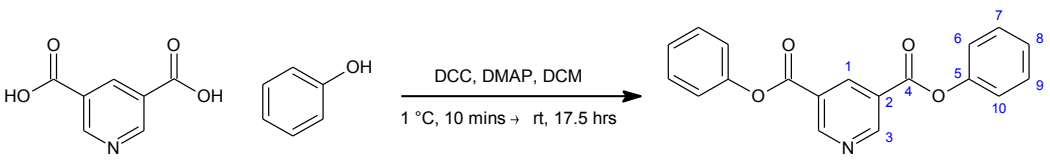

$C_7H_5NO_4$
Fw = 167.12

C_6H_6O
Fw = 94.11

47
$C_{19}H_{13}NO_4$
Fw = 319.31

DMAP (98 mg, 0.80 mmol) was added to a solution of pyridine-3,5-dicarboxylic acid (489 mg, 2.93 mmol), phenol (570 mg, 6.05 mmol) and 1,3-dicyclohexylcarbodiimide (610 mg, 5.86 mmol) in DCM (60 mL) at 1 °C. The reaction mixture was stirred for 10 minutes before warming to room temperature and stirring for a further 17.5 hours.

Solvent was removed from the resulting suspension *in vacuo* and the solid produced was dissolved in DCM (50 mL) and filtered. The residue was washed with DCM (30 mL) and the combined filtrates were partitioned sequentially against an aqueous solution of HCl (2M, 50 mL) and a saturated aqueous solution of $NaHCO_3$ (50 mL). Removal of solvent from the organic phase *in vacuo* yielded a white solid (1.05 g) which was crystallised from $CHCl_3$ and light petroleum ether (bpt 60-80 °C) to give colourless crystals (94 mg, 37%).

Mpt: 120-121 °C.

^{1}H NMR (400 MHz, $CDCl_3$): **7.32** (4H, d, J = 7.5 Hz, **H6**, **H10**); **7.38** (2H, t, J = 7.5 Hz, **H8**); **7.52** (4H, t, J = 7.8 Hz, **H7**, **H9**); **9.24** (1H, t, J = 2.0 Hz, **H1**); **9.66** (2H, d, J = 2.0 Hz, **H3**).

^{13}C NMR (100 MHz, $CDCl_3$): **121.41** (**C6**, **C10**); **125.79** (**C2**); **126.44** (**C8**); **129.66** (**C7**, **C9**); **138.93** (**C1**); **150.32** (**C5**); **155.11** (**C3**); **162.91** (**C4**).

MS (ES+) M/Z: **320** (100%, $M+H^+$); **361** (50%, $M+MeCN+H^+$); **661** (23%, $2M+Na^+$).

FTIR ν_{max} cm^{-1}: **(solid-state, selected)** **3075**, **3040** (wk, aromatic C-H stretch); **1733** (s, ester C=O stretch); **1588** (s, aromatic C=C stretch).

DSC: 2 cycles were performed between 25 and 170 °C using a 2.88 mg sample. Heating and cooling rates of 10 °C min^{-1} were used and end-point temperatures were held for 2 minutes.

Cycle	Onset temperature/°C	Peak temperature/°C	Integral/mJ
1 - heating	124.42	127.01	-307.42
1 - cooling	92.20	91.18	291.27
2 - heating	122.89	125.68	-303.43
2 - cooling	88.79	87.84	288.16

Elemental analysis: Found: C, 71.67%; H, 3.93%; N, 4.99%
Calculated: C, 71.47%; H, 4.10%; N, 4.38%

X-ray diffraction: All atoms were found from the electron density map.

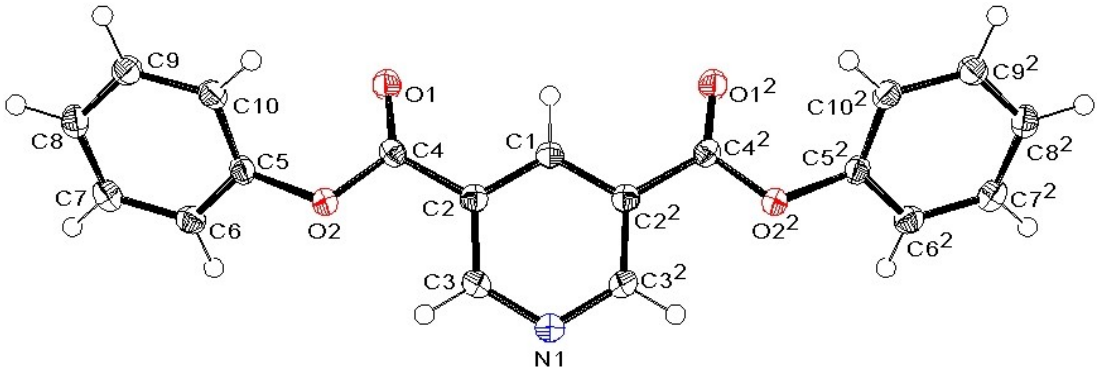

$C_{19}H_{13}NO_4$	a = 10.9016 (2) Å	T 120 K
Orthorhombic P n m a	b = 35.2929 (9) Å	λ = 0.71073 Å
V = 1464.09 (1) $Å^3$	c = 3.80530 (10) Å	D_c = 1.45 g cm^{-3}
Z = 4	α = 90.000 (0)°	μ = 0.103 mm^{-1}
R_1 = 4.4%	β = 90.000 (0)°	0.14 x 0.12 x 0.04 mm^3
R_{all} = 4.8%	γ = 90.000 (0)°	Clear, colourless cut plate

9.12 - *bis*-(2,4,6-Trimethylbenzyl) 2,6-pyridinedicarboxylate (61)

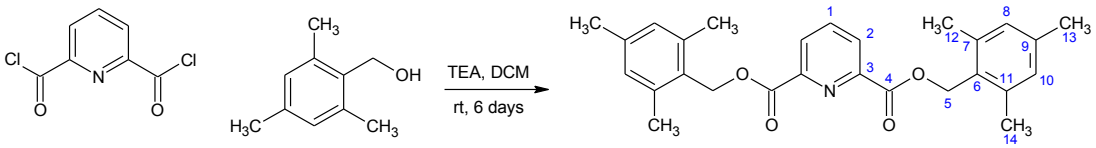

$C_7H_3Cl_2NO_2$
Fw = 204.01

$C_{10}H_{14}O$
Fw = 150.22

61
$C_{27}H_{29}NO_4$
Fw = 431.52

TEA (0.56 mL, 3.7 mmol) was added to a solution of 2,6-pyridinedicarbonyl dichloride (678 mg, 3.33 mmol) and 2,4,6-trimethylbenzyl alcohol (1.01 g, 6.71 mmol) in DCM (150 mL). The solution was stirred at room temperature for 148 hours after which the solvent was removed *in vacuo*.

The resultant solid was dissolved in DCM (50 mL) and partitioned against water (50 mL). The phases were separated and the aqueous phase was washed with further portions of DCM (2 x 50 mL). The combined organic phases were washed with brine (50 mL) and dried over $MgSO_4$. Removal of the solvent *in vacuo* gave a pale yellow solid (1.28 g) which was crystallised from DCM to give a white crystalline solid (193 mg, 13%).

Mpt: 120-123 °C.

^{1}H NMR (300 MHz, $CDCl_3$): **2.30** (6H, s, **H13**); **2.42** (12H, s, **H12**, **H14**); **5.50** (4H, s, **H5**); **6.89** (4H, s, **H8**, **H10**), **7.90** (1H, t, J = 8.1 Hz, **H1**); **8.17** (2H, d, J = 8.1 Hz, **H2**).

^{13}C NMR (75 MHz, $CDCl_3$): **19.68** (**C12**, **C14**); **20.99** (**C13**); **62.51** (**C5**); **127.57** (**C2**); **128.69** (**C6**); **129.04** (**C8**, **C10**); **137.89** (**C1**); **138.41** (**C7**, **C11**); **138.48** (**C9**); **148.61** (**C3**); **164.45** (**C4**).

MS (ES+) M/Z: **432** (100%, $M+H^+$); **454** (40%, $M+Na^+$); **885** (50%, $2M+Na^+$).

HRMS (ES+) M/Z: Found: 454.1980; calculated: 454.1989 ($C_{27}H_{29}NNaO_4$, $M+Na^+$) error = 1.97 ppm.

FTIR ν_{max} cm^{-1}: **(solid-state, selected)** **3064**, **3003** (m, aromatic C-H stretch); **2962**, **2913**, **2856** (m, alkyl C-H stretch); **1724** (s, ester C=O stretch)

Elemental analysis: Found: C, 75.16%; H, 6.39%; N, 3.35%
Calculated: C, 75.15%; H, 6.77%; N, 3.24%

X-ray diffraction: All atoms, including protons, were found from the electron density map.

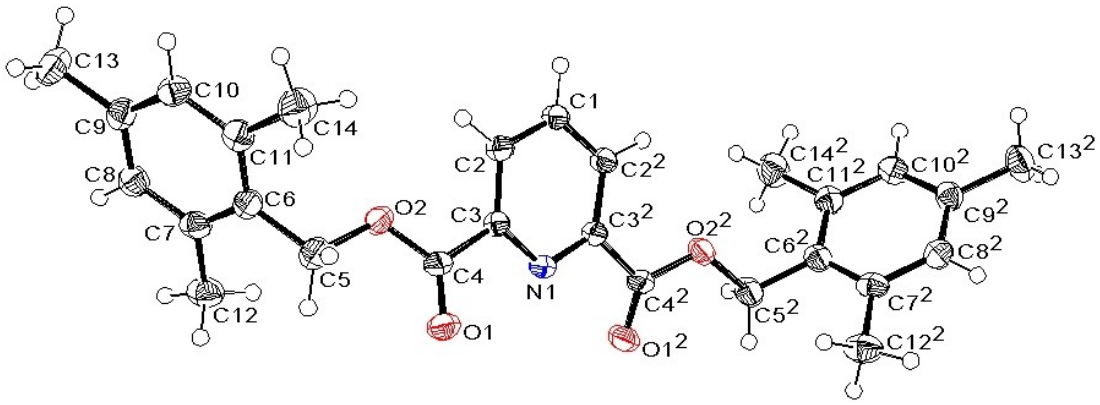

$C_{27}H_{29}NO_4$	a = 21.4705 (8) Å	T = 120 K
Monoclinic C 2/c	b = 6.1963 (2) Å	λ = 0.71073 Å
V = 2323.90 (23) $Å^3$	c = 19.1792(6) Å	D_c = 1.23 g cm^{-3}
Z = 4	α = 90.00 (0)°	μ = 0.082 mm^{-1}
R_1 = 7.0 %	β = 114.387 (2)°	0.1 x 0.04 x 0.02 mm^3
R_{all} = 11.6 %	γ = 90.00 (0)°	Clear, colourless cut plate

9.13 - *bis*(2,4,6-Trimethylbenzyl) 3,5-pyridinedicarboxylate (64)

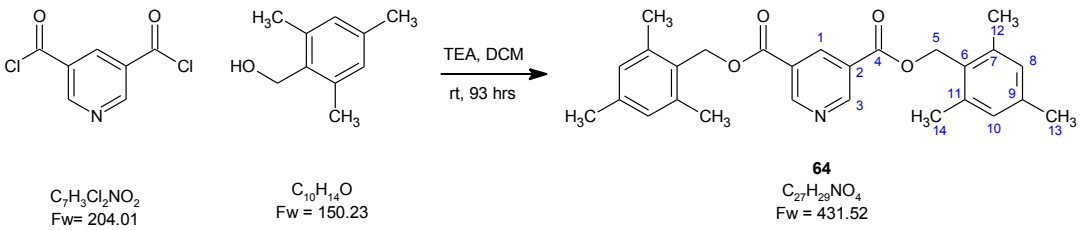

$C_7H_3Cl_2NO_2$
Fw= 204.01

$C_{10}H_{14}O$
Fw = 150.23

64
$C_{27}H_{29}NO_4$
Fw = 431.52

Addition of TEA (0.57 mL, 4.1 mmol) to a solution of 3,5-pyridinedicarbonyl dichloride (689 mg, 3.38 mmol) and 2,4,6-trimethylbenzyl alcohol (1.01 g, 6.76 mmol) in DCM (150 mL) caused the solution to turn orange pink in colour and white vapour to form. The reaction mixture was stirred at room temperature for 93 hours after which TLC showed that the reaction had not gone to completion. Additional TEA (0.3 mL, 2.15 mmol) was added, causing more vapour to be produced. The reaction mixture was stirred at room temperature for a further 36 hours after which the solvent was removed *in vacuo*.

The resulting solid was dissolved in DCM (60 mL) and partitioned against water (50 mL). The phases were separated and the aqueous phase was washed with further portions of DCM (3 x 30 mL). The combined organic extractions were washed with brine (50 mL) and dried over $MgSO_4$. The solvent was removed *in vacuo* to give a crude product (971 mg, 72 %) which was crystallised from acetonitrile to give fine white needles (118 mg, 8%).

Mpt: 137-139 °C (MeCN); 143-145 °C (EtOAc).

^{1}H NMR (300 MHz, $CDCl_3$): **2.31** (6H, s, **H13**); **2.42** (12H, s, **H12**, **H14**); **5.49** (4H, s, **H5**); **6.92** (4H, s, **H8**, **H10**); **8.80** (1H, t, J = 2.0 Hz, **H1**); **9.32** (2H, d, J = 2.0 Hz, **H3**).

^{13}C NMR (75 MHz, $CDCl_3$): **19.62** (**C12**, **C14**); **21.02** (**C13**); **62.34** (**C5**); **126.10** (**C2**); **128.40** (**C6**); **129.18** (**C8**, **C10**); **138.07** (**C9**); **138.31** (**C1**); **138.83** (**C7**, **C11**); **154.17** (**C3**); **164.47** (**C4**).

MS ES+ M/Z: **218** (90%, $M+2H^+$); **432** (100%, $M+H^+$).

FTIR ν_{max} cm^{-1}: **(solid-state, selected)** **3007** (m, aromatic C-H stretch); **2970**, **2915** (m, alkyl C-H stretch); **1720** (s, ester C=O stretch).

Elemental analysis: Found: C, 75.32%; H, 6.62%; N, 3.20%
Calculated: C, 75.15%; H, 6.77%; N, 3.24%

X-ray diffraction: All atoms were found from the electron difference map.

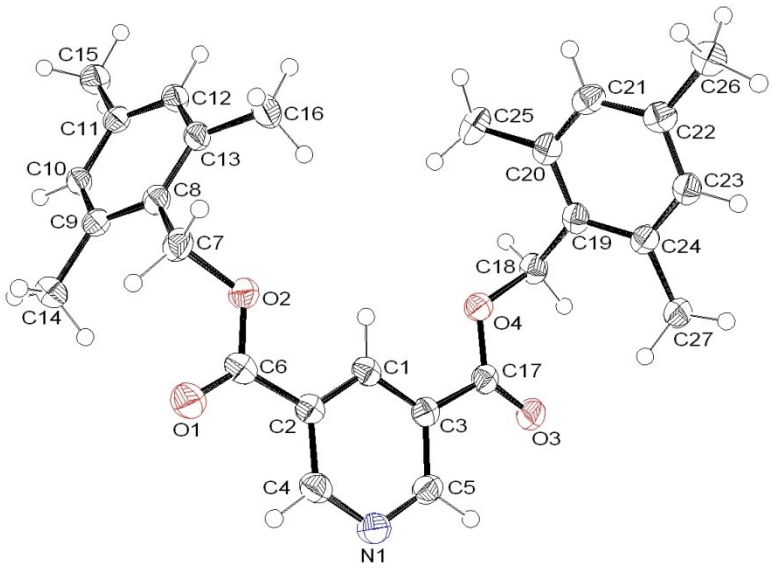

$C_{27}H_{29}NO_4$	a = 4.44630 (10) Å	T = 120 K
Monoclinic P $2_1/c$	b = 22.6226 (6) Å	λ = 0.71073 Å
V = 2253.96 (4) $Å^3$	c = 22.4960 (5) Å	D_c = 1.27 g cm^{-3}
Z = 4	α = 90.000 (0)°	μ = 0.085 mm^{-1}
R_1 = 6.2 %	β = 95.068 (2)°	0.02 x 0.02 x 0.14 mm^3
R_{all} = 9.8 %	γ = 90.000 (0)°	Clear, colourless cut needle

9.14 - *bis*(2,4,6-Trichlorobenzyl) 2,6-pyridinedicarboxylate (67)

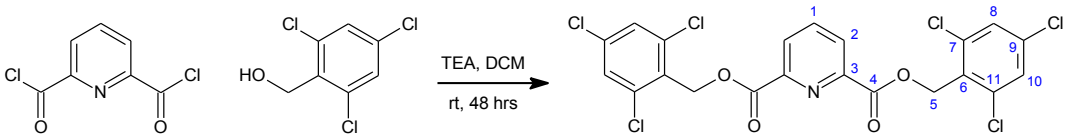

$C_7H_3Cl_2NO_2$
Fw = 204.01

$C_7H_5Cl_3O$
Fw = 211.47

67
$C_{21}H_{11}Cl_6NO_4$
Fw = 554.03

TEA (0.40 mL, 2.9 mmol) was added to a solution of 2,6-pyridinedicarbonyl dichloride (479 mg, 2.35 mmol) and 2,4,6-trichlorobenzyl alcohol (994 mg, 4.70 mmol) in DCM (150 mL). The reaction mixture was stirred at room temperature for 48 hours.

Removal of the solvent *in vacuo* gave a crude solid which was dissolved in DCM (50 mL) and partitioned against water (50 mL). The aqueous phase was washed with further portions of DCM (2 x 50 mL) and the combined organic phases were washed with brine (50 mL) and dried over $MgSO_4$. The solvent was removed *in vacuo* to yield a solid product (1.29 g) which was crystallised from DCM to give a white crystalline solid (272 mg, 21%). Extraction of a second crop was not possible as the filtrate was inadvertently discarded.

Mpt: 220-223 °C.

^{1}H NMR (300 MHz, $CDCl_3$): **5.65** (4H, s, **H5**); **7.38** (4H, s, **H8**, **H10**), **7.95** (1H, t, J = 7.8, **H1**); **8.21** (2H, d, J = 7.7, **H2**).

^{13}C NMR (75 MHz, $CDCl_3$): **61.94** (**C5**); **128.03** (**C2**); **128.49** (**C8**, **C10**); **129.70** (**C6**); **135.83** (**C9**); **137.67** (**C7**, **C11**); **138.16** (**C1**); **148.17** (**C3**); **163.84** (**C4**).

MS ES+ M/Z: **554** (100%, M^+).

HRMS (ES+) M/Z: Found: 575.8687; calculated: 573.8711 ($C_{21}H_{11}Cl_6NNaO_4$, $M+Na^+$) error = 0.50 ppm.

FTIR ν_{max} cm^{-1}: **3072**, **3003** (m, aromatic C-H stretch); **2962**, **2909** (m, alkyl C-H stretch); **1748** (s, ester C=O stretch).
(solid-state, selected)

Elemental analysis: Found: C, 45.81%; H, 2.01%; N, 2.70%
Calculated: C, 45.53%; H, 2.00%; N, 2.53%

X-ray diffraction: All atoms were found from the electron density map.

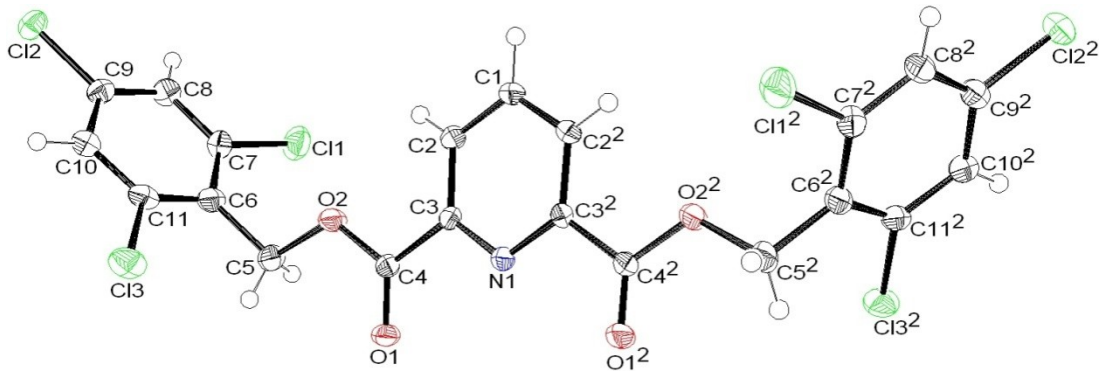

$C_{21}H_{11}Cl_6NO_4$	a = 21.1045 (14) Å	T = 120 K
Monoclinic C 2/c	b = 6.2400 (2) Å	λ = 0.71073 Å
V = 2229.62 (32) $Å^3$	c = 18.5046 (14) Å	D_c = 1.65 g cm^{-3}
Z = 4	α = 90.000 (0)°	μ = 0.801 mm^{-1}
R_1 = 5.5 %	β = 113.803 (3)°	0.08 x 0.04 x 0.04 mm^3
R_{all} = 7.6 %	γ = 90.000 (0)°	Clear, colourless block

9.15 - *bis*(2,4,6-Trichlorobenzyl) 3,5-pyridinedicarboxylate (69)

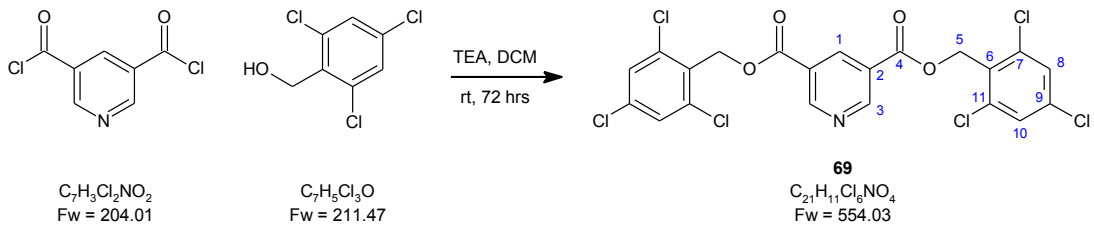

$C_7H_3Cl_2NO_2$
Fw = 204.01

$C_7H_5Cl_3O$
Fw = 211.47

69
$C_{21}H_{11}Cl_6NO_4$
Fw = 554.03

Addition of TEA (0.33 mL, 2.4 mmol) to a stirred solution of 3,5-pyridinedicarbonyl dichloride (486 mg, 2.38 mmol) and 2,4,6-trichlorobenzyl alcohol (1.01 g, 4.77 mmol) in DCM (150 mL) caused the solution to turn from colourless to orange/pink with the formation of white vapour. The reaction mixture was stirred at room temperature for 72 hours after which time the solvent was removed *in vacuo*.

The resulting solid was dissolved in DCM (80 mL) and partitioned against water (50 mL). The aqueous phase was washed with further portions of DCM (3 x 30 mL), and the organic phases were combined, washed with brine (50 mL) and dried over $MgSO_4$. Removal of the solvent *in vacuo* gave a crude solid. Crystallisation from chloroform gave poor quality crystals, which were recrystallised from toluene to give white needles (430 mg, 32%).

Mpt: 196-200 ºC.

^{1}H NMR (300 MHz, $CDCl_3$): **5.83** (4H, s, **H5**); **7.416** (4H, s, **H8**, **H10**); **8.82** (1H, t, J = 2.1 Hz, **H1**); **9.33** (2H, d, J = 2.1 Hz, **H3**).

^{13}C NMR (75 MHz, $CDCl_3$): **61.83** (**C5**); **125.72** (**C2**); **128.64** (**C8**, **C10**); **129.47** (**C6**); **136.12** (**C9**); **137.56** (**C7**, **C11**); **138.51** (**C1**); **154.30** (**C3**); **163.87** (**C4**).

MS ES+ M/Z: **554** (100%, M+).

HRMS (ES+) M/Z: Found: 551.8885; calculated: 551.8892 ($C_{21}H_{12}C_{l6}NO_4$, $M+H^+$) error = 1.34 ppm.

FTIR ν_{max} cm^{-1}: **3081**, **3052** (wk, aromatic C-H stretch); **1724** (s, ester C=O stretch).

(solid-state, selected)

Elemental analysis: Found: C, 45.89%; H, 2.07%; N, 2.93%
Calculated: C, 45.53%; H, 2.00%; N, 2.53%

X-ray diffraction: Data was collected and processed at the Diamond synchrotron by the EPSRC NCS. All non-hydrogen atoms were found from the electron density map. Protons were identified from the density map and then modelled based on an idealised geometry with coordinates and C-H distances refined from the data.

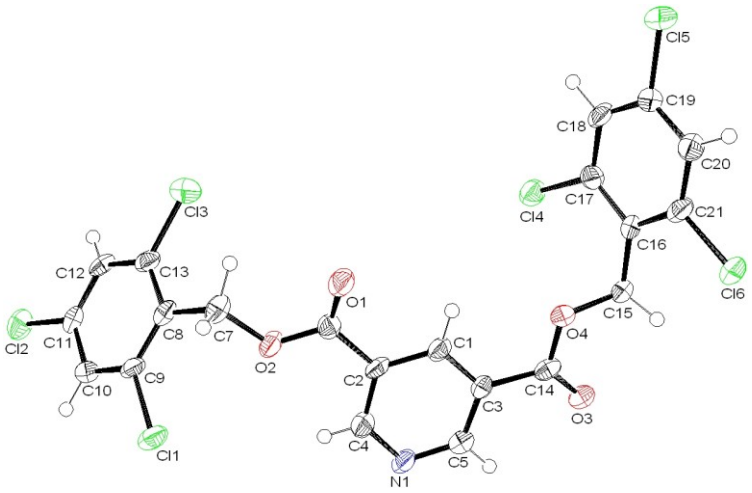

$C_{21}H_{11}Cl_6NO_4$	a = 22.452 (13) Å	T 120 K
Monoclinic P 2_1/C	b = 4.010 (2) Å	λ = 0.6889 Å
V = 2188.79 (65) $Å^3$	c = 25.969 (15) Å	Dc = 1.68 g cm^{-3}
Z = 4	α = 90.000 (0)°	μ = 0.677 mm^{-1}
R_1 = 4.8%	β = 110.584 (7)°	0.05 x 0.01 x 0.01 mm^3
R_{all} = 5.9%	γ = 90.000 (0)°	Clear, colourless rod

9.16 - *bis*(*N*,*O*-Dimethylhydroxyl) 3,5-pyridinediamide (74)

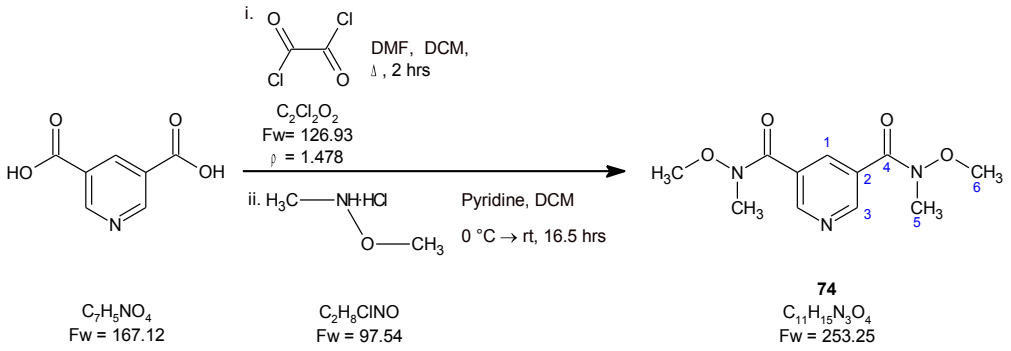

The synthesis was conducted following the procedure described by West *et al.*[115] DMF (10 drops) was added to a suspension of pyridine-3,5-dicarboxylic acid (1.51 g, 9.04 mmol) and oxalyl chloride (1.71 mL, 19.9 mmol) in dry DCM (75 mL). The reaction mixture was heated at reflux under nitrogen for 2 hours after which a clear orange solution had been formed. Removal of the solvent *in vacuo* gave a pale orange solid which was re-dissolved in dry DCM (75 mL).

N,O-Dimethylhydroxylamine hydrochloride (1.96 g, 20.1 mmol) was added to the resulting solution and the suspension was stirred under nitrogen at room temperature for 15 minutes during which time a brown solution was formed. The reaction mixture was cooled in an ice/salt slush bath for 10 minutes. Pyridine (1.62 mL, 20.0 mmol) was added dropwise to the cooled solution producing white vapour; the reaction mixture was stirred at reduced temperature for a further 5 minutes and was then allowed to warm to room temperature. The reaction mixture was stirred for 16.5 hours during which time it turned opaque. The suspension was poured into water (75 mL) and basified to pH 11 with an aqueous solution of KOH (2 M). The biphasic mixture was separated and the dark orange aqueous phase washed with further portions of DCM (3 x 30 mL). The combined organic phases were washed with brine (50 mL) and dried over Na_2SO_4. Removal of the solvent *in vacuo* gave a pale brown solid (1.85 g, 82 %) which was used without further purification.

^{1}H NMR (400 MHz, $CDCl_3$): **3.40** (6H, s, **H5**); **3.56** (6H, s, **H6**); **8.36** (1H, t, J = 2.0 Hz, **H1**); **9.01** (2 H, d, J = 2.0 Hz, **H3**); the data was in good agreement with that published by West,[115] although the peaks at 9.01 and 8.36 ppm were reported as singlets not multiplets.

^{13}C NMR (100 MHz, $CDCl_3$): **33.13** (**C5**); **61.34** (**C6**); **129.20** (**C2**); **136.15** (**C1**); **150.86** (**C3**); **166.64** (**C4**).

MS ES+ M/Z: **254** (39%, $M+H^+$); **276** (100%, $M+Na^+$); **308** (73%, $M+MeOH+Na^+$); **317** (87%, $M+MeCN+Na^+$); **529** (60%, $2M+Na^+$).

9.17 - 3,5-Diacetylpyridine (73)

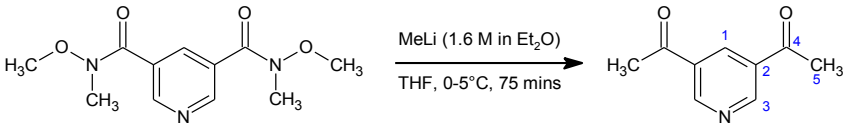

74
$C_{11}H_{15}N_3O_4$
Fw = 253.25

73
$C_9H_9NO_2$
Fw = 163.17

The synthesis was performed following the procedure described by West *et al.*[115] *bis*(*N*,*O*-Dimethylhydroxyl)-pyridine-3,5-diamide (**74**, 1.78 g, 7.13 mmol) was dissolved in THF (75 mL) and cooled in an ice slush bath. A solution of methyl lithium in diethyl ether (1,6 M, 30 mL, 48.0 mmol) was added, turning the reaction mixture deep orange in colour and causing a precipitate to form. The reaction mixture was stirred at reduced temperature for 75 minutes and was then poured in to an aqueous solution of HCL (1 M, 70 mL).

The biphasic mixture was separated and the aqueous phase was basified from pH 2 to pH 11 with an aqueous solution of KOH (2 M). Brine (35 mL) was added and the aqueous phase was washed with diethyl ether (3 x 30

mL). The aqueous phase was reduced *in vacuo* to remove the residual THF and was then washed with further portions of diethyl ether (3 x 30 mL). The combined organic phases were dried over Na_2SO_4 and the solvent was removed *in vacuo* to give an orange solid (902 mg, 78%). Crystallisation from chloroform and light petroleum ether (bpt 60-80 °C) produced off-white needle-shaped crystals (211.0 mg, 18%).

Mpt: 66-68 °C (lit.[115] 68.5-70.5 °C (hexanes/EtOAc)).

^{1}H NMR (400 MHz, $CDCl_3$): **2.68** (6H, s, **H5**); **8.69** (1H, t, J = 2.0 Hz, **H1**); **9.30** (2 H, d, J = 2.0 Hz, **H3**).
Lit.[115] (300 MHz, $CDCl_3$): 2.70 (2H,s); 8.72 (1H, s); 9.33 (2H, s).

^{13}C NMR (100 MHz, $CDCl_3$): **26.84** (**C5**); **132.04** (**C2**); **134.83** (**C1**); **153.06** (**C3**); **195.93** (**C4**) .
Lit.[115] (75 MHz, $CDCl_3$): 26.75; 131.95; 134.71; 152.94; 195.83.

MS ES+ M/Z: **164** (84%, $M+H^+$); **205** (57%, $M+MeCN+H^+$)

FTIR ν_{max} cm^{-1}: **(solid-state, selected)** **3049** (wk, aromatic C-H stretch); **2914** (wk, alkyl C-H stretch); **1683** (s, ester C=O stretch); **1588**, **1572** (m, aromatic C=C stretch)

X-ray diffraction: All atoms were found from the electron density map apart from the methyl protons; these were identified from the density map and then modelled based on an idealised geometry with the torsion angle refined from the electron density data.

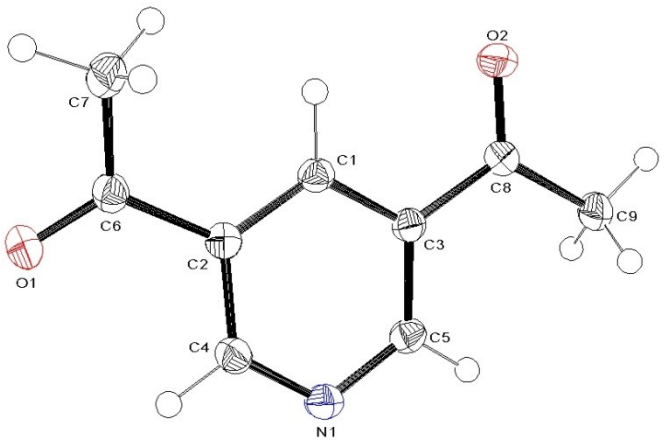

$C_9H_9NO_2$	a = 5.2666 (10) Å	T = 120 K
Monoclinic P $2_1/c$	b = 10.5126 (3) Å	λ = 0.71073 Å
V = 798.15 (1) Å^3	c = 14.4250 (4) Å	D_c = 1.36 g cm^{-3}
Z = 4	α = 90.000 (0)°	μ = 0.097 mm^{-1}
R_1 = 5.2%	β = 92.023 (2)°	0.04 x 0.05 x 0.10 mm^3
R_{all} = 6.9%	γ = 90.000 (0)°	Clear, colourless, cut needle

9.18 - 6-Ethoxycarbonyl-2-pyridinecarboxylic acid (76)

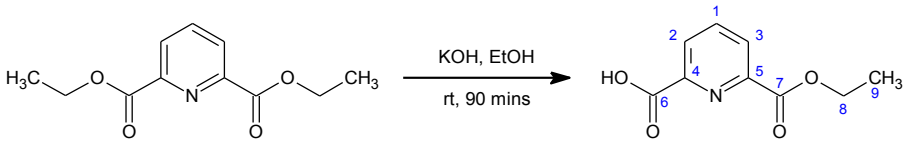

40
$C_{11}H_{13}NO_4$
Fw = 223.23

76
$C_9H_9NO_4$
Fw = 195.17

A suspension of KOH (380 mg, 6.78 mmol) in ethanol (65 mL) was added to a solution of diethyl 2,6-pyridinedicarboxylate (**40**, 3.01 g, 13.5 mmol) in ethanol (15 mL). The reaction mixture was stirred at room temperature for 90 minutes after which time the solvent was removed *in vacuo*. The resulting solid was dissolved in water (50 mL) and partitioned against DCM (50 mL); additional KOH (2 M aqueous solution) was added to ensure a basic pH and water (25 mL) and brine (25 mL) were added to aid the separation of the phases. The aqueous phase was washed with further potions of DCM (3 x 30 mL). The organic phases were combined and removal of the solvent *in*

vacuo gave a white solid (1.67 g) which was shown by TLC to be unreacted diester (R_f = 0.66, MeOH (10% v/v) in DCM).

The aqueous phase was acidified to pH 1 with an aqueous solution of HCl (2M) and washed with DCM (3 x 30 mL). Removal of the solvent *in vacuo* from this second organic phase yielded a white solid (507 mg, 19% R_f = 0.06, MeOH (10% v/v) in DCM). Crystallisation from toluene and light petroleum ether (bpt 60-80 °C) gave small crystals.

Mpt: 115 °C (lit.[118, 119] 116-117 °C).

^{1}H NMR (400 MHz, $CDCl_3$): **1.46** (3H, t, J = 7.1 Hz, **H9**); **4.50** (2H, q, J = 7.1 Hz, **H8**); **8.12** (1 H, t, J = 7.8 Hz, **H1**); **8.36** (1 H, dd, J = 7.8, 1.0 Hz, **H3**); **8.41** (1 H, dd, J = 7.8, 1.0 Hz, **H2**).
Lit.[164] (400 MHz, $CDCl_3$): 1.46 (3H, t, J = 7.13 Hz); 4.50 (2H, q, J = 7.13 Hz); 8.13 (1H, t, J = 7.77 Hz); 8.37 (1H, d, J = 7.80 Hz); 8.41 (1H, d, J = 7.74 Hz).

^{13}C NMR (100 MHz, $CDCl_3$): **14.21** (**C9**); **62.42** (**C8**); **126.65** (**C3**); **128.68** (**C2**); **139.55** (**C1**); **146.37** (**C5**); **147.09** (**C4**); **163.50** (**C7**); **163.60** (**C6**).

MS ES+ M/Z: **124** (100%, $M+K^+ + NH_4^+$); **218** (10%, $M+Na^+$).

MS ES- M/Z: **194** (70%, $M-H^+$).

FTIR ν_{max} cm^{-1}: **(solid-state, selected)** **3063** (w, aromatic C-H stretch); **2983** (w, alkyl C-H stretch); **3000**-**2200** (br, H-bonded carboxylic acid O-H stretch); **1737** (s, ester C=O stretch); **1697** (s, carboxylic acid C=O stretch).

DSC: Two cycles were performed on a 2.32 mg sample between -10 and 135 °C. Heating and cooling rates of 10 °C min^{-1} were used and the end point temperatures were held for 2 minutes.

Cycle	Onset temperature/°C	Peak temperature/°C	Integral/mJ
1 - heating	120.56	123.01	-365.52
1 - cooling	110.08	107.84	341.92
1 - cooling	69.51	47.52	-101.89
2 - heating	119.94	122.62	-357.52
2 - cooling	110.62	108.15	334.99
2 - cooling	74.98	52.85	-92.30

Elemental analysis: Found: C, 55.38%; H, 4.52%; N, 7.15%
Calculated: C, 55.39%; H, 4.65%; N, 7.17%

X-ray diffraction: All atoms were found from the electron density map, except for the alkyl protons which were modelled on idealised geometries with atomic coordinates, C-H distances and X-C torsion angles refined from the electron density data.

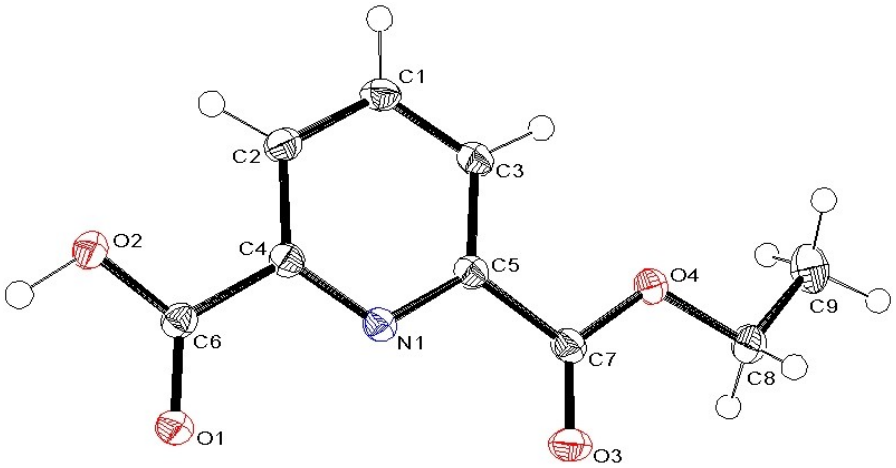

$C_9H_9NO_4$	a = 9.7569 (2) Å	T 120 K
Monoclinic C 2/c	b = 8.2160 (2) Å	λ = 0.71073 Å
V = 1820.63 (7) Å^3	c = 23.0602 (5) Å	D_c = 1.42 g cm^{-3}
Z = 8	α = 90.00 (0)°	μ = 0.114 mm^{-1}
R_1 = 3.5%	β = 99.973 (2)°	0.12 x 0.06 x 0.04 mm^3
R_{all} = 4.4%	γ = 90.00 (0)°	Clear, colourless block

9.19 - 6-Benzyloxycarbonyl-2-pyridinecarboxylic acid (77)

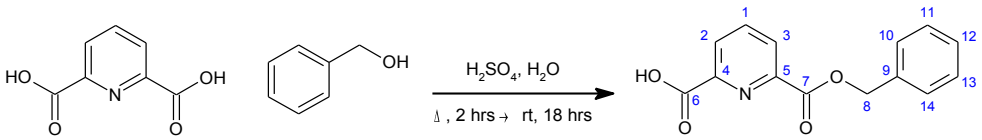

$C_7H_5NO_4$
Fw= 167.12

C_7H_8O
Fw = 108.14

77
$C_{14}H_{11}NO_4$
Fw = 257.24

This product was synthesised by a summer intern, R. Foti, following a procedure adapted from Reddy *et al.*[121] A suspension of pyridine-2,6-dicarboxylic acid (16.69 g, 0.998 mol) in a solution of benzyl alcohol (115 mL, 1.11 mol), water (40 mL) and concentrated H_2SO_4 (5.5 mL) was heated at reflux for 2 hours and then stirred at room temperature for 18 hours.

The reaction mixture was basified with a saturated solution of $NaHCO_3$ in water (1 L) and partitioned against chloroform (100 mL). The aqueous phase was separated and washed with further portions of chloroform (2 x 100 mL). Acidification of the aqueous phase to pH 4 with HCl (2 M) caused a white

precipitate to form. The suspension was allowed to settle and the resultant crystals were collected by filtration.

The combined organic phases were washed with a saturated solution of $NaHCO_3$ (3 x 30 mL). The aqueous phase from this second extraction was acidified to pH 4 with HCl (2 M) and washed with DCM (3 x 30 mL). Removal of the solvent *in vacuo* gave further material.

From both extractions, a white solid (2.80 g, 1.1%) was obtained. Crystallisation of this from toluene and chloroform gave crystals suitable for single crystal X-ray diffraction.

Mpt: 129-130 °C (lit.[117] 132-133 °C (AcOEt/Hexane)).

^{1}H NMR (400 MHz, DMSO): **5.36** (2H, s, **H8**); **7.21**-**7.33** (3H, m, **H11**, **H12**, **H13**); **7.38** (2H, d, J = 6.5 Hz, **H10**, **H14**); **7.96** (1H, t, J = 7.9 Hz, **H1**); **8.19** (1H, dd, J = 7.9, 1.0 Hz, **H3**); **8.21** (1H, dd, J = 7.9, 1.0 Hz, **H2**). Lit.[121] ($CDCl_3$): 5.48 (2H, s); 7.48 (5H, m); 8.12 (1H, t, J = 7.6 Hz); 8.40 (2H, t, J = 7.6 Hz).

^{13}C NMR (100 MHz, DMSO): **66.84** (**C8**); **127.71** (**C3**); **127.88** (**C2**); **128.24** (**C12**); **128.28** (**C11**, **C13**); **128.49** (**C10**, **C14**); **135.72** (**C9**); **139.04** (**C1**); **147.57** (**C5**); **148.90** (**C4**); **164.04** (**C7**); **165.55** (**C6**).

MS ES- M/Z: **256** (23%, M-H^+).

FTIR ν_{max} cm^{-1}: (solid-state, selected) **3064** (wk, aromatic C-H stretch); **2967** (wk, alkyl C-H stretch); **3000**-**2400** (br, H-bonded carboxylic acid O-H stretch); **1737** (s, ester C=O stretch); **1694** (s, carboxylic acid C=O stretch).

DSC: Two cycles were performed on a 2.39 mg sample between -10 and 150 °C. Heating and cooling rates of 10 °C min^{-1} were used and the end point temperatures were held for 2 minutes.

Cycle	Onset temperature/°C	Peak temperature/°C	Integral/mJ
1 - heating	134.66	136.53	-359.59
1 - cooling	124.11	125.22	335.44
1 - cooling	91.34	64.19	-134.80
2 - heating	131.08	135.98	-340.85
2 - cooling	124.96	123.54	326.54
2 - cooling	88.11	56.68	-179.51

Elemental analysis: Found: C, 65.09%; H, 4.21%; N, 5.51%
Calculated: C, 65.37%; H, 4.31%; N, 5.44%

X-ray diffraction: All non-hydrogen atoms were found from the electron density map. Protons were identified from the density map and were then modelled based on an idealised geometry with coordinates and C-H distance refined from the density map.

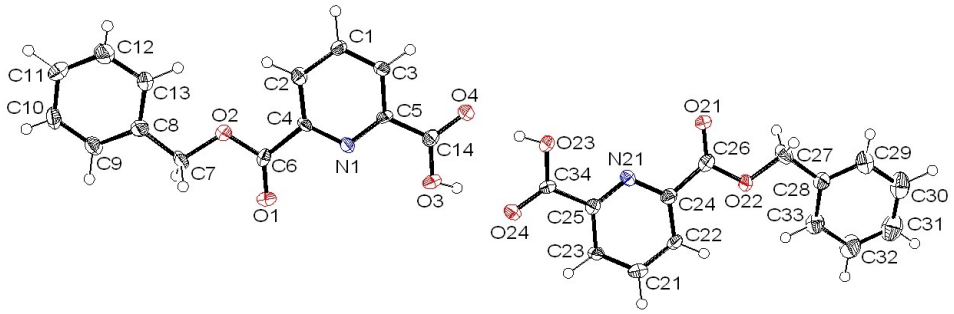

$C_{14}H_{11}NO_4$	a = 11.2792(4) Å	T 120 K
Orthorhombic P n a 2_1	b = 6.5284(2) Å	λ = 0.71073 Å
V = 2341.43 (1) $Å^3$	c = 31.7977(11) Å	D_c = 1.28 g cm^{-3}
Z = 7	α = 90.000 (0)°	μ = 0.095 mm^{-1}
R_1 = 7.9%	β = 90.000 (0)°	0.15 x 0.1 x 0.02 mm^3
R_{all} = 14.2%	γ = 90.000 (0)°	Clear, colourless plate

9.20 - 5-Methoxycarbonyl-3-pyridinecarboxylic acid (78)

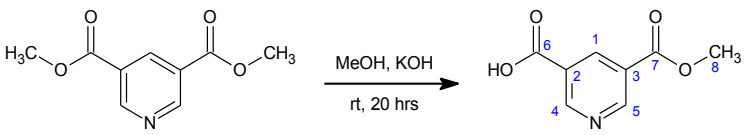

39
$C_9H_9NO_4$
Fw = 195.17

78
$C_8H_7NO_4$
Fw = 181.15

A solution of KOH (278 mg, 5.24 mmol) in methanol (20 mL) was added to a solution of dimethyl 3,5-pyridinedicarboxylate (**39**, 1.023 g, 5.24 mmol) in methanol (20 mL). The reaction mixture was stirred at room temperature for 20 hours and was then poured into DCM (40 mL) and partitioned against water (40 mL). The biphasic mixture was separated and the aqueous phase was washed with further portions of DCM (2 x 30 mL). The combined organic phases were dried over Na_2SO_4 and removal of the solvent *in vacuo* gave a pale yellow solid (249 mg), which was shown by TLC to be unreacted starting material (R_f = 0.69, in an eluent of MeOH (10%) in DCM).

The aqueous phase was acidified from pH 9 to pH 2 with an aqueous solution of HCl (2 M) and washed with DCM (40 mL, then 2 x 30 mL). The organic phases from this second washing were then combined and dried over Na_2SO_4. Removal of the solvent *in vacuo* gave a white solid (607 mg, 64%).

Mpt: 207-216 °C (decomp) (lit.[120] 207-210 °C).

^{1}H NMR (400 MHz, DMSO): **3.90** (3H, s, H8); **8.70** (1H, t, J = 2.0 Hz, H1); **9.21** (1H, d, J = 2.0 Hz, H5); **9.22** (1H, d, J = 2.0 Hz, H4).
Lit.[165] (300 MHz, DMSO): 3.89 (3H, s); 8.57 (1H, t, J = 2 Hz); 8.97 (1H, d, J = 2 Hz); 9.12 (1H, d, J = 2 Hz).

^{13}C NMR (100 MHz, DMSO): **52.10** (**C8**); **125.29** (**C3**); **126.46** (**C2**); **137.25** (**C1**); **153.00** (**C5**); **153.65** (**C4**); **164.20** (**C7**); **165.22** (**C6**).
Lit.[165] (75 MHz, DMSO): 52.8; 125.1; 136.2; 137.2; 150.0; 154.9; 166.2; 166.3.

MS (ES-) M/Z: **180** (100%, M-H$^+$).

FTIR ν_{max} cm^{-1}: **(solid-state, selected)** **3083** (wk, aromatic C-H stretch); **2800**-**2200** (br, carboxylic acid O-H stretch); **1731** (s, C=O stretch); **1602** (m, aromatic C=C stretch).

DSC: Two cycles were performed on a 2.19 mg sample between 25 and 270 °C. Heating and cooling rates of 10 °C min^{-1} were used and the end point temperatures were held for 2 minutes.

Cycle	Onset temperature/°C	Peak temperature/°C	Integral/mJ
1 - heating	221.22	224.65	-680.60
1 - heating	236.36	238.98	-693.32

Elemental analysis: Found: C, 52.89%; H, 3.87%; N, 7.75%
Calculated: C, 53.04%; H, 3.89%; N, 7.73%

9.21 - 5-Ethoxycarbonyl-3-pyridinecarboxylic acid (79)

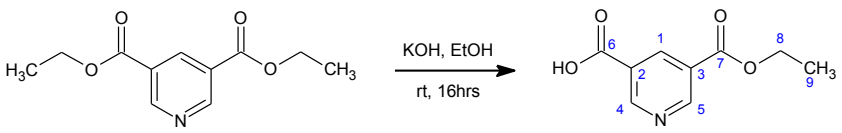

41
$C_{11}H_{13}NO_4$
Fw = 223.23

79
$C_9H_9NO_4$
Fw = 195.17

Diethyl 3,5-pyridinedicarboxylate (**41**, 246 mg, 1.05 mmol) was added to a solution of KOH (62 mg, 1.18 mmol) in ethanol (20 mL). The solution was stirred at room temperature for 16 hours and was then poured into DCM (30 mL). Water (30 mL) was added to give a biphasic mixture which was basified to pH 9 by the addition of an aqueous solution of KOH (2M, 10 drops). The phases were separated and the organic phase was washed with water (20 mL). The combined aqueous phases were washed with further portions of DCM (2 x 30 mL), and brine was then added to aid separation. Removal of the solvent from the organic phase *in vacuo* yielded a white solid (90 mg) which was shown by TLC to be unreacted diester (R_f = 0.35 in DCM).

The aqueous phase was then acidified to pH 2 with an aqueous solution of HCl (2M) and washed with DCM (3 x 30 mL). The organic phase was concentrated *in vacuo* to afford a white solid (105 mg, R_f = 0.00).

Crystallisation from chloroform and acetonitrile yielded a white micro-crystalline powder (55 mg, 27%) but it was not possible to obtain a sample suitable for single crystal diffraction.

Mpt: 183-185 °C (lit.[116] 182 °C).

^{1}H NMR (400 MHz, DMSO): **1.35** (3H, t, J = 7.0 Hz, **H9**); **4.38** (2H, q, J = 7.0 Hz, **H8**); **8.64** (1H, t, J = 2.0 Hz, **H1**); **9.26** (2H, dd, J = 2.0, 1.0 Hz, **H4**, **H5**).

^{13}C NMR (100 MHz, DMSO): **14.01** (**C9**); **61.54** (**C8**); **125.83** (**C3**); **126.72** (**C2**); **137.07** (**C4**); **153.20** (**C5**); **153.74** (**C4**); **163.95** (**C7**); **165.35** (**C6**).

MS (ES-) M/Z: **194** (100%, M-H$^+$).

FTIR ν_{max} cm^{-1}: **(solid-state, selected)** **3065** (wk, aromatic C-H stretch); **2980** (wk, alkyl C-H stretch); **3000**-**2200** (br. H-bonded carboxylic acid O-H stretch); **1720** (s, C=O stretch); **1596** (m, aromatic C=C stretch).

DSC: Two cycles were performed on a 3.25 mg sample between 25 and 250 °C. Heating and cooling rates of 10 °C min^{-1} were used and the end point temperatures were held for 2 minutes.

Cycle	Onset temperature/°C	Peak temperature/°C	Integral/mJ
1 - heating	185.42	188.05	-576.01
1 - heating	236.36	237.39	-27.46

A second experiment was performed on a 2.94 mg sample. The first cycle was performed between 25 and 220 ° and the second between 25 and 250 °C. Heating and cooling rates of 10 °C min^{-1} were used and the end point temperatures were held for 2 minutes.

Cycle	Onset temperature/°C	Peak temperature/°C	Integral/mJ
1 - heating	185.62	187.85	-509.46
1 - 220 °C isotherm	220.01	220.01	-41.97
1 - cooling	139.00	129.34	218.54
1 - heating	161.62	173.85	-273.32
2 - heating	244.55	246.01	-1339.19

Elemental analysis: Found: C, 55.40%; H, 4.49%; N, 7.22%
Calculated: C, 55.39%; H, 4.65%; N, 7.17%

9.22 - 5-Benzyloxycarbonyl-3-pyridinecarboxylic acid (80)

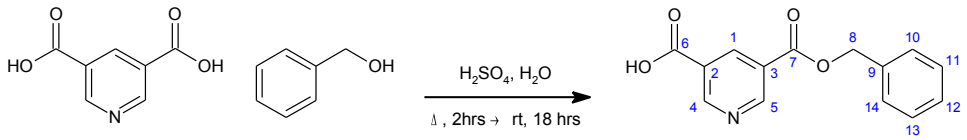

$C_7H_5NO_4$
Fw= 167.12

C_7H_8O
Fw = 108.14

80
$C_{14}H_{11}NO_4$
Fw = 257.24

The synthesis was performed using a procedure adapted from Reddy *et al.*[121] for the 2,6-isomer. A suspension of pyridine-3,5-dicarboxylic acid (2.59 g, 15.5 mmol) in benzyl alcohol (17.8 mL, 172 mmol), concentrated H_2SO_4 (0.85 mL) and water (6.2 mL) was heated at reflux for 2 hours. The reaction mixture was cooled to room temperature and stirred for a further 18 hours after which a biphasic system was formed. (The lower layer was observed to be a white, opaque oil whilst the upper layer appeared pale yellow and clear.)

Basification of the mixture to pH 9 with a saturated aqueous solution of $NaHCO_3$ gave a white suspension which was extracted with DCM (60 mL then 2 x 35 mL). The combined organic phases were washed with water (35 mL) and the combined aqueous phases were acidified to pH 3-4 with concentrated HCl, producing a white suspension. This suspension was washed with DCM (3 x 40 mL) but failed to clear. A white solid (124.9 mg,

3%) was observed to form in the combined organic phases and was collected by filtration. Analysis by NMR showed this to be the desired product and crystallisation from acetonitrile gave clear, colourless platelets.

The aqueous phase was filtered to remove the remaining solid, the melting point of which was found to be greater than 250°C, indicating it to be unreacted diacid. The filtrate was washed with further portions of DCM (3 x 40 mL) and the organic phases were combined and dried over Na_2SO_4. Removal of the solvent *in vacuo* gave a pink solid (760.5 mg, 19%), a portion of which was crystallised from a mixture of DCM, acetonitrile and diethyl ether to give clear, pink plate-like crystals (20.6 mg). Analysis by NMR and melting point showed this solid to be the same material as the first crop.

Mpt: 1st crop: 180-182 °C (MeCN).
2nd crop: 181-183 °C (DCM/MeCN/Ether).

^{1}H NMR (400 MHz, DMSO): **5.42** (2H, s, **H8**); **7.33-7.46** (3H, m, **H11** - **H13**); **7.51** (2H, d, J = 7.0 Hz, **H10**, **H14**); **8.65** (1H, t, J = 2.1 Hz, **H1**); **9.27** (1H, d, J = 2.1 Hz, **H3**); **9.29** (1H, d, J = 2.1 Hz, **H2**).

^{13}C NMR (100 MHz, DMSO): **66.89** (**C8**); **125.63** (**C3**); **126.78** (**C2**); **128.18** (**C12**); **128.30** (**C11**, **C13**); **128.55** (**C10**, **C14**); **135.57** (**C9**); **137.18** (**C1**); **153.28** (**C5**); **153.91** (**C4**); **163.86** (**C7**); **165.32** (**C6**).

MS (ES-) M/Z: **256** (100%, M-H^+).

HRMS (ES+) M/Z: Found: 258.0762; calculated: 258.0761 ($C_{14}H_{12}NO_4$, M+H^+) error = -0.34 ppm.

FTIR ν_{max} cm^{-1}:
(solid-state, selected)

3150-**2200** (br, hydrogen bonded carboxylic acid O-H stretch); **3067**, **3033** (wk, aromatic C-H stretch); **2926**, **2849** (wk, alkyl C-H stretch); **1715** (s, ester C=O stretch); **1588** (m, aromatic C=C stretch).

DSC:

Two cycles were performed on a 1.86 mg sample between 25 and 250 °C. Heating and cooling rates of 10 °C min^{-1} were used and the end point temperatures were held for 2 minutes.

Cycle	Onset temperature/°C	Peak temperature/°C	Integral/mJ
1 - heating	181.13	184.86	-276.95
1 - heating	211.75	234.36	-114.06

Elemental analysis:

Found: C, 65.09%; H, 4.33%; N, 5.44%
Calculated: C, 65.37%; H, 4.31%; N, 5.83%

X-ray diffraction:

All non-hydrogen atoms were found from the electron density map. Protons were identified from the density map and then modelled based on idealised geometry. No electron density peak was observed for the proton attached to C73, this has not been modelled. Isotropic constraints were applied to atoms C6, C33, C66, O1 and O2 and the distances between C6 and O2, C62 and C66, C66 and O62 were fixed.

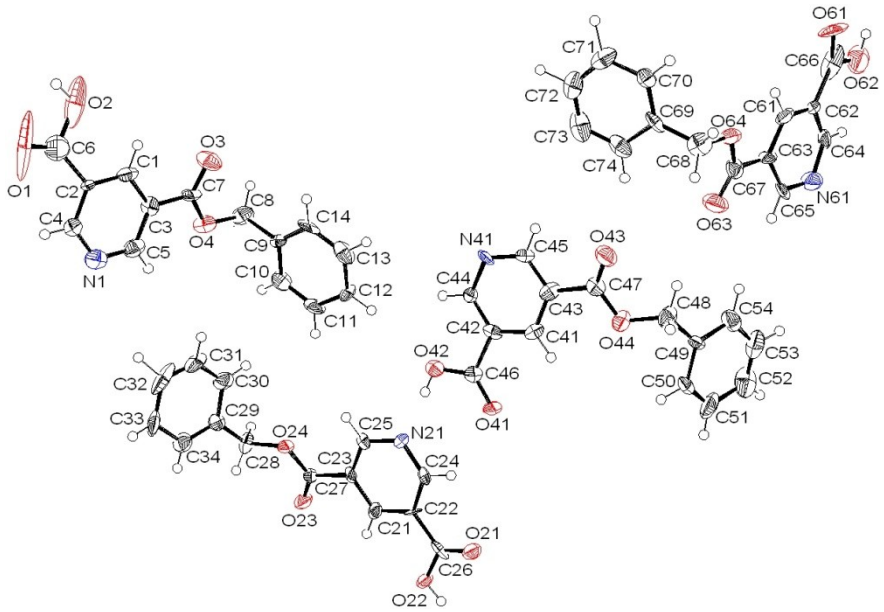

C14 H11 N O4	a = 5.8935 (3) Å	T 120 K
Triclinic P 1	b = 8.4872 (4) Å	λ = 0.71073 Å
V = 1190.66 (8) Å^3	c = 24.8589 (10) Å	Dc = 1.43 g cm^{-3}
Z = 4	α = 82.421 (3)°	μ = 0.107 mm^{-1}
R_1 = 12.0%	β = 83.473 (3)°	0.14 x 0.06 x mm^3
R_{all} = 15.2%	γ = 75.809(2)°	Clear, colourless, cut plate

9.23 - *bis*(Cinnamyl) 2,6-pyridinedicarboxylate (81)

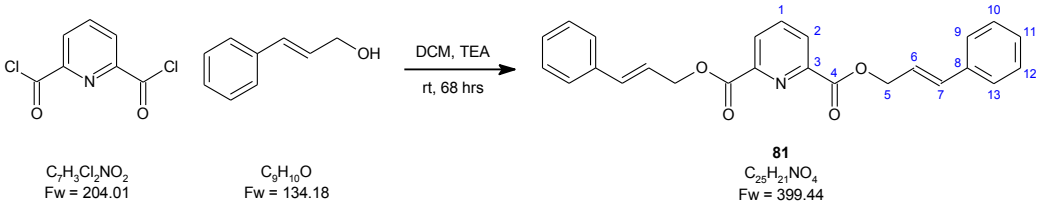

$C_7H_3Cl_2NO_2$
Fw = 204.01

$C_9H_{10}O$
Fw = 134.18

81
$C_{25}H_{21}NO_4$
Fw = 399.44

A solution of cinnamyl alcohol (1.5178 g, 11.3 mmol) in DCM (25 mL) was added to a suspension of 2,6-pyridinedicarbonyl dichloride (1.1531 g, 5.65 mmol) in DCM (25 mL). Addition of TEA (1.1 mL, 11.4 mmol) resulted in the formation of white vapour. The reaction mixture was stirred at room temperature for 68 hours, forming a clear, green solution. The solvent was removed *in vacuo* and the resulting solid was dissolved in DCM (40 mL). Addition of a saturated aqueous solution of $NaHCO_3$ (40 mL) caused a white

precipitate to form and the solution to turn pink. Water (40 mL) was then added to aid the separation of the phases.

The aqueous phase was separated and washed with further portions of DCM (2 x 30 mL). The combined organic phases were washed sequentially with brine (60 mL) and water (40 mL) but still did not show full separation. The emulsion was spun in a centrifuge at 2000 rpm for 15 minutes giving two distinct phases. The organic phase was isolated and dried over $MgSO_4$. Removal of the solvent *in vacuo* yielded a beige solid (1.9266 g, 85%).

This crude product was combined with that obtained from a second reaction (performed with 1.06 g, 5.20 mmol of 2,6-pyridinedicarbonyl dichloride) and purified by flash column chromatography using DCM as the eluent (R_f = 0.03). Removal of the solvent *in vacuo* yielded a white solid (2.55 g, 39%), which was crystallised from DCM and light petroleum ether (bpt 40-60 °C) to produced crystals suitable for study by X-ray diffraction.

Mpt: 107-110°C

^{1}H NMR (400 MHz, $CDCl_3$): **5.14** (4H, d, J = 6.6 Hz, **H5**); **6.51** (2H, dt, J = 16.0, 6.6 Hz, **H6**); **6.83** (2H, d, J = 16.0 Hz, **H7**) **7.25**-**7.41** (6H, m, **H10**, **H11**, **H12**); **7.46** (4H, d, J = 7.3 Hz, **H9**, **H13**); **8.07** (1H, t, J = 7.8 Hz, **H1**); **8.37** (2H, d, J = 7.8 Hz **H2**)

^{13}C NMR (100 MHz, $CDCl_3$): **66.83** (**C5**); **122.54** (**C6**); **126.68** (**C9**, **C13**); **128.01** (**C2**); **128.14** (**C11**); **128.58** (**C10**, **C12**); **135.29** (**C7**); **136.08** (**C8**); **138.23** (**C1**); **148.51** (**C3**); **164.39** (**C4**)

MS ES+ M/Z: **422** (65%, $M+Na^+$); **821** (70%, $2M+Na^+$)

FTIR ν_{max} cm^{-1}: **3072** (wk, sp^2 C-H stretch); **3055**-**3017** (wk, aromatic C-H stretch); **1729** (s, ester C=O stretch); **1576** (m, aromatic C=C stretch)

(solid-state, selected)

UV/Vis: A single absorption was observed at 254.5 nm, the extinction coefficient was calculated to be 0.0348 μM^{-1} cm^{-1}.

Concentration/μM	Peak λ/nm	Absorbtion
24.40	254.5	0.927
19.54	254.5	0.801
15.63	254.5	0.633
12.51	254.0	0.525
9.77	254.0	0.430

Elemental analysis: Found: C, 74.96%; H, 5.23%; N, 3.34%
Calculated: C, 75.17%; H, 5.30%; N, 3.50%

X-ray diffraction: All atoms were found from the electron density map.

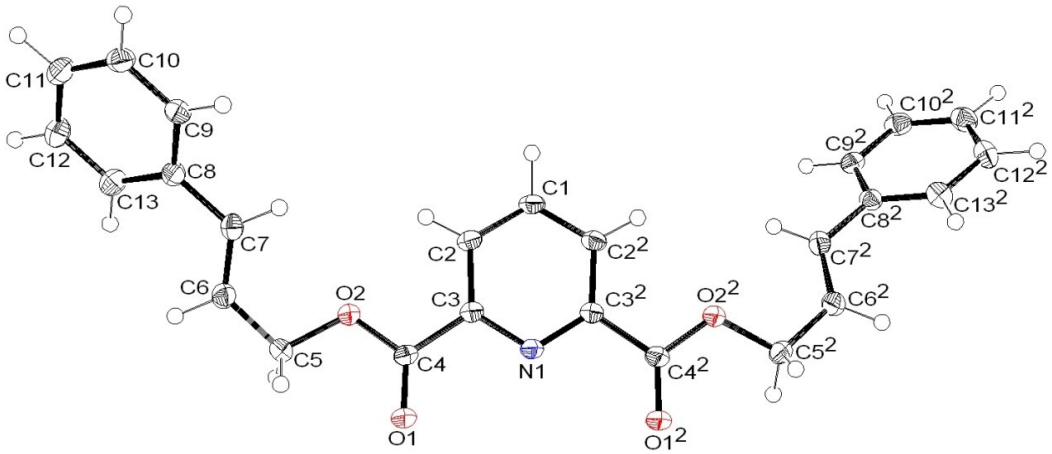

$C_{25}H_{21}NO_4$	a = 28.0169 (12) Å	T = 120 K
Monoclinic C 2/c	b = 6.3647 (2) Å	λ = 0.71073 Å
V = 2023.60 (3) Å^3	c = 11.3681 (5) Å	D_c = 1.31 g cm^{-3}
Z = 4	α = 90.000 (0)°	μ = 0.089 mm^{-1}
R_1 = 4.6%	β = 93.391 (2)°	0.21 x 0.14 x 0.05 mm^3
R_{all} = 7.4%	γ = 90.000 (0)°	Clear, colourless cut plate

9.24 - 4-Formyl-tetrathiafulvalene (82)

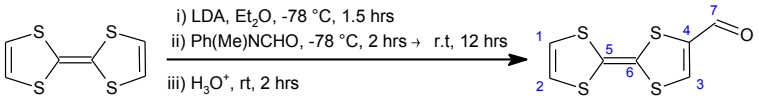

$C_6H_4S_4$
Fw = 204.36

82
$C_7H_4OS_4$
Fw = 232.37

The synthesis was performed following the procedure described by Garin *et al.*[135] A solution of TTF (1.11 g, 5.42 mmol) in sodium dried diethyl ether (85 mL) was cooled to -78 °C under N_2. Addition of a solution of LDA-monoTHF in cyclohexane (1.27 M, 4.4 mL, 5.6 mmol) over 5 minutes caused the formation of a yellow precipitate. The reaction mixture was stirred at reduced temperature for a further 90 minutes after which time a solution of methyl(phenyl)formamide (1.34 mL, 10.8 mmol) in dry diethyl ether (15 mL) was added, causing the yellow suspension to take on a greenish tinge. The reaction mixture was stirred for a further 2 hours at -78 °C and then warmed to room temperature and stirred for 12 hours.

Water (80 mL) was added to the reaction mixture causing the suspension to turn deep red. The mixture was acidified to pH 3 with an aqueous solution of HCl (2 M). The phases were separated and the aqueous phase was washed with further portions of diethyl ether (5 x 60 mL). The combined organic phases were divided into two portions; each was washed with brine (50 mL) and dried over $MgSO_4$. Removal of the solvent *in vacuo* gave a dark powder which was purified by flash column chromatography using chloroform as the eluent to afford a dark red solid (R_f = 0.42, 843 mg, 67%).

Mpt: 96-101 °C (lit.[166] 98-99 °C (benzene)).

^{1}H NMR (300 MHz, $CDCl_3$): **6.35** (2H, dd, J = 6.4, 10.9 Hz, **H1**, **H2**); **7.43** (1H, s, **H3**); **9.48** (1H, s, **H7**).
Lit.[135] ($CDCl_3$): 6.30 (1H, d, J = 6.4 Hz); 6.33 (1H, d, J= 6.4 Hz); 7.41 (1H, s); 9.44 (1H, s).

9.25 - 4-Hydroxymethyl-tetrathiafulvalene (83)

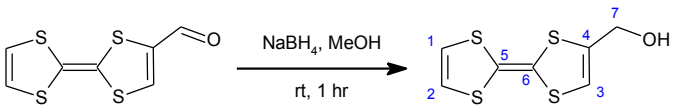

82
$C_7H_4OS_4$
Fw = 232.37

83
$C_7H_6OS_4$
Fw = 234.38

The synthesis was performed following the procedure described by Garin *et al.*[135] Addition of $NaBH_4$ (152 mg, 4.02 mmol) to a solution of 4-formyl-TTF (**82**, 780 mg, 3.36 mmol) in methanol (60 mL) at room temperature resulted in an almost instantaneous colour change from deep red to golden yellow. The reaction mixture was stirred at room temperature for 60 minutes and was then poured into DCM (70 mL).

The solution was partitioned against brine (50 mL) and a white precipitate was observed to form. The organic phase was separated and washed sequentially with further portions of brine (1 x 50 mL) and water (2 x 50 mL). The combined aqueous phases were observed to be strongly coloured; washing with DCM (3 x 50 mL) removed most of the colour. The organic phases were combined and dried over Na_2SO_4.

Removal of the solvent *in vacuo* gave a yellow solid (808 mg, 98%) which was used without further purification.

Mpt: 64-65 °C (lit.[167] 70-71 °C (isooctane/toluene)).

^{1}H NMR (400 MHz, $CDCl_3$): **1.58** (1H, s, **H_2O**); **1.79** (1H, br. s, **OH**); **4.41** (2 H, d, J = 4.1 Hz, **H7**); **6.24** (1 H, t, J = 1.2 Hz, **H3**) **6.32** (2 H, s, **H1**, **H2**).
Lit.[135] ($CDCl_3$): 1.90 (1H, br. s); 4.38 (2H, s); 6.20 (1H, s); 6.29 (2H, s).

9.26 - *bis*(4-Methyl-tetrathiafulvalene) 2,6-pyridinedicarboxylate (84)

9.26.1 - Reaction with acid chloride

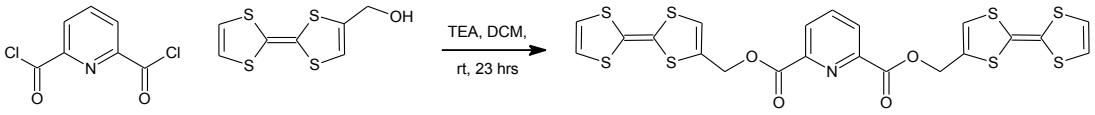

$C_7H_3Cl_2NO_2$
Fw = 204.01

83
$C_7H_6OS_4$
Fw = 234.38

84
$C_{21}H_{13}NO_4S_8$
Fw = 599.85

4-Hydroxymethyl-TTF (**83**, 699 mg, 2.85 mmol) was suspended in DCM (20 mL). The opaque, brown suspension was added to a stirred solution of 2,6-pyridinedicarbonyl dichloride (238 mg, 1.42 mmol) in DCM (30 mL). Addition of TEA (0.45 mL, 3.23 mmol) produced a large amount of white vapour and caused the suspension to darken. The reaction mixture was stirred at room temperature for 23 hours during which time the solvent turned yellow. Analysis of the reaction mixture by TLC showed the reaction to be incomplete but, owing to concerns about the stability of the alcohol, it was decided to quench the reaction. Additional DCM (50 mL) was added and the reaction mixture was partitioned against water (90 mL). The precipitate was found to be insoluble in both phases and was removed by filtration. The phases were separated and the aqueous phase was washed with a further portion of DCM (50 mL). The combined organic phases were dried over $MgSO_4$ and removal of the solvent *in vacuo* gave a brownish yellow solid (702 mg).

The crude solid was purified by flash column chromatography. A 1:4 mixture of diethyl ether in light petroleum ether (bpt 40-60 °C) was used to elute the first component (R_f = 0.36, diethyl ether (25% v/v) light petroleum ether). Removal of the solvent *in vacuo* yielded a brown solid (324 mg) which was shown by NMR to be unreacted alcohol (**83**).

A second component was eluted using 100% diethyl ether (R_f = 0.08, diethyl ether (25% v/v) in light petroleum ether) and removal of the solvent *in vacuo* afforded a yellow/brown solid (123 mg). The ^{1}H NMR spectrum for this

compound contained peaks corresponding to both the TTF unit and the pyridine dicarboxylate core. However the integrals for the pyridyl protons were higher than expected for the diester.

The sample was dissolved in DCM (25 mL) and partitioned against an aqueous solution of KOH (2M, 20 mL). The phases were separated and the organic phase was washed with further portions of KOH solutions (2 x 20 mL). The combined organic phases were washed with DCM (20 mL) and the combined organic phases were washed with brine (25 mL) and dried over Na_2SO_4. Removal of the solvent *in vacuo* gave a sticky yellow solid (82.7 mg). NMR analysis (see below) showed evidence for decomposition of the TTF moiety.

^{1}H NMR (400 MHz, $CDCl_3$): **4.03** (9H, s); **4.40** (1H, s); **5.15** (2H, d, J =0.8 Hz); **6.30** (H, d, J =1.1 Hz); **6.48** (1H, s); **8.02** (2H, t, J =7.7 Hz); **8.27** (0.5H, d, J = 1.1 Hz); **8.31** (3H, d, J =7.9 Hz).

FTIR ν_{max} cm^{-1}: **3062** (wk, aromatic C-H stretch); **2966** (wk, alkyl C-H stretch); **1740** (s, C=O stretch).
(solid-state, selected)

9.26.2 - Synthesis via DCC coupling

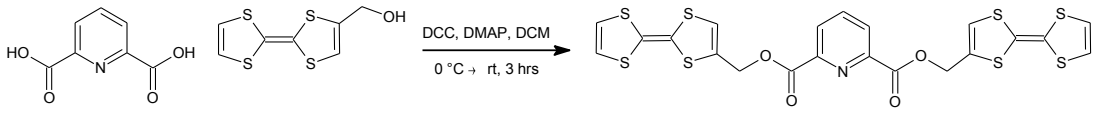

$C_7H_5NO_4$
Fw = 167.12

83
$C_7H_6OS_4$
Fw = 234.38

84
$C_{21}H_{13}NO_4S_8$
Fw = 599.85

DMAP (9 mg, 77 μmol) was added to a suspension of 4-hydroxymethyl-TTF (**83**, 40 mg, 0.24 mmol) and pyridine-2,6-dicarboxylic acid (18 mg, 0.11 mmol) in DCM (50 mL) at 0 °C. DCC (45 mg, 0.22 mmol) was added and the reaction mixture was stirred at 0 °C for 5 minutes. The reaction mixture was

then warmed to room temperature and stirred for a further 3 hours during which time a fine white precipitate was formed.

The reaction mixture was filtered to remove the precipitate and the filtrate was partitioned against an aqueous solution of HCl (0.5 M, 60 mL). The phases were separated and the organic phase was washed with a saturated aqueous solution of $NaHCO_3$ (60 mL) before drying over Na_2SO_4. Removal of the solvent *in vacuo* gave an orange/yellow solid.

NMR analysis of the crude product showed a high level of impurities with a low chemical shift and several different environments for the pyridyl protons indicating that the coupling reaction had not worked effectively.

^{1}H NMR (400 MHz, $CDCl_3$): **1.05**-**1.23** (15H, m); **1.24**-**1.39** (16H, m); **1.40** (1H, s); **1.54**-**1.84** (26H, m); **1.84**-**2.04** (14H, m); **2.18** (2H, br. s); **3.21** (1H, br. s); **3.49** (4H, dd, J = 7.3, 3.5 Hz); **4.40** (4H, br. s); **5.14** (2H, d, J = 12.8 Hz); **6.23** (2H, s); **6.29**-**6.34** (6H, m); **6.49** (1H, s); **7.82**-**7.89** (1H, m); **7.96** (2H, t, J = 7.8 Hz); **8.03** (1H, t, J = 7.8 Hz); **8.18** (2H, dd, J = 7.8, 1.0 Hz); **8.30** (1H, d, J = 7.8 Hz).

9.27 - 4,5-Ethylenedithio-4'-carbomethoxy-tetrathiafulvalene (85)

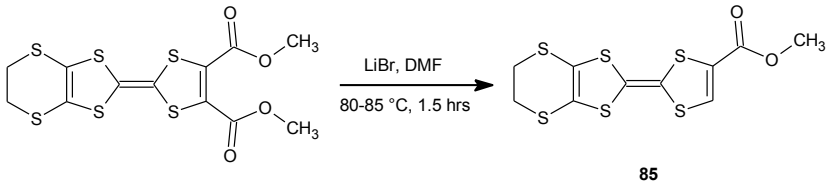

$C_{12}H_{10}O_4S_6$
Fw = 410.60

85
$C_{10}H_8O_2S_6$
Fw = 352.56

The synthesis was performed in collaboration with the Batail group at the University of Angers following the procedure described by Kilburn *et al.*[168] A solution of LiBr (11.6 g, 133.0 mmol) and 4',5'-*bis*(carbomethoxy)-EDT-TTF (4.77 g, 11.6 mmol, previously prepared by the Batail group) was heated to

between 80 and 85 °C for 1.5 hours, during the course of which the dark brown solution was observed to turn red.

The reaction mixture was poured into water (200 mL), causing a red precipitate to form. An additional portion of water (200 mL) was added and the precipitate was collected by filtration; the filtrate was observed to be golden yellow in colour. The precipitate was washed with water (200 mL) and dissolved in DCM (300 mL). This solution was partitioned against water (150 mL), the phases were separated and the organic phase was washed with further portions of water (2 x 150 mL). The aqueous phases were combined and washed with DCM (100 mL). The combined organic phases were dried over $MgSO_4$ and the solvent was removed *in vacuo* to give a dark red solid (3.92 g, 96%) which was used without further purification.

Mpt: 156 °C (lit.[168] 150-153 °C (DCM/hexane)).

9.28 - 4,5-Ethylenedithio-4'-hydroxymethyl-tetrathiafulvalene (86)

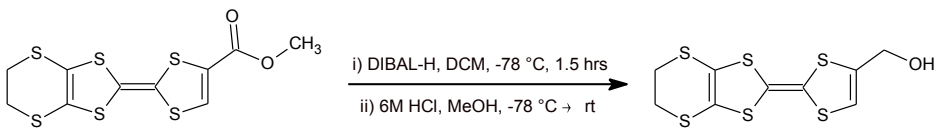

85
$C_{10}H_8O_2S_6$
Fw = 352.56

86
$C_9H_8OS_6$
Fw = 324.55

The synthesis was performed in collaboration with the Batail group. Addition of a solution of DIBAL-H in DCM (1.0 M, 14 mL, 14 mmol) to a stirred solution of 4'-carbomethoxy-EDT-TTF (**85**, 1.01 g, 2.86 mmol) in DCM (25 mL) at -78 °C caused the formation of yellow bubbles. The reaction mixture was stirred for 1.5 hours during which time the dark red solution was observed to turn brownish orange.

Addition of a 1:1 mixture of methanol and aqueous HCl (2 M; 2 mL) resulted in effervescence and the solution was temporarily observed to turn yellow. The reaction mixture was warmed to room temperature and poured into DCM

(30 mL). The solution was partitioned against an aqueous solution of HCl (1 M, 50 mL), the phases were separated and the organic phase was washed with water (3 x 50 mL). The aqueous phases were combined and washed with DCM (2 x 50 mL) before the combined organic phases were dried over $MgSO_4$. Removal of the solvent *in vacuo* yielded an orange/red solid (0.92 g, 99%) which was used without further purification.

Mpt: 121-123 °C.

9.29 - *bis*(4,5-Ethylenedithio-4'-methyl-tetrathiafulvalene) 2,6-pyridinedicarboxylate (87)

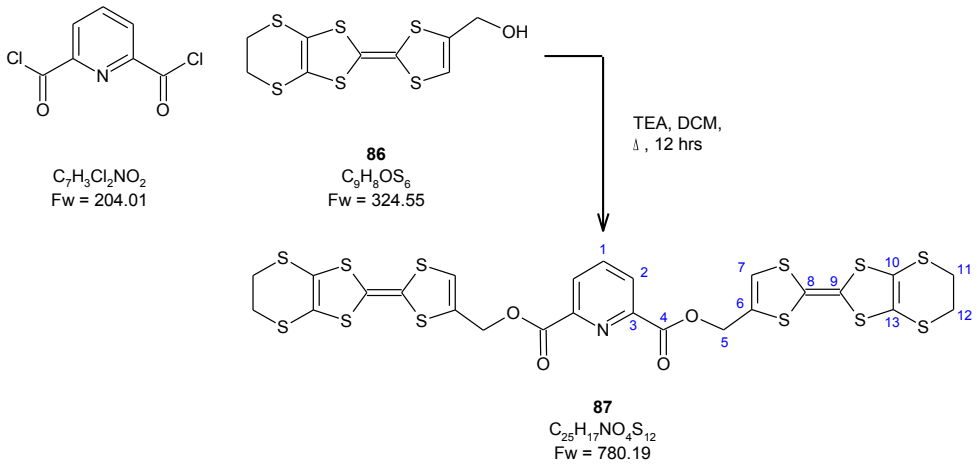

$C_7H_3Cl_2NO_2$
Fw = 204.01

86
$C_9H_8OS_6$
Fw = 324.55

87
$C_{25}H_{17}NO_4S_{12}$
Fw = 780.19

The synthesis was performed in collaboration with the Batail group. A solution of 2,6-pyridinedicarbonyl dichloride (0.10 g, 0.49 mmol) in DCM (10 mL) was added to a solution of EDT-TTF-4'-methanol (**86**, 350 mg, 1.08 mmol) and TEA (40 drops) in DCM (15 mL). The reaction mixture was stirred at reflux under N_2 for 12 hours during which time an orange precipitate was observed to form.

The precipitate was isolated by filtration and was washed sequentially with DCM (50 mL), a saturated aqueous solution of $NaHCO_3$ (50 mL) and a further portion of DCM (50 mL). The aqueous filtrate was partitioned against DCM (50 mL) and the phases were separated. The organic phases from the

filtration and separation were combined and dried over $MgSO_4$. Removal of the solvent *in vacuo* failed to yield any additional material.

The precipitate was dried *in vacuo* (290 mg) and analysis by NMR showed evidence of the pyridine diester but was dominated by an impurity at low chemical shift. Due to time constraints it was not possible to isolate the pure product.

^{1}H NMR (500 MHz, DMSO): **3.12** (81H, s unknown contaminant); **3.38** (9H, s, **H11**, **H12**); **5.22** (4H, s, **H5**); **5.70** (1H, s, residual DCM) **7.01** (2H, s, **H7**); **8.20**-**8.25** (1H, m, **H1**); **8.25**-**8.32** (2H, m, **H2**).

9.30 - 4,5-Dimethyl-4'-hydroxymethyl-tetrathiafulvalene (88)

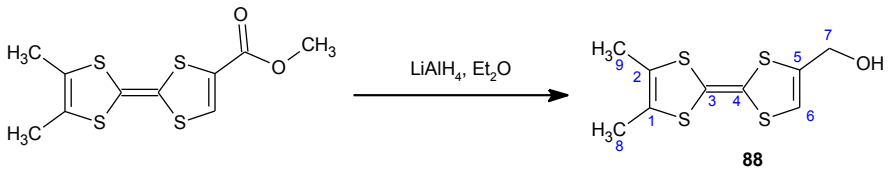

$C_{10}H_{10}O_2S_4$
Fw = 290.45

88
$C_9H_{10}OS_4$
Fw = 262.44

A solution of 4,5-dimethyl-4'-carbomethoxy-TTF (100.3 mg, 0.343 mmol) in diethyl ether (30 mL) was added dropwise to a stirred suspension of $LiAlH_4$ (18 mg, 0.47 mmol) in diethyl ether (30 mL) under nitrogen. The reaction mixture was stirred at room temperature for 2 hours after which the reaction was quenched by the dropwise addition of ethyl acetate (5 mL).

The resultant suspension was poured into water (80 mL) and basified by the addition of an aqueous solution of NaOH (15% w/v, 20 mL). The phases were separated and the aqueous phase was washed with further portions of ether (3 x 50 mL). The combined organic phases were dried over Na_2SO_4 and removal of the solvent *in vacuo* gave an orange/brown micro-crystalline solid (82.2 mg, 91%) which was used without further purification.

Mpt: 102-105°C.

^{1}H NMR (400 MHz, $CDCl_3$): **1.95** (6H, s, **H8**, **H9**); **4.39** (2H, d, J = 1.0 Hz, **H7**); **6.22** (1H, s, **H6**).

MS ES+ M/Z: **262** (29%, M^+); **405** (100%, $3M+H^++Na^+$).

9.31 - *bis*(4,5-Dimethyl-4'-methyl-tetrathisfulvalene) 2,6-pyridinedicarboxylate (89)

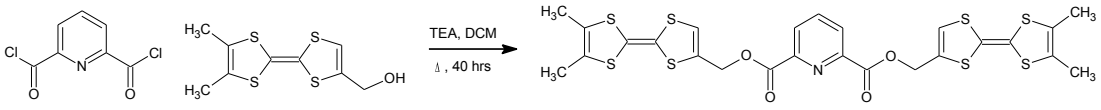

$C_7H_3Cl_2NO_2$
Fw = 204.01

88
$C_9H_{10}OS_4$
Fw = 262.44

89
$C_{25}H_{21}NO_4S_8$
Fw = 655.96

A solution of 2,6-pyridinedicarbonyl dichloride (26.6 mg, 0.130 mmol) in DCM (13 mL) was added to a stirred solution of 4,5-dimethyl-4'-hydroxymethyl-TTF (**88**, 70.5 mg, 0.267 mmol) and TEA (0.04 mL, 0.287 mmol) in DCM (10 mL). The reaction was heated at reflux under nitrogen for 40 hours after which time an orange precipitate had formed.

The solvent was removed *in vacuo* and the residual solid was suspended in THF (50 mL). Chloroform (50 mL), and a saturated aqueous solution of $NaHCO_3$ (100 mL) were added to the suspension. The phases were separated and the aqueous phase was washed with an additional portion of chloroform (50 mL). The combined organic phases were washed with brine (50 mL) and dried over Na_2SO_4. The solvent was removed *in vacuo* and NMR analysis of the crude product showed the reaction to have failed; no pyridyl protons were observed and the integrals of the peaks corresponding to the TTF substituent indicated that degradation had occured.

^{1}H NMR (400 MHz, $CDCl_3$): **1.27** (4H, s); **1.38**-**1.48** (20H, m); **1.85** (3H, br. s); **1.94** (3H, s); **2.28** (3H, s); **3.76** (3H, s); **5.01** (1H, s); **6.99** (2H, s).

9.32 - Pyridine-2,6-dicarbaldehyde (90)

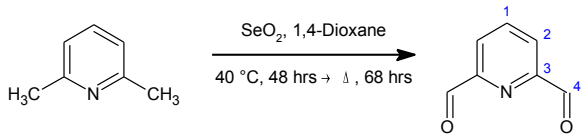

C_7H_9N
Fw= 107.15

90
$C_7H_5NO_2$
Fw = 135.12

The synthesis was performed following a procedure adapted from Chandler *et al.*[169] 2,6-Lutidene (1.95 mL, 16.7 mmol) was added to a suspension of selenium dioxide (6.08 g, 54.8 mmol) in 1,4-dioxane (50 mL). The reaction mixture was stirred at 40 °C for 48 hours during which time the selenium dioxide turned pinkish brown and the solvent turned pale yellow. Analysis by TLC showed no evidence of reaction occurring so additional selenium dioxide (3.82 g, 34.4 mmol) was added and the reaction mixture was heated at reflux. After a further 68 hours, the selenium dioxide was found to have turned black and the solvent was observed to be greenish yellow in colour. The suspension was hot filtered and the residue was washed with additional portions of dioxane (2 x 30 mL)

The filtrate was reduced *in vacuo* to give a white solid which subsequently turned pink under continued vacuum. This solid was found to be insoluble in neat DCM. A biphasic solution was obtained by dissolving the solid in 1,4-dioxane (20 mL), DCM (80 mL) and water (40 mL); the organic phase was observed to be pale yellow in colour. The phases were separated and the aqueous phase was washed with further portions of DCM (3 x 30 mL). The combined organic phases were washed with brine (30 mL) and dried over Na_2SO_4. Removal of the solvent *in vacuo* yielded an off-white solid (1.5798 g, 70%).

The crude solid was purified by flash column chromatography; initially neat DCM was used as the eluent, although the polarity was subsequently increased by the addition of methanol to a maximum of 10% (v/v). A pure sample was obtained (800 mg, 35%) along with a mixed sample (400 mg).

Although the R_f of the pure compound was the same as the starting material (R_f = 0.46, methanol (10% v/v) in DCM), NMR analysis showed it to be the target aldehyde.

A sample of the pure material was crystallised from DCM and light petroleum ether (bpt 60-80°C) yielding plate-like crystals (125 mg) suitable for X-ray diffraction.

Mpt: 117-120 °C (lit.[138] 115-117 °C ($CHCl_3$/light petroleum ether)).

^{1}H NMR (400 MHz, $CDCl_3$): **8.08** (1H, t, J = 7.5 Hz, **1H**); **8.17** (2H, d, J = 7.5 Hz, **H2**); **10.16** (2H, s, **H4**).
lit.[138] (220 MHz, CHCl3): 8.15 (3H, m); 10.16 (2H, s).

^{13}C NMR (100 MHz, $CDCl_3$): **125.28** (**C2**); **138.35** (**C1**); **152.97** (**C3**); **192.29** (**C4**).

FTIR ν_{max} cm^{-1}: (solid-state, selected) **3083**, **3017** (m, aromatic C-H stretch); **2860** (m, aldehyde C-H stretch); **1712** (s, aldehyde C=O stretch); **1682** (s, aromatic C=C stretch).

X-ray diffraction: All non-hydrogen atoms were found from the electron density map; protons were identified in the density map and modelled based on idealised geometries with their coordinates refined from the data set.

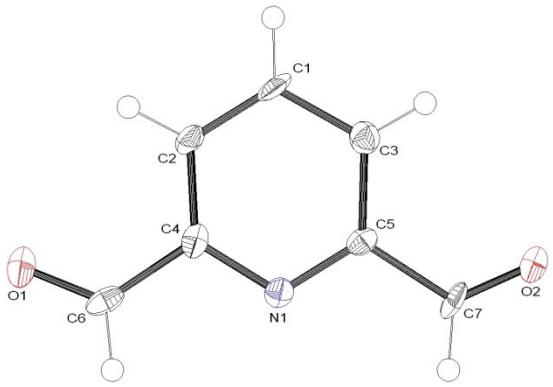

$C_7H_5NO_2$	a = 15.1214 (9) Å	T = 120 K
Monoclinic C c	b = 6.4421 (3) Å	λ = 0.71073 Å
V = 614.51 (8) Å^3	c = 6.7767 (3) Å	D_c = 1.46 g cm^{-3}
Z = 4	α = 90.000 (0)°	μ = 0.109 mm^{-1}
R_1 = 4.4 %	β = 111.429 (3)°	0.16 x 0.06 x 0.01 mm^3
R_{all} = 4.9 %	γ = 90.000 (0)°	Clear, colourless cut plate

9.33 - Pyridine-3,5-dicarbaldehyde (91)

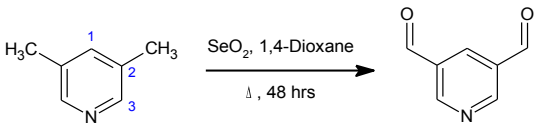

C_7H_9N
Fw= 107.15

91
$C_7H_5NO_2$
Fw = 135.12

The synthesis was performed following a procedure adapted from Chandler *et al.*[169] 3,5-Lutidine (2.25 g, 21.0 mmol) was added to a suspension of SeO_2 (7.51 g, 67.7 mmol) in 1,4-dioxane (50 mL). The reaction mixture was stirred at reflux under N_2 for 48 hrs after which time the SeO_2 was observed to have turned dark grey and the solution had become greenish yellow.

The volume of solvent was reduced *in vacuo* to approximately one third of its original volume and the selenium residue was removed by filtration. The residue was washed with DCM (3 x 25 mL) and the combined filtrates were partitioned against water (40 mL). The phases were separated and the aqueous phase was washed with further portions of DCM (3 x 30 mL). The

combined organic layers were washed with brine (40 mL) and dried over Na_2SO_4.

Analysis by TLC using an eluent of methanol (10% v/v) in DCM showed the organic phase to contain a single component (R_f = 0.45). Purification of the crude product by flash column chromatography using an eluent of methanol (5% v/v) in DCM produced a yellow oil (R_f = 0.29, 456 mg) which was shown by NMR to be unreacted starting material.

^{1}H NMR (400 MHz, $CDCl_3$): **2.27** (2H, s, **Me**); **2.28** (4H, s, **Me**); **7.28** (1H, s, **H1**); **8.23** (2H, s, **H3**).

^{13}C NMR (100 MHz, $CDCl_3$): **18.16** (**Me**); **132.43** (**C2**); **137.06** (**C1**); **147.34** (**C3**).

9.34 - *bis*(*N*,*N*-Dimethyl) 2,6-pyridinediamide (92)

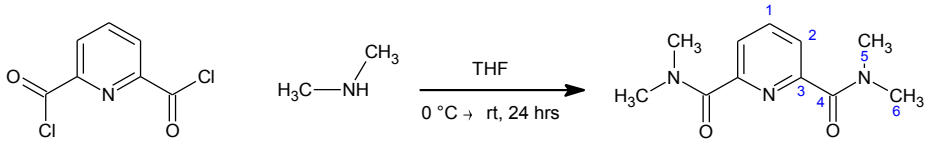

$C_7H_3Cl_2NO_2$
Fw = 204.01

C_2H_7N
Fw = 45.08

92
$C_{11}H_{15}N_3O_2$
Fw = 221.26

The synthesis was performed using a procedure adapted from D. Marlin *et al.*[170] A solution of 2,6-pyridinedicarbonyl dichloride (1.00 g, 4.91 mmol) in THF (75 mL) was added to a solution of dimethylamine in THF (2.0 M, 5 mL, 10.0 mmol) at 0 °C. The reaction mixture was warmed to room temperature, stirred for 24 hours and filtered.

The solvent was removed from the filtrate *in vacuo* and the resulting solid was dissolved in DCM and partitioned against an aqueous solution of KOH (2 M, 50 mL). The phases were separated and the aqueous phase was washed with further portions of DCM (2 x 50 mL). The combined organic

phases were washed with brine (50 mL) and dried over Na_2SO_4. Removal of the solvent *in vacuo* gave a white solid (602 mg, 55%)

Crystallisation from ethyl acetate gave large, colourless, multi-domain crystals (93.1 mg).

Mpt: 141-142 °C (lit.[171] 82 °C (Et_2O)).

^{1}H NMR (400 MHz, $CDCl_3$): **3.03** (6 H, s, **H5**, **H6**); **3.11** (6 H, s, **H5**, **H6**); **7.63** (2 H, d, *J* = 7.9 Hz, **H2**); **7.87** (1 H, t, *J* = 7.9 Hz, **H1**).
Lit.[171] (500MHz, DMSO): 2:89 (6H, d); 8.15 (3H, m); 9.27 (2H, q).

^{13}C NMR (100 MHz, $CDCl_3$): **35.65** (**C5**, **C6**); **38.97** (**C5**, **C6**); **123.94** (**C2**); **137.99** (**C1**); **153.10** (**C3**); **168.20** (**C4**).

MS ES+ M/Z: **222** (100%, $M+H^+$); **244** (20%, $M+Na^+$).

FTIR ν_{max} cm^{-1}: **2938** (br. w, alkyl C-H stretch); **1632** (s, tertiary amide C=O stretch).
(solid-state, selected)

Elemental analysis: Found: C, 59.72%; H, 6.74%; N, 19.11%
Calculated: C, 59.71%; H, 6.74%; N, 18.98%

X-ray Diffraction: All atoms were found from the electron density map.

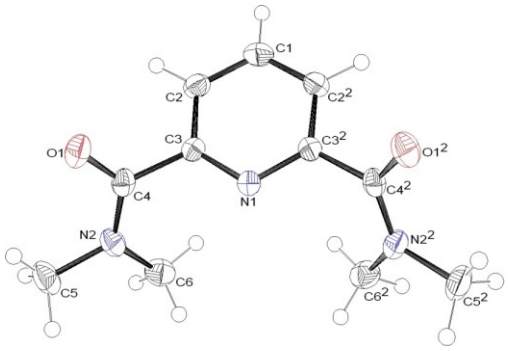

$C_{11}H_{15}N_3O_2$	a = 8.7712 (4) Å	T = 120 K
Orthorhombic Pnma	b = 18.9397 (7) Å	λ = 0.71073 Å
V = 1149.91 (1) Å^3	c = 6.9220 (3) Å	D_c = 1.28 g cm^{-3}
Z = 4	α = 90.000 (0)°	μ = 0.090 mm^{-1}
R_1 = 3.9%	β = 90.000 (0)°	0.3 x 0.2 x 0.1 mm^3
R_{all} = 5.5%	γ = 90.000 (0)°	Clear, colourless cut block

9.35 - *bis*(*N*,*N*-Dimethyl)-pyridine-3,5-diamide (93)

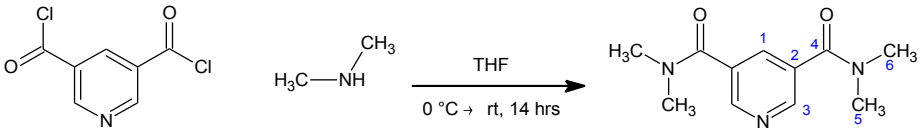

$C_7H_3Cl_2NO_2$
Fw = 204.01

C_2H_7N
Fw = 45.08

93
$C_{11}H_{15}N_3O_2$
Fw = 221.26

The synthesis was performed using a procedure adapted from D. Marlin *et al.*[170] A solution of 3,5-pyridinedicarbonyl dichloride (1.02 g, 4.99 mmol) in THF (100 mL) was added to a solution of dimethylamine in THF (2.0 M, 5 mL, 10.0 mmol) at 0 °C. The solution was warmed to room temperature and stirred for 14 hours.

The resulting suspension was filtered and the precipitate was suspended in DCM (80 mL). Addition of an aqueous solution of K_2CO_3 (2 M, 100 mL) caused the suspension to clear. The aqueous phase was separated and washed with further portions of DCM (2 x 50 mL). The combined organic

phases were washed with brine (50 mL) and dried over $MgSO_4$. Removal of the solvent *in vacuo* gave a pink solid (630 mg, 57 %).

Crystallisation of the crude product from ethyl acetate gave colourless plate-like crystals (137 mg, 12%) which were unsuitable for study by X-ray diffraction. Recrystallisation from ethyl acetate gave crystalline needles.

Mpt: 109-110 °C (lit.[172] 120-122 °C (EtOH/hexane)).

^{1}H NMR (400 MHz, $CDCl_3$): **3.02** (6H, br. s, **H6**) **3.14** (6H, br. s, **H5**) **7.83** (1H, t, *J* = 1.9 Hz, **H1**) **8.71** (2H, d, *J* = 1.9 Hz, **H3**).

^{13}C NMR (100 MHz, $CDCl_3$): **35.35** (**C5**, **C6**); **39.41** (**C5**, **C6**); **131.81** (**C2**); **133.62** (**C1**); **148.55** (**C3**); **167.98** (**C4**).

MS ES+ M/Z: **222** (100%, $M+H^+$); **244** (32%, $M+Na^+$).

FTIR ν_{max} cm^{-1}: **3017** (w, aromatic C-H stretch); **2935** (w, alkyl
(solid-state, selected) C-H stretch); **1625** (s, tertiary amide C=O stretch).

Elemental analysis: Found: C, 59.87%; H, 6.79%; N, 19.05%
Calculated: C, 59.71%; H, 6.83%; N, 18.98%

X-ray diffraction: All non-hydrogen atoms and pyridyl protons were found from the electron density map. The methyl protons were modelled from an idealised geometry with coordinates and X-C torsion refined from electron density.

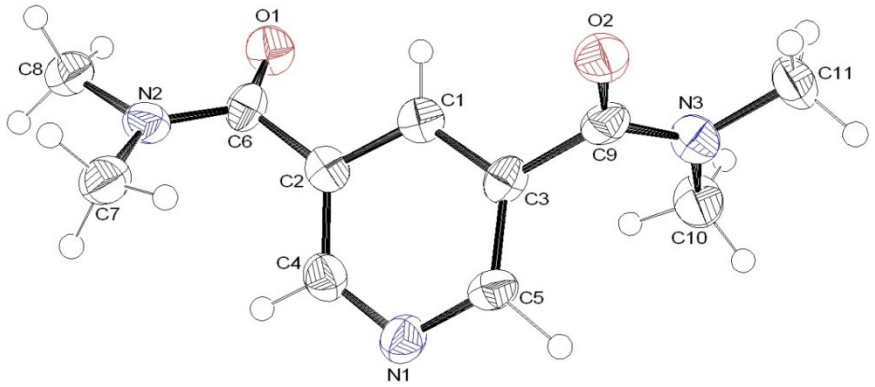

$C_{11}H_{15}N_3O_2$	a = 6.3705 (11) Å	T 120 K
Orthorhombic Pbca	b = 9.4907 (15) Å	λ = 0.71073 Å
V = 2218.50 (7) Å^3	c = 36.6933 (67) Å	D_c = 1.32 g cm^{-3}
Z = 8	α = 90.000 (0)°	μ = 0.094 mm^{-1}
R_1 = 9.1 %	β = 90.000 (0)°	0.4 x 0.1 x 0.04 mm^3
R_{all} = 22.2 %	γ = 90.000 (0)°	Clear, colourless cut needle

9.36 - *bis*(Morpholino) 2,6-pyridinediamide (94)

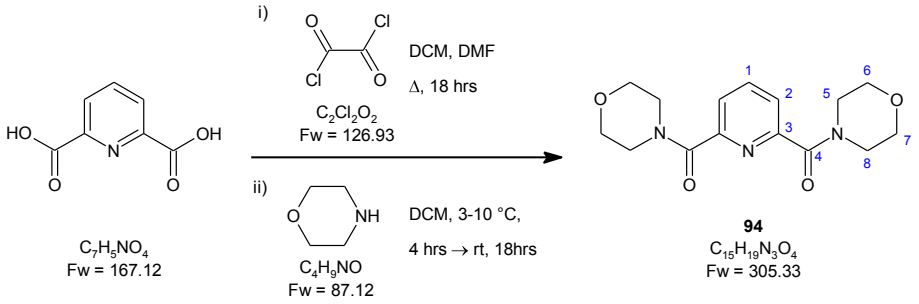

Oxalyl chloride (1.26 mL, 14.7 mmol) was added to a suspension of pyridine-2,6-dicarboxylic acid (2.20 g, 13.2 mmol) in DCM (55 mL). Addition of DMF (20 drops) caused the reaction mixture to effervesce. The reaction mixture was heated at reflux under nitrogen for 90 minutes, after which time additional oxalyl chloride (1.3 mL, 15.14 mmol) was added. Heating the reaction mixture for a further 16.5 hours gave a dark orange/red solution which was cooled to 3 °C.

The reaction mixture was kept below 10 °C whilst a solution of morphline (4.70 mL, 53.4 mmol) in DCM (55 mL) was added over a period of 4 hours,

forming an orange suspension. The reaction mixture was warmed to room temperature and stirred for a further 18 hours, after which it was poured into water (50 mL) forming a biphasic system containing an opaque, pale orange organic phase and a clear, dark orange aqueous phase.

The mixture was filtered through celite which was subsequently washed with DCM (2 x 50 mL) and water (50 mL). The resulting clear, biphasic mixture was separated and the aqueous phase was basified from pH 3 to pH 9 with a saturated aqueous solution of $NaHCO_3$. The aqueous phase was washed with DCM (2 x 40 mL) and the combined organic phases were dried over Na_2SO_4. Removal of the solvent *in vacuo* gave a dark orange oil from which crystals formed upon standing. Crystallisation from chloroform gave white block-like crystals (250 mg, 28%).

Mpt: 139-141 °C (lit.[173] 126 °C (Et_2O)).

^{1}H NMR (300 MHz, $CDCl_3$): **3.58** (4H, d, J = 4.8 Hz, **H5**); **3.64** (4H, d, J = 4.8 Hz, **H6**); **3.79** (8H, br. s, **H7**, **H8**); **7.72** (2H, d, J = 7.8 Hz, **H2**); **7.92** (1H, t, J = 7.8 Hz; **H1**).

^{13}C NMR (75 MHz, $CDCl_3$): **42.74** (**C8**); **47.67** (**C5**); **66.73** (**C6**); **66.90** (**C7**); **124.95** (**C2**); **138.36** (**C1**); **152.18** (**C3**); **166.57** (**C4**).

MS ES+ M/Z: **328** (100%, $M+Na^+$).

FTIR ν_{max} cm^{-1}: **2907**, **2861** (br. wk, alkyl C-H stretch); **1624** (s, amide C=O stretch).
(solid-state, selected)

Elemental analysis: Found: C, 58.87%; H, 6.25%; N, 13.65%
Calculated: C, 59.01%; H, 6.27%; N, 13.76%

X-ray diffraction: All atoms were found from the electron density map.

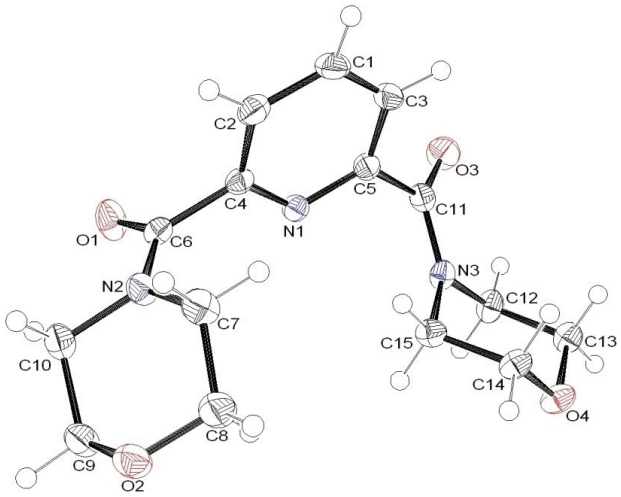

$C_{15}H_{19}N_3O_4$	a = 9.7730 (3) Å	T 120 K
Orthorhombic P n a 2_1	b = 11.4534 (3) Å	λ = 0.71073 Å
V = 1492.53 (1) $Å^3$	c = 13.3340 (4) Å	D_c = 1.36 g cm^{-3}
Z = 4	α = 90.000 (0)°	μ = 0.100 mm^{-1}
R_1 = 3.8%	β = 90.000 (0)°	0.3 x 0.16 x 0.14 mm^3
R_{all} = 5.0%	γ = 90.000 (0)°	Clear, colourless, cut shard

9.37 - *bis*(Morpholino) 3,5-pyridinediamide (95)

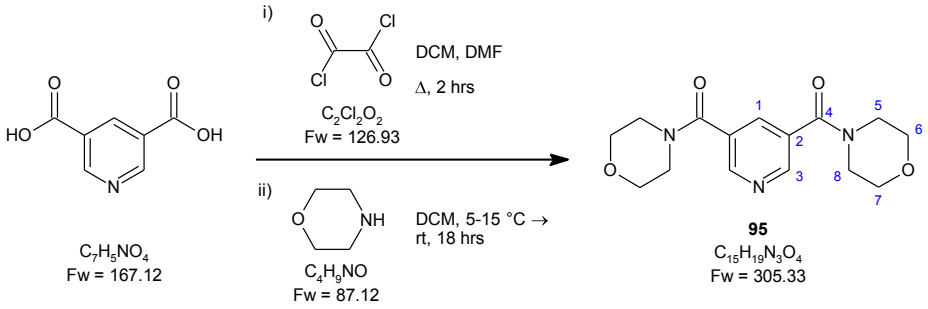

DMF (10 drops) was added to a suspension of oxalyl chloride (2.1 mL, 25 mmol) and pyridine-3,5-dicarboxylic acid (1.99 g, 11.9 mmol) in DCM (30 mL). The reaction mixture was heated at reflux for 2 hours after which time a clear, yellow solution had been formed. This solution was cooled to 5 °C and a solution of morpholine (2.15 mL, 24.4 mmol) in DCM (20 mL) was added,

keeping the temperature below 15 °C. The reaction mixture was warmed to room temperature and stirred for 18 hours.

The resulting cream suspension was poured into water where a biphasic system was formed; the organic phase was observed to be opaque and milky whilst the aqueous phase was a clear, pale yellow. The mixture was poured through wet celite and the filter aid was washed sequentially with DCM (80 mL) and water (50 mL). The phases were separated and the aqueous phase was washed with DCM (3 x 40 mL). The combined organic phases were then washed sequentially with a saturated aqueous solution of $NaHCO_3$ and brine (50 mL of each) and dried over Na_2SO_4. Removal of the solvent *in vacuo* gave an opaque oil (2.04 g, 56%).

The oil was purified by flash column chromatography using an eluent of methanol (10% v/v) in DCM (R_f = 0.43). Removal of the solvent *in vacuo* gave a colourless solid (1.32 g, 36%) A portion of the solid obtained was crystallised from chloroform and acetonitrile giving clear, colourless block crystals suitable for single crystal X-ray diffraction (242 mg).

Mpt: 120-122 °C.

^{1}H NMR (400 MHz, $CDCl_3$): **3.45**-**3.78** (16H, br. m, **H5**, **H6**, **H7**, **H8**); **7.82** (1H, t, J = 2.1 Hz, **H1**); **8.70** (2H, d, J = 2.1 Hz, **H3**).

^{13}C NMR (100 MHz, $CDCl_3$): **66.70** (**C5**, **C6**, **C7**, **C8**); **131.25** (**C2**); **134.11** (**C1**); **148.83** (**C3**); **166.75** (**C4**).

MS ES+ M/Z: **306** (7%, $M+H^+$); **328** (32%, $M+Na^+$); **360** (65%, $M+MeOH+Na^+$); **633** (100%, $2M+Na^+$).

FTIR ν_{max} cm^{-1}: (solid-state, selected) **2962** (m, aromatic C-H stretch); **2911**-**2858** (m, alkyl C- H stretch); **1622** (s, amide C=O stretch).

Elemental analysis: Found: C, 58.96%; H, 6.36%; N, 13.75%
Calculated: C, 59.01%; H, 6.27%; N, 13.76%

X-ray diffraction: All atoms were found from the electron density map.

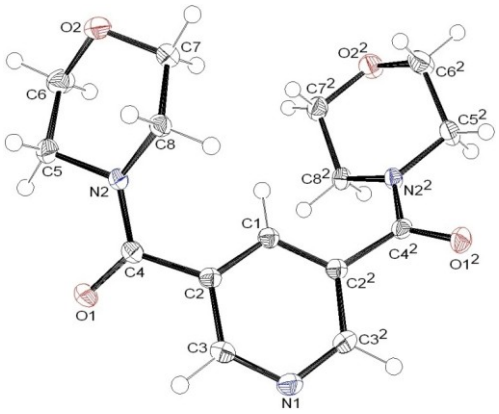

$C_{15}H_{19}N_3O_4$	a = 14.6968 (4) Å	T = 120 K
Orthorhombic Pbcn	b = 8.7319 (3) Å	λ = 0.71073 Å
V = 1443.98 (1) Å^3	c = 11.2520 (4) Å	D_c = 1.40 g cm^{-3}
Z = 4	α = 90.000 (0)°	μ = 0.103 mm^{-1}
R_1 = 3.9 %	β = 90.000 (0)°	0.3 x 0.26 x 0.12 mm^3
R_{all} = 5.5 %	γ = 90.000 (0)°	Clear, colourless cut plate

9.38 - Collection of crystallographic data on diesters with naphthyl and anthryl substituents

The naphthyl and anthryl substituted diesters were synthesised by undergraduate project students, R. Parker[111] (**50**, **52**, **53**, **59**) and S. Twiddy[112] (**49**, **51**, **54**, **55**, **58**). Summaries of the crystallographic data collected for each compound are presented below.

9.38.1 - bis((2-Naphthyl)methyl) 2,6-pyridinedicarboxylate (49)

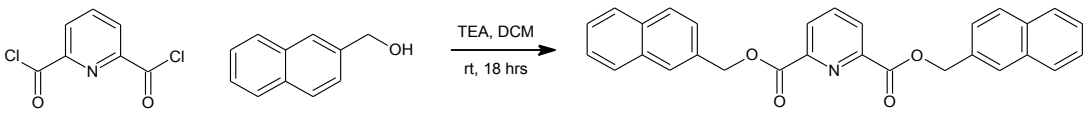

$C_7H_3Cl_2NO_2$
Fw = 204.01

$C_{11}H_{10}O$
Fw = 158.20

49 (55%)
$C_{29}H_{21}NO_4$
Fw = 447.48

Crystalline platelets were grown by crystallisation from chloroform and light petroleum ether (bpt 40-60 °C).

Mpt: 187-189 °C.

Elemental analysis: Found: C, 77.84%; H, 4.73%; N, 3.13%
Calculated: C, 77.98%; H, 4.64%; N, 3.16%

X-ray diffraction: All atoms were found from the electron density map.

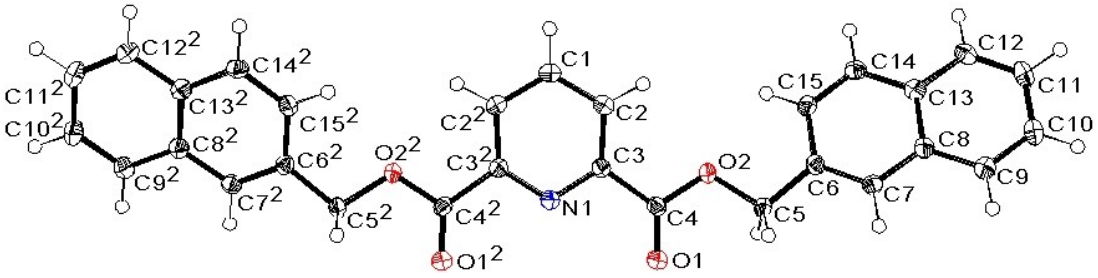

$C_{29}H_{21}NO_4$	a = 40.3698 (19) Å	T 120 K
Monoclinic C 2/c	b = 6.2536 (3) Å	λ = 0.71073 Å
V = 2113.22 (5) $Å^3$	c = 8.4296 (3) Å	D_c = 1.41 g cm^{-3}
Z = 4	α = 90.00 (0)˚	μ = 0.094 mm^{-1}
R_1 = 6.0%	β = 96.781 (2)˚	0.08 x 0.08 x 0.04 mm^3
R_{all} = 8.3%	γ = 90.00 (0)˚	Clear, colourless cut plate

9.38.2 - bis((2-Naphthyl)ethyl) 2,6-pyridinedicarboxylate (50)

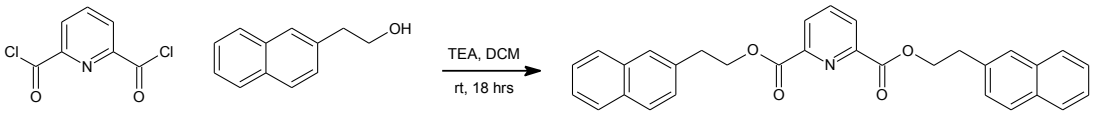

$C_7H_3Cl_2NO_2$
Fw = 204.01

$C_{12}H_{12}O$
Fw = 172.22

50 (75%)
$C_{31}H_{25}NO_4$
Fw = 475.53

Crystals were obtained by slow evaporation of a solution of the product in DCM.

Mpt: 147-149 °C.

X-ray diffraction: All atoms were found from the electron density map.

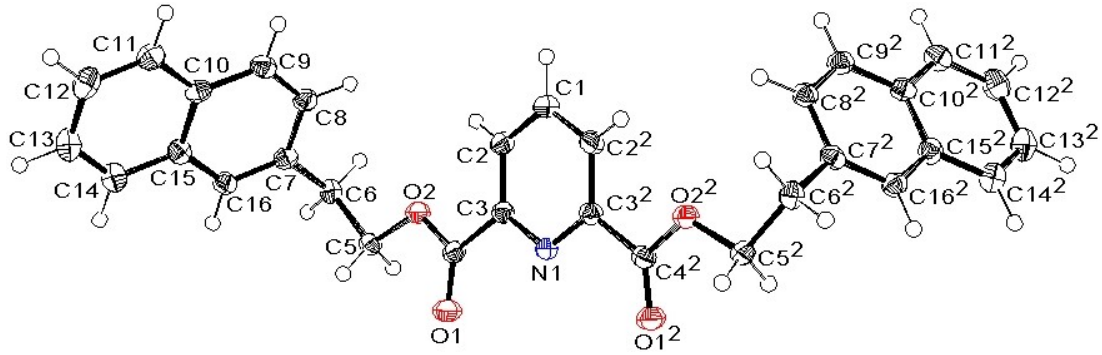

$C_{31}H_{25}NO_4$	a = 42.5463 (26) Å	T 120 K
Monoclinic C 2/c	b = 6.3191 (4) Å	λ = 0.71073 Å
V = 2388.15 (5) $Å^3$	c = 8.8893 (6) Å	D_c = 1.32 g cm^{-3}
Z = 4	α = 90.000 (0)°	μ = 0.087 mm^{-1}
R_1 = 5.1 %	β = 92.209 (4)°	0.28 x 0.12 x 0.03 mm^3
R_{all} = 11.8 %	γ = 90.000 (0)°	Clear, colourless plate

9.38.3 - bis(1-Naphthyl) 2,6-pyridinedicarboxylate (51)

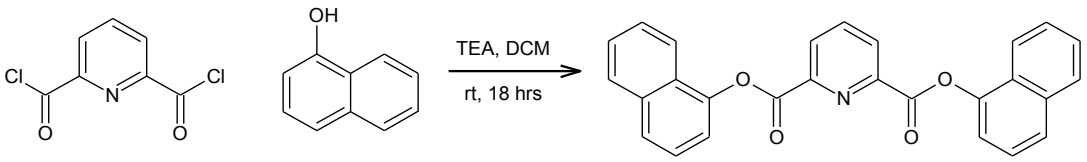

$C_7H_3Cl_2NO_2$
Fw = 204.01

$C_{10}H_8O$
Fw = 144.17

51 (75%)
$C_{27}H_{17}NO_4$
Fw = 419.43

Crystallisation from diethyl ether and light petroleum ether (bpt 40-60 °C) produced red crystals.

Mpt: 131-133 ºC.

Elemental analysis: Found: C, 77.43%; H, 3.93%; N, 3.36%
Calculated: C, 77.32%; H, 4.09%; N, 3.34%

X-ray diffraction: All atoms were found from the electron density map.

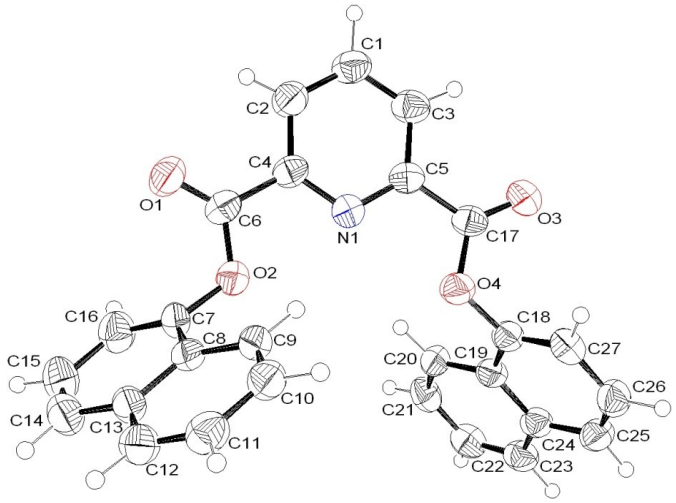

$C_{27}H_{17}NO_4$	a = 8.4772 (3) Å	T 120 K
Monoclinic P $2_1/c$	b = 28.7239 (19) Å	λ = 0.71073 Å
V = 2090.52 (29) Å^3	c = 9.3134 (5) Å	D_c = 1.33 g cm^{-3}
Z = 4	α = 90.000 (0)°	μ = 0.090 mm^{-1}
R_1 = 6.6 %	β = 112.805 (3)°	0.25 x 0.16 x 0.08 mm^3
R_{all} = 14.2 %	γ = 90.000 (0)°	Clear, colourless cut block

9.38.4 - bis((1-Naphthyl)methyl) 2,6-pyridinedicarboxylate (52)

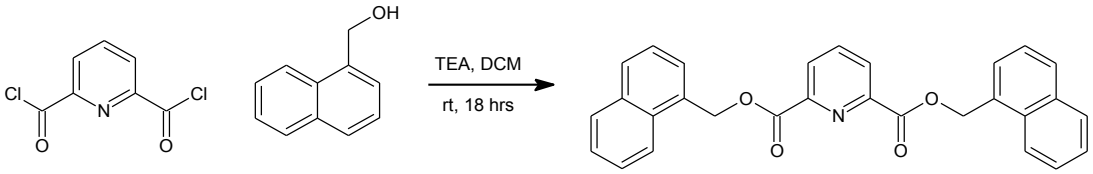

$C_7H_3Cl_2NO_2$
Fw = 204.01

$C_{11}H_{10}O$
Fw = 158.20

52 (71%)
$C_{29}H_{21}NO_4$
Fw = 447.4

Crystals were grown from a solution of the product in DCM and light petroleum ether (bpt 40-60 °C).

Mpt: 129-130 ºC.

Elemental analysis: Found: C, 77.53%; H, 3.93%; N, 3.47%
Calculated: C, 77.84%; H, 4.73%; N, 3.13%

X-ray diffraction: Non-hydrogen atoms and pyridyl protons were found from the electron density map. Naphthyl and methylene protons were identified from the density map and were then modelled based on an idealised geometry. The 6-membered ring defined by C10 - C15 was constrained to an idealised geometry.

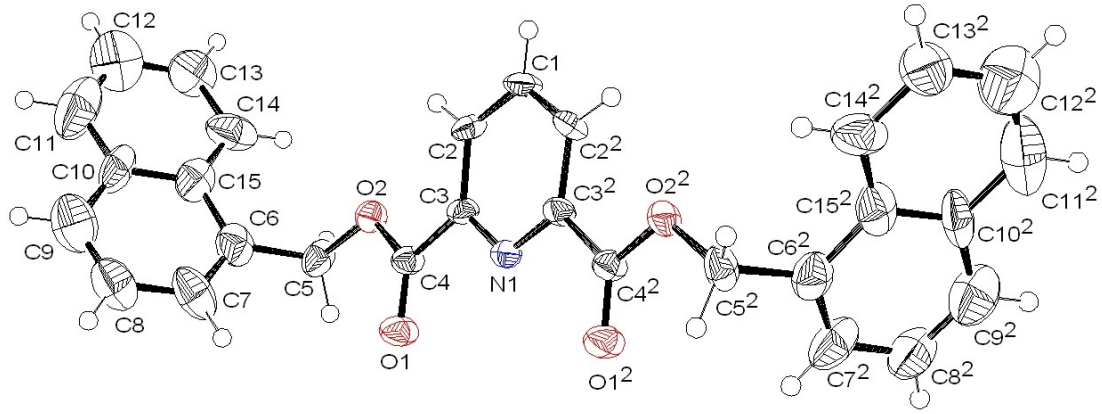

$C_{15}H_{11}NO_2$	a = 35.4864 (16) Å	T 120 K
Monoclinic C 2 /c	b = 6.3576 (3) Å	λ = 0.71073 Å
V = 2217.85 (16) Å^3	c = 10.1021 (5) Å	D_c = 1.34 g cm^{-3}
Z = 4	α = 90.000 (0)°	μ = 0.089 mm^{-1}
R_1 = 13.1%	β = 103.315 (3)°	0.08 x 0.08 x 0.01 mm^3
R_{all} = 18.3%	γ = 90.000 (0)°	Clear, colourless, cut plate

9.38.5 - bis((9-Anthryl)methyl) 2,6-pyridinedicarboxylate (53)

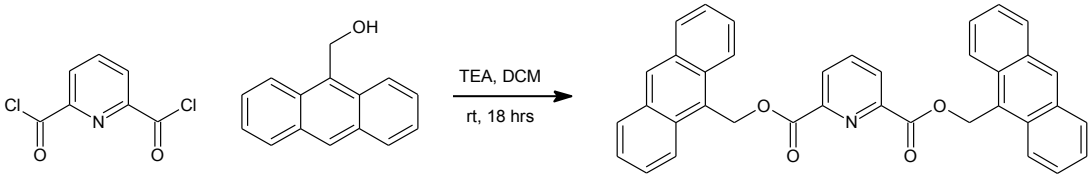

$C_7H_3Cl_2NO_2$
Fw = 204.01

$C_{15}H_{12}O$
Fw = 208.26

53 (43%)
$C_{37}H_{25}NO_4$
Fw = 547.60

White crystalline platelets were obtained by slow evaporation of a solution of the product in DCM.

Mpt: 234-236 °C.

Elemental analysis: Found: C, 80.49%; H, 4.41%; N, 2.93%
Calculated: C, 81.15%; H, 4.60%; N, 2.56%

X-ray diffraction: All atoms were found from the electron density map.

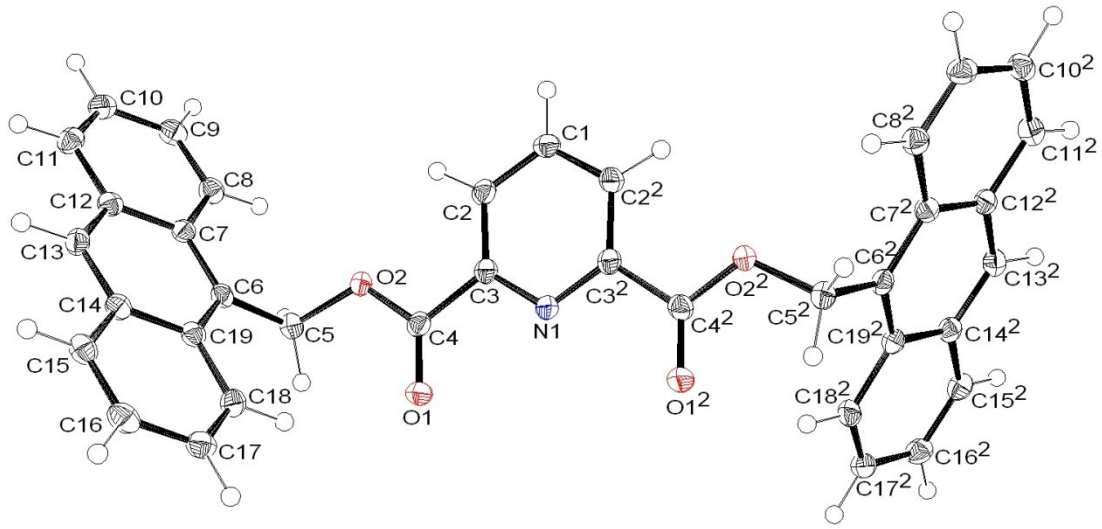

$C_{37}H_{25}NO_4$	a = 17.2053 (8) Å	T 120 K
Monoclinic P2/c	b = 6.3704 (2) Å	λ = 0.71073 Å
V = 1302.51 (3) $Å^3$	c = 11.9432 (4) Å	D_c = 1.40 g cm^{-3}
Z = 2	α = 90.000 (0)°	μ = 0.091 mm^{-1}
R_1 = 6.9 %	β = 95.723 (2)°	0.1 x 0.1 x 0.02 mm^3
R_{all} = 10.0 %	γ = 90.000 (0)°	Clear, pale yellow cut plate

9.38.6 - bis(2-Naphthyl) 3,5-pyridinedicarboxylate (54)

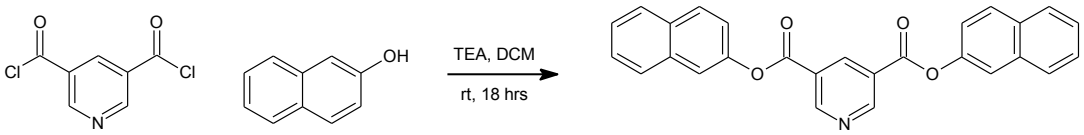

$C_7H_3Cl_2NO_2$
Fw = 204.01

$C_{10}H_8O$
Fw = 144.17

54 (84%)
$C_{27}H_{17}NO_4$
Fw = 419.43

Crystals were grown by soxhlet extraction with chloroform over a period of 4 days.

Mpt: 222 °C.

Elemental analysis: Found: C, 77.41%; H, 4.06%; N, 3.93%
Calculated: C, 77.32%; H, 4.09%; N, 3.34%

X-ray diffraction: All atoms were found from the electron density map.

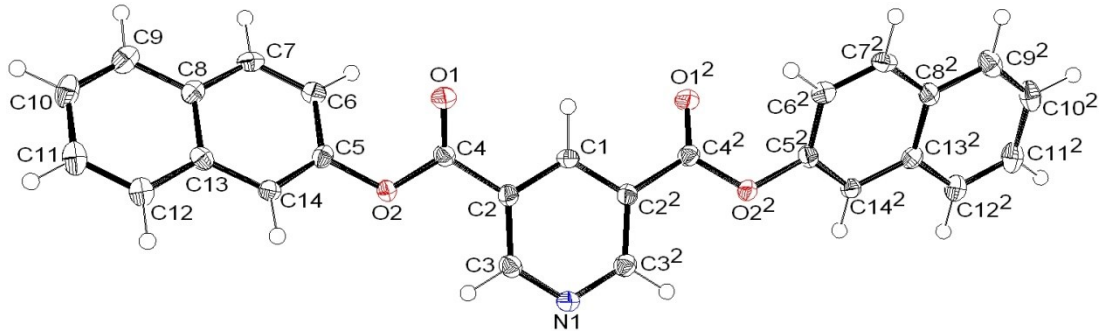

$C_{29}H_{21}NO_4$	a = 44.4470 (26) Å	T 120 K
Monoclinic C 2/c	b = 6.4550 (3) Å	λ = 0.71073 Å
V = 1961.19 (6) $Å^3$	c = 7.2073 (4) Å	D_c = 1.42 g cm^{-3}
Z = 4	α = 90.000 (0)°	μ = 0.096 mm^{-1}
R_1 = 5.8 %	β = 95.922 (3)°	0.12 x 0.10 x 0.02 mm^3
R_{all} = 8.5 %	γ = 90.000 (0)°	Clear, colourless plate

9.38.7 - bis((2-Naphthyl)methyl) 3,5-pyridinedicarboxylate (55)

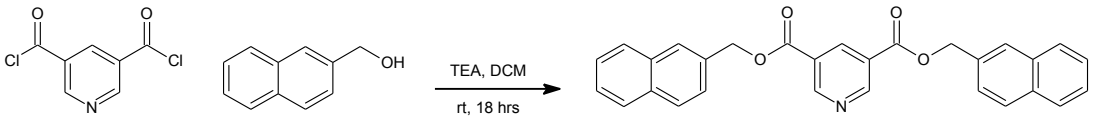

$C_7H_3Cl_2NO_2$
Fw = 204.01

$C_{11}H_{10}O$
Fw = 158.20

55 (93%)
$C_{29}H_{21}NO_4$
Fw = 447.48

Crystallisation by vapour diffusion of light petroleum ether into a solution of the product in chloroform gave small platelets.

Mpt: 159-161 °C.

Elemental analysis: Found: C, 77.42%; H, 4.61%; N, 3.21%
Calculated: C, 77.84%; H, 4.73%; N, 3.13%

X-ray diffraction: Data was collected by the NCS using the high flux X-ray synchrotron source at the Daresbury Laboratory. All non-hydrogen atoms were found from the electron density map; protons were identified from the density map and were then modelled based on an idealised geometry with bond length and torsion angles refined from the density data.

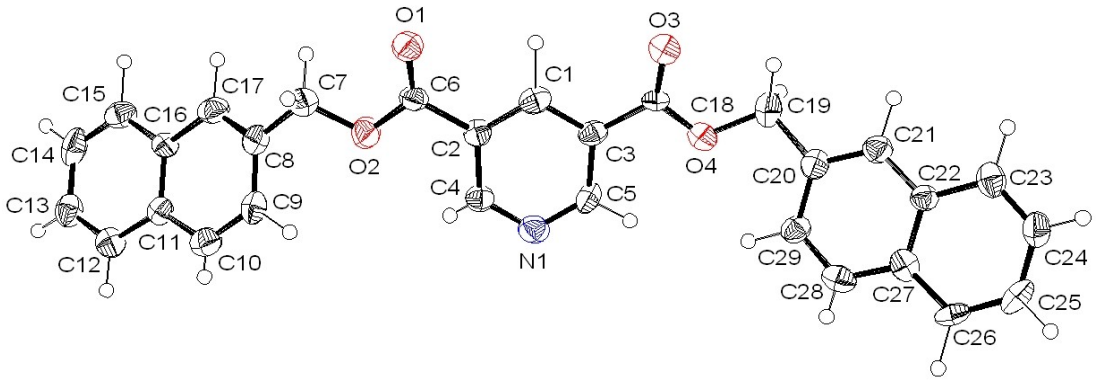

$C_{29}H_{21}NO_4$	a = 7.40 (2) Å	T 120 K
Monoclinic P $2_1/n$	b = 6.113 (17) Å	λ = 0.71073 Å
V = 2094.31 (100) $Å^3$	c = 46.30 (13) Å	D_c = 1.42 g cm^{-3}
Z = 4	α = 90.00 (0)˚	μ = 0.053 mm^{-1}
R_1 = 15.4%	β = 90.63 (2)˚	0.05 x 0.05 x 0.005 mm^3
R_{all} = 16.6%	γ = 90.00 (0)˚	Colourless plate

9.38.8 - bis((1-Naphthyl)methyl) 3,5-pyridinedicarboxylate (58)

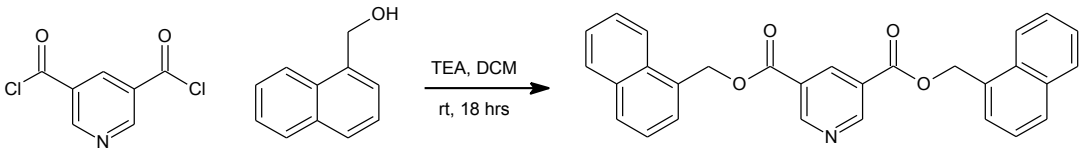

$C_7H_3Cl_2NO_2$
Fw = 204.01

$C_{11}H_{10}O$
Fw = 158.20

58 (66%)
$C_{29}H_{21}NO_4$
Fw = 447.4

Yellow crystals were obtained by vapour diffusion of a solution of the product in chloroform with light petroleum ether (bpt 40-60 °C).

Mpt: 140-144 °C.

Elemental analysis: Found: C, 77.30%; H, 3.84%; N, 3.53%
Calculated: C, 77.84%; H, 3.73%; N, 3.13%

X-ray diffraction: All atoms were found from the electron density map.

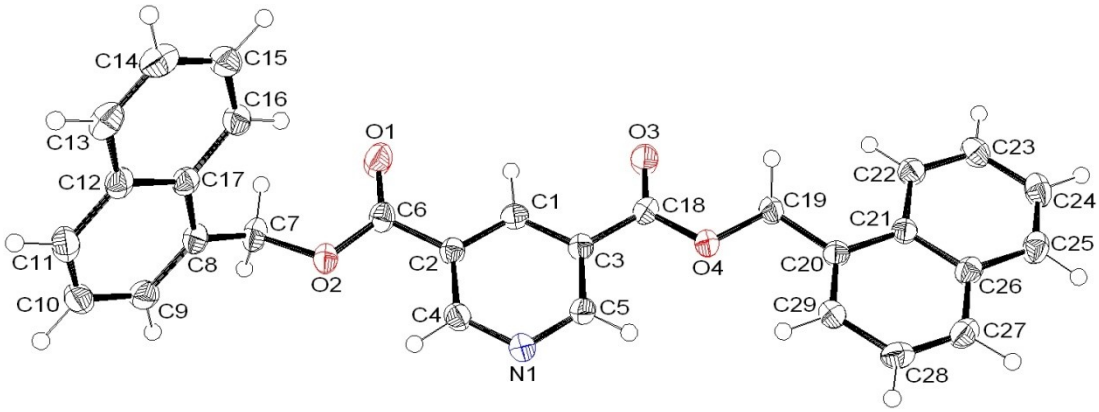

$C_{29}H_{21}NO_4$	a = 8.0715 (4) Å	T 120 K
Triclinic P-1	b = 8.5049 (3) Å	λ = 0.71073 Å
V = 1077.08 (10) Å^3	c = 17.1901 (7) Å	D_c = 1.38 g cm^{-3}
Z = 2	α = 86.222 (3)°	μ = 0.92 mm^{-1}
R_1 = 5.8 %	β = 85.597 (2)°	0.18 x 0.16 x 0.06 mm^3
R_{all} = 11.6 %	γ = 66.365 (2)°	Clear, pale yellow cut fragment

9.38.9 - bis((9-Anthryl)methyl) 3,5-pyridinedicarboxylate (59)

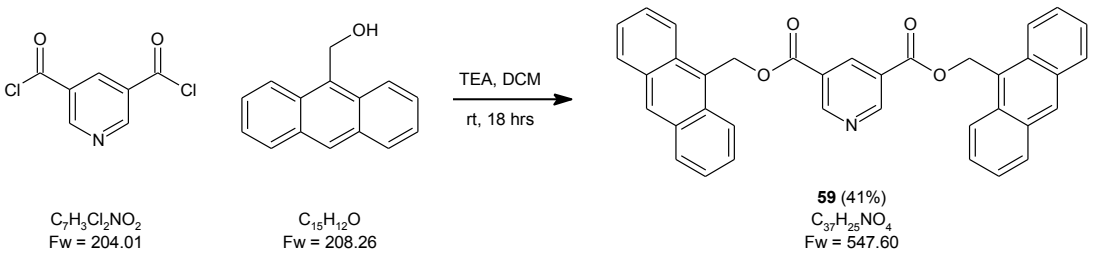

$C_7H_3Cl_2NO_2$
Fw = 204.01

$C_{15}H_{12}O$
Fw = 208.26

59 (41%)
$C_{37}H_{25}NO_4$
Fw = 547.60

White crystalline platelets were obtained by slow evaporation of a solution of the product in toluene.

Mpt: 207-209 °C.

Elemental analysis: Found: C, 80.87%; H, 4.55%; N, 2.96%
Calculated: C, 81.15%; H, 4.60%; N, 2.56%

X-ray diffraction: All atoms were found from the electron density map.

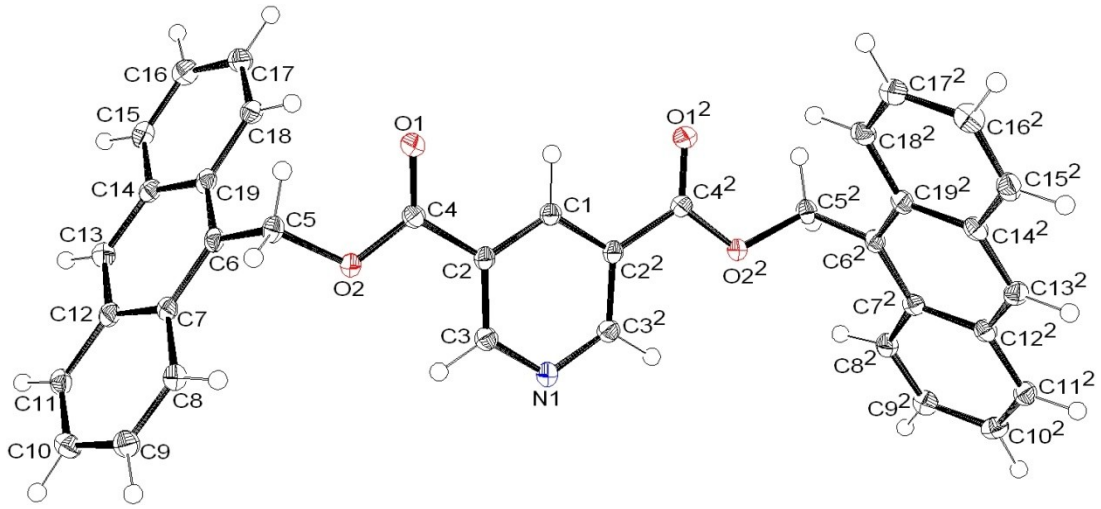

$C_{17.5}H_{12.5}N_{0.5}O_2$	a = 17.1840 (0) Å	T 120 K
Monoclinc P 2/c	b = 6.2990 (0) Å	λ = 0.71073 Å
V = 1305.53 (0) Å^3	c = 12.1480 (0) Å	D_c = 1.33 g cm^{-3}
Z = 4	α = 90.000 (0)°	μ = 0.087 mm^{-1}
R_1 = 5.8 %	β = 96.852 (0)°	0.38 x 0.32 x 0.02 mm^3
R_{all} = 6.8 %	γ = 90.000 (0)°	Clear, colourless cut plate

Appendix A - ^{1}H NMR titration spectra

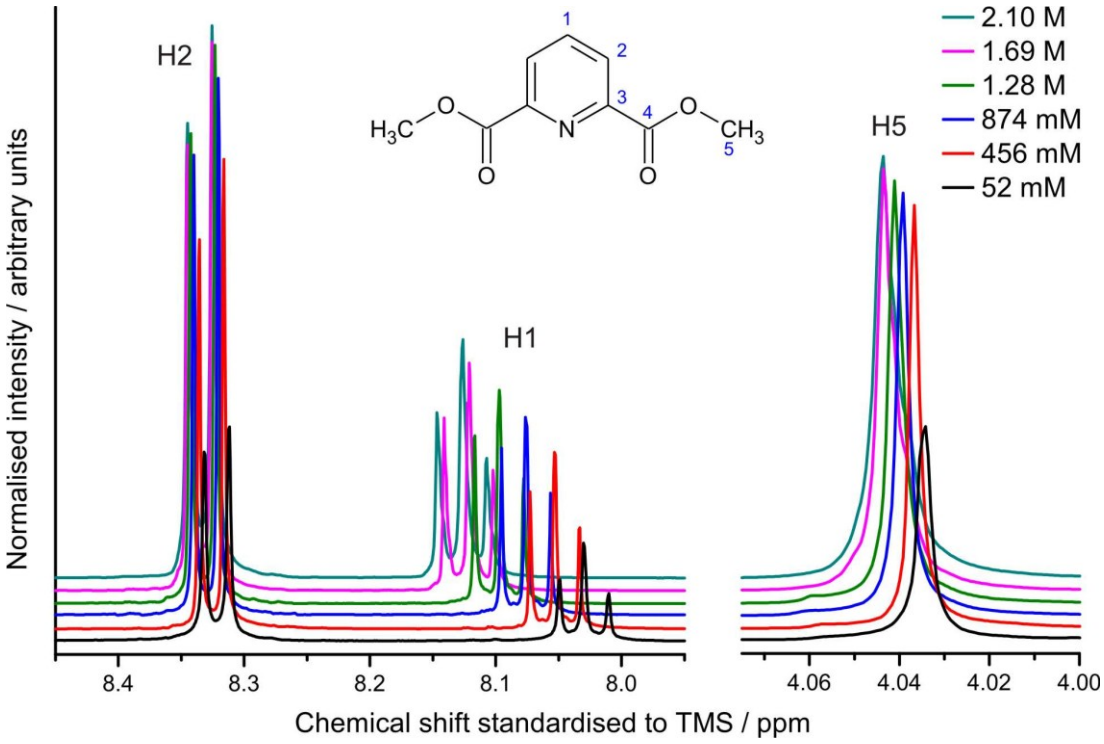

*Figure 96: ^{1}H NMR titration spectra for dimethyl 2,6-pyridinedicarboxyate (**38**).*

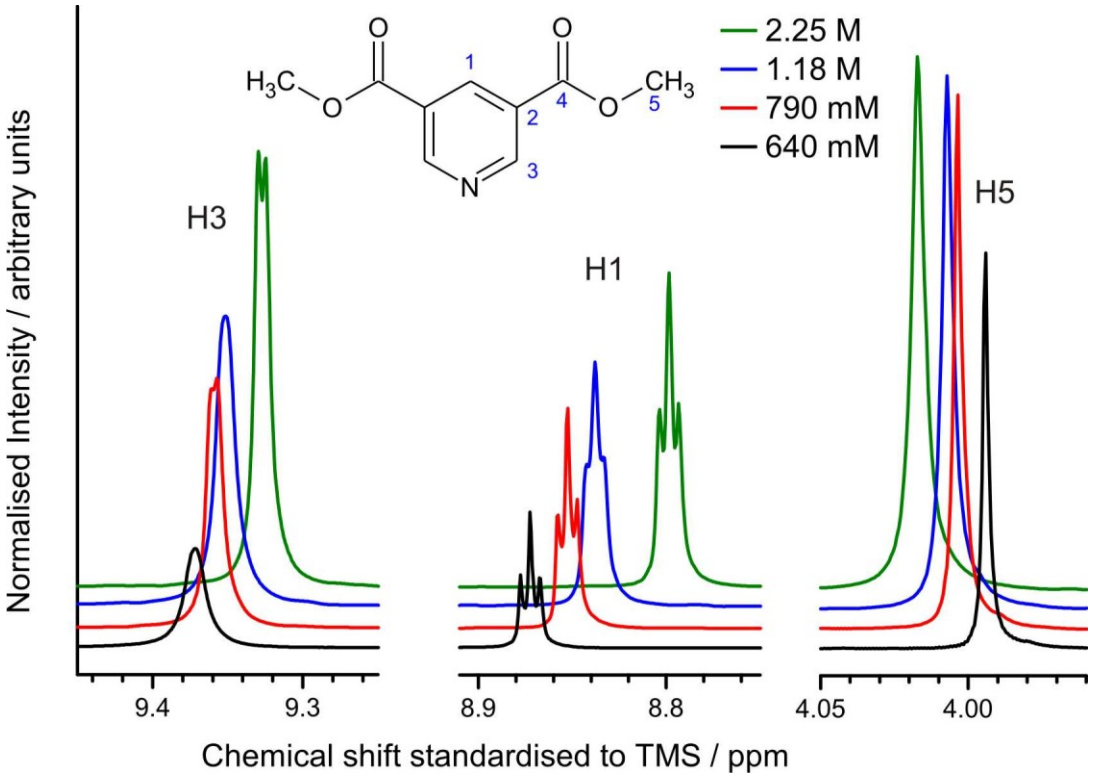

*Figure 97: ^{1}H NMR titration spectra for dimethyl 3,5-pyridinedicarboxyate (**39**).*

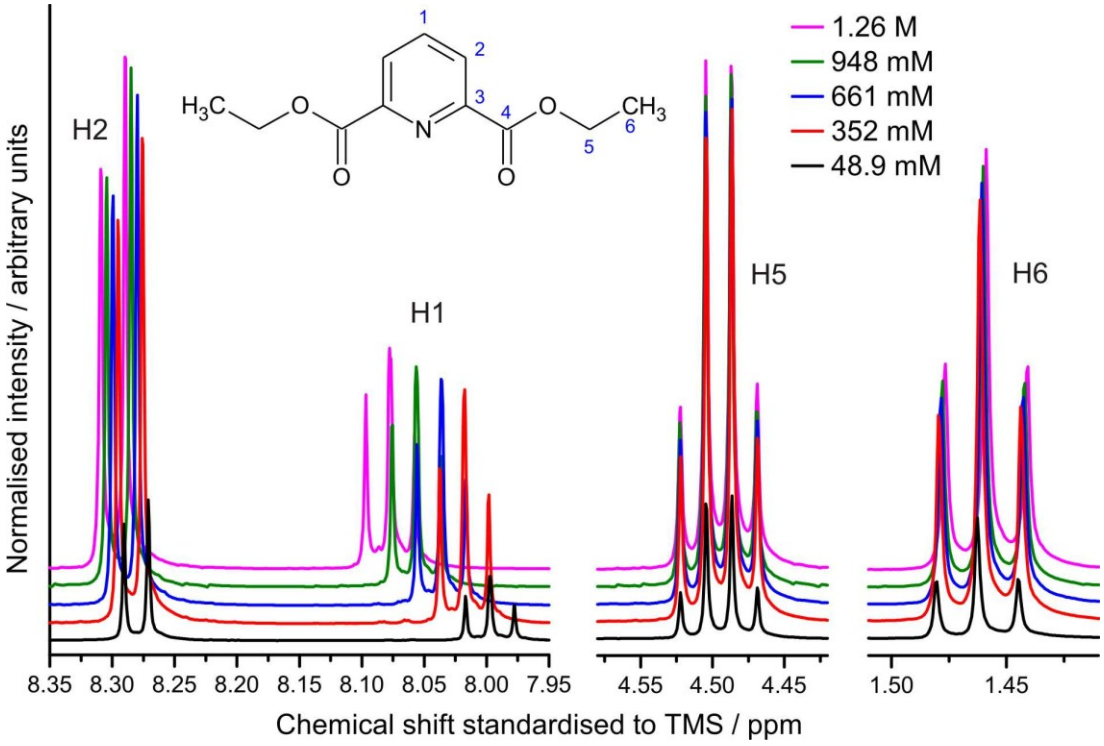

*Figure 98: ^{1}H NMR titration spectra for diethyl 2,6-pyridinedicarboxyate (**40**).*

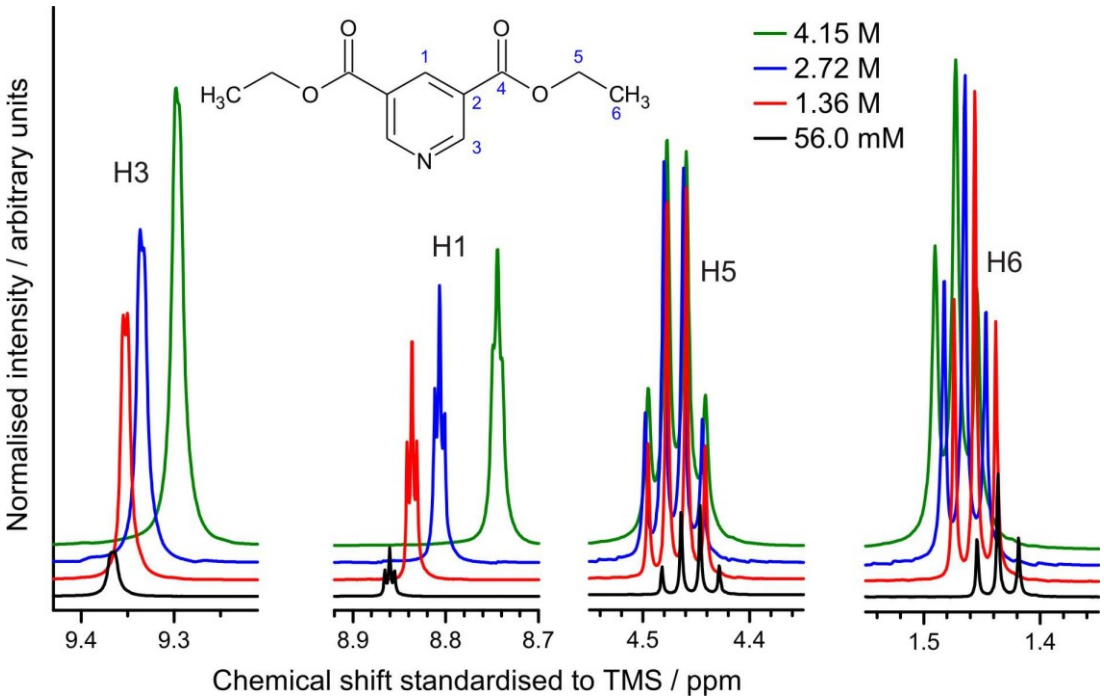

*Figure 99: ^{1}H NMR titration spectra for diethyl 3,5-pyridinedicarboxyate (**41**).*

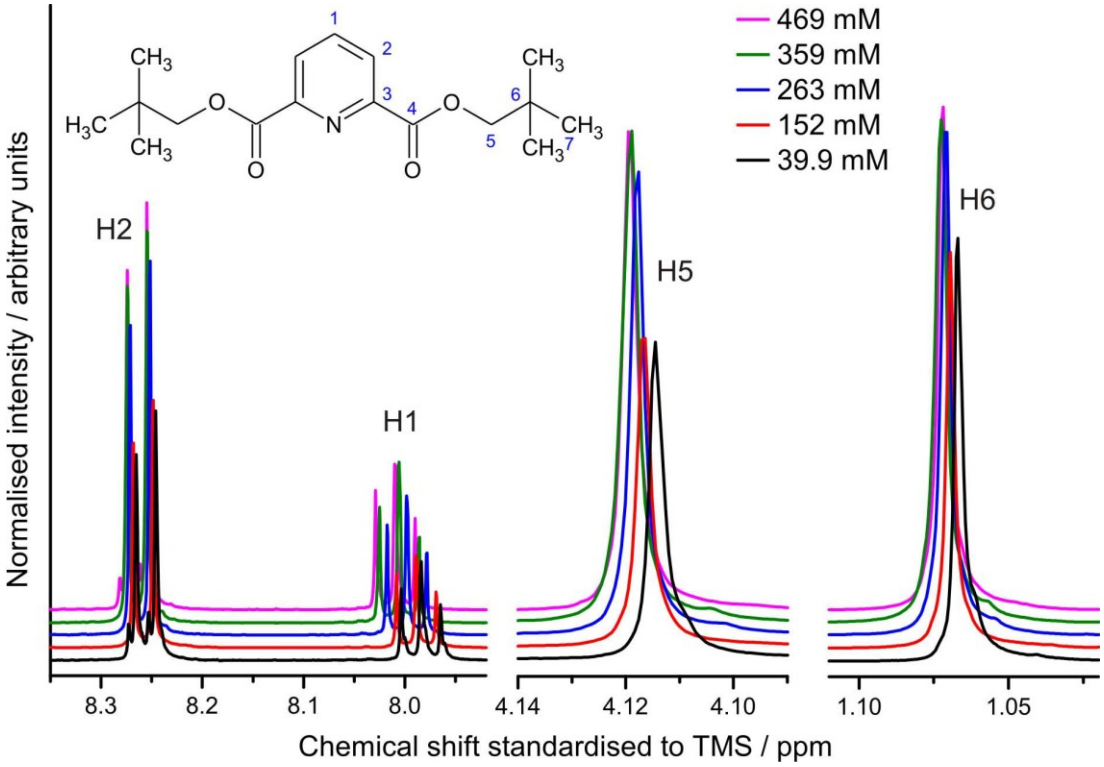

*Figure 100: ^{1}H NMR titration spectra bis(neopentyl) 2,6-pyridinedicarboxyate (**42**).*

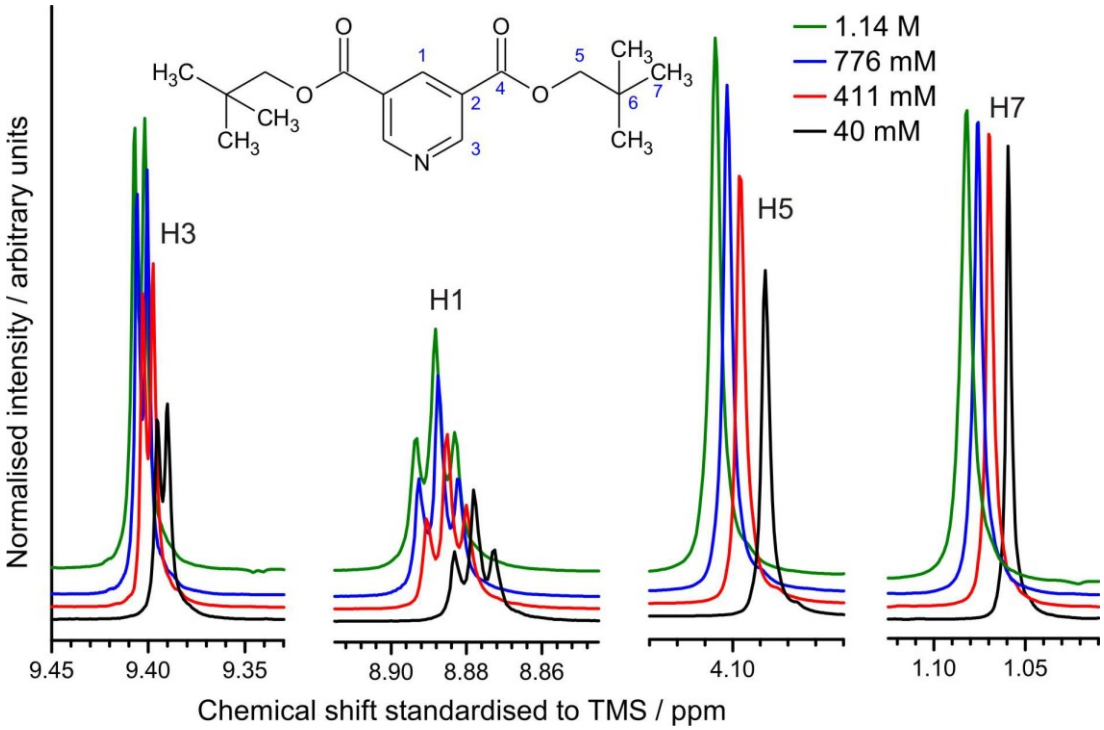

*Figure 101: ^{1}H NMR titration spectra for bis(neopentyl) 3,5-pyridinedicarboxyate (**43**).*

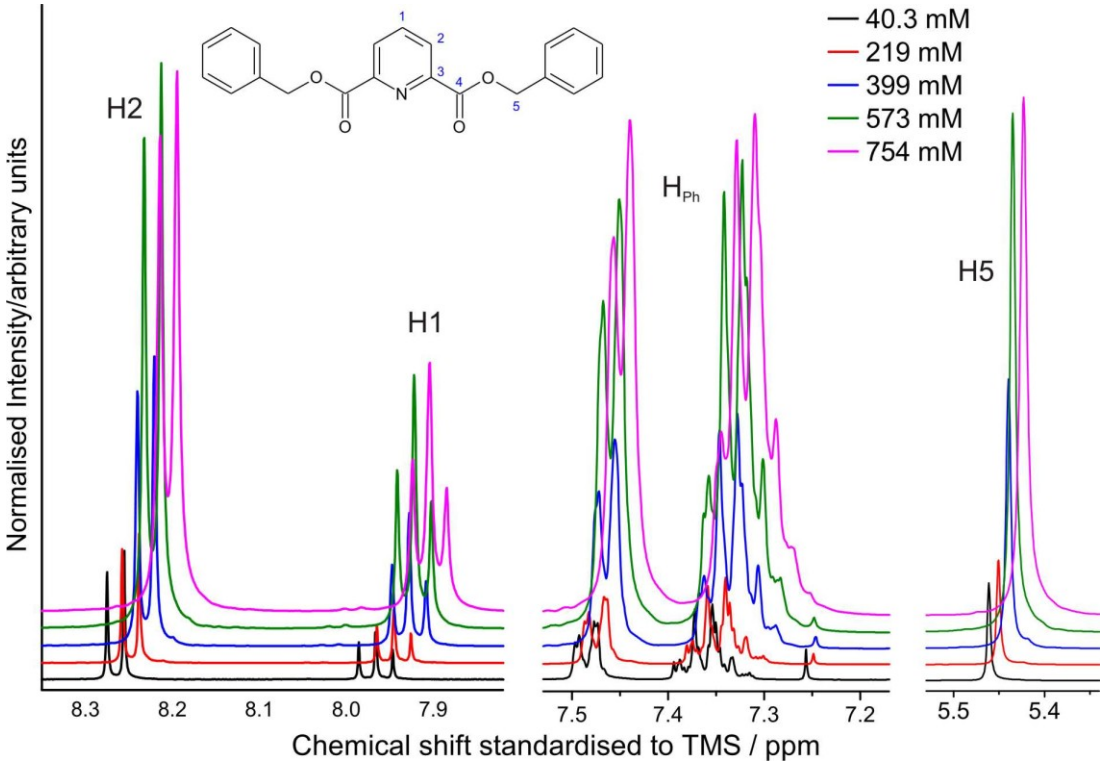

*Figure 102: ^{1}H NMR titration spectra for bis(benzyl) 2,6-pyridinedicarboxyate (**44**).*

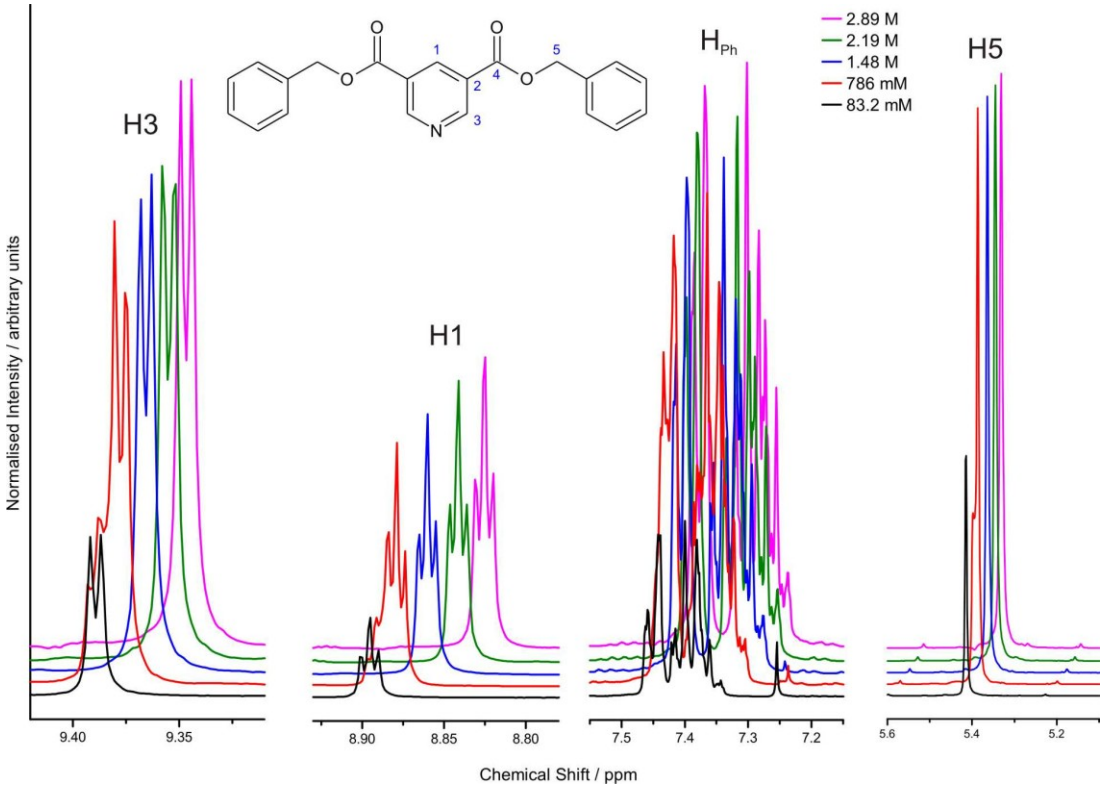

*Figure 103: ^{1}H NMR titration spectra for bis(benzyl) 3,5-pyridinedicarboxyate (**45**).*

Appendix B - Variable temperature Raman spectra

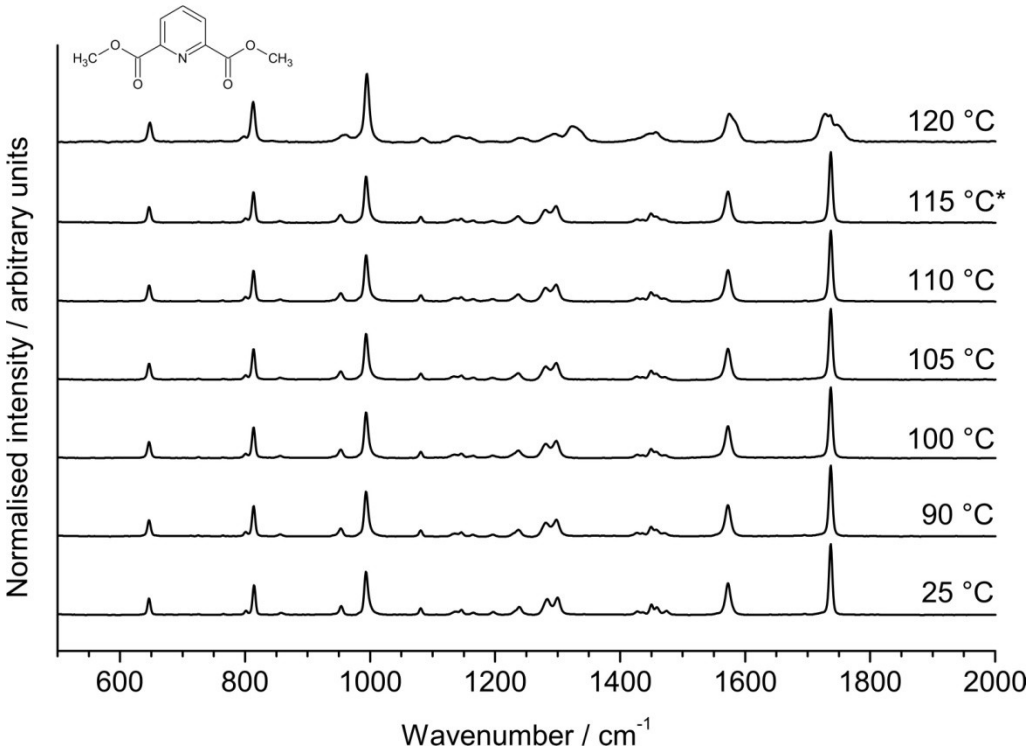

*Figure 104: Variable temperature Raman spectra for dimethyl 2,6-pyridinedicarboxyate (**38**); * indicates sample melting point.*

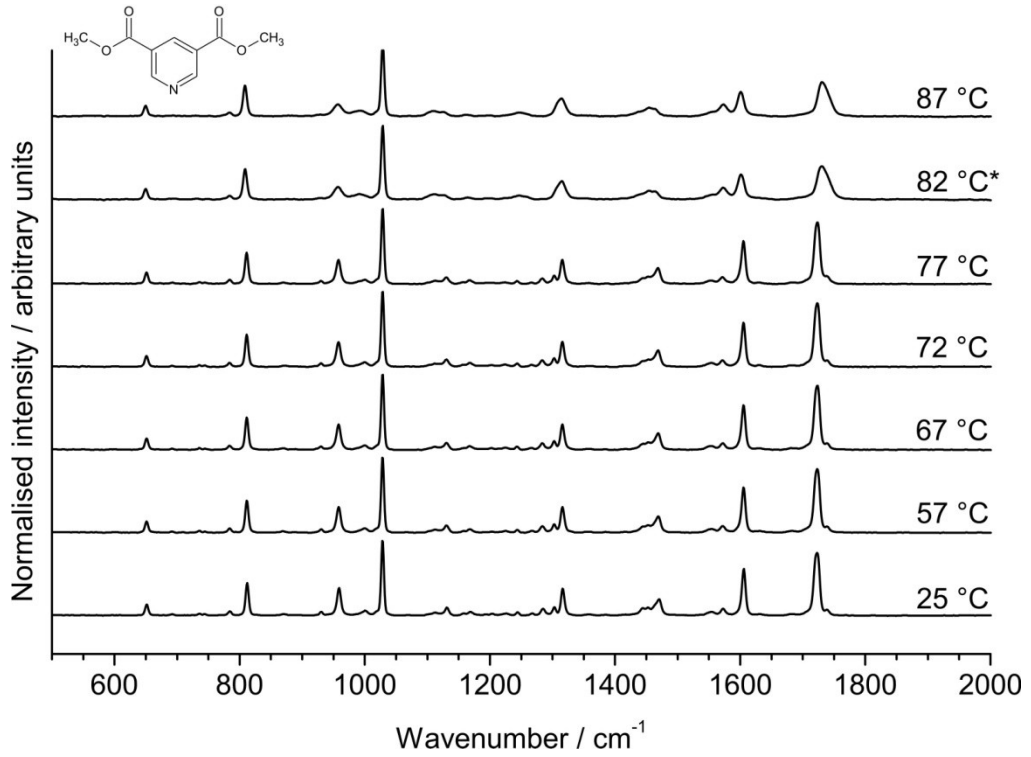

*Figure 105: Variable temperature Raman spectra for dimethyl 3,5-pyridinedicarboxyate (**39**); * indicates sample melting point.*

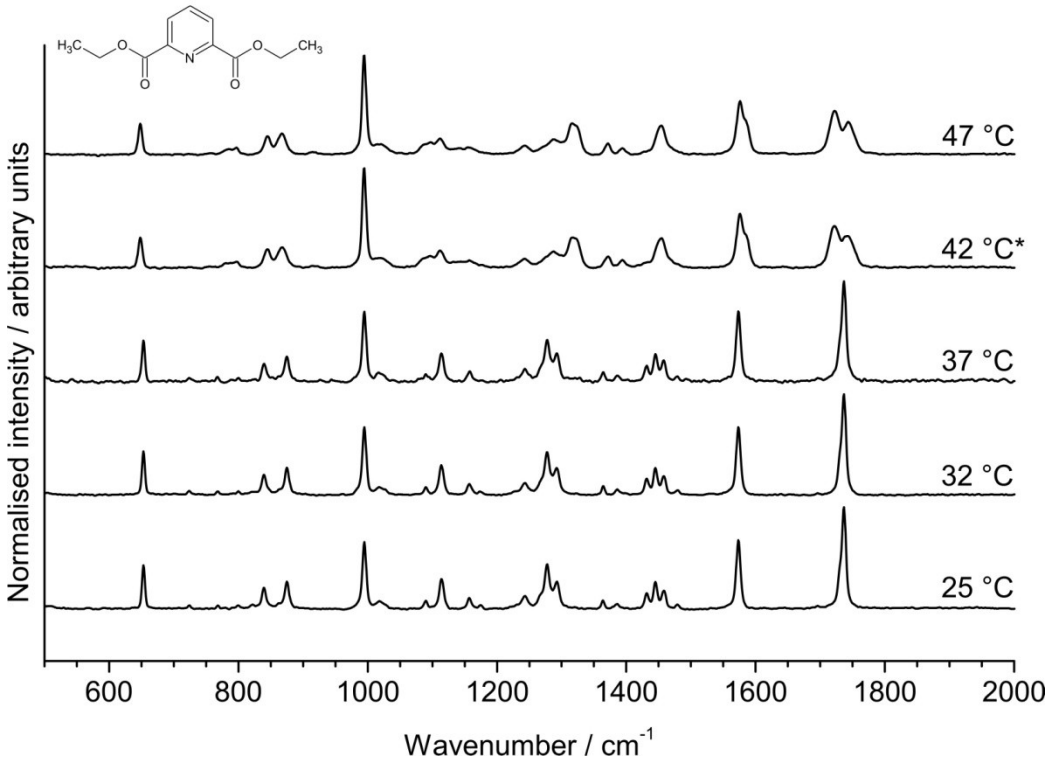

*Figure 106: Variable temperature Raman spectra for diethyl 2,6-pyridinedicarboxyate (**40**); * indicates sample melting point.*

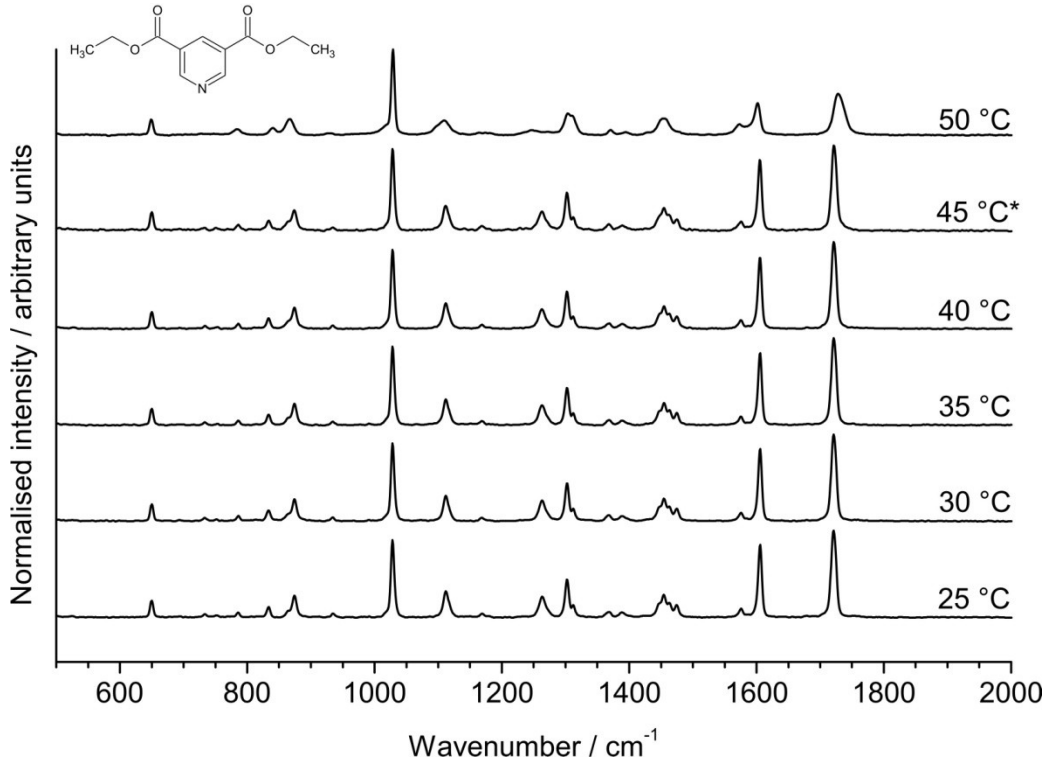

*Figure 107: Variable temperature Raman spectra for diethyl 3,5-pyridinedicarboxyate (**41**); * indicates sample melting point.*

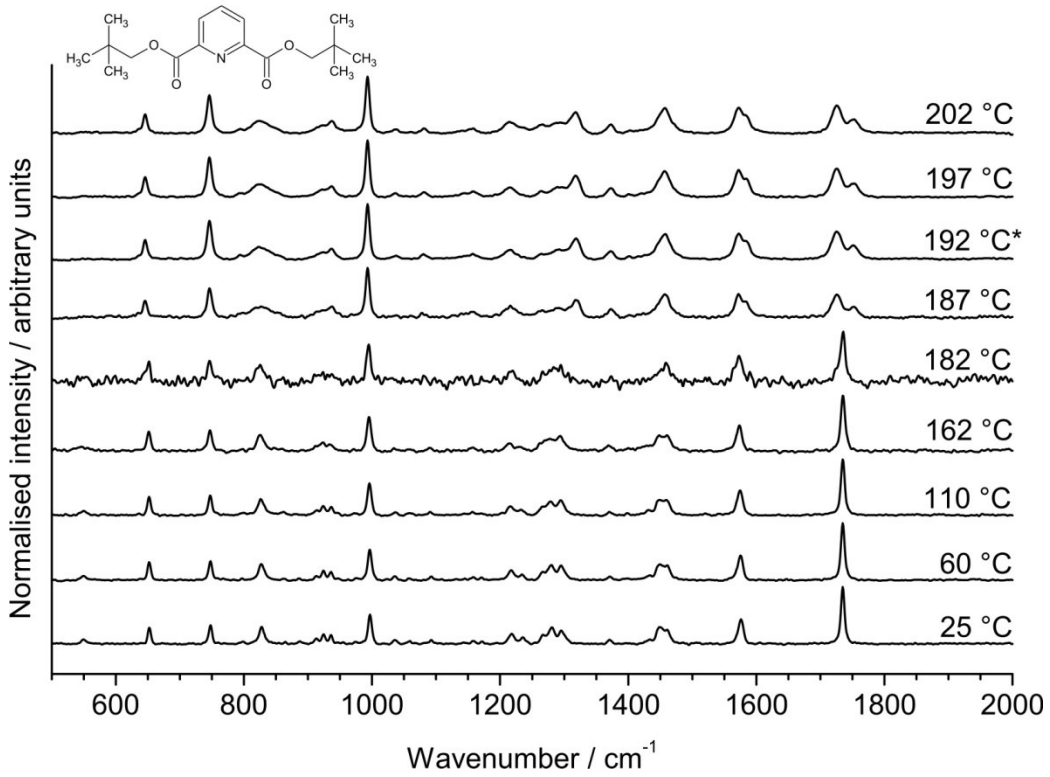

*Figure 108: Variable temperature Raman spectra for bis(neopentyl) 2,6-pyridinedicarboxyate (**42**); * indicates sample melting point.*

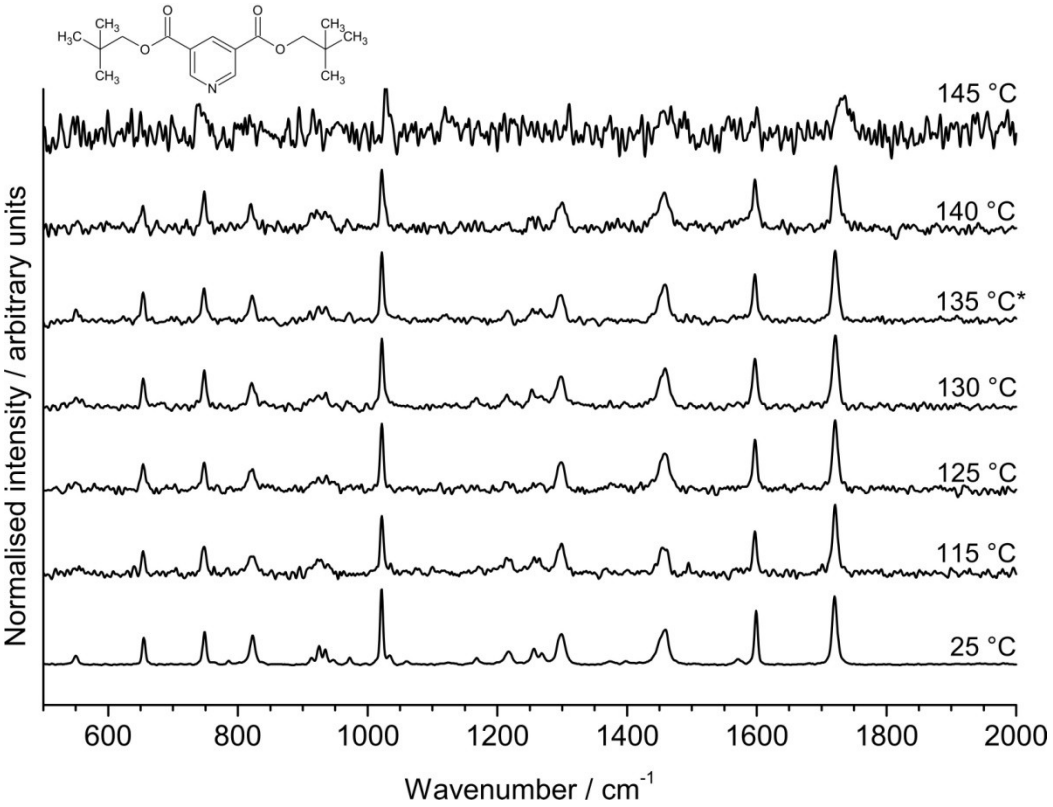

*Figure 109: Variable temperature Raman spectra for bis(neopentyl) 3,5-pyridinedicarboxyate (**43**); * indicates sample melting point.*

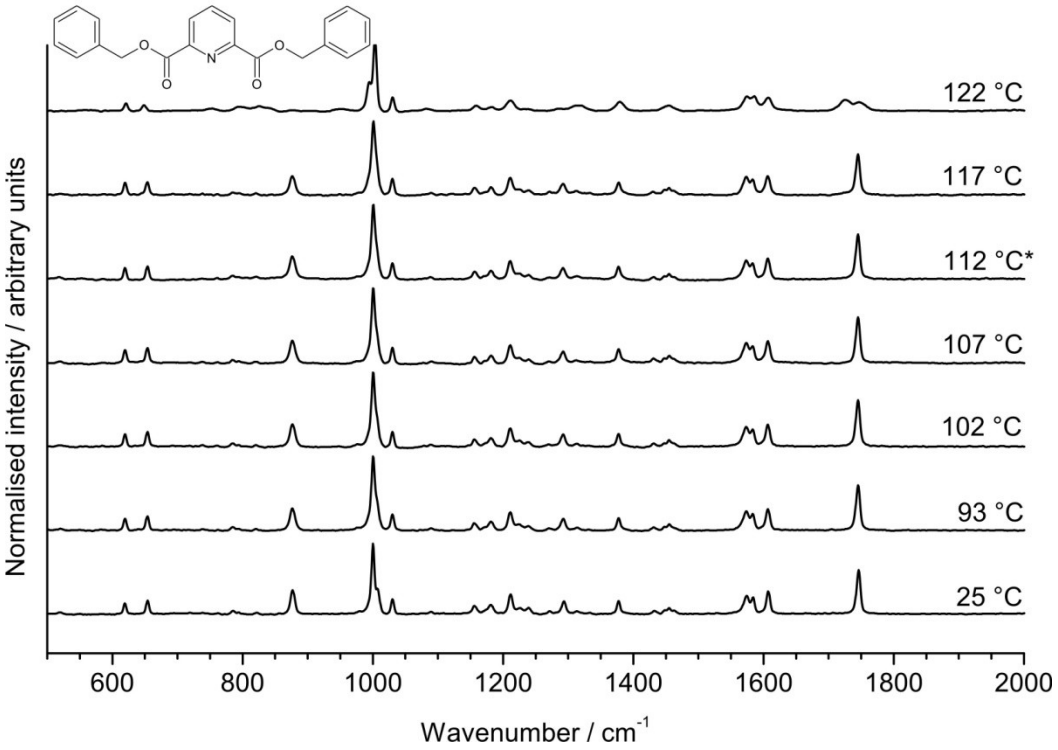

*Figure 110: Variable temperature Raman spectra for bis(benzyl) 2,6-pyridinedicarboxyate (**44**); * indicates sample melting point.*

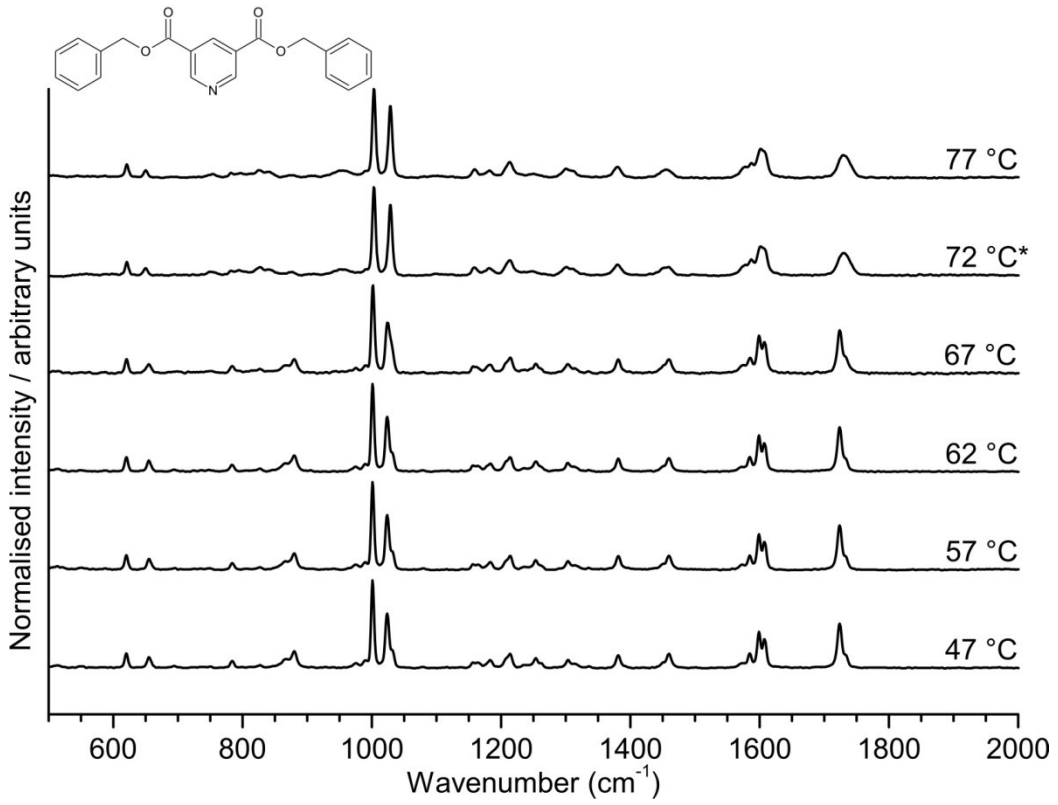

*Figure 111: Variable temperature Raman spectra for bis(benzyl) 3,5-pyridinedicarboxyate (**45**); * indicates sample melting point.*

Appendix C - DSC data

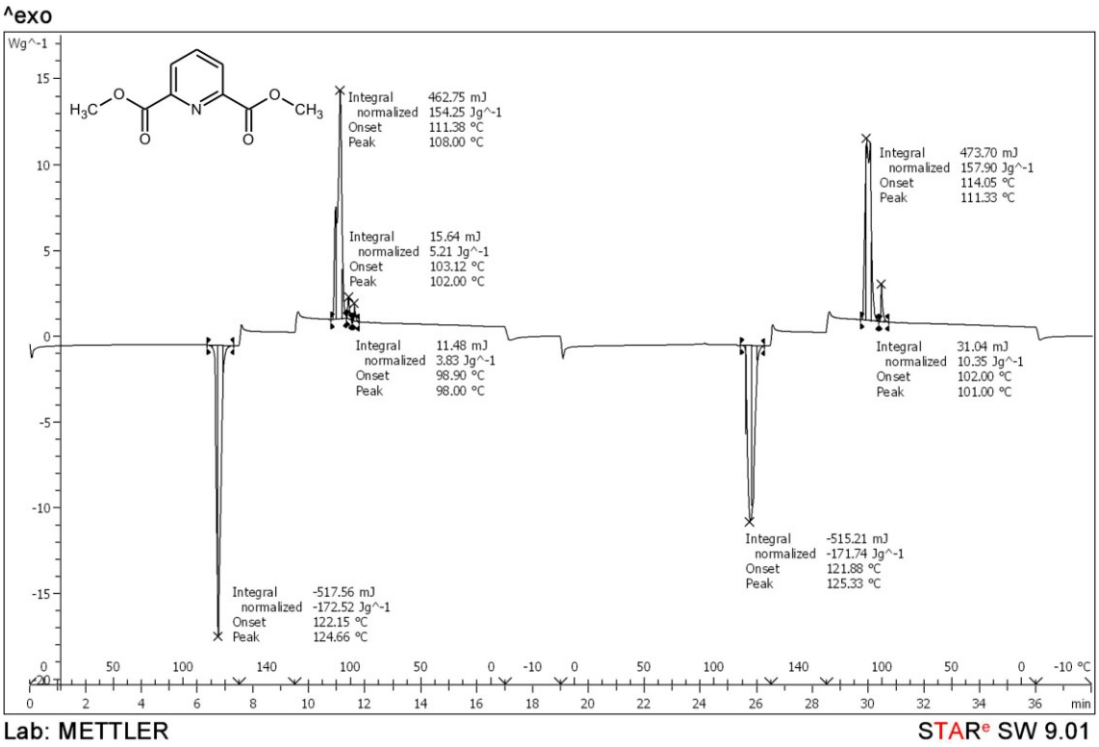

*Figure 112: DSC curve for dimethyl 2,6-pyridinedicarboxyate (**38**); a 3.00 mg sample was heated and cooled at 20 °C min^{-1} between -10 and 140 °C.*

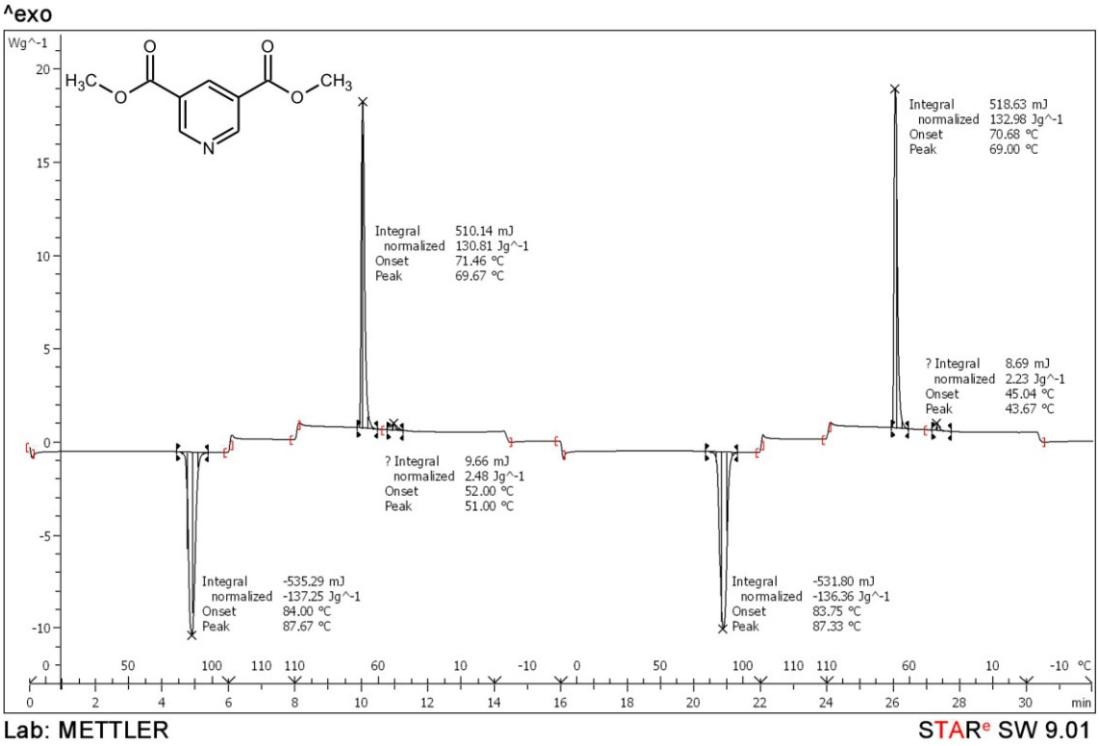

*Figure 113: DSC curve for dimethyl 3,5-pyridinedicarboxyate (**39**); a 3.90 mg sample was heated and cooled at 20 °C min^{-1} between -10 and 110 °C.*

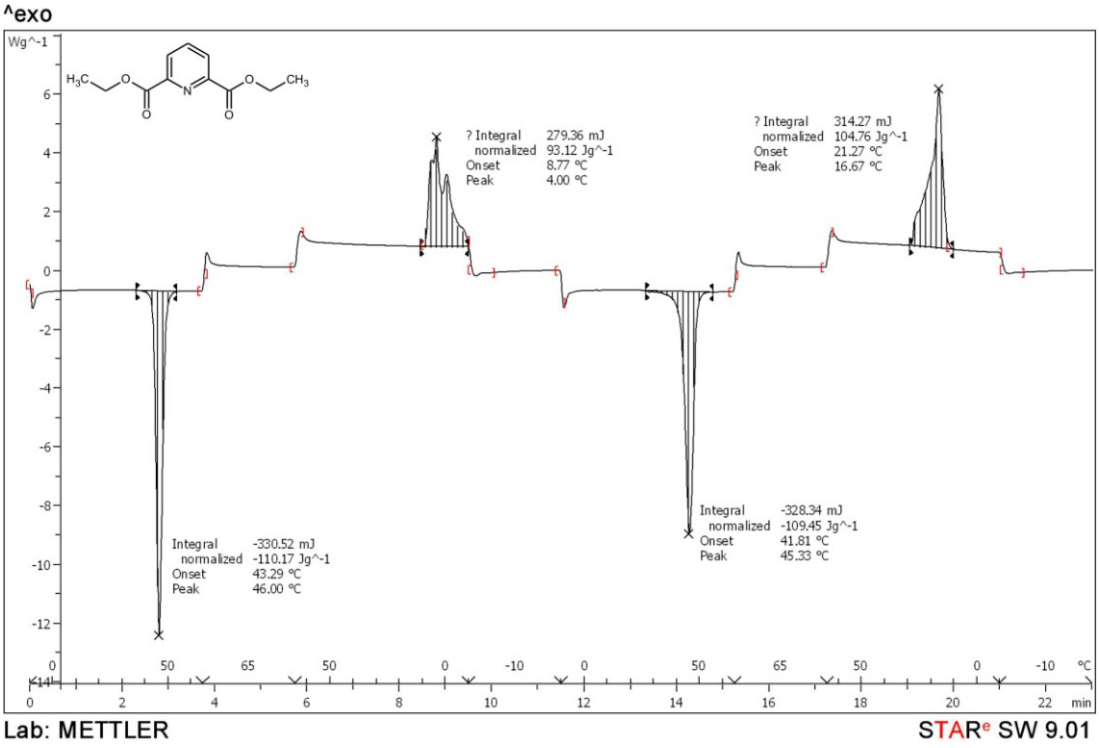

*Figure 114: DSC curve for diethyl 2,6-pyridinedicarboxyate (**40**); a 3.00 mg sample was heated and cooled at 20 °C min^{-1} between -10 and 65 °C.*

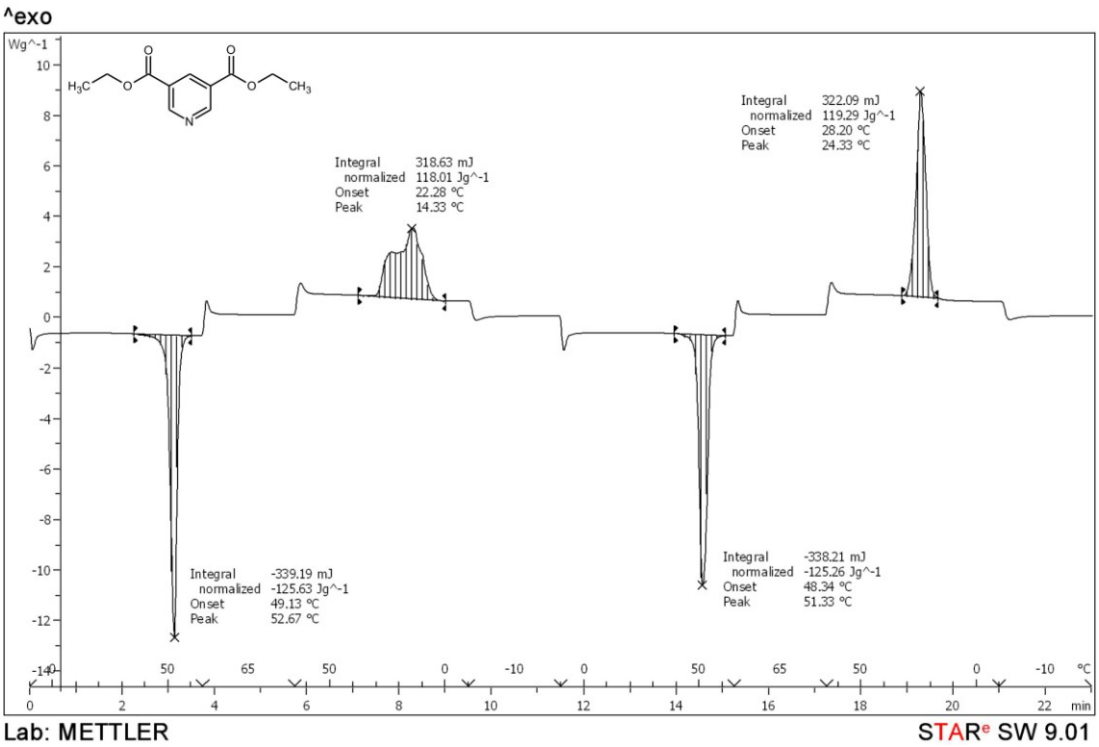

*Figure 115: DSC curve for diethyl 3,5-pyridinedicarboxyate (**41**); a 2.70 mg sample was heated and cooled at 20 °C min^{-1} between -10 and 65 °C.*

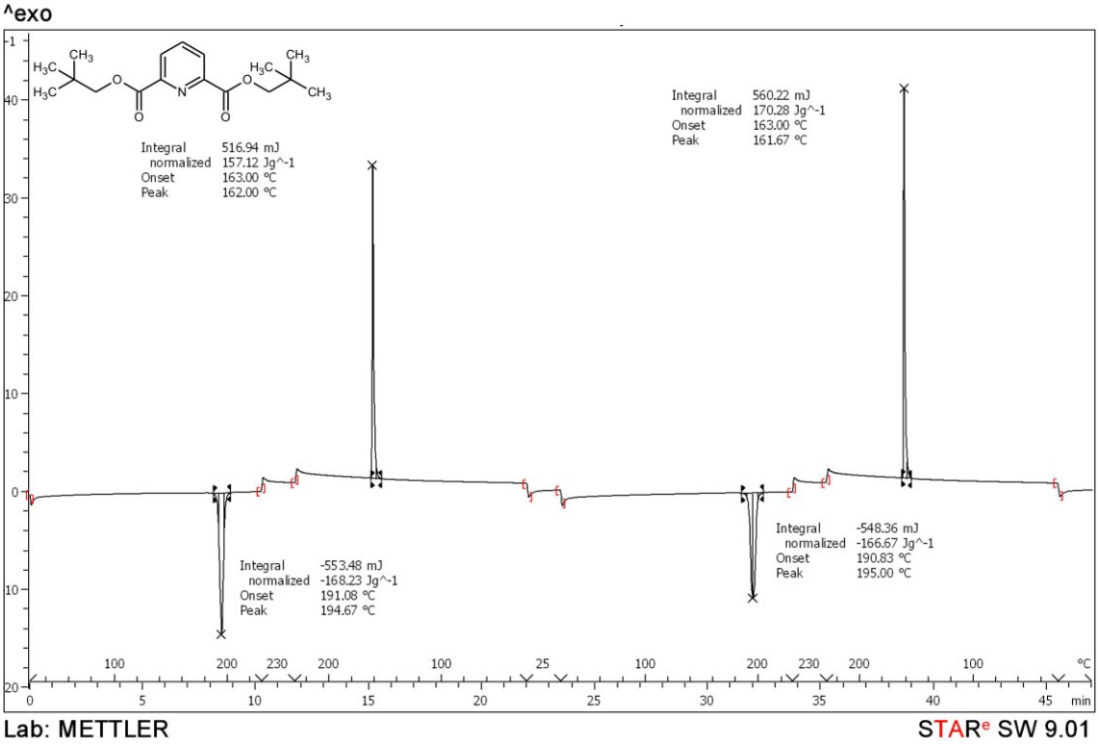

*Figure 116: DSC curve for bis(neopentyl) 2,6-pyridinedicarboxyate (**42**); a 3.29 mg sample was heated and cooled at 20 °C min^{-1} between 25 and 230 °C.*

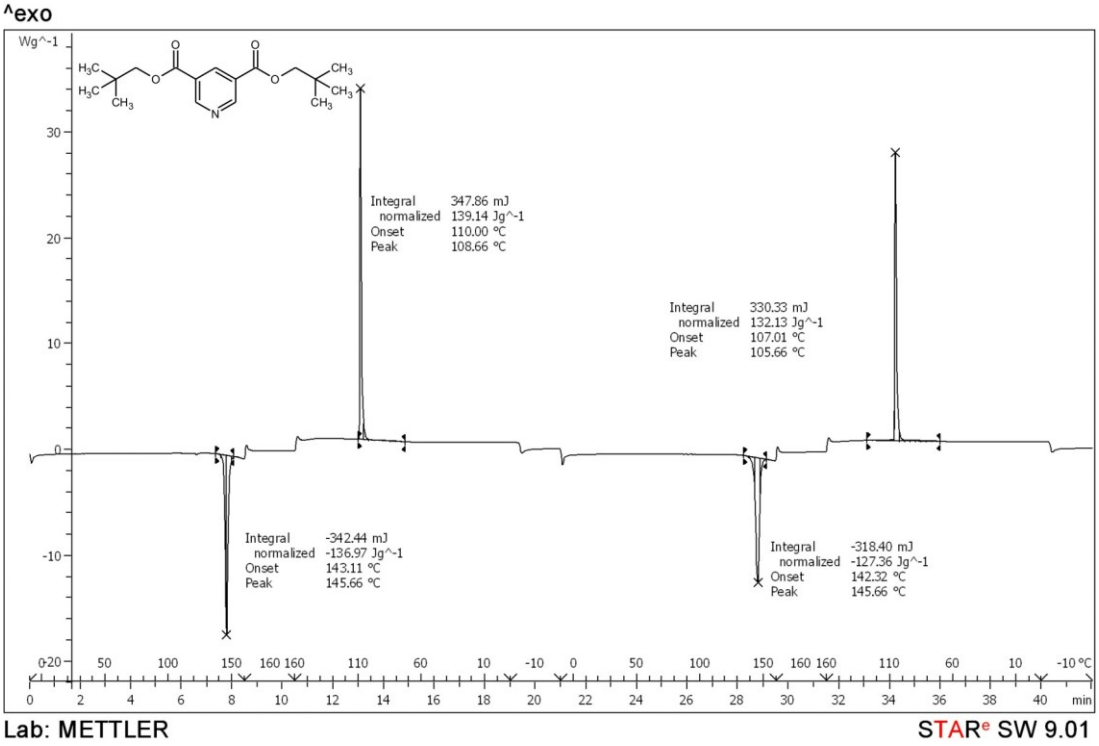

*Figure 117: DSC curve for bis(neopentyl) 3,5-pyridinedicarboxyate (**43**); a 2.50 mg sample was heated and cooled at 20 °C min^{-1} between -10 and 160 °C.*

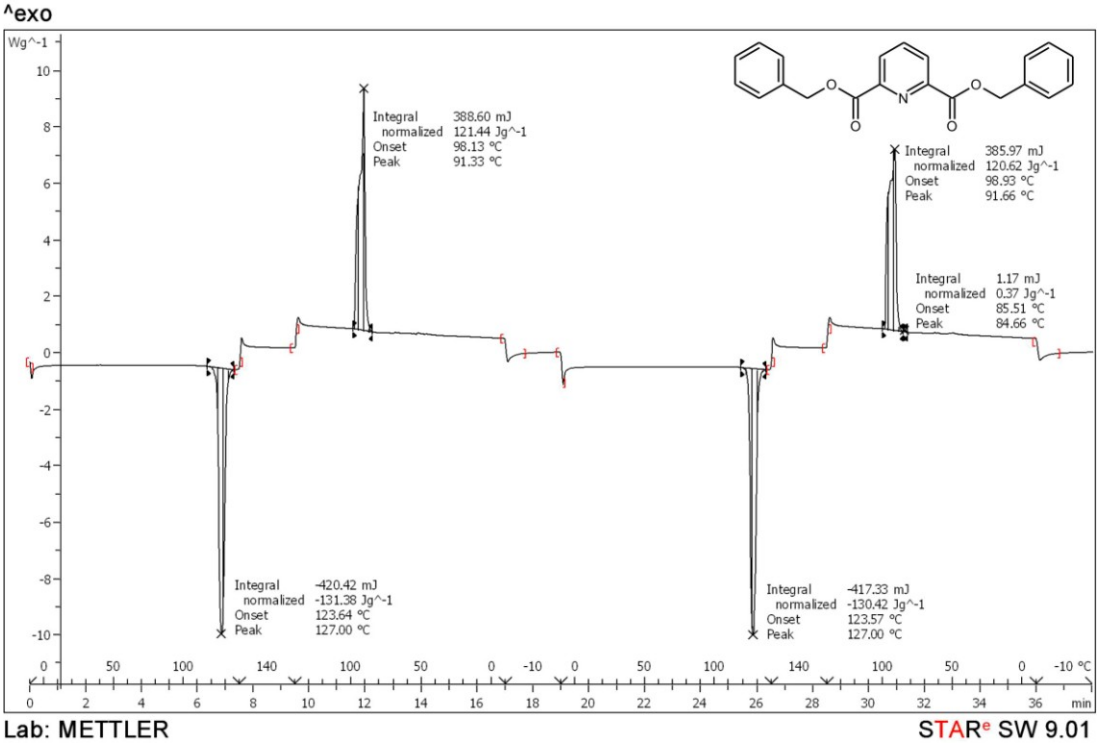

*Figure 118: DSC curve for bis(benzyl) 2,6-pyridinedicarboxyate (**44**); a 3.20 mg sample was heated and cooled at 20 °C min^{-1} between -10 and 140 °C.*

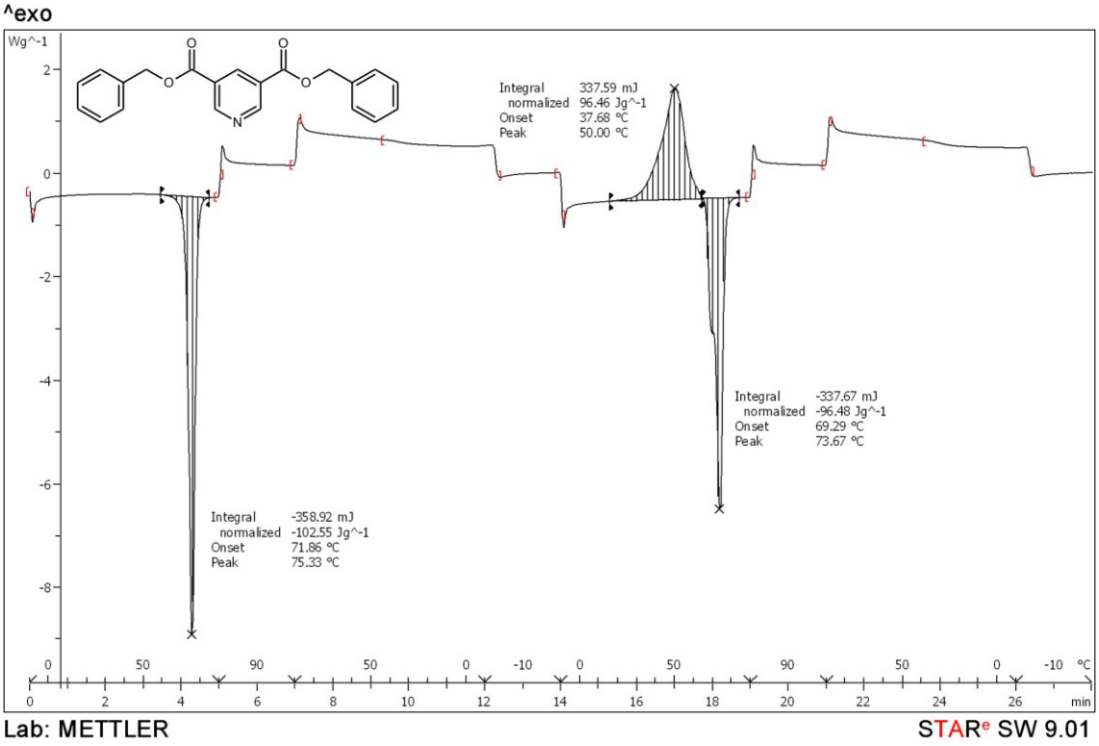

*Figure 119: DSC curve for bis(benzyl) 3,5-pyridinedicarboxyate (**45**); a 3.50 mg sample was heated and cooled at 20 °C min^{-1} between -10 and 90 °C.*

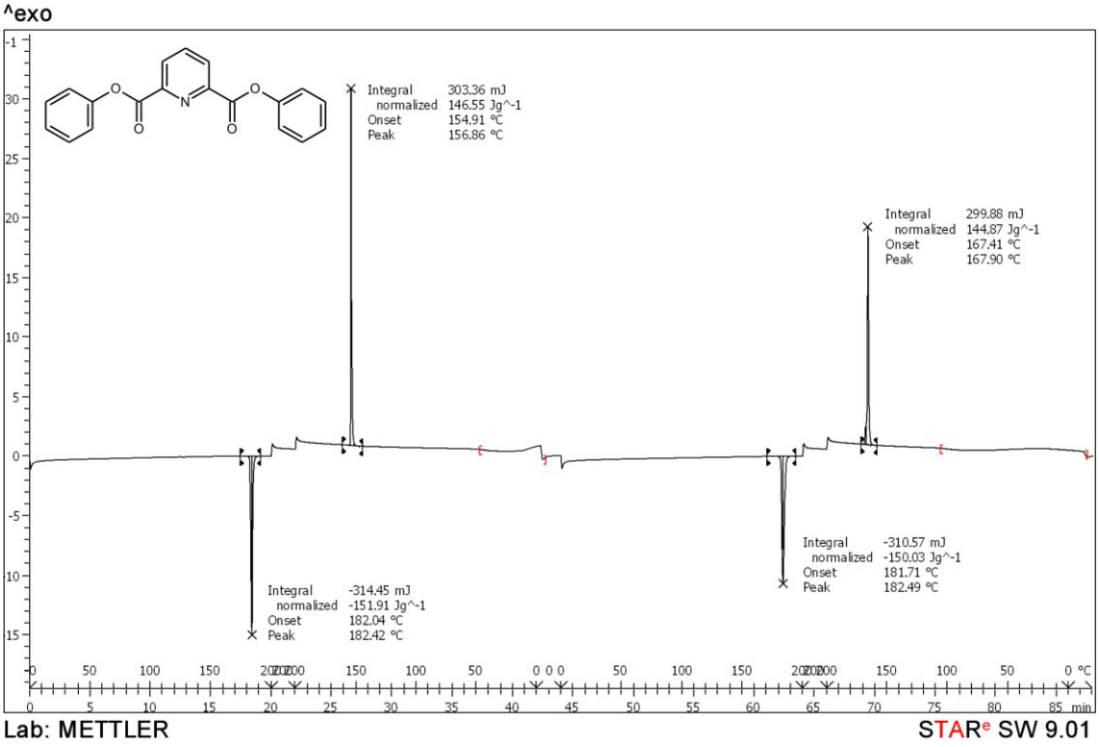

*Figure 120: DSC curve for bis(phenyl) 2,6-pyridinedicarboxylate (**46**); a 2.07 mg sample was heated and cooled at 10 °C min^{-1} between 0 and 200 °C.*

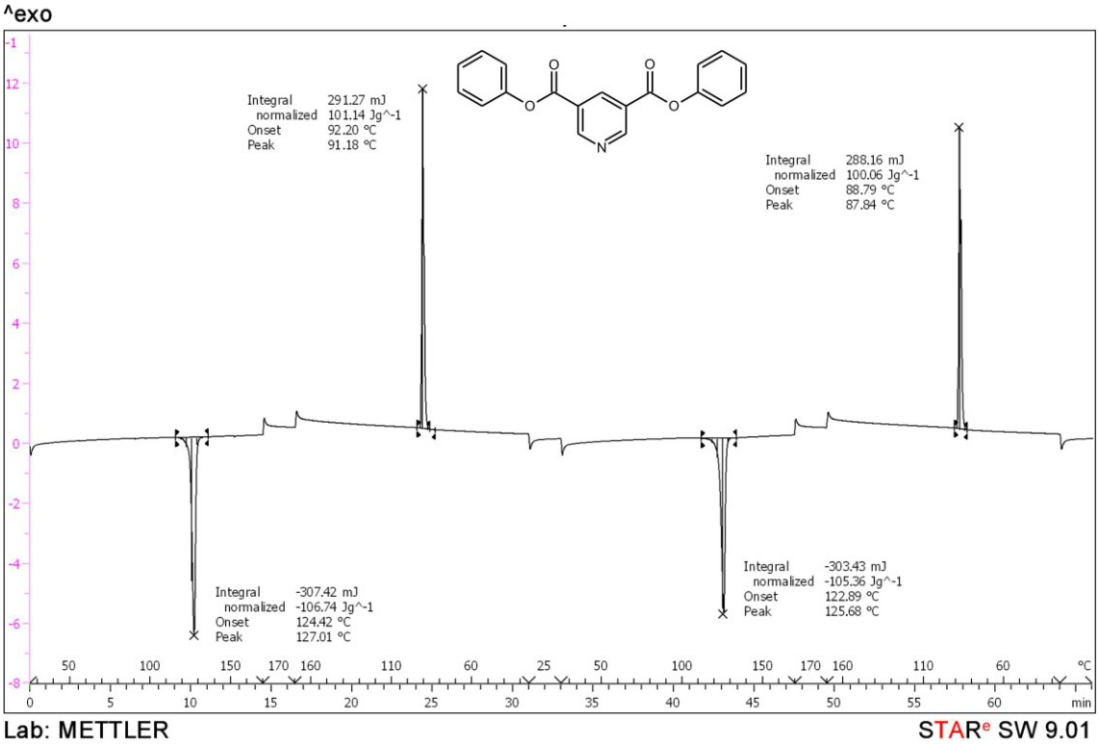

*Figure 121: DSC curve for bis(phenyl) 3,5-pyridinedicarboxylate (**47**); a 2.88 mg sample was heated and cooled at 10 °C min^{-1} between 25 and 170 °C.*

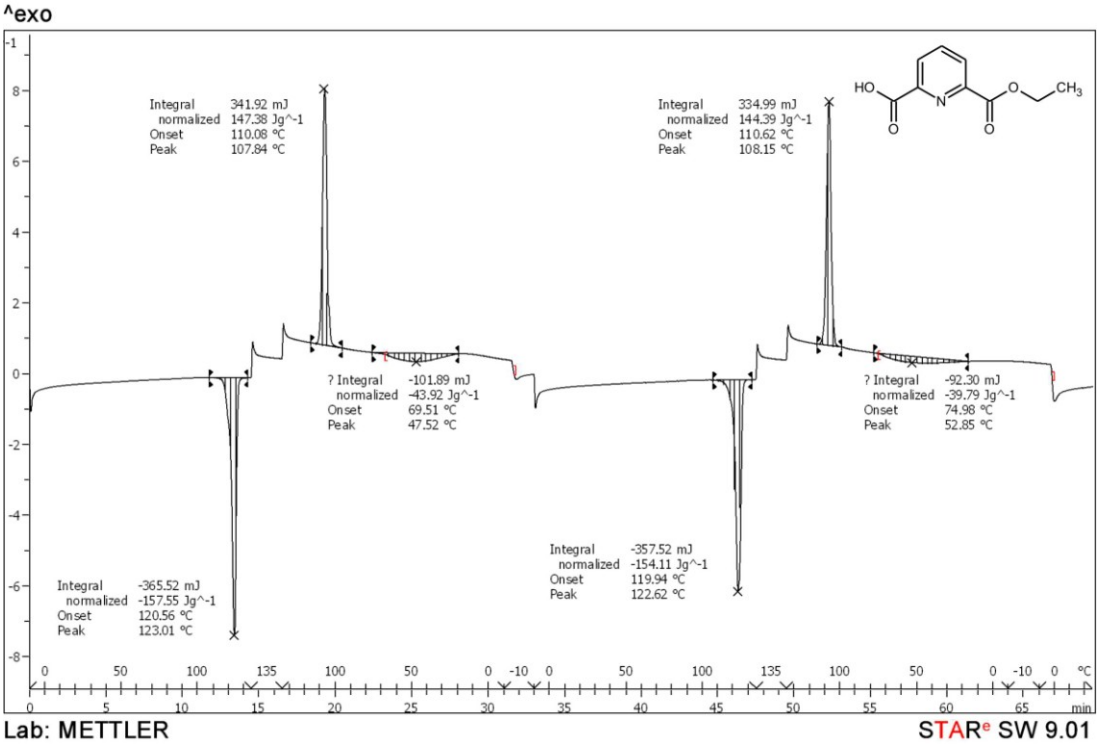

*Figure 122: DSC curve for 6-ethoxycarbonyl-2-pyridinecarboxylic acid (**76**); a 2.32 mg sample was heated and cooled at 10 °C min^{-1} between -10 and 135 °C.*

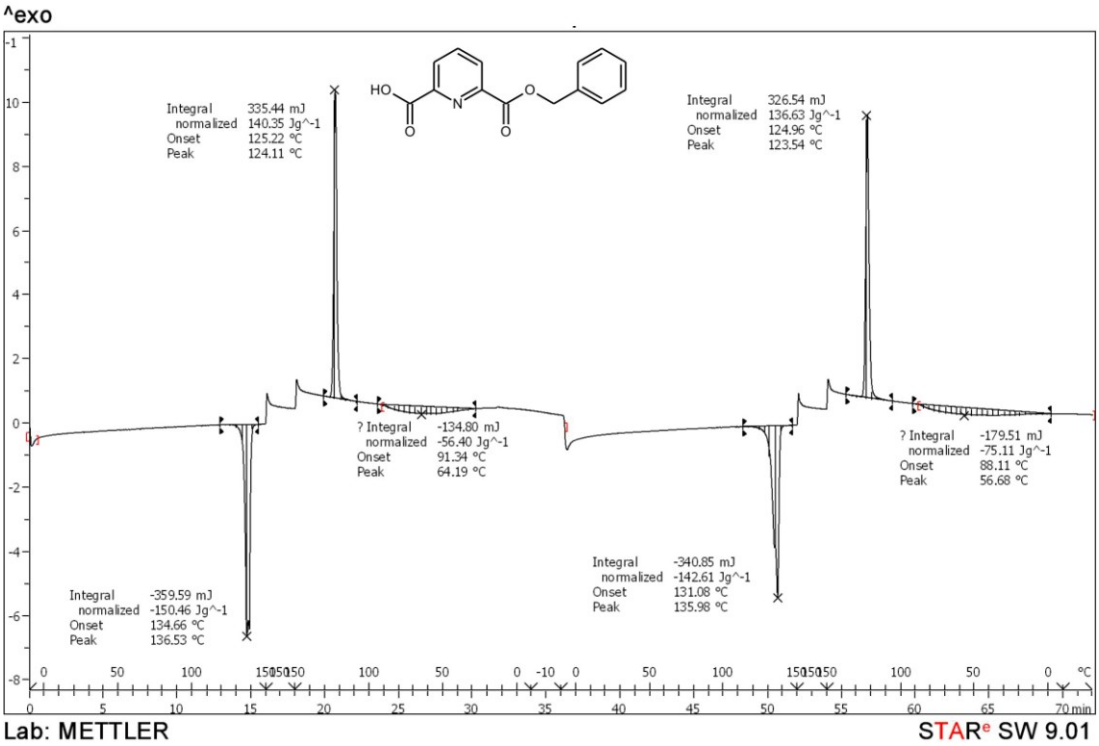

*Figure 123: DSC curve for 6-benzyloxycarbonyl-2-pyridinecarboxylic acid (**77**); a 2.39 mg sample was heated and cooled at 10 °C min^{-1} between -10 and 150 °C.*

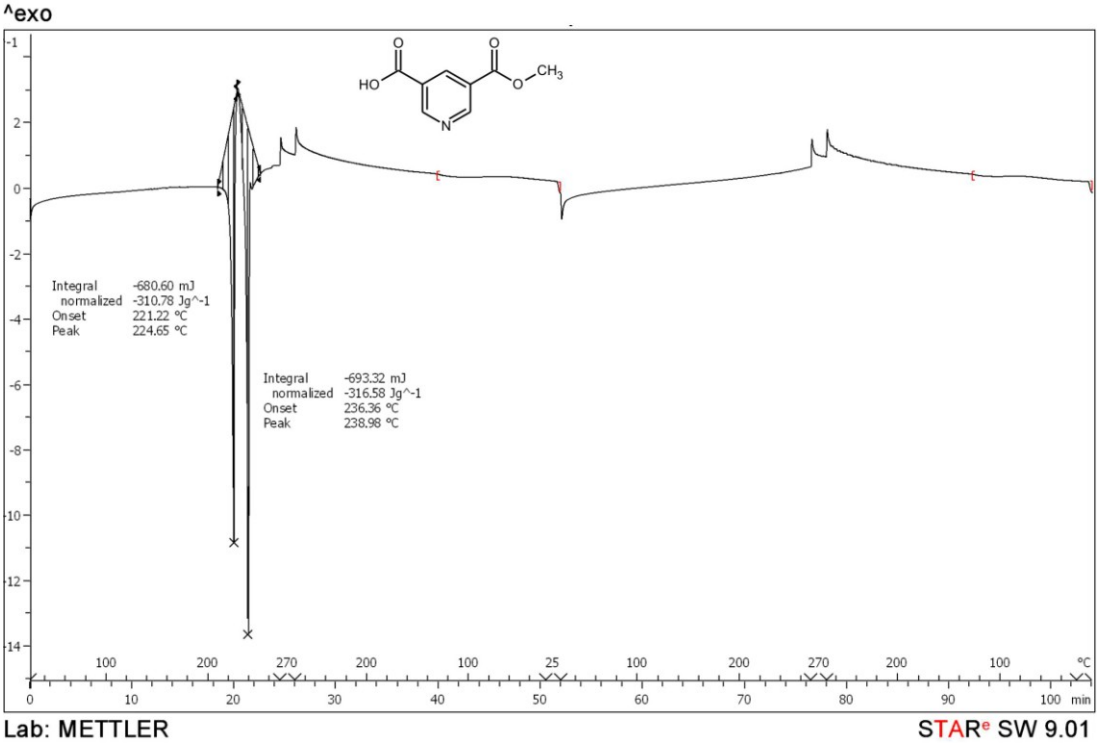

*Figure 124: DSC curve for 5-methoxycarbonyl-3-pyridinecarboxylic acid (**78**); a 2.19 mg sample was heated and cooled at 10 °C min^{-1} between 25 and 270 °C.*

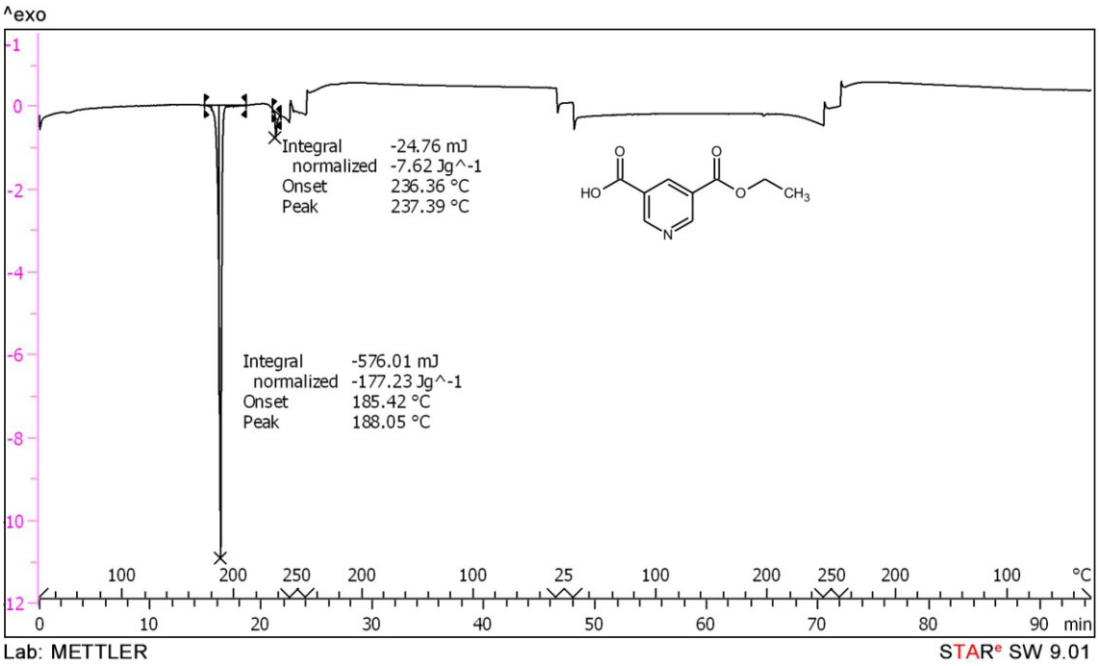

*Figure 125: DSC curve for 5-ethoxycarbonyl-3-pyridinecarboxylic acid (**79**); a 3.25 mg sample was heated and cooled at 10 °C min^{-1} between 25 and 250 °C.*

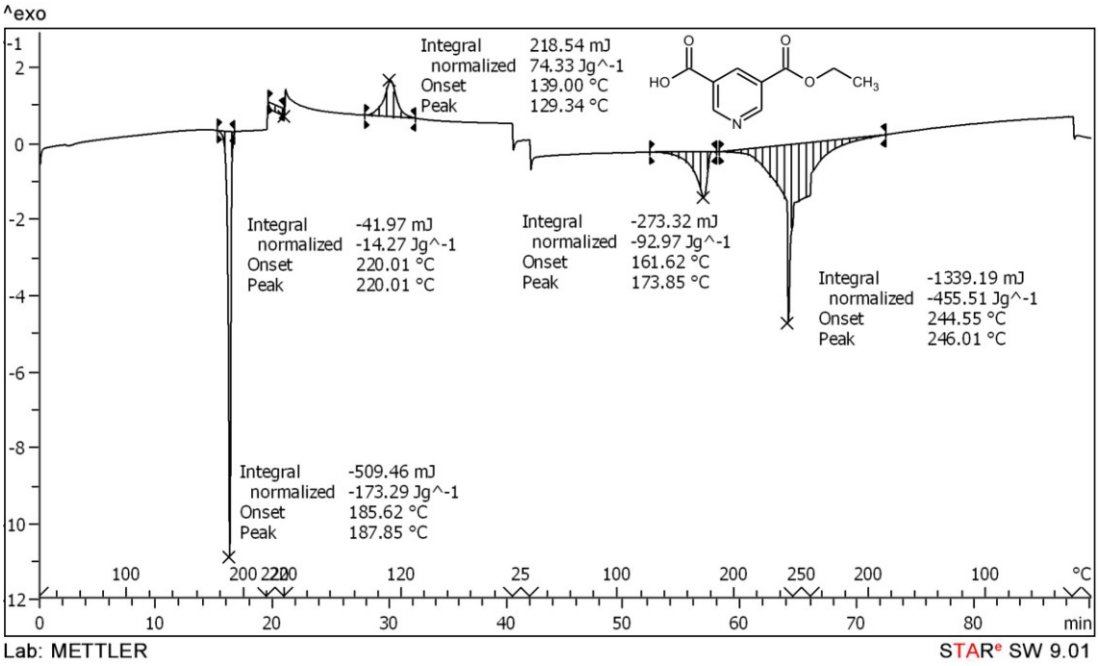

*Figure 126: DSC curve for 5-ethoxycarbonyl-3-pyridinecarboxylic acid (**79**); a 2.94 mg sample was heated and cooled at 10 °C min^{-1} between 25 and 220 °C for the first cycle, and between 25 and 250 °C for the second.*

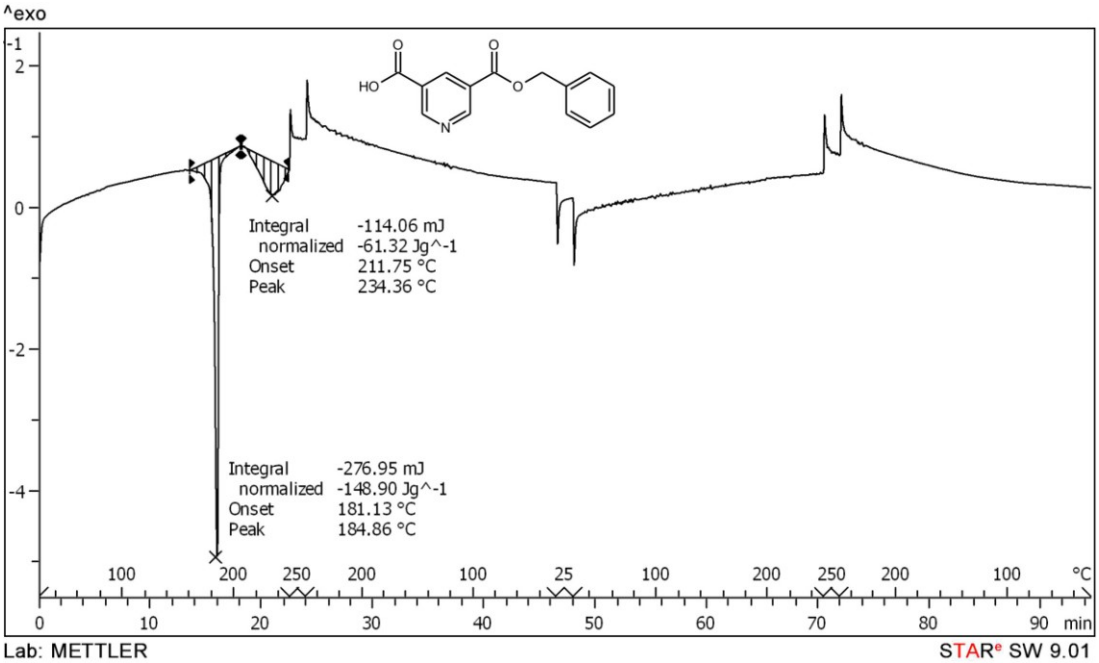

*Figure 127: DSC curve for 5-benzyloxycarbonyl-3-pyridinecarboxylic acid (**80**); a 1.86 mg sample was heated and cooled at 10 °C min^{-1} between 25 and 250 °C.*

Appendix D - Fingerprint plots

Fingerprint plots were determined using CrystalExplorer[107] and are given below for all of the crystal structures discussed in Chapters 2 - 7.

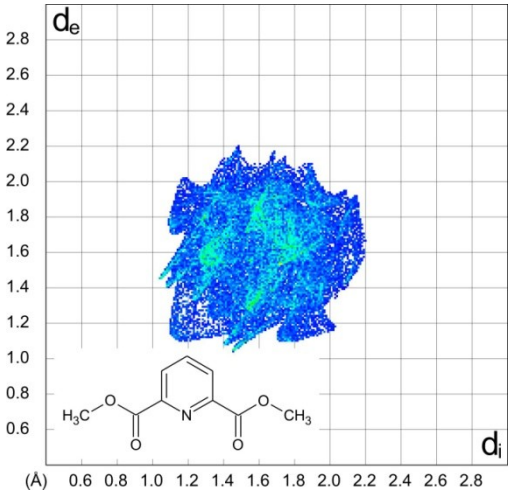

*Figure 128: Fingerprint plot for compound **38**.[92]*

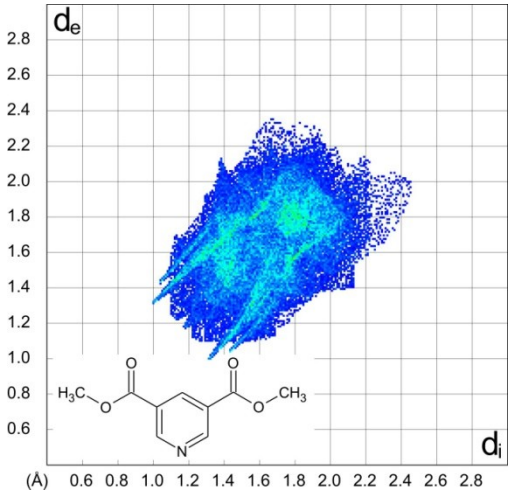

*Figure 129: Fingerprint plot for compound **39**.[91]*

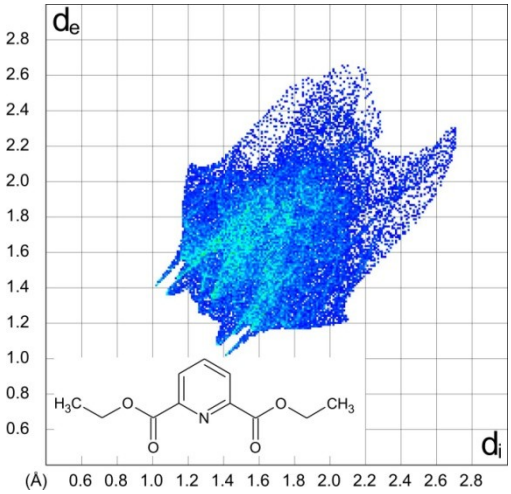

*Figure 130: Fingerprint plot for compound **40**.[91]*

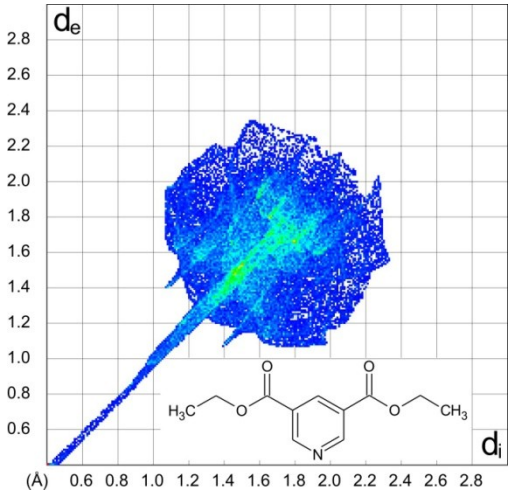

*Figure 131: Fingerprint plot for compound **41**.[91]*

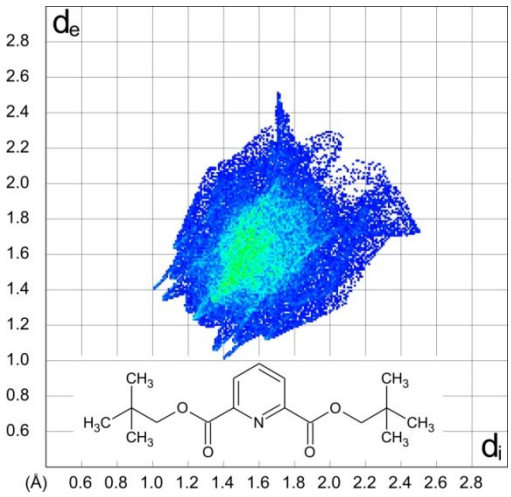

*Figure 132: Fingerprint plot for compound **42**.*[91]

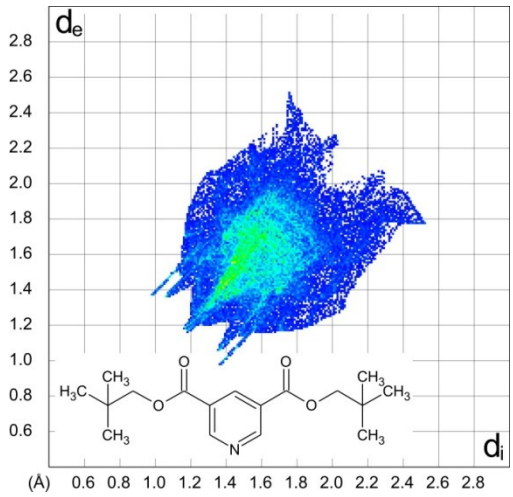

*Figure 133: Fingerprint plot for compound **43**.*[91]

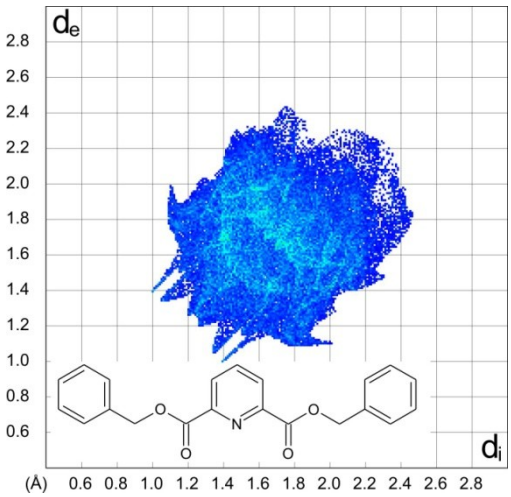

*Figure 134: Fingerprint plot for compound **44**.*[92]

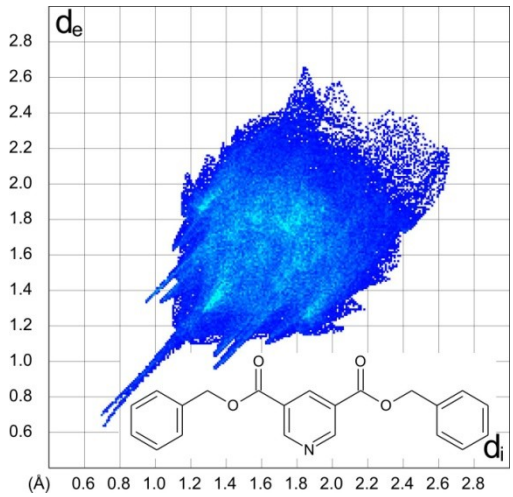

*Figure 135: Fingerprint plot for compound **45**.*[91]

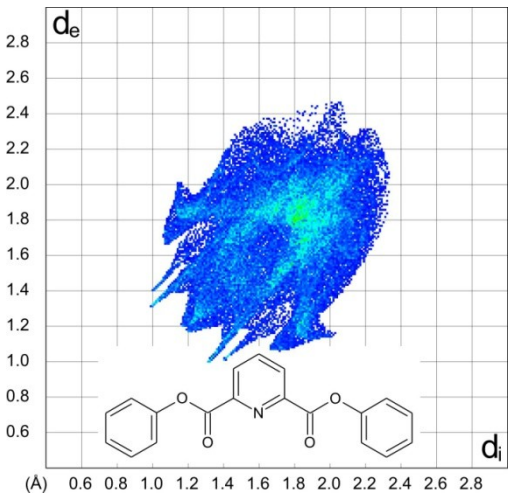

*Figure 136: Fingerprint plot for compound **46**.*

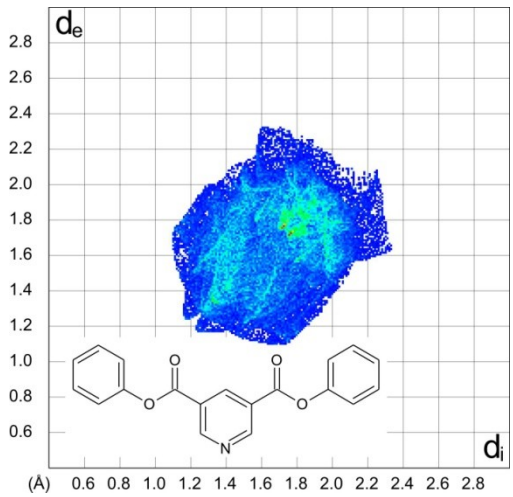

*Figure 137: Fingerprint plot for compound **47**.*

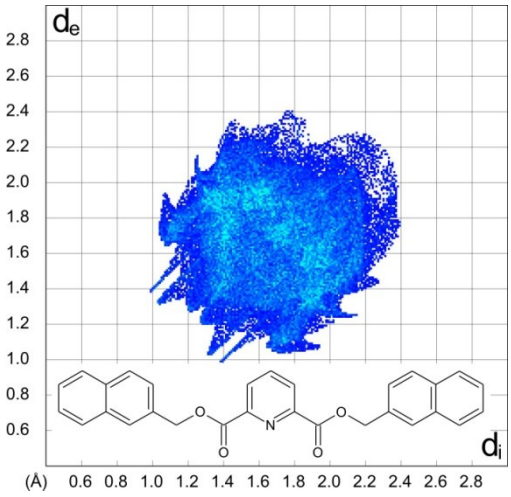

*Figure 138: Fingerprint plot for compound **49**.*

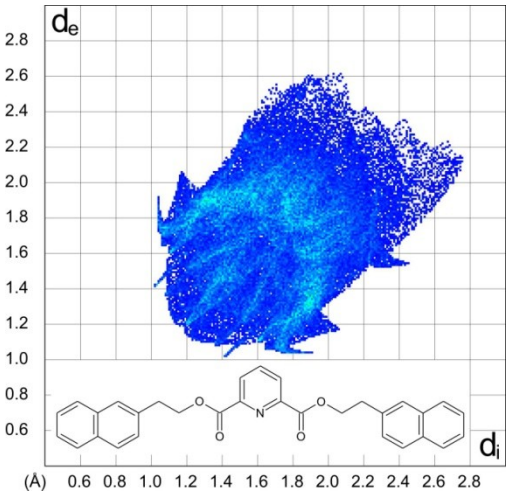

*Figure 139: Fingerprint plot for compound **50**.*

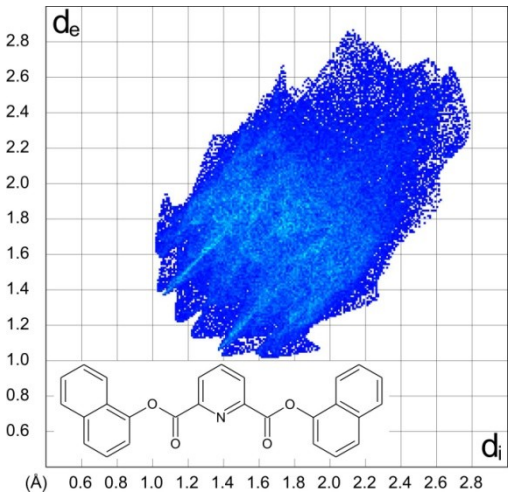

*Figure 140: Fingerprint plot for compound **51**.*

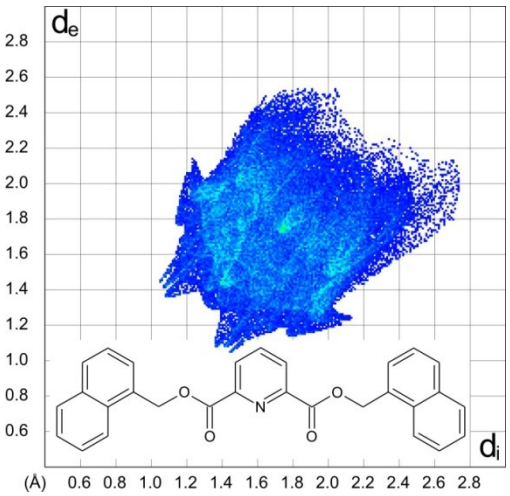

*Figure 141: Fingerprint plot for compound **52**.*

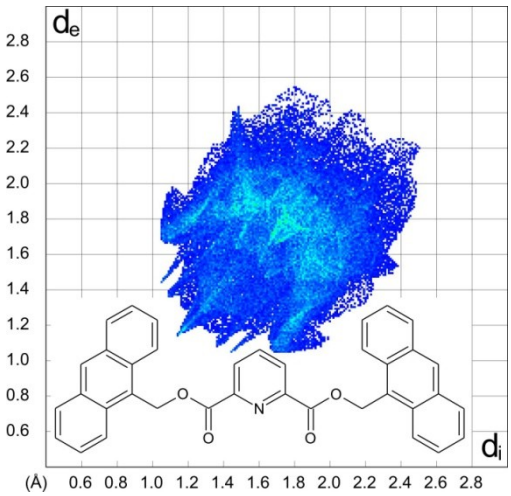

*Figure 142: Fingerprint plot for compound **53**.*

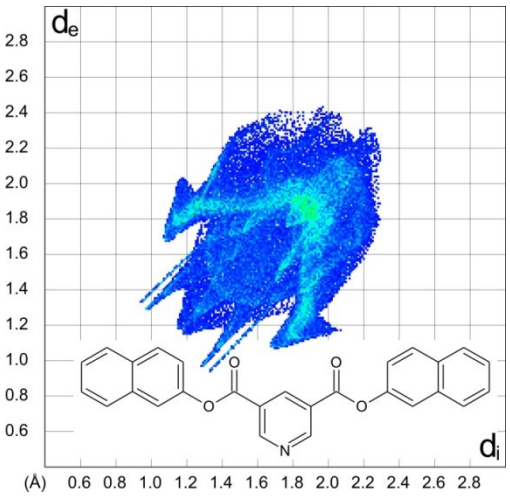

*Figure 143: Fingerprint plot for compound **54**.*

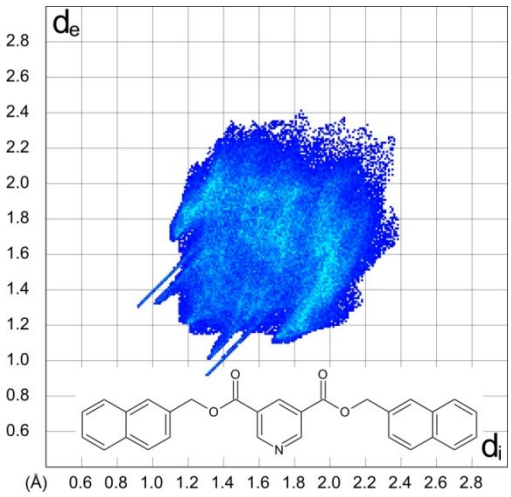

*Figure 144: Fingerprint plot for compound **55**.*

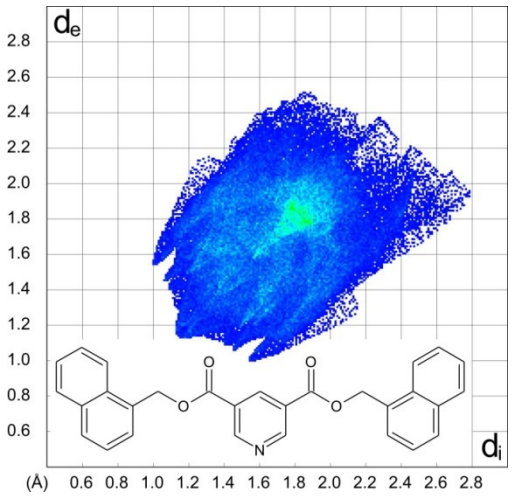

*Figure 145: Fingerprint plot for compound **58**.*

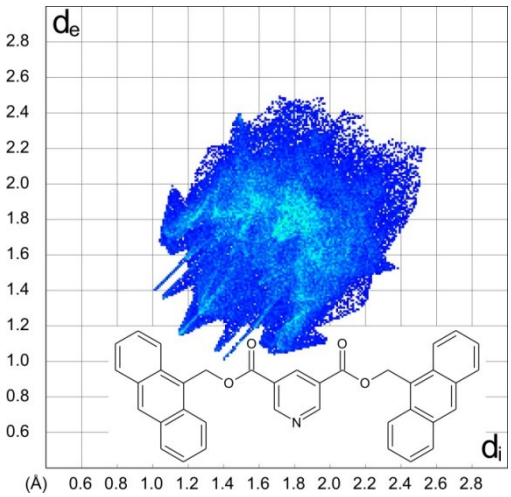

*Figure 146: Fingerprint plot for compound **59**.*

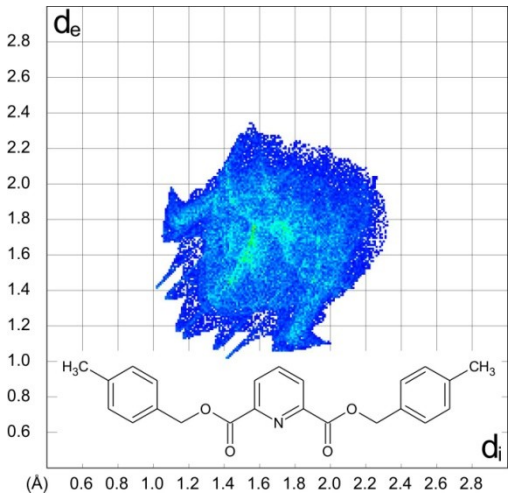

*Figure 147: Fingerprint plot for compound **60**.[95]*

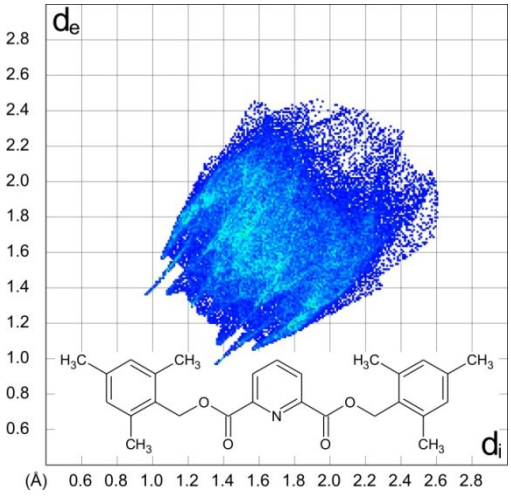

*Figure 148: Fingerprint plot for compound **61**.*

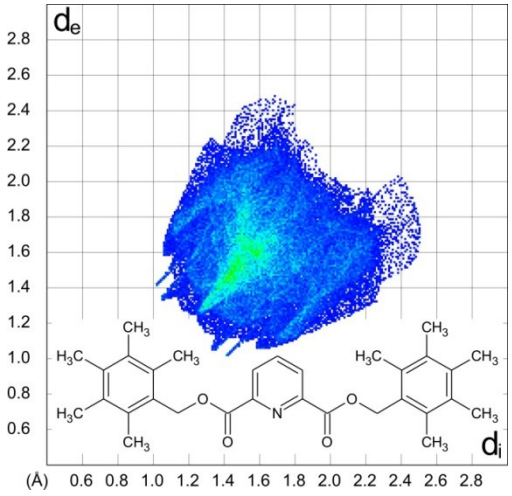

*Figure 149: Fingerprint plot for compound **62**.[91]*

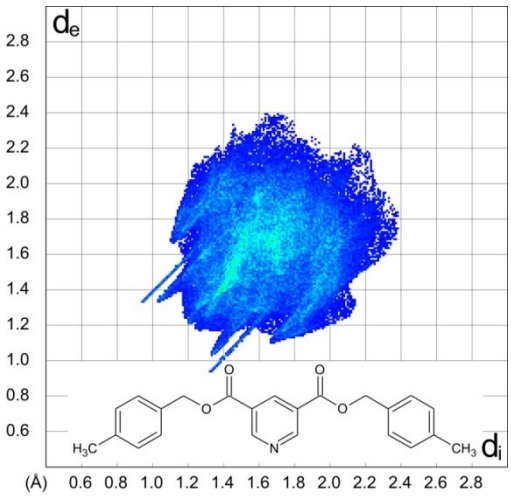

*Figure 150: Fingerprint plot for compound **63**.*[91]

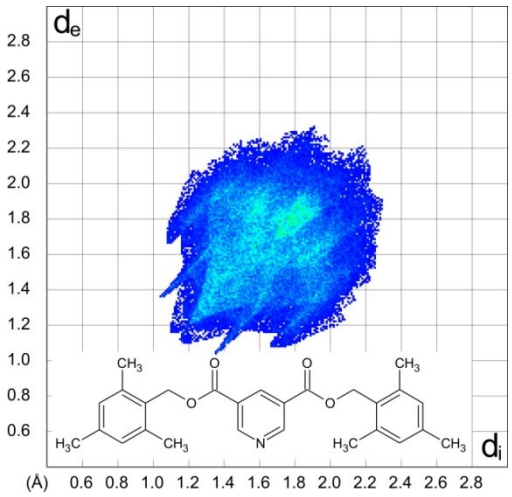

*Figure 151: Fingerprint plot for compound **64**.*

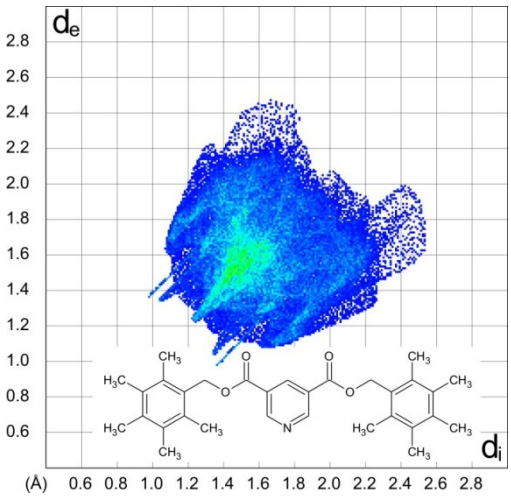

*Figure 152: Fingerprint plot for compound **65**.*[91]

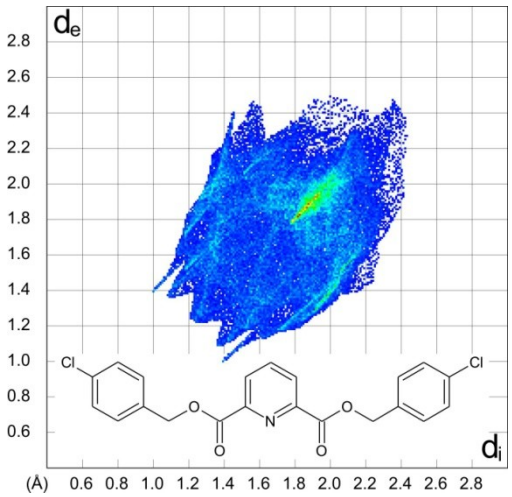

*Figure 153: Fingerprint plot for compound **66**.*[92]

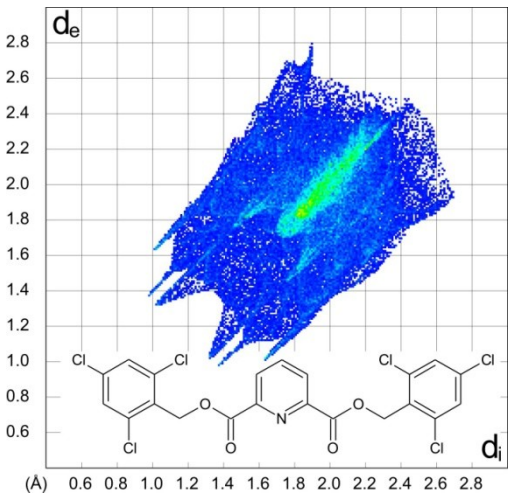

*Figure 154: Fingerprint plot for compound **67**.*

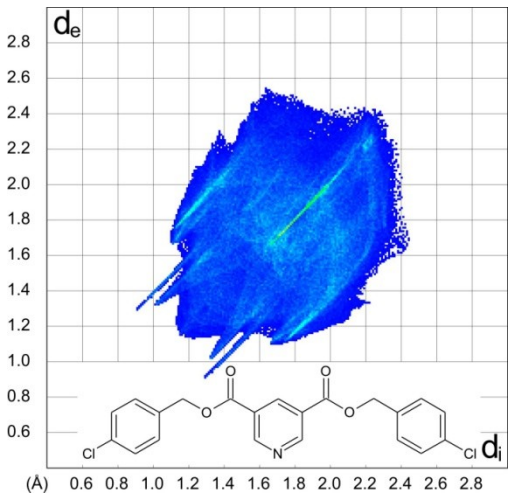

*Figure 155: Fingerprint plot for compound **68**.*[91]

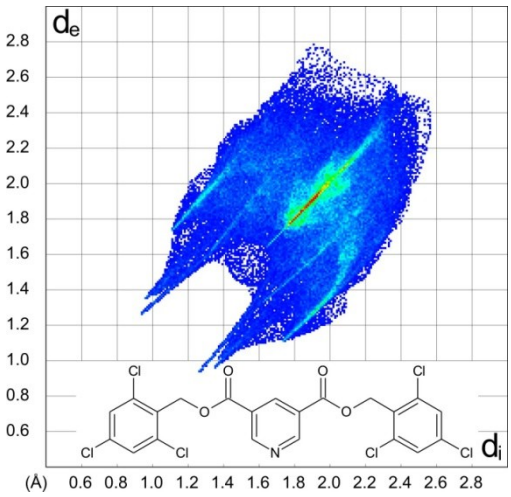

*Figure 156: Fingerprint plot for compound **69**.*

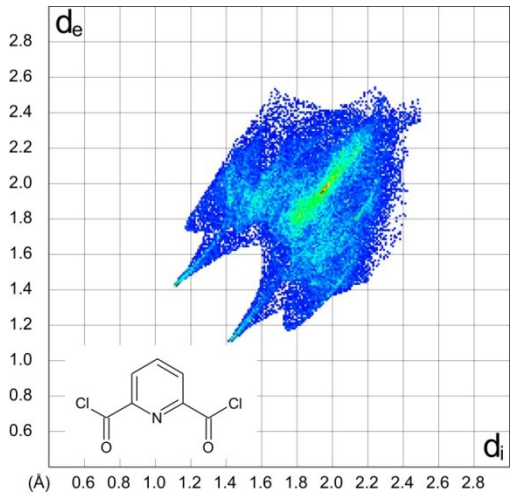

*Figure 157: Fingerprint plot for compound **70**.[113]*

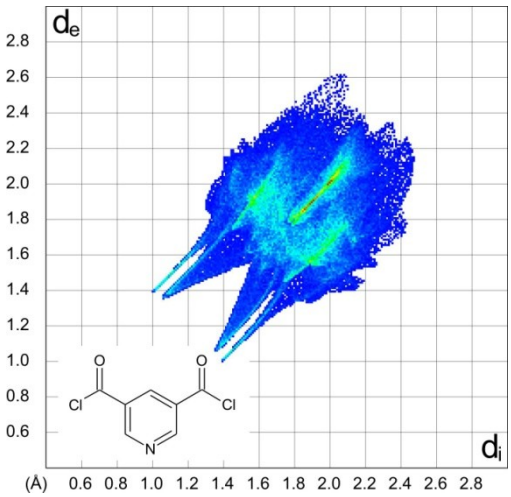

*Figure 158: Fingerprint plot for compound **71**.[113]*

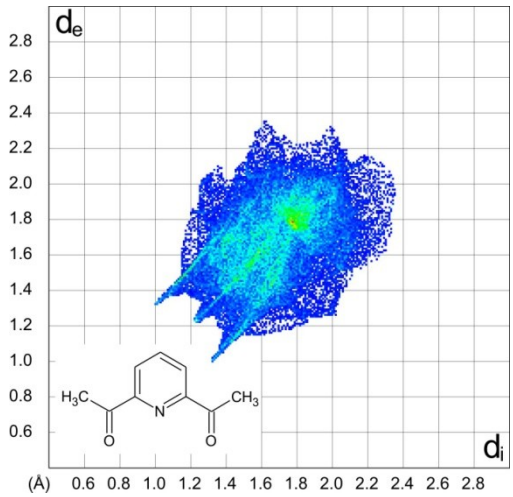

*Figure 159: Fingerprint plot for compound **72**.[114]*

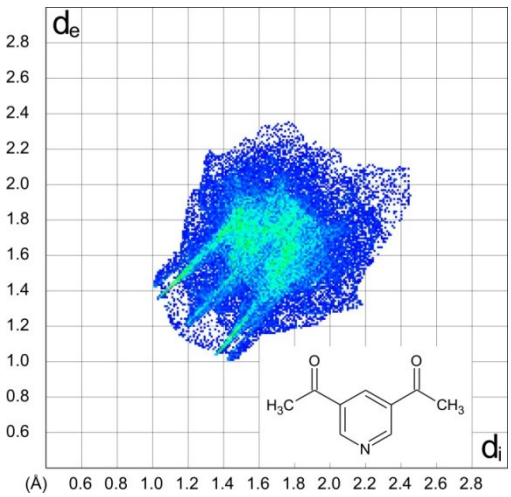

*Figure 160: Fingerprint plot for compound **73**.*

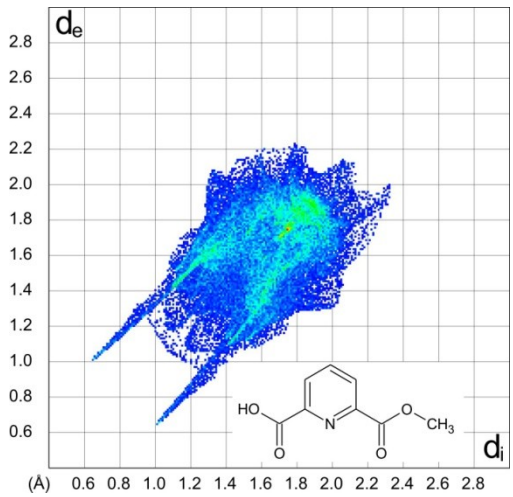

*Figure 161: Fingerprint plot for compound **75**.[94]*

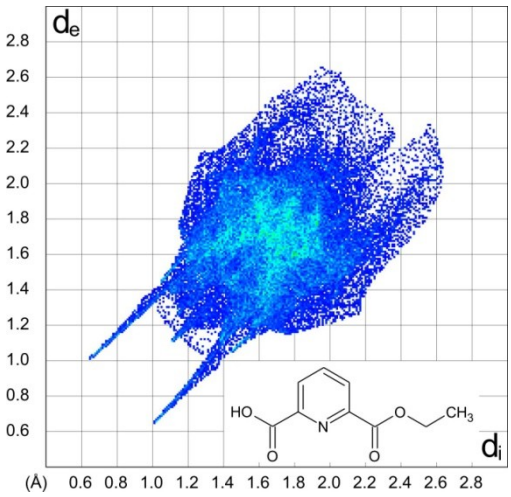

*Figure 162: Fingerprint plot for compound **76**.*

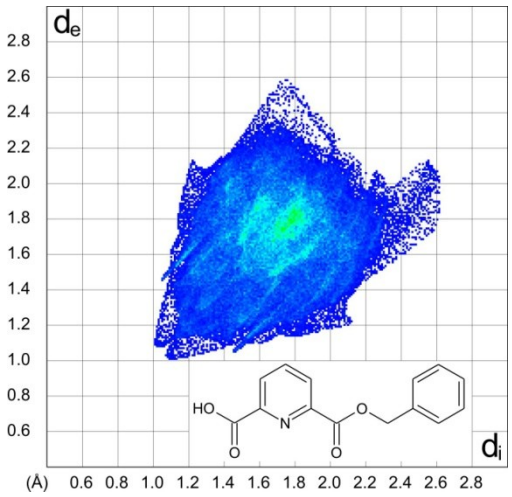

*Figure 163: Fingerprint plot for compound **77**.*

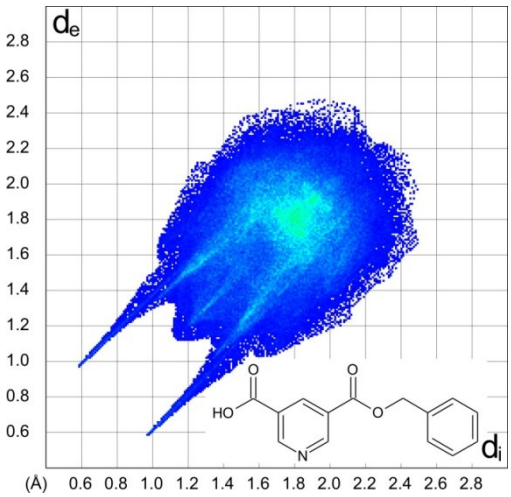

*Figure 164: Fingerprint plot for compound **80**.*

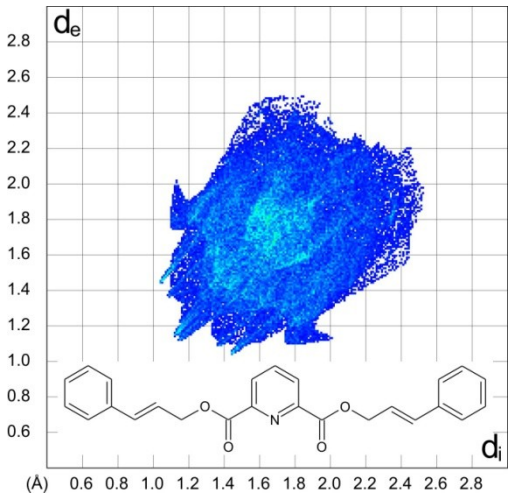

*Figure 165: Fingerprint plot for compound **81**.*

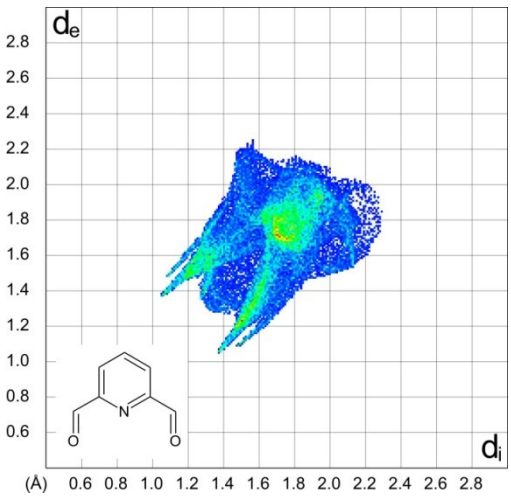

*Figure 166: Fingerprint plot for compound **90**.*

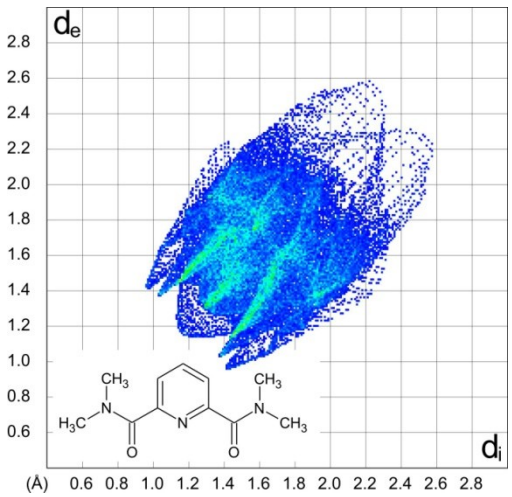

*Figure 167: Fingerprint plot for compound **92**.*

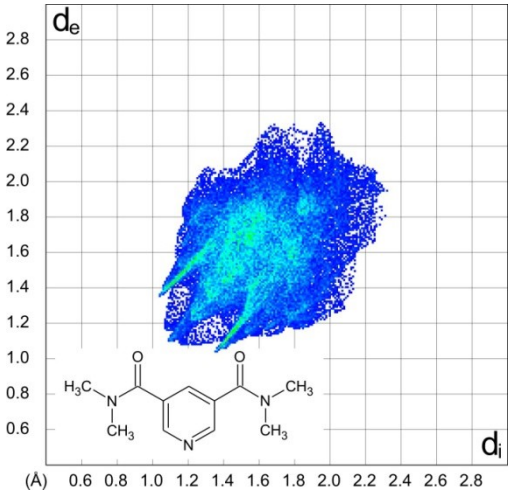

*Figure 168: Fingerprint plot for compound **93**.*

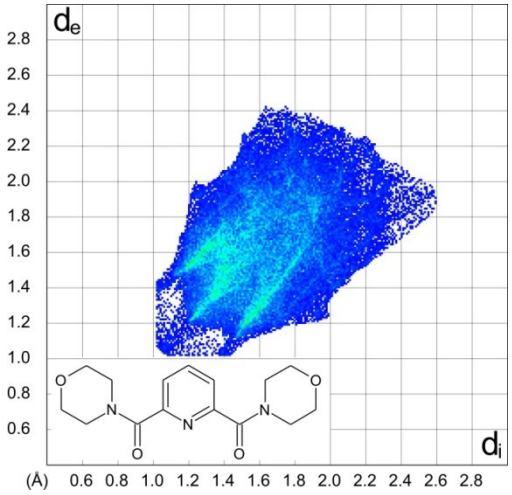

*Figure 169: Fingerprint plot for compound **94**.*

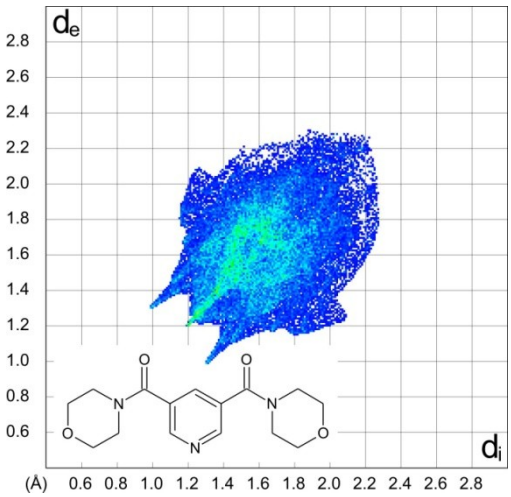

*Figure 170: Fingerprint plot for compound **95**.*

Appendix E - Structures of compounds discussed in Chapters 2 - 7

Chapter 2

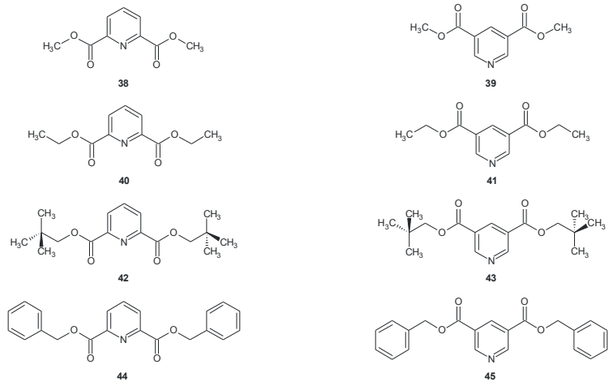

Chapter 3

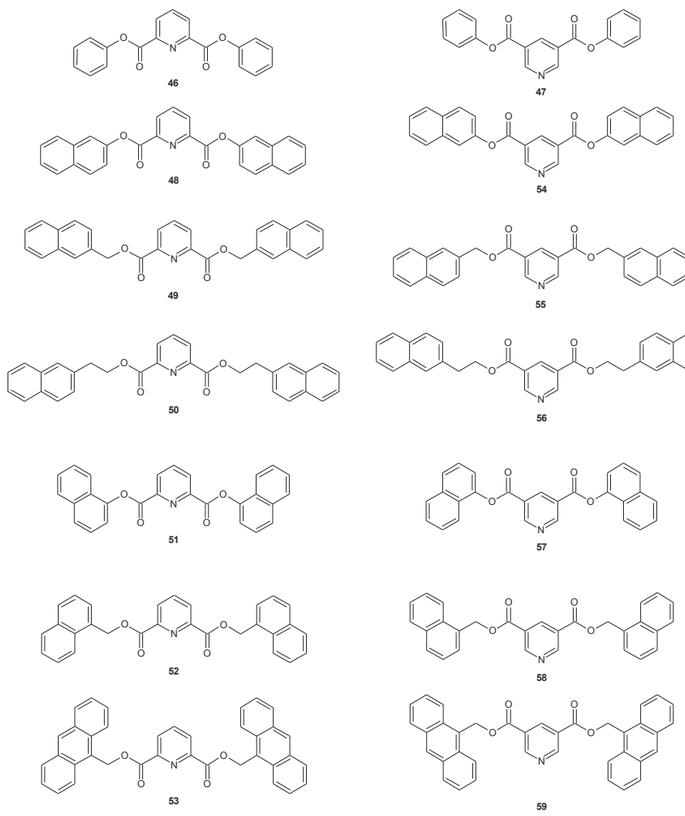

Chapter 4

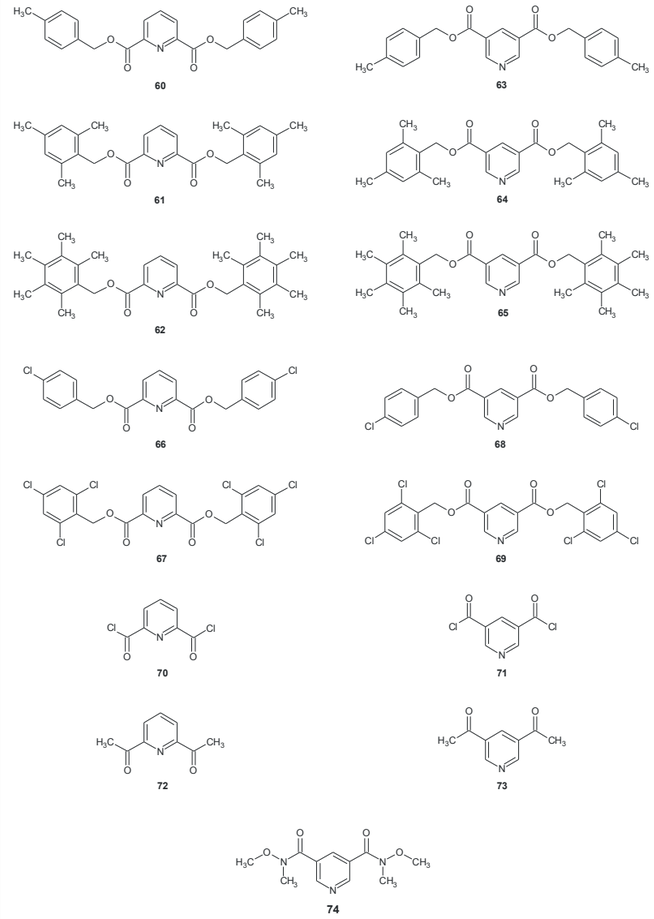

Chapter 5

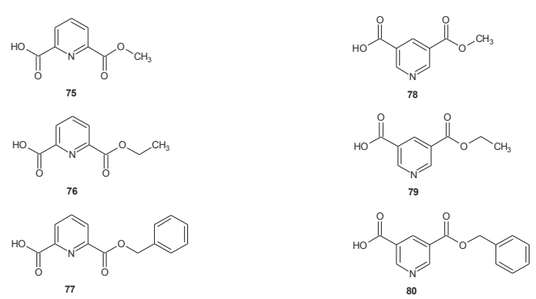

Chapter 6

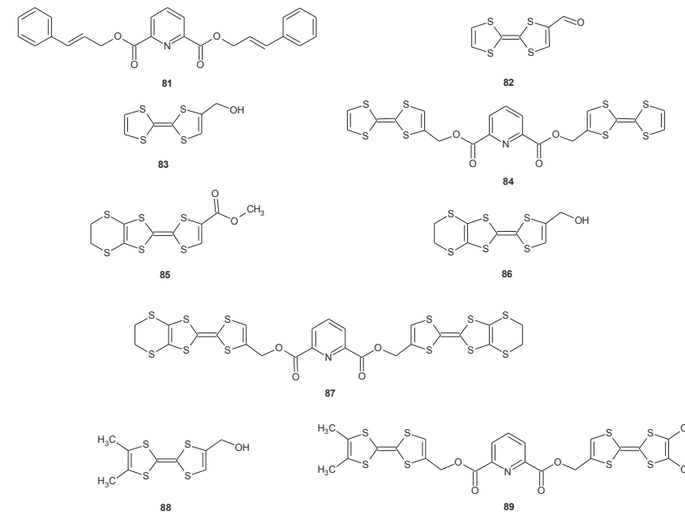

Chapter 7

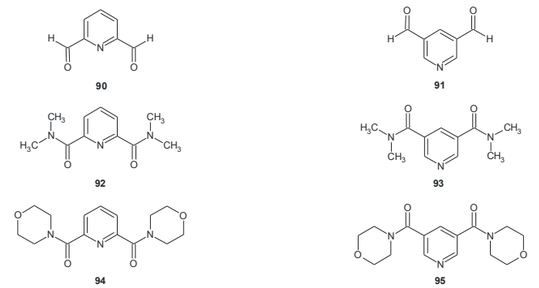

Distances & angles used in the definition of tape-like assemblies

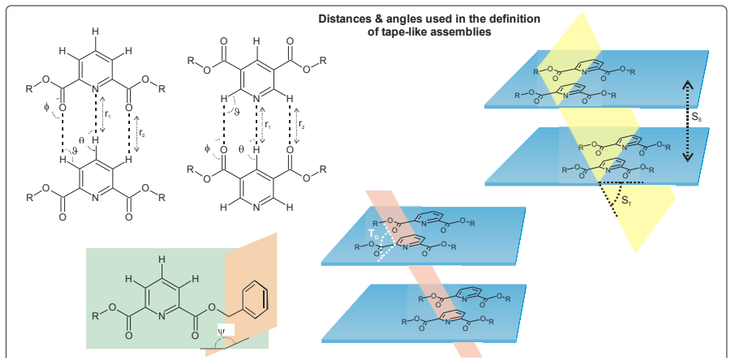

References

1. J. M. Lehn, *Angew. Chem., Int. Ed. Engl.*, 1988, **27**, 89-112.
2. C. J. Pedersen, *Angew. Chem., Int. Ed. Engl.*, 1988, **27**, 1021-1027.
3. J. M. Spruell, W. F. Paxton, J.-C. Olsen, D. Benítez, E. Tkatchouk, C. L. Stern, A. Trabolsi, D. C. Friedman, W. A. Goddard and J. F. Stoddart, *J. Am. Chem. Soc.*, 2009, **131**, 11571-11580.
4. A. P. de Silva and S. Uchiyama, *Nat Nano*, 2007, **2**, 399-410.
5. H.-J. Kim, E. Lee, H.-s. Park and M. Lee, *J. Am. Chem. Soc.*, 2007, **129**, 10994-10995.
6. K. Yoosaf, A. Belbakra, N. Armaroli, A. Llanes-Pallas and D. Bonifazi, *Chem. Commun.*, 2009, 2830-2832.
7. L. R. MacGillivray, *J. Org. Chem.*, 2008, **73**, 3311-3317.
8. X. Li, I. S. Nandhakumar, G. S. Attard, M. L. Markham, D. C. Smith and J. J. Baumberg, *Microporous and Mesoporous Materials*, 2009, **118**, 403-407.
9. M. C. Branco and J. P. Schneider, *Acta Biomater.*, 2009, **5**, 817-831.
10. E. Fischer, *Ber. Dtsch. Chem. Ges.*, 1894, **27**, 2984–2993.
11. J. D. Dunitz, in *The Crystal as a Supramolecular Entity*, Ed. G. R. Desiraju, John Wiley & Sons Ltd., Chichester, Editon edn., 1996, pp. 1 - 30.
12. G. M. J. Schmidt, *Pure Appl. Chem.*, 1971, **27**, 647-678.
13. G. R. Desiraju, *Chem. Commun.*, 1997, 1475-1482.
14. G. R. Desiraju, *Angew. Chem., Int. Ed. Engl.*, 2007, **46**, 8342-8356.
15. G. R. Desiraju, *Crystal Engineering. The Design of Organic Solids.*, Elsevier, 1989.
16. E. Fan, C. Vicent, S. J. Geib and A. D. Hamilton, *Chem. Mat.*, 1994, **6**, 1113-1117.
17. D. B. Amabilino, J. F. Stoddart and D. J. Williams, *Chem. Mat.*, 1994, **6**, 1159-1167.
18. S. J. Cantrill, K. S. Chichak, A. J. Peters and J. F. Stoddart, *Accounts Chem. Res.*, 2005, **38**, 1-9.
19. G. R. Desiraju and C. V. K. Sharma, in *The Crystal as a Supramolecular Entity*, Ed. G. R. Desiraju, John Wiley & Sons Ltd., Chichester, Editon edn., 1996, pp. 31 - 61.
20. C. A. Hunter, *Angew. Chem., Int. Ed. Engl.*, 2004, **43**, 5310-5324.
21. C. B. Aakeröy and K. R. Seddon, *Chem. Soc. Rev.*, 1993, **22**, 397-407.
22. T. Steiner and W. Saenger, *J. Am. Chem. Soc.*, 1993, **115**, 4540-4547.
23. T. Steiner, *Angew. Chem., Int. Ed. Engl.*, 2002, **41**, 48-76.
24. G. C. Pimentel and A. L. McClellan, *The hydrogen bond*, W. H. Freeman, San Francisco, 1960.
25. G. A. Jeffrey, *An Introduction to Hydrogen Bonding*, Oxford University Press, Oxford, 1997.
26. M. C. Grossel, D. A. S. Merckel and M. G. Hutchings, *Cryst. Eng. Comm.*, 2003, 77-81.
27. M. Kaftory, M. Kapon and M. Botoshanksy, *Chem. Mat.*, 1994, **6**, 1245-1249.

28. J. H. Loehlin, M. C. Etter, C. Gendreau and E. Cervasio, *Chem. Mat.*, 1994, **6**, 1218-1221.
29. L. M. Toledo, J. W. Lauher and F. W. Fowler, *Chem. Mat.*, 1994, **6**, 1222-1226.
30. J. A. Zerkowski, J. C. Macdonald and G. M. Whitesides, *Chem. Mat.*, 1994, **6**, 1250-1257.
31. L. Orola and M. V. Veidis, *Cryst. Eng. Comm.*, 2009, **11**, 415-417.
32. C. Avendaño and A. Briceño, *Cryst. Eng. Comm.*, 2009, **11**, 408-411.
33. M. Nishio, Y. Umezawa, K. Honda, S. Tsuboyama and H. Suezawa, *Cryst. Eng. Comm*, 2009, **11**, 1757-1788.
34. G. R. Desiraju, *Accounts Chem. Res.*, 1991, **24**, 290-296.
35. T. Steiner and G. R. Desiraju, *Chem. Commun.*, 1998, 891-892.
36. C. Janiak and T. G. Scharmann, *Polyhedron*, 2003, **22**, 1123-1133.
37. C. Gatti, E. May, R. Destro and F. Cargnoni, *J. Phys. Chem. A*, 2002, **106**, 2707-2720.
38. C. Schmuck and J. Lex, *Eur. J. Org. Chem.*, 2001, 1519-1523.
39. P. K. Thallapally and A. Nangia, *Cryst. Eng. Comm.*, 2001, 114-119.
40. M. Nishio, Y. Umezawa, M. Hirota and Y. Takeuchi, *Tetrahedron*, 1995, **51**, 8665-8701.
41. S. K. Burley and G. A. Petsko, *J. Am. Chem. Soc.*, 1986, **108**, 7995-8001.
42. C. A. Hunter and J. K. M. Sanders, *J. Am. Chem. Soc.*, 1990, **112**, 5525-5534.
43. F. Cozzi, M. Cinquini, R. Annunziata, T. Dwyer and J. S. Siegel, *J. Am. Chem. Soc.*, 1992, **114**, 5729-5733.
44. C. V. K. Sharma, K. Panneerselvam, L. Shimoni, H. Katz, H. L. Carrell and G. R. Desiraju, *Chem. Mat.*, 1994, **6**, 1282-1292.
45. Y. C. Chang, Y. D. Chen, C. H. Chen, Y. S. Wen, J. T. Lin, H. Y. Chen, M. Y. Kuo and I. Chao, *J. Org. Chem.*, 2008, **73**, 4608-4614.
46. J. M. Serrano-Becerra, S. Hernandez-Ortega, D. Morales-Morales and J. Valdes-Martinez, *Cryst. Eng. Comm.*, 2009, **11**, 226-228.
47. G. R. Desiraju and A. Gavezzotti, *Acta Crystallogr. Sect. B: Struct. Sci.*, 1989, **45**, 473-482.
48. S. Grimme, *Angew. Chem., Int. Ed. Engl.*, 2008, **47**, 3430-3434.
49. A. Sygula, F. R. Fronczek, R. Sygula, P. W. Rabideau and M. M. Olmstead, *J. Am. Chem. Soc.*, 2007, **129**, 3842-3843.
50. M. C. Grossel, A. K. Cheetham, D. A. O. Hope, K. P. Lam and M. J. Perkins, *Tetrahedron Lett.*, 1979, 1351-1354.
51. M. C. Grossel, A. K. Cheetham, D. A. O. Hope and S. C. Weston, *J. Org. Chem.*, 1993, **58**, 6654-6661.
52. S. Paliwal, S. Geib and C. S. Wilcox, *J. Am. Chem. Soc.*, 1994, **116**, 4497-4498.
53. K. M. Sureshan, T. Uchimaru, Y. H. Yao and Y. Watanabe, *Cryst. Eng. Comm.*, 2008, **10**, 493-496.
54. O. Takahashi, Y. Kohno, S. Iwasaki, K. Saito, M. Iwaoka, S. Tomoda, Y. Umezawa, S. Tsuboyama and M. Nishio, *Bull. Chem. Soc. Jpn.*, 2001, **74**, 2421-2430.
55. H. Suezawa, T. Yoshida, Y. Umezawa, S. Tsuboyama and M. Nishio, *Eur. J. Inorg. Chem.*, 2002, 3148-3155.
56. A. Bondi, *J. Phys. Chem.*, 1964, **68**, 441-451.

57. P. Ganguly and G. R. Desiraju, *Chem. Asian J.*, 2008, **3**, 868-880.
58. P. Metrangolo, H. Neukirch, T. Pilati and G. Resnati, *Accounts Chem. Res.*, 2005, **38**, 386-395.
59. A. R. Voth, P. Khuu, K. Oishi and P. S. Ho, *Nat. Chem.*, 2009, **1**, 74-79.
60. P. Metrangolo, F. Meyer, T. Pilati, G. Resnati and G. Terraneo, *Angew. Chem., Int. Ed. Engl.*, 2008, **47**, 6114-6127.
61. S. C. Nyburg and C. H. Faerman, *Acta Crystallogr. Sect. B: Struct. Sci.*, 1985, **41**, 274-279.
62. T. Clark, M. Hennemann, J. S. Murray and P. Politzer, *J. Mol. Model.*, 2007, **13**, 291-296.
63. P. Metrangolo and G. Resnati, *Chem. Eur. J.*, 2001, **7**, 2511-2519.
64. N. Ramasubbu, R. Parthasarathy and P. Murray-Rust, *J. Am. Chem. Soc.*, 1986, **108**, 4308-4314.
65. K. Rissanen, *Cryst. Eng. Comm.*, 2008, **10**, 1107-1113.
66. P. Metrangolo and G. Resnati, *Science*, 2008, **321**, 918-919.
67. A. R. Voth, F. A. Hays and P. S. Ho, *Proc. Natl. Acad. Sci. U.S.A.*, 2007, **104**, 6188-6193.
68. V. R. Thalladi, H. C. Weiss, R. Boese, A. Nangia and G. R. Desiraju, *Acta Crystallogr. Sect. B: Struct. Sci.*, 1999, **55**, 1005-1013.
69. R. Liantonio, P. Metrangolo, F. Meyer, T. Pilati, W. Navarrini and G. Resnati, *Chem. Commun.*, 2006, 1819-1821.
70. J. Sarma, F. H. Allen, V. J. Hoy, J. A. K. Howard, R. Thaimattam, K. Biradha and G. R. Desiraju, *Chem. Commun.*, 1997, 101-102.
71. V. R. Pedireddi, D. S. Reddy, B. S. Goud, D. C. Craig, A. D. Rae and G. R. Desiraju, *J. Chem. Soc., Perkin Trans. 2*, 1994, 2353-2360.
72. S. L. Price, A. J. Stone, J. Lucas, R. S. Rowland and A. E. Thornley, *J. Am. Chem. Soc.*, 1994, **116**, 4910-4918.
73. G. R. Desiraju and J. Sarma, *Proc. Indian Acad. Sci. (Chem. Sci.)*, 1986, **96**, 599-605.
74. I. Csöregh, T. Brehmer, P. Bombicz and E. Weber, *Crystal Engineering*, 2001, **4**, 343-357.
75. O. Guvench and A. D. MacKerell Jr, *Curr. Opin. Struct. Biol.*, 2009, **19**, 56-61.
76. L. Y. Han, H. H. Lin, Z. R. Li, C. J. Zheng, Z. W. Cao, B. Xie and Y. Z. Chen, *Journal of Chemical Information and Modeling*, 2005, **46**, 445-450.
77. M. C. Etter, *Accounts Chem. Res.*, 1990, **23**, 120-126.
78. C. B. Aakeroy, J. Desper and M. M. Smith, *Chem. Commun.*, 2007, 3936-3938.
79. B. K. Saha, A. Nangia and M. Jaskolski, *Cryst. Eng. Comm*, 2005, **7**, 355-358.
80. C. B. Aakeroy, M. Fasulo, N. Schultheiss, J. Desper and C. Moore, *J. Am. Chem. Soc.*, 2007, **129**, 13772-13773.
81. R. E. Davis, J. K. Whitesell, M. Wong and N. Chang, in *The Crystal as a Supramolecular Entity*, Ed. G. R. Desiraju, John Wiley & Sons Ltd., Chichester, Editon edn., 1996, pp. 63 - 106.
82. D. Das, R. K. R. Jetti, R. Boese and G. R. Desiraju, *Cryst. Growth Des.*, 2003, **3**, 675-681.

83. N.-F. She, M. Gao, X.-G. Meng, G.-F. Yang, J. A. A. W. Elemans, A.-X. Wu and L. Isaacs, *J. Am. Chem. Soc.*, 2009, **131**, 11695-11697.
84. J. D. Wuest, *Chem. Commun.*, 2005, 5830-5837.
85. J.-H. Fournier, T. Maris and J. D. Wuest, *J. Org. Chem.*, 2003, **69**, 1762-1775.
86. J. M. Lehn, M. Mascal, A. Decian and J. Fischer, *J. Chem. Soc., Perkin Trans. 2*, 1992, 461-467.
87. J. A. Zerkowski, C. T. Seto, D. A. Wierda and G. M. Whitesides, *J. Am. Chem. Soc.*, 1990, **112**, 9025-9026.
88. P. Vishweshwar, A. Nangia and V. M. Lynch, *J. Org. Chem.*, 2001, **67**, 556-565.
89. R. P. Sijbesma, F. H. Beijer, L. Brunsveld, B. J. B. Folmer, J. Hirschberg, R. F. M. Lange, J. K. L. Lowe and E. W. Meijer, *Science*, 1997, **278**, 1601-1604.
90. M. C. Grossel, C. A. Golden, J. R. Gomm, P. N. Horton, D. A. S. Merckel, M. E. Oszer and R. A. Parker, *Cryst. Eng. Comm*, 2001, **3**, 170-173.
91. J. B. Orton, PhD thesis, University of Southampton, 2006.
92. J. R. Gomm, PhD thesis, University of Southampton, 2002.
93. C. A. Golden, PhD thesis, University of Southampton, 2005.
94. A. N. Dwyer, PhD thesis, University of Southampton, 2004.
95. M. E. Oszer, M.Res. thesis, University of Southampton, 1998.
96. R. A. Parker, PhD thesis, University of Southampton, 1999.
97. W. L. Jorgensen and J. Pranata, *J. Am. Chem. Soc.*, 1990, **112**, 2008-2010.
98. S. N. Qu, F. Li, H. T. Wang, B. L. Bai, C. Y. Xu, L. J. Zhao, B. H. Long and M. Li, *Chem. Mat.*, 2007, **19**, 4839-4846.
99. W. F. Cooper, N. C. Kenny, J. W. Edmonds, A. Nagel, F. Wudl and P. Coppens, *J. Chem. Soc. D*, 1971, 889-890.
100. F. Wudl, G. M. Smith and E. J. Hufnagel, *J. Chem. Soc. D*, 1970, 1453-1454.
101. F. Wudl, Wobschal.D and E. J. Hufnagel, *J. Am. Chem. Soc.*, 1972, **94**, 670-672.
102. M. R. Bryce, *J. Mater. Chem.*, 2000, **10**, 589-598.
103. J. Puigmarti-Luis, A. Minoia, A. P. del Pino, G. Ujaque, C. Rovira, A. Lledos, R. Lazzaroni and D. B. Amabilino, *Chem. Eur. J.*, 2006, **12**, 9161-9175.
104. J. P. Griffiths, R. J. Brown, P. Day, C. J. Matthews, B. Vital and J. D. Wallis, *Tetrahedron Lett.*, 2003, **44**, 3127-3131.
105. *Mercury CSD*, version 2.2 (build RC5), CCDC, 2008.
106. C. F. Macrae, I. J. Bruno, J. A. Chisholm, P. R. Edgington, P. McCabe, E. Pidcock, L. Rodriguez-Monge, R. Taylor, J. van de Streek and P. A. Wood, *J. Appl. Crystallogr.*, 2008, **41**, 466-470.
107. S. K. Wolff, D. J. Grimwood, J. J. McKinnon, D. Jayatilaka and M. A. Spackman, *CrystalExplorer*, version 2.1, 2007.
108. J. J. McKinnon, D. Jayatilaka and M. A. Spackman, *Chem. Commun.*, 2007, 3814-3816.
109. H. L. Turner, BSc dissertation, University of Southampton, 2001.
110. J. B. Orton, MPhil/PhD Transfer Thesis, University of Southampton, 2003.

111. R. M. Parker, MChem. dissertation, University of Southampton, 2006.
112. S. Twiddy, MChem. dissertation, University of Southampton, 2007.
113. M. C. Grossel, M. B. Hursthouse and J. B. Orton, *Cryst. Eng. Comm*, 2005, **7**, 279-283.
114. S. Burnet, A. K. Hall, J. M. Harrowfield, G. A. Koutsantonis, V. Sanford, D. Sauter, B. W. Skelton and A. H. White, *Supramol. Chem.*, 2003, **15**, 291-312.
115. A. P. West, S. K. Silverman and D. A. Dougherty, *J. Am. Chem. Soc.*, 1996, **118**, 1452-1463.
116. F. Bobhlmann, A. Englisch, N. Ottawa, H. Sander and W. Weise, *Chem. Ber.*, 1956, **89**, 792-799.
117. Y. Hamuro, S. J. Geib and A. D. Hamilton, *J. Am. Chem. Soc.*, 1997, **119**, 10587-10593.
118. E. I. Levkoeva, L. I. Mastafanova, D. M. Krasnokutskaya, M. I. Evstratova, Y. S. Karpman, I. S. Tubina, I. L. Ivanova and L. N. Yakhontov, *Khimiya Geterotsiklicheskikh Soedinenii*, 1976, 233-237.
119. E. I. Levkoeva, L. I. Mastafanova, D. M. Krasnokut-skaya, M. I. Evstratova, Y. S. Karpman, I. S. Tubina, I. L. Ivanova and L. N. Yakhontov, *Chem. Heterocycl. Compd. (N. Y.)*, 1976, **12**, 201-204.
120. M. Misicvukovic, D. M. Dimitrijevic, M. D. Muskatirovic, M. Radojkovicvelickovic and Z. D. Tadic, *J. Chem. Soc., Perkin Trans. 2*, 1978, 34-38.
121. K. V. Reddy, S. J. Jin, P. K. Arora, D. S. Sfeir, S. C. F. Maloney, F. L. Urbach and L. M. Sayre, *J. Am. Chem. Soc.*, 1990, **112**, 2332-2340.
122. K. G. Hull, M. Visnick, W. Tautz and A. Sheffron, *Tetrahedron*, 1997, **53**, 12405-12414.
123. G. K. S. Ooi and R. J. Magee, *Journal of Inorganic & Nuclear Chemistry*, 1970, **32**, 3315-3320.
124. L. Thunus and M. Dejardin-Duchene, *J Pharm Belg*, 1969, **24**, 3-21.
125. F. H. Allen, *Acta Crystallogr. Sect. B-Struct. Commun.*, 2002, **58**, 380-388.
126. I. J. Bruno, J. C. Cole, P. R. Edgington, M. Kessler, C. F. Macrae, P. McCabe, J. Pearson and R. Taylor, *Acta Crystallogr. Sect. B-Struct. Commun.*, 2002, **58**, 389-397.
127. D. A. Haynes, W. Jones and W. D. S. Motherwell, *Cryst. Eng. Comm.*, 2006, **8**, 830-840.
128. J. A. Cowan, J. A. K. Howard, G. J. McIntyre, S. M. F. Lo and I. D. Williams, *Acta Crystallogr. Sect. B-Struct. Commun.*, 2005, **61**, 724-730.
129. K. Hayakawa, D. Shiomi, T. Ise, K. Sato and T. Takui, *J. Phys. Chem. B*, 2005, **109**, 9195-9197.
130. L. B. Jerzykiewicz, Z. Malarski, L. Sobczyk, T. Lis and E. Grech, *J. Mol. Struct.*, 1998, **440**, 175-185.
131. B. R. Bhogala, S. Basavoju and A. Nangia, *Cryst. Eng. Comm.*, 2005, **7**, 551-562.
132. R. F. Evans, E. F. G. Herington and W. Kynaston, *Trans. Faraday Soc.*, 1953, **49**, 1284-1292.
133. R. W. Green and H. K. Tong, *J. Am. Chem. Soc.*, 1956, **78**, 4896-4900.

134. E. P. Oliveto, in *Pyidine and Its Derivatives*, Ed. E. Klingsberg, Interscience Publishers, New York, Editon edn., 1962, vol. 3, pp. 179-346.
135. J. Garin, J. Orduna, S. Uriel, A. J. Moore, M. R. Bryce, S. Wegener, D. S. Yufit and J. A. K. Howard, *Synthesis*, 1994, 489-493.
136. M. R. Bryce, W. Devonport, L. M. Goldenberg and C. S. Wang, *Chem. Commun.*, 1998, 945-951.
137. V. C. Tellez, B. S. Gaytan, S. Bernes and E. G. Vergara, *Acta Crystallogr. Sect. C: Cryst. Struct. Commun.*, 2002, **58**, O228-O230.
138. N. W. Alcock, R. G. Kingston, P. Moore and C. Pierpoint, *J. Chem. Soc., Dalton Trans.*, 1984, 1937-1943.
139. J. P. Collman, R. A. Decreau and S. Costanzo, *Org. Lett.*, 2004, **6**, 1033-1036.
140. *ACD/SpecManager*, version 11.01, Advanced Chemistry Development, Inc., Toronto, Ontario, Canada, 2007.
141. *Omnic*, version 7.2, Thermo Electron Corporation, 2005.
142. *Spectrum*, version 2.00, Perkin-Elmer Ltd., 1998.
143. *OriginPro 8*, version 8.0987, OriginLab Corportation, Northampton, MA, USA, 2009.
144. *STARe Software*, version 9.01, Mettler-Toledo GmbH, 2006.
145. *UVPC Personal Spectroscopy Software*, version 3.5, Shimadzu Scientific Instruments Inc., 1994.
146. R. W. W. Hooft, *"Collect" data collection software*, B. V. Nonius, 1998.
147. Z. Otwinowski and W. Minor, in *Macromolecular Crystallography, Pt A*, Eds. C. W. J. Carter and R. M. Sweet, Academic Press Inc., San Diego, Editon edn., 1997, vol. 276, pp. 307-326.
148. A. J. M. Duisenberg, R. W. W. Hooft, A. M. M. Schreurs and J. Kroon, *J. Appl. Crystallogr.*, 2000, **33**, 893-898.
149. A. J. M. Duisenberg, *J. Appl. Crystallogr.*, 1992, **25**, 92-96.
150. G. M. Sheldrick, *SADABS*, version 2.10, Bruker AXS Inc., Madison, Wisconsin, USA, 2003.
151. G. M. Sheldrick, *SADABS*, version 2007/2, Bruker AXS Inc., Madison, Wisconsin, USA, 2007.
152. *XPREP - Data Preparation & Reciprocal Space Exploration*, version 5.1/NT Bruker AXS Inc., Madison, Wisconsin, USA, 1997.
153. G. M. Sheldrick, *SHELX-97 - Programs for Crystal Structure Analysis* Release 97-2, Institut fűr Anorganische Chemie der Universikit, Gottingen, Germany, 1998.
154. G. M. Sheldrick, *Acta Crystallogr. Sect. A: Fundam. Crystallogr.*, 2008, **64**, 112-122.
155. L. J. Farrugia, *J. Appl. Crystallogr.*, 1999, **32**, 837.
156. A. L. Spek, *J. Appl. Crystallogr.*, 2003, **36**, 7-13.
157. L. J. Farrugia, *J. Appl. Crystallogr.*, 1997, **30**, 565.
158. W. H. Tallent and E. C. Horning, *J. Am. Chem. Soc.*, 1956, **78**, 4467-4469.
159. R. M. Kellogg and T. J. Van Bergen, *J. Org. Chem.*, 1971, **36**, 978-983.
160. R. A. Barnes and H. M. Fales, *J. Am. Chem. Soc.*, 1953, **75**, 3830-3831.
161. V. D. Adams and R. C. Anderson, *Synthesis*, 1974, **1974**, 286-288.

162. W. Mothersole, MChem. dissertation, University of Southampton, 2008.
163. W. Raßofer, W. Müller, M. and F. Vögtle, *Chem. Ber.*, 1979, **112**, 2095-2119.
164. X. Li, C. L. Zhan, Y. B. Wang and J. N. Yao, *Chem. Commun.*, 2008, 2444-2446.
165. K. M. Broadus and S. R. Kass, *J. Am. Chem. Soc.*, 2000, **122**, 9014-9018.
166. D. C. Green and R. W. Allen, *J. Chem. Soc., Chem. Commun.*, 1978, 832-833.
167. D. C. Green, *J. Org. Chem.*, 1979, **44**, 1476-1479.
168. R. P. Parg, J. D. Kilburn, M. C. Petty, C. Pearson and T. G. Ryan, *J. Mater. Chem.*, 1995, **5**, 1609-1615.
169. C. J. Chandler, L. W. Deady, J. A. Reiss and V. Tzimos, *Journal of Heterocyclic Chemistry*, 1982, **19**, 1017-1019.
170. D. S. Marlin, M. M. Olmstead and P. K. Mascharak, *J. Mol. Struct.*, 2000, **554**, 211-223.
171. E. Buhleier, W. Wehner and F. Vögtle, *Chem. Ber.*, 1979, **112**, 559-566.
172. N. Kanomata, H. Nagahara and M. Tada, *J. Heterocycl. Chem.*, 1992, **29**, 1567-1571.
173. E. Buhleier, W. Wehner and F. Vogtle, *Chem. Ber.*, 1979, **112**, 559-566.